Mechanisms of Dysregulated Calcitonin Signalling in Cardiac Fibroblasts in Atrial Fibrillation



Aaron Michael Johnston

Magdalen College

Radcliffe Department of Medicine, University of Oxford

A thesis submitted for the degree of

Doctor of Philosophy

Trinity Term 2026

Abstract

Atrial fibrillation (AF) is the most prevalent sustained cardiac arrhythmia and is associated with substantial morbidity and mortality. Atrial fibrosis, driven by the excessive activation of atrial cardiac fibroblasts (ACFs), is a hallmark of the structural substrate that perpetuates AF, yet no approved therapies primarily target this process. Paracrine calcitonin (CT), secreted by atrial cardiomyocytes, suppresses adjacent ACF fibrogenesis via the calcitonin receptor (CALCR). This antifibrotic axis is disrupted in persistent AF owing to reduced CT production and aberrant CALCR internalisation in ACFs, rendering fibroblasts refractory to its protective effects.[1] This thesis had two overarching aims: (i) to identify the molecular mechanisms underlying AF-associated CALCR internalisation in primary human ACFs, and (ii) to unbiasedly identify pharmacological compounds capable of restoring CALCR surface expression and thereby resensitising AF-ACFs to CT.

Hypothesis-driven, mechanistic investigation systematically evaluated filamin A (FLNa) and its proteolytic fragments, clathrin-mediated endocytosis, alternative splicing, receptor-activity modifying proteins, β-arrestins, and N-linked glycosylation, and found no evidence that these were major determinants of the CALCR internalisation phenotype in primary human ACFs. Immunoprecipitation-mass spectrometry identified substantial AF-associated remodelling of the CALCR interactome, with enrichment of endocytic and retromer recycling machinery suggesting impaired receptor recycling or failed surface delivery as the predominant trafficking defects.

Given the absence of a single causal mechanism, an unbiased high-throughput screen of 3,091 clinically approved compounds in primary AF-ACFs identified levamlodipine as a reproducible restorer of CALCR surface localisation. Functional validation demonstrated levamlodipine restores CALCR-dependent suppression of collagen I in AF-ACFs when combined with human calcitonin. Mechanistic investigations revealed

this effect is possibly L-type Ca^{2+} channel independent and is associated with transcriptional induction of mevalonate/cholesterol biosynthesis pathways and downregulation of cytoskeletal motor proteins. These findings establish a proof-of-principle for pharmacological re-engagement of an endogenous, antifibrotic, paracrine axis in human AF, identifying levamlodipine as a candidate for repurposing in this indication.

Acknowledgements

This DPhil thesis would not have been possible without the steadfast support - and often patience - of the remarkable individuals around me. First and foremost, I would like to express my gratitude to my supervisors, Professors Svetlana Reilly and Nicola Smart. Your wisdom, encouragement, insightful guidance, and confidence in me have shaped not only this work but also my growth as a scientist. I remain enduringly indebted to you both.

To my biggest champions - my parents, Lauren, Meng, and Grandma - I owe an immeasurable debt of gratitude. Your love, encouragement, and inspiration made this endeavour possible. I look forward to spending more time with you now that it has come to an end. I also wish to acknowledge, with both love and sadness, those I lost during this period: Auntie Colette and Uncle Jason. Your absence is deeply felt.

To my cherished friends - particularly Marianne, Luke, Jacinta, Lauren, Maria, Flair, Emma, Noah, Max, Sam, Michail - thank you for your humour, kindness, reassurance, and companionship through long hours, failed experiments, and sleep-deprived days. Your presence made it endurable. My colleagues and now friends – particularly Kendrick, Lucia, Sam, Val, and Danny – your support and expertise kept me sane. Each of you inspires me.

I would also like to thank the British Heart Foundation for funding my studentship, with particular gratitude to Dr Robert Easton and Mr Andrew Spokes for their generous donations in support of my research. I am equally grateful for the supportive and stimulating environments provided by Magdalen and Wadham Colleges, which formed an important foundation for my time in Oxford. Finally, and most importantly, I wish to thank the extraordinarily generous patients who donated samples for this research. This thesis was inspired by their contribution and would not have been possible without them.

Publications

Leblanc, F.J.A., Yiu, C.H.K., Moreira, L.M., Johnston, A.M., Mehta, N., Kourliouros, A., Sayeed, R., Nattel, S., Reilly, S., & Lettre, G. Single-nucleus multi-omics implicates androgen receptor signaling in cardiomyocytes and NR4A1 regulation in fibroblasts during atrial fibrillation. *Nat Cardiovasc Res*. **4**. (2025). https://doi.org/10.1038/s44161-025-00626-0

Zhao, S., *Johnston, A.M., Yiu C.H.K., Moreira, L.M., Reilly, S., & Wehrens, X.H.T. Aging-associated mechanisms of atrial fibrillation progression and their therapeutic potential. *J Cardiovasc Aging*. **4**. (2024). https://doi.org/10.20517/jca.2024.12

*Johnston, A.M., Yiu, C.H.K., & Reilly, S. Decoding Long Noncoding RNAs in Myocardial Infarction: A Step Closer to a "Magic Bullet"? *Can J Cardiol*. **40**. (2024). https://doi.org/10.1016/j.cjca.2024.01.016.

Wallis, L., Donovan, L., Johnston, A., Phillips, L.C., Lin, J., Garland, C.J., & Dora, K.A. Tracking endothelium-dependent NO release in pressurized arteries. *Front Physiol*. **14**. (2023). https://doi.org/10.3389/fphys.2023.1108943

*First or joint first authorship

Table of Contents

CHAPTER 1: INTRODUCTION ***1***

1.1 Atrial Fibrillation (AF) **2**

1.1.1 Epidemiology and clinical definition 2

1.1.2 Aetiology of atrial fibrillation (AF) 4

1.1.3 Principles of AF management 6

1.2 Fibrosis **9**

1.2.1 Introduction to fibrosis 9

1.2.2 Atrial fibrosis as a hallmark of the AF substrate 10

1.3 Calcitonin and Atrial Fibrillation **13**

1.3.1 Calcitonin (CT) 13

1.3.2 Calcitonin receptor (CALCR) 14

1.4 Regulation of CALCR Localisation and Activity **16**

1.4.1 Genetic polymorphisms and alternative splicing 16

1.4.2 β-arrestin recruitment 17

1.4.3 Receptor-activity modifying proteins 18

1.4.4 Filamin A (FLNa) regulates CALCR membrane recycling 20

1.4.5 Post-translational modifications of CALCR 21

1.4.6 The '*Escape Phenomenon*' 22

1.5 High-throughput drug repurposing screens **24**

1.5.1 Drug repurposing 24

1.5.2 High throughput screening (HTS) 25

1.6 Hypotheses, Aims and Objectives **29**

CHAPTER 2: MATERIALS AND METHODS ***30***

2.1 Patient recruitment and cardiac fibroblast isolation 31

2.2 Real-time quantitative polymerase chain reaction (RT-qPCR) 35

2.3 Western blot (WB) 36

2.4 Immunoprecipitation of FLNa and CALCR 40

2.5 siRNA transfection of ACFs 40

2.6 ACF immunostaining and confocal microscopy 42

2.7 Statistical analyses 42

CHAPTER 3: THE ROLE OF FILAMIN A AND ITS PROTEOLYTIC FRAGMENTS IN CALCR LOCALISATION 44

3.1 Introduction 45

3.2 Methods & Materials 49

3.2.1 Subcellular fractionation 49

3.2.2 Calpain activity assay 49

3.2.3 Calpain 1 pharmacological inhibition 49

3.2.4 Proteasome and lysosome inhibition in human ACFs 50

3.2.5 Tandem ubiquitin-binding entity (TUBE) pulldown assay 50

3.2.6 Cycloheximide chase assay 51

3.2.7 Cloning and transfection of a CALCR-FLNa interaction disrupting peptide 52

3.3 Results 54

3.3.1 Confirmation of CALCR internalisation 54

3.3.2 Reduced expression of $FLNa^{CT}$ in AF-ACFs 56

3.3.3 Unaltered calpain expression and activity in AF-ACFs 58

3.3.4 Caspase 3 knockdown does not alter $FLNa^{CT}$ abundance in ACFs 62

3.3.5 Proteasome, but not lysosome, inhibition reduces $FLNa^{CT}$ expression 64

3.3.6 $FLNa^{CT}$ is not degraded by the lysosomal pathway 69

3.3.7 FLNa is not a major regulator of CALCR localisation in ACFs 71

3.4 Discussion 77

3.4.1 CALCR internalisation in AF-ACFs reflects redistribution to cytoskeletal compartments 77
3.4.2 FLNa processing is altered in ACFs in patients with AF 78
3.4.3 Calpains and caspase 3 are not the predominant proteases responsible for $FLNa^{CT}$ generation in human ACFs 79
3.4.4 $FLNa^{CT}$ is not degraded by proteasomal or lysosomal pathways 79
3.4.5 FLNa-CALCR interaction is not a major determinant of CALCR localisation in ACFs 81
3.4.6 Conclusions and implications 82

CHAPTER 4: MECHANISTIC INTERROGATION OF ALTERNATIVE REGULATORS OF CALCR LOCALISATION 83

4.1 Introduction 84

4.2 Methods & Materials 85

4.2.1 Sample preparation, mass spectrometry (MS) & data analysis of the CALCR interactome 85
4.2.2 Data Analysis and KEGG pathway analysis 87
4.2.3 Endocytosis and N-glycosylation inhibition 87
4.2.4 RT-qPCR for CALCR splice variants 87

4.3 Results 89

4.3.1 Quality assessment and global overview of the CALCR interactome 89
4.3.2 KEGG pathway analysis of unique interactors 91
4.3.3 Inhibition of endocytosis does not affect CALCR localisation 96
4.3.4 CALCR isoform expression in human ACFs 99
4.3.5 Assessment of RAMP1-3 expression in human ACFs 99
4.3.6 Assessment of β-arrestin expression and function in human ACFs 102
4.3.7 Assessment of CALCR N-glycosylation 102

4.4 Discussion 106

4.4.1 CALCR interactome profiling reveals AF-specific remodelling 106
4.4.2 Pharmacological inhibition of CME and actin polymerisation does not rescue CALCR surface expression 108
4.4.3 CALCR splice variant expression is conserved between SR- and AF-ACFs 112
4.4.4 RAMP proteins are not detectable at the protein level in human ACFs 112
4.4.5 β-arrestins are unlikely to promote CALCR internalisation 113
4.4.6 Inhibition of N-glycosylation does not significantly alter CALCR localisation 114
4.4.7 Conclusions and implications 114

CHAPTER 5: DEVELOPMENT OF A HIGH-THROUGHPUT DRUG SCREENING PLATFORM IN AF-ACFs TO ASSESS CALCR LOCALISATION 116

5.1 Introduction 117

5.2 Methods & Materials 119

5.2.1 Seeding density and antibody optimisation 119
5.2.2 High-throughput drug screening assay 119
5.2.3 High content imaging and image analysis 121
5.2.4 Definition of toxic and hit compounds 122

5.3 Results 124

5.3.1 Optimisation of HTS conditions 124
5.3.2 Selection of an assay readout for CALCR localisation 127
5.3.3 Comparative analysis of screen-level performance metrics 130
5.3.4 Identification of CALCR Localisation Hits 132
5.3.5 Secondary screening of the effects of cytotoxic compounds on CALCR localisation 135
5.3.6 Identification of Collagen I hits 137

5.4 Discussion 143

5.4.1 Assay development and performance 143
5.4.2 CALCR localisation hit identification and reproducibility 145

5.4.3 CALCR hits: L-type calcium channel blockers 146

5.4.4 CALCR hits: integrin inhibitors 147

5.4.5 CALCR hits: deprioritised compounds 148

5.4.6 Secondary collagen I readouts 148

5.4.7 Conclusions and implications 149

CHAPTER 6: MECHANISTIC INVESTIGATIONS INTO THE ANTIFIBROTIC EFFECTS OF SELECTED HIT COMPOUNDS 151

6.1 Introduction 152

6.2 Methods & Materials 155

6.2.1 *In silico* prediction of protein targets of CALCR hits 155

6.2.2 Determination of concentration-response relationships 155

6.2.3 *In vitro* validation of levamlodipine besylate 156

6.2.4 RNA sequencing (RNAseq) analysis 157

6.2.5 Assessment of CALCR localisation in ACFs from CREM-IBΔC-X-Tg mice 159

6.3 Results 161

6.3.1 Further characterisation of CALCR hits identified in ≥2 donors 161

6.3.2 Assessment of TRPC channel antagonists on CALCR localisation 168

6.3.3 Functional validation of levamlodipine on CALCR localisation and antifibrotic signalling 171

6.3.4 Knockdown of the canonical molecular target of levamlodipine 172

6.3.5 Transcriptomic changes induced by levamlodipine treatment in AF-ACFs 176

6.3.6 Establishing the reproducibility of the levamlodipine-mediated effects on CALCR localisation 180

6.4 Discussion 182

6.4.1 Shared pharmacological targets among CALCR-restoring compounds 182

6.4.2 Concentration-response relationships and potency considerations 184

6.4.3 Levamlodipine restores functional CALCR-dependent antifibrotic signalling 185

6.4.4 The effects of levamlodipine on CALCR localisation are possibly independent of $Ca_v1.2$ inhibition 185
6.4.5 Transcriptomic profiling reveals levamlodipine affects lipid metabolic and inflammatory pathways 187
6.4.6 Mechanistic insight provided by genes downregulated by levamlodipine 188
6.4.7 Conservation of the CALCR internalisation phenotype in the CREM-Tg mouse model 190
6.4.8 Conclusions and implications 190

CHAPTER 7: CONCLUSIONS AND FUTURE DIRECTIONS 192

7.1 Overview 193

7.2 Principal findings 194

7.2.1 FLNa is not a major regulator of CALCR localisation in primary human ACFs 194
7.2.2 Systematic exploration of six candidate trafficking mechanisms narrows the mechanistic field and identifies CALCR interactome remodelling in AF 195
7.2.3 CALCR internalisation in AF-ACFs: a complex, potentially redundant, aetiology 196
7.2.4 A high-throughput phenotypic screen identified levamlodipine as a reproducible restorer of surface CALCR localisation 196
7.2.5 Levamlodipine rescues CALCR-dependent antifibrotic signalling possibly via a $Ca_v1.2$-independent mechanism 197

7.3 Limitations and future directions 201

7.3.1 The primary human ACF model 201
7.3.2 Measurement of CALCR localisation 202
7.3.3 Limitations of mechanistic experiments 203

7.4 Final conclusions 205

CHAPTER 8: APPENDICES 206

Appendix 1: List of the 169 unique CALCR interactors in SR-ACFs 207

Appendix 2: List of the 427 unique CALCR interactors in AF-ACFs 209

Appendix 3: Full list of the compounds that reduced cell count by ≥2 SD for each donor 211

Appendix 4: RNA quality, sequencing depth, and alignment quality-control metrics for RNAseq libraries. 217

Appendix 5: Genes upregulated by levamlodipine in AF-ACFs. 218

Appendix 6: Genes downregulated by levamlodipine in AF-ACFs. 220

CHAPTER 9: REFERENCES ***222***

List of Figures

Figure 1.1 Mechanisms of atrial fibrillation pathogenesis……12

Figure 1.2 Diversification of CALCR and CRLR ligand specificity by RAMPs……...19

Figure 1.3 Proposed regulators of CALCR surface expression……...23

Figure 2.1 Isolation of ACFs……..33

Figure 2.2 Validation of HPRT1 as an RT-qPCR housekeeping gene……36

Figure 3.1.1 Schematic representation of filamin A (FLNa) domain organisation and interaction with the calcitonin receptor……48

Figure 3.3.1 CALCR is aberrantly localised in AF-ACFs……..55

Figure 3.3.2 $FLNa^{CT}$ interacts with CALCR and is reduced in AF-ACFs……57

Figure 3.3.3 Calpain-like activity is not altered in AF, despite reduced calpain 1 expression……59

Figure 3.3.4 Pharmacological inhibition of classical calpains does not reduce $FLNa^{CT}$ expression in SR-ACFs. ……..……..60

Figure 3.3.5 Calpain 1 siRNA-knockdown does not affect $FLNa^{CT}$ in SR-ACFs……...61

Figure 3.3.6 Caspase 3 siRNA-knockdown does not affect $FLNa^{CT}$ expression in SR-ACFs……62

Figure 3.3.7 Effects of MG-132 on FLNa species……..……65

Figure 3.3.8 Cycloheximide chase assay to assess turnover of FLNa species……66

Figure 3.3.9 Assessment of $FLNa^{CT}$ ubiquitination using tandem ubiquitin-binding entity (TUBE) pulldown assays……..68

Figure 3.3.10 Effect of MG-132 on CALCR localisation…….69

Figure 3.3.11 Effect of bafilomycin A1 (BafA1) on $FLNa^{CT}$…….……70

Figure 3.3.12 Design and optimisation of a CALCR C-terminal disrupting peptide to interfere with FLNa-CALCR interactions……..73

Figure 3.3.13 Expression of a FLNa-CALCR disrupting peptide does not affect CALCR localisation…….……75

Figure 3.3.14 FLNa siRNA-knockdown does not affect CALCR localisation……..76

Figure 4.3.1 Quality assessment and overview of the CALCR interactome from 4 unique SR- and AF-ACFs……...90

Figure 4.3.2 KEGG pathway analysis of unique CALCR interactors in SR- and AF-ACFs…….93

Figure 4.3.3 Effect of endocytosis inhibition on CALCR localisation in AF-ACFs…….98

Figure 4.3.4 Analysis of CALCR splice variant expression in SR- and AF-ACFs…...100

Figure 4.3.5 Expression of RAMP1-2…….……..101

Figure 4.3.6 β-arrestin expression and effect on CALCR localisation in AF-ACFs……...103

Figure 4.3.7 Effect of N-glycosylation inhibition in ACFs……105

Figure 4.4.1 Schematic of CALCR trafficking dynamics and dysregulation in AF…….111

Figure 5.2.1 Knockdown validation for the confirmation of the CALCR antibody's specificity…….....122

Figure 5.2.2 Schematic overview of the high-content screening workflow and automated image analysis……..……123

Figure 5.3.1 Optimisation of seeding density and DMSO tolerance in SR- and AF-ACFs……...124

Figure 5.3.2 Selection of assay readout based on Z'-factor analysis……...129

Figure 5.3.3 Full screen assay performance and reproducibility……..131

Figure 5.3.4 Identification of CALCR localisation hits…..……..134

Figure 5.3.5 Re-evaluation of cytotoxic compounds at lower concentrations identifies additional CALCR localisation hits……..136

Figure 5.3.6 Identification of collagen I hits assessed by cytoplasmic staining intensity……..141

Figure 5.3.7 Identification of collagen I hits assessed by thresholded cytoplasmic area coverage……142

Figure 6.2.1 Experimental workflow for assessing restoration of calcitonin responsiveness in independent AF-ACFs…….……157

Figure 6.3.1 Concentration-dependent effects of prioritised compounds on CALCR localisation in AF-ACFs across each donor……...162

Figure 6.3.2 Concentration-response relationships of prioritised compounds on cell number and CALCR localisation in AF-ACFs……167

Figure 6.3.3 Concentration-response relationships of TRPC3/6 or store-operated calcium entry (SOCE) modulators on cell number, CALCR localisation, and collagen 1……170

Figure 6.3.4 Levamlodipine restores CALCR-dependent antifibrotic signalling in human AF-ACFs……173

Figure 6.3.5 Effect of CACNA1C siRNA-knockdown on the antifibrotic response to human calcitonin (hCT)……175

Figure 6.3.6 Transcriptomic profiling of AF-ACFs following levamlodipine treatment……177

Figure 6.3.7 CALCR internalisation and pharmacological rescue in ACFs from CREM-Tg mice……..……181

Figure 7.1 Schematic summarising the principal findings of this thesis……200

List of Tables

Table 1.1 Summary of active clinical trials with calcitonin as an intervention or treatment……..……..……...15

Table 2.1 Clinical characteristics of study participants……34

Table 2.2 RT-qPCR TaqManTM assay IDs……35

Table 2.3 Details of primary antibodies used for immunocytochemistry and Western blot……38

Table 2.4 Details of secondary antibodies used for immunocytochemistry and Western blot……39

Table 2.5 Details of ON-TARGETplus human siRNAs used in this study……41

Table 3.1 List of proteases (HGNC symbols) in the MEROPS database also identified in a human ACF proteomic database……...63

Table 4.1 Summary of differential protein enrichment across comparisons in the CALCR interactome dataset……..…91

Table 4.2 Significantly enriched KEGG pathways (ranked by fold enrichment) among putative CALCR interactors in SR-ACFs……....92

Table 4.3 Top 20 enriched KEGG pathways (ranked by fold enrichment) among putative CALCR interactors in AF-ACFs……..94

Table 5.1 Summary of FDA Approved & Pharmacopeial Drug Library……....120

Table 5.2 Clinical characteristics of the three AF donors and common SR control used in each HTS……..125

Table 5.3 CALCR localisation compound hits in each donor, ranked by Z-score..133

Table 5.4 Re-evaluation of cytotoxic compounds at lower concentrations identifies additional CALCR localisation hits……..136

Table 5.5 Collagen I compound hits in each donor, ranked by Z-score, as defined by mean collagen I cytoplasmic staining intensity…….138

Table 5.6 Collagen I compound hits in each donor, ranked by Z-score, as defined by proportion of the cytoplasm covered by a binary collagen I mask…..139

Table 6.1 Protein target prediction for mutual CALCR hit compounds by two *in silico* ligand-target prediction tools……...164

Table 6.2 Summary of TRPC antagonists and SOCE modifiers……..169

Table 6.3 Top 20 enriched KEGG pathways (ranked by fold enrichment) among genes upregulated in levamlodipine-treated AF-ACFs……178

Table 6.4 Enriched KEGG pathways (ranked by fold enrichment) among genes downregulated (based on unadjusted p-value) in levamlodipine-treated AF-ACFs……...179

List of Abbreviations

5-HT	5-hydroxytryptamine or serotonin
5-HT1AR	Serotonin 1A receptor
ACF	Atrial cardiac fibroblast
ACM	Atrial cardiomyocyte
ACTA2 or αSMA	Alpha smooth muscle actin or actin alpha 2
AF	Atrial fibrillation
AF-ACF	Atrial cardiac fibroblast derived from donors with persistent AF
AP-2	Adaptor protein 2
AT1R	Angiotensin II type 1 receptor
CABG	Coronary artery bypass grafting
CACNA1C	Calcium voltage-gated channel subunit alpha 1 C
CALCR	Calcitonin receptor
CALCRL	Calcitonin receptor-like receptor
CaMKII	Ca^{2+}/calmodulin-dependent protein kinase II
cAMP	Cyclic adenosine monophosphate
CASP3	Caspase 3
CGRP	Calcitonin gene-related peptide
CME	Clathrin-mediated endocytosis
CMR	Cardiac magnetic resonance
CRAPome	Contaminant repository for affinity purification
CRC	Concentration-response curves
CREM-Tg	cAMP-Response Element Modulator-Ib∆C-X isoform overexpressing transgenic
CryoEM	Cryo-electron microscopy
CT	Calcitonin
CVD	Cardiovascular disease
DAD	Delayed afterdepolarisation
DAPI	4',6-diamidino-2-phenylindole
DHP	Dihydropyridine
DMSO	Dimethylsulfoxide
DOAC	Direct oral anticoagulant
EAD	Early afterdepolarisation
ECD	Extracellular domain
ECG	Electrocardiogram
ECM	Extracellular matrix
EGFP	Enhanced green fluorescent protein
ESC	European Society of Cardiology
FDA	Food and Drug Administration
FDR	False discovery rate
FGF	Fibroblast growth factors
FLNa	Filamin A
$FLNa^{CT}$	Filamin A C-terminal fragment
$FLNa^{NT}$	Filamin A N-terminal fragment

GAPDH	Glyceraldehyde 3-phosphate dehydrogenase
GPCR	G-protein coupled receptor
GRK	G-protein coupled receptor kinase
hCT	Human calcitonin
HEK293	Human embryonic kidney 293 cells
Ig	Immunoglobulin
IL-1	Interleukin-1
IL-6	Interleukin-6
IP	Immunoprecipitation
IQR	Interquartile range
JPH2	Junctophilin-2
kDa	Kilodalton
KEGG	Kyoto Encyclopaedia of Genes and Genomes
LTCC	L-type Calcium Channel
MS	Mass spectrometry
NCX	Sodium-Calcium exchanger
NHS	National Health Service
NICE	National Institute for Health and Care Excellence
NLS	Nuclear localisation signal
NPC	Nuclear pore complexes
NUP155	Nucleoporin 155
PDGF	Platelet derived growth factors
persAF	Persistent atrial fibrillation
PITX2	Paired-like homeodomain 2
PKA	Protein kinase A
PNS	Perinuclear space
PRDX4	Peroxiredoxin 4
RAAS	Renin-angiotensin-aldosterone system
RGD	Arginine-glycine-aspartic acid
RNA	Ribonucleic acid
RNAseq	Ribonucleic acid sequencing
RyR	Ryanodine receptor
scRNAseq	Single-cell RNA sequencing
sCT	Salmon calcitonin
SD	Standard deviation
SEM	Standard error of the mean
SK2	Small-conductance Ca^{2+}-activated K^+ channels
SMILES	Simplified Molecular Input Line Entry System
SR	Sinus Rhythm
SR-ACF	Atrial cardiac fibroblast derived from donors in sinus rhythm
STITCH	Search Tool for Interacting Chemicals
TAC	Transverse aortic constriction
TGF-β	Transforming growth factor-beta
TUBE	Tandem ubiquitin-binding entity
UPS	Ubiquitin proteasome system
V_{GLA}	Global left atrial voltage

WB	Western blot
αMHC	Alpha myosin heavy chain

CHAPTER 1: INTRODUCTION

Even in classical antiquity, the heart was recognised to be more than a simple, mechanical pump. Philosophers and physicians such as Aristotle and Galen attributed to it functions beyond circulation, encompassing emotion, intellect, and sensation, thereby establishing its central place in both physiological and metaphysical axes.[2] While many of these early interpretations were later revised through the functional and anatomical studies of Vesalius, Colombo, Harvey and many others, they nevertheless represent an important stage in the evolution of cardiovascular thought. Their tradition of inquiry established the intellectual foundation for modern cardiovascular science, as Harvey observed "there is no science which does not spring from pre-existing knowledge".[3,4]

In this chapter, I outline the epidemiology, pathophysiology, and current management of atrial fibrillation (AF), with particular emphasis on atrial structural remodelling. On this basis, I introduce a novel, antifibrotic, paracrine signalling axis which has been shown to be impaired in AF owing to loss of receptor expression at the cell surface in atrial fibroblasts. Mechanisms governing receptor trafficking and internalisation are subsequently reviewed, followed by a discussion of approaches to identify compounds capable of restoring this protective pathway. Upon these discussions evolve the hypotheses, aims, and objectives underpinning this thesis.

1.1 Atrial Fibrillation (AF)

1.1.1 Epidemiology and clinical definition

Owing to improvements in medicine, public health, sanitation and the security of food and water supplies, the global population is both expanding and ageing. This is forecast to significantly increase the number of people living with cardiovascular disease (CVD), which currently affects 8 million people in the UK and accounts for 27% of all deaths (NICE, July 2025). Among CVDs, atrial fibrillation (AF) is a significant contributor to mortality and morbidity. AF is the most common, sustained cardiac arrhythmia, estimated

to affect ~0.5% of the global population with a lifetime risk approaching 1 in 3 and a European Union incidence predicted to double by 2060, due to advancing age, increased prevalence of comorbidities, and improved detection.[5-7]

AF is a supraventricular arrhythmia characterised by irregular and rapid, uncoordinated atrial electrical activity. This arrhythmia is associated with increased risk of mortality (1.95-fold) and morbidity, primarily due to ischaemic stroke (5-fold) and heart failure (4.62-fold) as well as thromboembolic damage to other organs.[8-11] AF also poses a substantial economic burden, estimated to cost the National Health Service (NHS) between £1.4-2.5 billion per year, accounting for ~1% of the service's total expenditure.[12]

Diagnosis relies on single- or twelve-lead electrocardiogram (ECG)-confirmed episodes, which reveal chaotic atrial electrical activity that manifests as absent P waves and the presence of fibrillatory (f) waves. When this aberrant atrial activity propagates to the ventricles, variable ventricular rates (inconsistent RR interval) and narrow QRS complexes (<120ms) can be observed. Symptoms of AF are variable and can include palpitations, shortness of breath, fatigue, chest pain, dizziness, reduced exercise capacity, syncope, and sleep disturbance.[11] Notably, up to one-third of patients are asymptomatic, and symptoms do not reliably predict incident stroke, systemic embolism, nor mortality.[13] AF exhibits important sex-specific differences: women tend to develop AF later in life, experience a greater symptom burden, and poorer quality of life due to higher comorbidity prevalence, yet remain underrepresented in clinical trials, highlighting the importance of inclusive studies.[11,14]

AF is clinically classified by episode duration and persistence.[11]

- Paroxysmal: self-terminating episodes lasting ≤7 days.
- Persistent (persAF): non-self-terminating episodes lasting >7 days, with ≥12 months duration typically defining long-standing persistent AF.
- Permanent: persAF when sinus rhythm restoration is no longer pursued.

- Post-operative: newly occurring AF episodes immediately after surgery, particularly cardiac surgery.

Largely disfavoured in modern parlance, lone AF was used to describe idiopathic AF in younger individuals without underlying risk factors (e.g. structural heart disease, hypertension).[15] Due to improvements in diagnostic techniques, it is increasingly recognised that probable causes can be identified in virtually all patients leading to the term being largely abandoned in contemporary guidelines.[11] Furthermore, alternative classification schemes, based on aetiology or underlying pathophysiology, also exist; however, a consensus driver-based framework has yet to be incorporated into clinical guidelines.[11]

1.1.2 Aetiology of atrial fibrillation (AF)

AF represents a final common phenotype of atrial cardiomyopathy, arising from progressive, electrical and structural atrial myocardial remodelling (**Fig 1.1**).[16] In some cases, AF presents with a clear precipitant (termed primary or trigger-induced AF) that acts on a vulnerable heart to instigate the arrhythmia. Common AF triggers include valvular and structural heart disease, sepsis, cardiac surgery, excessive alcohol consumption, drug use and endocrine disorders (primarily thyroid, adrenal and pituitary).[11] Exposures also interact with a complex genetic architecture with additive genetic variation estimated to be 22% (UK Biobank), driven largely by common polymorphisms.[17] Family-based studies, which may overestimate genetic risk due to the confounding effect of shared environmental exposures, have estimated heritability to be 2-3-times higher.[18] Genetic variants increasing AF risk cluster near, or within, genes encoding ion channels (e.g. *HCN4*, *KCNH2*, *KCNN2, KCNN3*, *KCNQ1*, *SCN5A*, *SCN10A*), transcription factors (e.g. *GATA4*, *GATA6*, *PITX2*, *PRRX1*, *SHOX2*, *TBX3*, *TBX5, ZFHX3*) and structural or contractile proteins (e.g. *MYBPC3*, *MYH6*, *MYH7, MYL4, TTN*).[18] The heterogenous genetic landscape associated with AF reflects the

complexity of its aetiology, whereby the manifest electrical phenotype commonly co-occurs with developmental and structural perturbations of the atrial myocardium.

Pathophysiologically, AF ensues when electrical triggers, mostly originating from the pulmonary veins, spontaneously depolarise faster than sinus rhythm (**Fig 1.1**).[19] This initiates an electrical wavefront that interacts with a permissive, vulnerable atrial substrate capable of sustaining fibrillatory conduction.[20] The substrate is rooted in heterogenous electrical, structural, and autonomic changes to the heart that vary between individuals and disease states. As set forth by Wijffels and colleagues, once established, AF promotes progressive atrial remodelling such that "*AF begets AF*" which further shortens atrial refractoriness and promotes ion mishandling and myocardial fibrosis.[21] This provides a mechanistic explanation as to why many interventions become less effective with disease progression.[21]

Electrical remodelling of cardiac ion channels and Ca^{2+} handling contribute to the proarrhythmic substrate.[22] Electrical triggers may emerge following early and after delayed depolarisations (EADs, DADs) in cardiomyocytes, typically in the pulmonary veins.[19] Aberrant depolarisations are driven by enhanced diastolic Ca^{2+} leak from the sarcoplasmic reticulum (SR) through 'leaky' ryanodine receptors (RyR), and spontaneous Ca^{2+} release events, which trigger Ca^{2+} outflux on the electrogenic Na^{+}-Ca^{2+} exchanger (NCX).[22-24] Moreover, shortening of the atrial cardiomyocyte (ACM) action potential duration and the atrial effective refractory period is a consistent observation in long-standing AF which, alongside membrane potential hyperpolarisation, promotes the formation of re-entry circuits that maintain the arrhythmia.[20] Concurrently, conduction abnormalities are promoted by the altered expression and lateralisation of connexins 40 and 43.[25] Therefore, a picture evolves whereby rapidly firing foci (triggers), interact with an electrically and structurally remodelled atrium – perhaps promoted by upstream pathology (e.g. hypertension, ischaemia, autonomic dysfunction) and genetic predisposition – to provoke wavefront fragmentation and, ultimately, fibrillation (**Fig 1.1**).

1.1.3 Principles of AF management

Current European Society of Cardiology (ESC) guidelines advocate a patient-centred, multidisciplinary framework for AF management (**AF-CARE**) which emphasises four pillars: **C**omorbidity and risk factor optimisation, **A**voidance of stroke and thromboembolism, **R**eduction of symptoms by rate and rhythm control and, **E**valuation and dynamic reassessment as the clinical picture develops. Optimising concomitant conditions enhances the effectiveness of other aspects of AF care. Robust evidence demonstrates the benefits of managing hypertension, heart failure, diabetes mellitus, obesity, and sleep apnoea alongside promoting physical activity and reducing alcohol consumption.[11]

Prevention of stroke and thromboembolic complications remains a cornerstone of therapy. In most patients, that is achieved with direct oral anticoagulants (DOACs), guided by thromboembolic risk (e.g. CHA_2DS_2-VA ≥2)[a] balanced against bleeding risk factors (e.g. hypertension, alcohol intake, antiplatelet drug use).

Interventions directly targeting the arrhythmia are broadly classified as rate control – aimed at limiting tachycardia – and rhythm control – aimed at restoring and maintaining sinus rhythm. These approaches primarily aim to manage symptoms, but do have prognostic benefit in specific cohorts.[11,26] The relative emphasis on rate versus rhythm control depends on AF duration, symptom burden, comorbidity profile, and overall cardiac function. Rate control can be achieved pharmacologically (e.g. with β-blockers or non-dihydropyridine Ca^{2+} channel blockers such as diltiazem or verapamil, or digoxin) or, when necessary, by atrioventricular node ablation and pacemaker implantation.

[a]CHA_2DS_2-VA is a clinical prediction score used to estimate the risk of stroke in patients with non-valvular AF. It assigns [C]ongestive heart failure 1 point, [H]ypertension 1 point, [A]ge 2 points (≥75 years) or 1 point (65-74), [D]iabetes 1 point, prior [S]troke/transient ischaemic attack or thromboembolism 2 points and [V]ascuar disease 1 point. A score ≥2 is usually considered to represent a high stroke risk.

Rhythm control strategies primarily target the electrical substrate. Antiarrhythmic drugs (AADs) – e.g. amiodarone, dronedarone, flecainide, propafenone, and sotalol – chiefly target ion channels.[27] However, their non-selective actions on ventricular electrophysiology confer risks such as life-threatening ventricular arrhythmias and negative inotropy.[16,28,29] Additionally, pharmacological cardioversion is reserved predominantly for acute-onset or paroxysmal AF. In chronic use, a meta-analysis revealed that many AADs are associated with high recurrence rates and have neutral effects on all-cause mortality, with some drugs possibly even increasing mortality.[11,30] Moreover, clinical trials that have compared rate- and rhythm-control strategies (e.g. RACE, PIAF, AFFIRM, STAF, AF-CHF, J-RHYTHM)[2] have mostly reported no significant differences in major composite cardiovascular endpoints nor on all-cause mortality, despite the higher rates of SR maintenance in patients randomised to rhythm-control.[26] It is important to note that these trials were mostly relatively small and conducted in an era with access to less atrial-specific AADs and the more recent EAST-AFNET 4 trial found evidence in favour of early rhythm control.[26,31]

Interventional approaches, such as catheter ablation, may be used as first-line rhythm control strategies or following AAD failure or intolerance.[11] Ablation aims to electrically isolate ectopic triggers (e.g. pulmonary veins) using radiofrequency, cryoablation, or pulsed-field electroporation.[19] Clinical trials and meta-analyses suggest ablation is more effective than AADs and may reduce mortality risk.[32,33] However, recurrence rates remain high (up to 50%), particularly in the presence of structural atrial remodelling, often necessitating repeat interventions and hospitalisations.[34,35] Electrical cardioversion is

[2] RACE = Rate Control versus Electrical Cardioversion for Persistent Atrial Fibrillation Group Study (2002); PIAF = Pharmacological Intervention in Atrial Fibrillation (2000); AFFIRM = Atrial Fibrillation Follow-Up Investigation of Rhythm Management (2002); STAF = Strategies of Treatment of Atrial Fibrillation (2003); AF-CHF = Atrial Fibrillation and Congestive Heart Failure (2008); J-Rhythm = Japanese Rhythm Management Trial for Atrial Fibrillation (2009).

recommended in acute-onset AF patients, particularly in haemodynamically unstable patients.[11]

Importantly, AF induction and progression are tightly linked with structural atrial remodelling, hallmarked by atrial dilatation and myocardial fibrosis, which hampers AF treatment.[36] Although electrical remodelling is relatively well defined, the key molecular, cellular and endocrine determinants of structural remodelling are less clearly delineated, motivating investigations into novel antifibrotic pathways. Amidst warnings of a global AF pandemic, the demand for pioneering rhythm-restoring therapies is urgent, yet unmet.

1.2 Fibrosis

1.2.1 Introduction to fibrosis

Fibrosis is the excessive accumulation of extracellular matrix (ECM) components, particularly fibrillar collagens and fibronectin, within tissues. It has been estimated fibrotic organ damage could account for up to 45% of all deaths in the industrialised world.[37] Although fibrosis is an important, physiological response to local insult, when it becomes chronically disproportionate to the initiating stimulus, it disrupts organ architecture and function.

Fibroblasts (Fbs), first described by Virchow (1858) and subsequently named by Ziegler (1895), are the foremost cellular instigators of organ fibrosis.[38,39] They are functionally defined as cells that secrete structural and signalling macromolecules, provide signalling niches for tissue-resident stem cells, and serve as progenitors for specialised mesenchymal cells.[39,40] Advances in *in vitro* practices in the early 20th century enabled the isolation and culture of primary Fbs and, subsequently, the generation of immortalised Fbs lines.[41] These foundational innovations permitted the extensive characterisation of Fb function, including their lineage potential and key synthetic outputs, establishing their role as key nexus cells that define tissue architecture and function.[40] Contemporary technologies, such as single-cell RNA sequencing, have exposed the extent of inter- and intra-organ Fb heterogeneity. Current theories of Fb origin propose a model whereby universal Fbs give rise to distinct, specialised phenotypes that subserve the specific homeostatic and repair requirements of their resident organs.[42,43]

Fbs, in most healthy, adult organs, are quiescent, but can be rapidly activated to generate ECM-producing Fbs, termed myofibroblasts, which are characterised by their expression of the contractile protein alpha smooth muscle actin (αSMA) and upregulated matrisome output. This differentiation is promoted by canonical signalling pathways (e.g.

transforming growth factor-beta [TGF-β], platelet derived growth factors [PDGF], Wnt, galectin-3, and fibroblast growth factors [FGF]), inflammatory cues (e.g. interleukin-1 [IL-1], interleukin-6 [IL-6]) and damage-associated molecular patterns (DAMPs e.g. heat shock proteins, histones, ribonucleic acid [RNA]).[40,44] Despite myofibroblasts serving an important and necessary role in the response to tissue injury, their aberrant and chronic activation promotes pathological organ fibrosis.

1.2.2 Atrial fibrosis as a hallmark of the AF substrate

Atrial fibrosis is defined as the endpoint of excessive extracellular matrix (particularly collagen fibres) accumulation within the myocardial interstitium by activated cardiac Fbs, which constitute approximately 20-30% of the atrial cell population.[45] Cardiac Fbs are a heterogenous population with multiple, context-dependent origins which include direct endothelial-to-mesenchymal transition from the epicardium and endocardium, as well as a small contribution from migrating neural crest cells.[46] Fibrosis, alongside other pathological changes including increased intercellular space, reduced nuclear density and myofibrillar loss, contributes to structural remodelling.[47-49] There are currently no approved therapies that primarily assuage cardiac fibrosis. Although there are CVD therapies that may retard progression of cardiac fibrosis as a secondary benefit to the treatment of the primary condition (e.g. inhibitors of the renin angiotensin-aldosterone system [RAAS] for the management of hypertension or heart failure), no current therapy primarily targets cardiac fibrosis to retard its progression or reverse it.[50] Pathophysiologically, interstitial fibrosis predisposes the atria to slow, non-uniform, anisotropic conduction which encourages formation of re-entry circuits (**Fig 1.1**).[20] Indeed, histopathological findings in atrial biopsies correspond with less invasive electroanatomic surrogates of structural remodelling, such as decreased global left atrial voltage (V_{GLA}) and fractionated electrograms.[47,51] Decreased V_{GLA} predisposes the atria to macro-re-entrant tachycardias which can degenerate into AF. Importantly, atrial fibrosis also influences treatment response in AF. For example, the DECAAF study found

fibrosis, determined by late gadolinium enhanced magnetic resonance imaging (LGE-MRI), independently correlated with recurrence of arrhythmia following catheter ablation.[52] However, the subsequent DECAAF II trial revealed adding MRI-guided fibrosis-targeting during catheter ablation did not affect atrial arrhythmia recurrence after a 90-day blanking period.[53] These disappointing results perhaps demonstrate that current imaging modalities cannot identify the most proarrhythmic regions or that modern ablation technologies have not been suitably optimised for fibrotic tissue. In sum, converging preclinical and clinical data establish a mechanistic coupling between cardiac fibrosis and AF. However, the precise timing, targets, and patient populations in which antifibrotic interventions may be most effective remain to be defined.

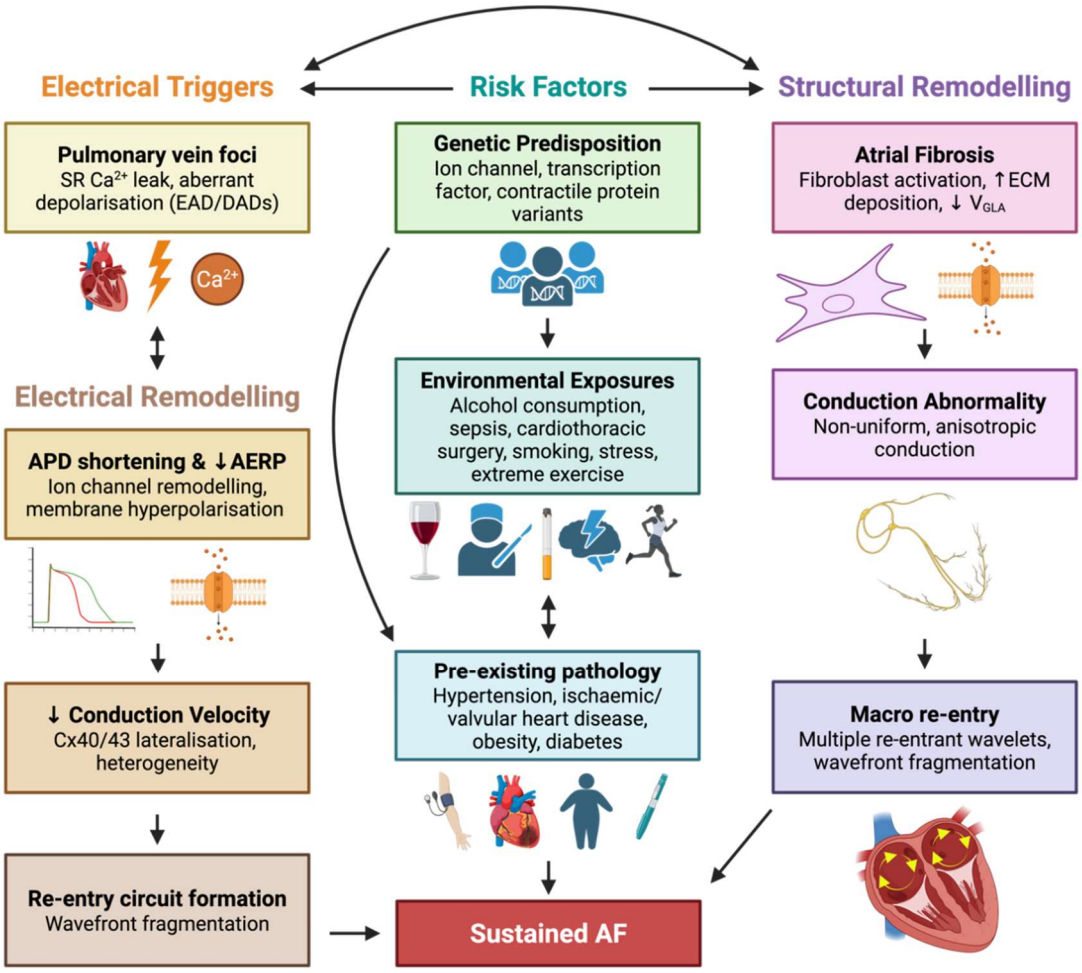


Figure 1.1 Mechanisms of atrial fibrillation pathogenesis. AF, atrial fibrillation; APD, action potential duration; AERP, atrial effective refractory period; Cx, connexin; DAD, delayed after depolarisation; EAD, early after depolarisation; ECM, extracellular matrix; V_{GLA}, global left atrial voltage.

1.3 Calcitonin and Atrial Fibrillation

1.3.1 Calcitonin (CT)

Fb biology, and hence fibrogenesis, is dynamically tuned by a complex array of autocrine, paracrine, and endocrine cues. Among the many regulators of ACF fibrotic activity is calcitonin (CT). Our group previously demonstrated that CT, acting via its receptor (CALCR) suppresses profibrotic ACF activity and its production by cardiomyocytes is reduced in AF.[1] *In vitro*, CT signalling suppressed ACF collagen production, proliferation, and migration.[1] Furthermore, *in vivo*, global CALCR knockout or atrial-specific CT knockdown promoted structural remodelling and rendered mice vulnerable to spontaneous and induced AF.[1] Therefore, disrupted CT-CALCR signalling can promote AF arrhythmogenesis.

CT is a 32 amino acid peptide hormone produced by the thyroid's parafollicular (or C) cells to defend serum Ca^{2+} homeostasis against hypercalcaemia.[54] Structurally, CT is synthesised as a prepropeptide following tissue-specific splicing of the *CALCA* gene from which the calcitonin gene-related peptide (CGRP) is also generated.[55] The mature hormone is produced by N-terminal cleavage, to yield proCT, and C-terminal amination by peptidyl-glycine N-amidating monooxygenase.[55]

Canonically, CT lowers circulating Ca^{2+} by its actions on osteoclasts, where it suppresses bone resorption, and the renal proximal tubule, where it promotes diuresis and Ca^{2+} excretion. However, the homeostatic significance of CT is controversial. Following thyroidectomy, hypercalcaemia is unusual, despite reduced CT levels.[56,57] Yet, a retrospective study associated thyroidectomy with osteoporosis indicating that CT may not be vestigial.[58] In lower vertebrates, such as fish, living in high Ca^{2+} environments, CT is produced by the ultimobranchial glands and serves a more significant role. The CT produced by salmon (sCT) is significantly more potent than human CT (hCT) and its intranasal formulation was approved by the Food and Drug Administration (FDA) for

postmenopausal osteoporosis, Paget's disease, and hypercalcaemia. However, sCT's clinical use has declined and its authorisation by the European Medicines Agency for use in osteoporosis was withdrawn in 2014 due to more effective alternatives with fewer side effects (bisphosphonates and RANKL inhibitors).[55,59] Despite its unclear physiological role, research into the therapeutic potential of CT for old indications and new (e.g. neuropathic pain, obesity) remains active (**Table 1.1**). A more complete elucidation of its unique physiological and therapeutic profile may reveal new indications for this hormone.

1.3.2 Calcitonin receptor (CALCR)

CT signals via its receptor, CALCR, which was identified molecularly by Lin *et al* (1991) and established as a G-protein coupled receptor (GPCR).[60] The GPCR family encompasses ~800 members in humans and regulates diverse cellular functions by transducing a variety of signals via their engagement of heterotrimeric G-proteins and myriad effector proteins.[61] CALCR belongs to the class B family of GPCRs which are subdivided into two subfamilies: the secretin (B1, 15 members) and adhesion (B2, 33 members). This B1 family is structurally identifiable by their large N-terminal extracellular domains (ECDs) - which serve an important role in ligand capture and selectivity - and have been resolved at near-atomic resolution by cryo-electron microscopy (cryoEM).[62,63] This family also includes the receptors for glucagon, glucagon-like peptide 1 & 2, gastric inhibitory polypeptide receptor, secretin, growth hormone-releasing hormone, vasoactive intestinal polypeptide 1 & 2, pituitary adenylate cyclase-activating polypeptide type 1, parathyroid hormone type 1 & 2, amylin 1-3, calcitonin gene-related peptide, adrenomedullin 1 & 2, and corticotropin-releasing factor 1 & 2.[64] Thus, the B1 family serves important functions in the regulation of metabolism, immunity and neuroendocrine activity.[64] CALCR is broadly expressed – including in the brain, bones, kidney, gastrointestinal tract, reproductive system, and lungs – and predominantly couples to $G_{\alpha s}$ to stimulate cyclic adenosine monophosphate (cAMP) production.[63,65] However,

subsequent work has also shown CALCR may engage other G proteins to activate $G_{\alpha i}$- and $G_{\alpha q}$-dependent pathways and this may depend on cell cycle stage.[62,66,67]

Table 1.1 Summary of active clinical trials with calcitonin as an intervention. Summary of active trials registered on ClinicalTrials.gov with "calcitonin" featured in their intervention/treatment description, accurate as of 11th January 2026. IU, international units; SPECT-CT, single-photon emission computed tomography.

Trial ID:	Indication:	Intervention:	Primary Outcome:
NCT03935984	Primary hyperthyroidism	200 IU CT b.d. for 2 days, then once on the day of SPECT-CT imaging.	Sensitivity of SPECT-CT to localise parathyroid adenoma.
NCT05805683	Spinal cord injury	100 IU of CT daily for 2 weeks, starting within 48h of injury.	Intensity of neuropathic pain and incidence of chronic pain
NCT06330168	Elective thoracotomy	Bupivacaine-calcitonin (100 IU)-fentanyl versus bupivacaine-fentanyl as a thoracic paravertebral block	Morphine consumption within 24h post-surgery and incidence of chronic pain at 3 months post-surgery
NCT07033104	Caesarean section with spinal anaesthesia	Addition of calcitonin to bupivacaine in transversalis fascia plane block	Time to first rescue analgesia
NCT03401619	Osteoporosis; cognitive impairment; arterial stiffness or healthy controls undergoing a DEXA examination.	Combination of exercise, nutrition, bisphosphonates, statins, calcitonin and vitamin D in patients with osteoporosis with cognitive impairment, osteoporosis with arterial stiffness, osteoporosis alone or healthy controls.	Cognitive impairment improvement
NCT06833749	Osteoarthritis and BMI ≥ 30	Weekly injection of KBP-336 (a long-acting dual amylin and calcitonin receptor agonist)	Proportional change in bodyweight and the change in Western Ontario and McMaster Universities Osteoarthritis Index (WOMAC) pain scale from baseline

1.4 Regulation of CALCR Localisation and Activity

Alongside reductions in atrial CT production, ACFs from donors with persistent AF (AF-ACFs) are refractory to exogenous CT administration, despite only a modest reduction in CALCR protein levels.[1] Compared to ACFs derived from donors in sinus rhythm (SR-ACFs), CALCR in AF-ACFs exhibited a striking internalisation (presented in **Fig 3.3.1**). Therefore, the success of any substrate-modifying CT-centred therapy is contingent upon the restoration of surface CALCR in AF-ACFs.

1.4.1 Genetic polymorphisms and alternative splicing

A priori, one may consider CALCR's surface expression to represent the balance between opposing fluxes: (i) biosynthetic delivery and membrane recycling versus (ii) endocytosis and degradation. The regulation of GPCR surface trafficking, endocytosis, and membrane compartmentalisation is conferred by numerous protein interactors and variations in the receptor's structure (**Fig 1.3**).[68] Alternative splicing and polymorphic variation in *CALCR* has been reported to affect its localisation and downstream coupling.[69] First cloned by Gorn and colleagues in 1992, the most common alternative splice variant, $CALCR_b$, includes an additional 16 amino acids in intracellular loop 1.[70] Compared with the insert-negative variant ($CALCR_a$), $CALCR_b$ is more restricted in its expression.[70,71] Moreover, a polymorphism at base position 1340 in $CALCR_a$ has been reported which codes either a proline or leucine.[72] In stably transfected COS7 cells (but not HEK293), flow cytometric analysis revealed $CALCR_b$ was expressed at a lower level at the cell surface and that proline variants of $CALCR_b$ had lower expression than their leucine equivalents. Similarly, these variations alter sCT ligand affinity, cAMP responses (10-100-fold reduced in $CALCR_b$ variant), and G-protein coupling (i.e. absent $G_{\alpha q}$ coupling with the $CALCR_b$ variant).[69] The isoform-specific expression of *CALCR* has not been assessed in human ACFs.

1.4.2 β-arrestin recruitment

An important facet of physiological GPCR regulation is ligand-induced receptor internalisation. The best studied mechanism of GPCR internalisation is the phosphorylation of C-terminal residues by GPCR kinases (GRKs) which recruits arrestin proteins to block further G-protein engagement. Arrestins interact with clathrin and adaptor protein-2 (AP-2) to drive clathrin-mediated endocytosis (CME).[73] The arrestin family comprises 4 members: arrestin-1 and arrestin-4, which are expressed in the eye, and β-arrestin-1 (arrestin-2) and β-arrestin-2 (arrestin-3) which are ubiquitously expressed.

However, the evidence for the role of β-arrestin-mediated internalisation of CALCR is conflicting. In a tour-de-force study, Dal Maso and colleagues generated CALCR and β-arrestin-1/2 fusion proteins to monitor possible ligand-induced β-arrestin recruitment by bioluminescence resonance energy transfer (BRET).[69] Despite overexpression of GRKs, the use of both CALCR splice variants and polymorphisms, two agonists (hCT and sCT), and two different cell backgrounds, there was no evidence of ligand promoted β-arrestin recruitment.[69] Similar results were observed with native CALCR, ruling out the possibility that the C-terminal reporter interfered with β-arrestin recruitment.[69] However, both ligand-dependent and -independent (constitutive) receptor internalisation was observed indicating that these cell lines were competent to sponsor CALCR internalisation. An earlier study, however, demonstrated β-arrestin recruitment at $CALCR_a$ which was sustained for longer with sCT when compared to hCT.[74] Yet, the EC_{50} for CT-mediated β-arrestin recruitment was ~3-4 orders of magnitude larger than that for the cAMP response which raises doubts about the physiological relevance of this internalisation mechanism. Notably, the β-arrestin-recruitment studies were conducted in the U2OS CALCR engineered cell line and thus the relevance of these results to native, primary cell systems is unclear.

These results were consistent with a recent study by Liu *et al* (2025) which systematically assessed the importance of β-arrestins to the ligand-induced internalisation of 60 GPCRs.[75] They uncovered cell background-specific patterns in the requirement of β-arrestin-1/2 for ligand-induced internalisation and, strikingly, discovered that the majority of GPCRs tested underwent agonist-induced internalisation in the absence of β-arrestins. Indeed, for the Class B1 receptors tested, β-arrestin overexpression had no effect on their internalisation. Although this study did not include CALCR, their results indicate that β-arrestins are not essential for the constitutive or ligand-induced internalisation of Class B1 GPCRs and that these receptors (as demonstrated for the glucagon-like peptide 1 receptor [GLP-1R]) may directly engage AP-2 to trigger CME.[75] However, the proposed binding motif (TSSLSS) is not present in CALCR. The study also found evidence of GRK-independent endocytosis which suggests GLP-1 may also be internalised by a non-CME pathway (e.g. caveolae-mediated or fast endophilin-mediated endocytosis). Whether the results derived for different Class B1 GPCRs, in an immortalised cell line background, are transferable to CALCR in primary cells with native levels of β-arrestin expression has not been explored.

1.4.3 Receptor-activity modifying proteins

The membrane trafficking, ligand specificity and G-protein coupling of several class B GPCRs, including CALCR and the calcitonin receptor-like receptor (CALCRL), is modified by their association with the single-span transmembrane family of receptor-activity modifying proteins (RAMPs).[76-79] The three RAMPs can allosterically modulate CALCR to bias ligand specificity to create amylin receptors (**Fig 1.2***, AMY*$_1$, AMY$_2$, and AMY$_3$).[80,81] Amylin is a glucoregulatory hormone; its physiological actions include the suppression of food intake, gastric emptying and glucagon secretion.[82] The RAMP-mediated diversification of receptor-ligand binding preference enriches CALCR pharmacology and provides a potentially targetable interaction for small molecules or peptides to prejudice ligand-GPCR signalling.[77]

In addition to modifying ligand preference, RAMPs have been shown to be required for the surface expression of CALCRL.[79] However, this has not been found to be the case for CALCR in immortalised cell lines.[83,84] Moreover, structural insight from cryo-EM studies has indicated distinct conformations of RAMP1-CALCR-CGRP complexes compared to RAMP1-CALCRL-CGRP, indicating a differential structural mechanism of RAMP regulation of CALCR function.[79,85] The cell-type specific expression of members of the RAMP family means their contribution to receptor surface expression and function is dependent on cell background. RAMP activity in ACFs has never been assessed.

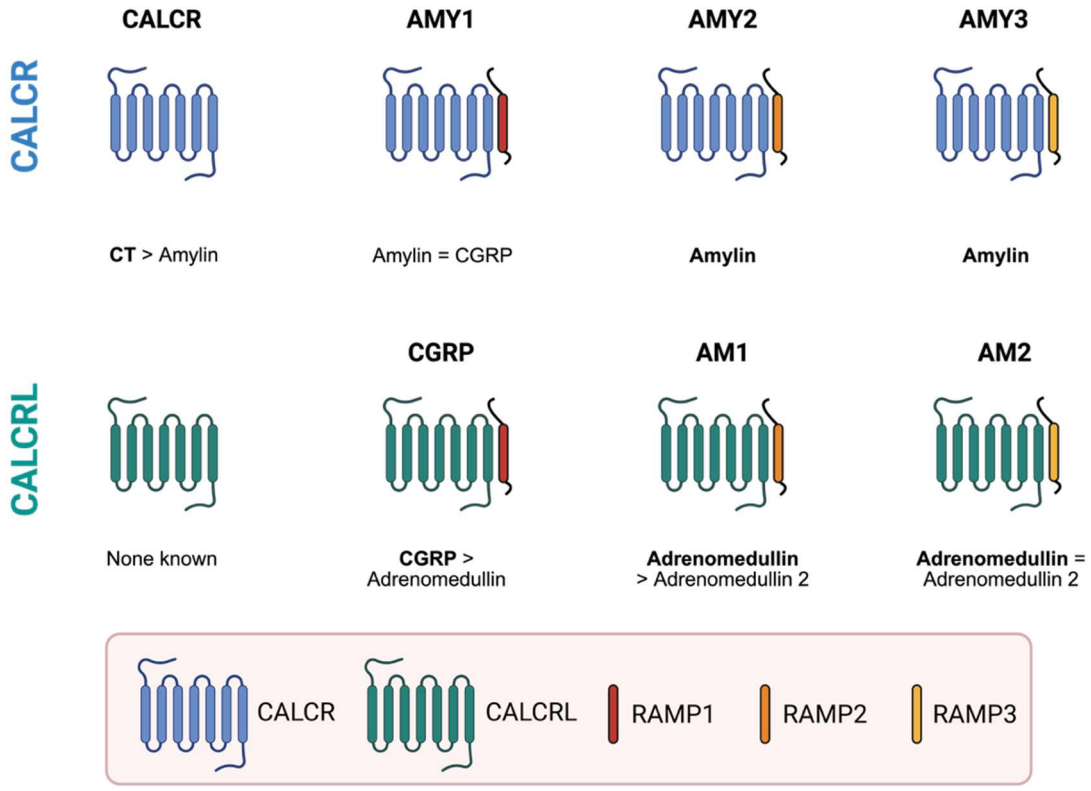


Figure 1.2 Diversification of CALCR and CRLR ligand specificity by RAMPs. Schematic illustration of the seven distinct receptors formed by association of the calcitonin receptor (CALCR) or calcitonin receptor-like receptor (CALCRL) with a receptor activity-modifying protein (RAMP). The most potent ligands, based on cAMP production, are shown beneath each quaternary receptor complex, adapted from Hay *et al* (2017) and the IUPHAR/BPS database.

1.4.4 Filamin A (FLNa) regulates CALCR membrane recycling

The literature also describes other protein regulators of CALCR trafficking (**Fig 1.3**). Among them is filamin A (FLNa), an actin-crosslinking and biomechanical signal-transducing protein that, via its known interactions with ~90 proteins, assembles scaffolding and signalling networks which regulate cell motility/adhesion, migration, proliferation, transcription, and signal transduction.[86-88] The phenotypic consequences of FLNa mutations reflect its multifaceted functions, and span nervous, cardiovascular, urological, skeletal, and respiratory system disorders.[89] FLNa comprises 24 Ig-like repeats which are interrupted by hinge regions at which FLNa is cleaved by proteases to generate N-terminal ($FLNa^{NT}$, ~170 kDa) and C-terminal fragments ($FLNa^{CT}$, ~100 kDa). FLNa's N-terminus contains the actin-binding domain, and the C-terminus contains the dimerization domain alongside binding motifs for other protein interactors, including CALCR.[90,91]

An important study by Seck *et al* (2003) demonstrated a physical interaction between CALCR's intracellular C-terminal (amino acids 397-474) and FLNa's C-terminal fragment ($FLNa^{CT}$, amino acids 2129-2647), as shown in **Fig 3.1.1**.[91] Compared to FLNa-deficient lines, FLNa expression reduces CALCR degradation and enhances its surface recycling following constitutive, ligand-independent internalisation.[91] Cleavage of FLNa would uncouple the CALCR-$FLNa^{CT}$ complex from the actin cytoskeleton. Indeed, inhibition of calpains, key mediators of FLNa cleavage, also reduced CALCR degradation in FLNa-expressing cells.[91] Taken together, this study built a model whereby CALCR is rescued from degradative pathways following constitutive internalisation by an interaction with FLNa. However, the use of heterologous overexpression systems with potentially artificial interaction stoichiometry and dynamics raises questions about the physiological relevance of this interaction, including in ACFs.

Building on this foundation, other studies have exposed functions for FLNa in GPCR and ion channel expression and trafficking. It is predicted more than 20% of GPCRs contain a FLNa-binding motif in their cytoplasmic regions. For the angiotensin II type 1 receptor (AT1R) and MAS receptor, agonist stimulation promotes FLNa recruitment and phosphorylation, mediated by protein kinase A (PKA) and serine/threonine kinases.[90] Additionally, $FLNa^{CT}$ has been reported to bind the N-terminus of the small-conductance Ca^{2+}-activated K^+ channels (SK2) and augment surface expression and function in neonatal rat cardiomyocytes, but not to confer the $[Ca^{2+}]_i$-dependence on its surface expression.[92] Intriguingly, SK2 channels exhibit a predominantly atrial expression in the human heart and I_{SK2} is enhanced in human AF due to altered channel gating and membrane trafficking.[93] These studies highlight the complex and varied functions of FLNa as a membrane protein organiser with the potential to impinge on both AF's electrical and structural substrate. These findings prompt FLNa's further exploration in the context of AF-associated structural remodelling in ACFs.

1.4.5 Post-translational modifications of CALCR

Phosphorylation: Post-translational modification of GPCRs has been reported to regulate their proper folding, surface expression and internalisation. As previously discussed, GPCR phosphorylation, the covalent addition of a phosphate moiety, by GRKs promotes the recruitment of β-arrestin proteins to curtail sustained, ligand-induced signalling. Phosphorylation of CALCR's C-terminal domain following sCT-stimulation has been described in baby hamster kidney fibroblasts; an effect preserved in the presence of protein kinase A (PKA) and protein kinase C (PKC) inhibition, suggesting a role for GRKs.[94]

N-glycosylation: describes the post-translational, enzymatic addition of glycans to asparagine (N) residues by glycosyltransferases.[95] Work from the laboratory of Augen Pioszak has demonstrated that N-glycosylation of asparagine 130 in CALCR's

extracellular domain (ECD) enhances ligand affinity likely by affecting ECD dynamics as the modification does not induce major conformational change nor make direct contact with the agonist.[96,97] N-glycosylation, typically occurring in the endoplasmic reticulum or Golgi apparatus, assists in protein folding and has been reported to enhance the surface delivery and half-life of other class B GPCRs.[98]

Palmitoylation: describes an evolutionarily conserved, reversible lipid modification. Most commonly, this involves the enzymatic addition of a 16-carbon fatty acid to a cysteine residue via the thiol functional group by palmitoyltransferases.[99] This modification enhances the hydrophobicity of proteins and therefore increases the propensity for membrane localisation by enhancing the thermodynamic stability in the lipid membrane.[99] The functional consequence of palmitoylation has been reported for several GPCRs. For example, in the case of serotonin (5-HT) receptor 1A (5-HT1AR) C-terminal palmitoylation promotes $G_{\alpha i}$-subunit interaction and serves as a targeting signal for lipid raft retention.[100] A limited number of studies have studied the effect of palmitoylation for Class B GPCRs. Yet, there has been a report that palmitoylation of GLP-1R does not affect surface receptor levels but does alter internalisation, membrane nanodomain localisation, and cAMP response following ligand stimulation.[101]

1.4.6 The '*Escape Phenomenon*'

Ligand-induced receptor desensitisation is considered to be an important phenomenon clinically.[54] Termed the '*escape phenomenon*', this manifests as reduced CT potency for calcium-lowering after a few days of treatment, as first described in hypercalcaemic oncology patients.[102] Subsequently, *in vitro* studies described CT-induced rapid and sustained downregulation of *CALCR* mRNA expression, even after a 1 hour treatment, as well as receptor internalisation.[103,104] However, as ACM CT production is markedly reduced in AF, and CALCR protein expression is not significantly altered, a ligand-induced *escape* as the underlying mechanism of reduced surface CALCR in AF-ACFs is

unlikely. However, the identification of an intervention which restores surface CALCR expression may help circumvent the *escape phenomenon*.

In summary, much remains unknown about the mechanisms of CALCR surface trafficking, internalisation (both ligand-induced and constitutive) and subsequent fate (recycling versus degradation). Significant conflict in the literature has emerged due to the differing use of internalisation protocols, cell lines, protein constructs, and CALCR variants. This work will aim to systematically explore which, if any, of the previously reported regulators (**Fig 1.3**) of the surface CALCR pool may contribute to the loss of surface localisation in the native AF-ACF context.

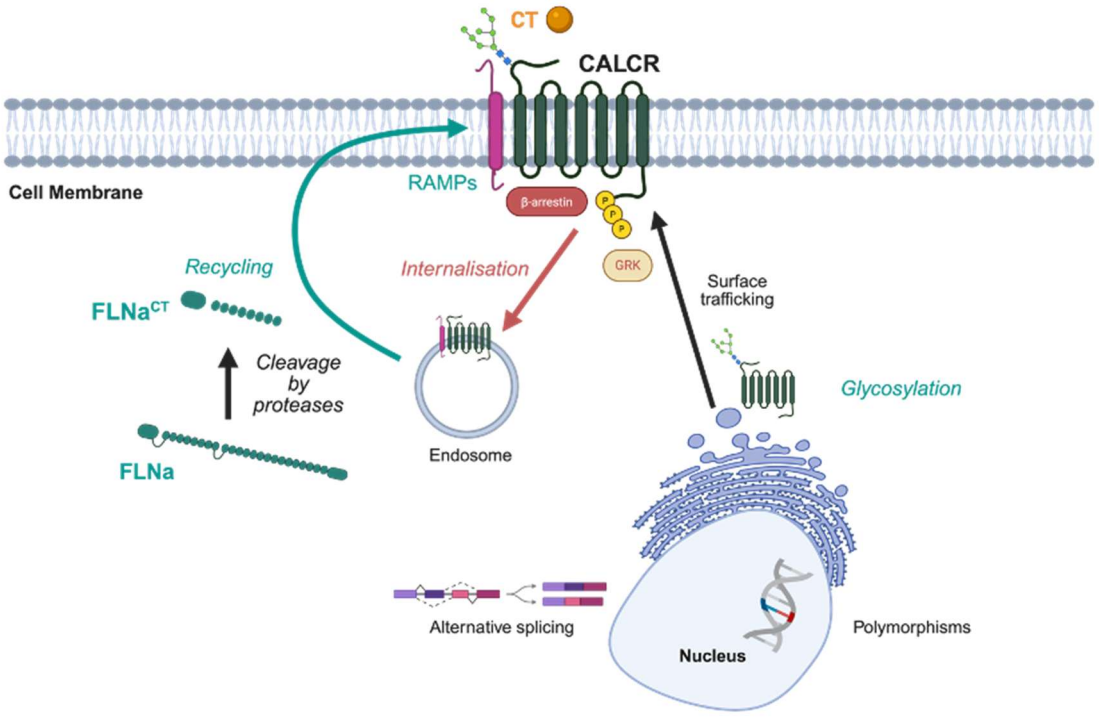


Figure 1.3 Proposed regulators of CALCR surface expression. Surface localisation of CALCR may be promoted by N-linked glycosylation in the endoplasmic reticulum or Golgi apparatus, receptor recycling after constitutive internalisation by FLNa, and association with receptor-activity modifying proteins (RAMPs). In contrast, C-terminal phosphorylation by G-protein receptor kinases (GRKs) and β-arrestin binding may favour loss from the cell surface. Genetic polymorphisms and alternative splicing are also reported to influence CALCR surface expression and function. CT, calcitonin.

1.5 High-throughput drug repurposing screens

1.5.1 Drug repurposing

To identify novel therapeutic candidates, this thesis also aims to unbiasedly screen well-characterised small molecules to identify those that may rescue surface CALCR expression to restore antifibrotic signalling in AF-ACFs.

The journey to clinical translation is fraught with pitfalls. Indeed, the progress of ~30% of preclinical candidates is prematurely terminated due to concerns of toxicology and only around 15% of drugs that enter phase I clinical trials receive regulatory approval for any indication.[105,106] Prominently, candidate compounds trialled in CVD have a particularly low success rate.[107] Likewise, even after regulatory approval there remain perils: post-marketing safety concerns led to the market withdrawal of 462 drugs between 1953-2013.[108]

Drug repurposing, or repositioning, describes the identification of new indications for existing drugs, including those compounds that are already approved, in late-stage development, or have well-characterised safety profiles but have been discontinued for non-safety reasons.[109] Historically, repurposing was serendipitous and relied on the opportunistic finding of an off-target effect or a novel on-target effect e.g. sildenafil for erectile dysfunction and pulmonary arterial hypertension or thalidomide for leprosy and multiple myeloma.[109] Subsequently, more systematic identification strategies have evolved based upon shared signature matching (e.g. identifying a drug effect on transcriptomic/proteomic/metabolomic profiles which would oppose a disease-associated profile), molecular docking and binding assays to identify and validate ligands for a specific target, or phenotypic screening with *in vitro* or *in vivo* disease models.[109] The progress of repurposing strategies was catalysed during the COVID-19 pandemic with notable successes e.g. dexamethasone, remdesivir and tocilizumab.[110]

Compared with conventional drug discovery, the principal advantages of a repurposing approach are its reduced developmental risk and accelerated timeline. Repurposing obviates several key drug-discovery constraints - especially those related to inappropriate drug absorption, distribution, metabolism, excretion, and toxicity profiles (ADMET) – thereby leaving efficacy for the repurposed indication as the dominant hurdle.

There are, however, some limitations of drug repurposing approaches. Firstly, intellectual property constraints can limit the commercial incentive for off-patent drugs. This poses challenges for large-scale clinical trial funding. A repurposed medical use can only be protected if it is new and inventive; that is to say, the knowledge underpinning the repurposed use cannot be found in the public domain. Even when a patent is awarded, if the dose and/or formulation is comparable to its previous indication, patent enforceability becomes a major challenge as clinicians can use generic forms off-label. Secondly, if a new indication requires a different dose, route of administration, or treatment duration, unanticipated toxicity may be unmasked. Finally, the data to support the clinical testing of repurposing candidates still relies on preclinical models that may lack human disease relevance in the new indication.

In summary, drug repurposing represents a powerful, and increasingly systematic, approach to therapeutic innovation, offering the prospect of faster, safer, and more cost-effective clinical translation. Consequently, in pursuit of therapies to restore antifibrotic CT-CALCR signalling in AF, the most obvious gains - in terms of logistical, economic, timescale and safety considerations - stand to be made in repurposing previously approved drugs. Therefore, this work will unbiasedly screen previously approved therapies to identify entities which may resensitise primary AF-ACFs to CT.

1.5.2 High throughput screening (HTS)

A successful drug repurposing pipeline requires the identification of a strong candidate. High-throughput screening (HTS) has emerged as a powerful experimental approach for

systematically identifying compounds with repurposing potential across diverse disease contexts. HTS describes the process of automatically monitoring the biological activity of cells following treatments with hundreds (or thousands) of interventions (e.g. small molecules, siRNAs) in a multi-well plate format. This approach enables the rapid, parallelised interrogation of compound activity against a robust, objective, and quantitative phenotype (e.g. CALCR localisation). When applied to drug repurposing, HTS examines libraries enriched for clinically approved drugs, investigational agents, or compounds with well-characterised pharmacological profiles, thereby uniting experimental breadth and translational relevance.

Unlike traditional target-based drug (TBD) discovery, which is predicated on *a priori* selection of a molecular target, HTS pursues drugs based on their ability to modify disease-relevant cellular phenotypes which affords distinct advantages. Firstly, this approach is well suited for complex, multifactorial diseases where there may not be a single molecular entity which drives disease. Secondly, systematic analysis of approved therapies between 1999 and 2008 revealed that phenotypic screening played a major role in the discovery of first-in-class small molecule drugs highlighting its translational efficacy in identifying drugs acting by novel mechanisms.[111] Thirdly, technological advances in high-content imaging and automated image analysis permit the simultaneous readout of several phenotypic parameters e.g. cell number, morphology and a target protein's subcellular localisation. This enhances the biological resolution and means secondary phenotypic outcomes can inform hit selection.

Sharing key similarities with this work, a recent HTS assessed the antifibrotic potential of ~5000 preclinical and clinical compounds across 7 doses (0.312-20 μM) in iPSC-derived cardiac fibroblasts expressing an *ACTA2* fluorescent reporter. Filtering of compounds for acceptable ADMET profiles and without cardiovascular toxicity (assessed in iPSC-ECs and iPSC-CMs counterscreens), identified artesunate as a potentially effective and safe compound. *In vivo* validation in a transverse aortic constriction (TAC)-

induced model of cardiac hypertrophy confirmed that artesunate prevented decline in left ventricular function and prevented fibrosis development even when treatment started 1-month post-surgery. Its antifibrotic effects were also demonstrated in an ischaemia-reperfusion model of myocardial infarction. One challenge facing HTS-derived hits can be mechanistic deconvolution, particularly when the effect of a drug is mediated through its interaction with several proteins. This study deployed single nuclear RNAseq to unveil that artesunate inhibited upregulation of key activated myofibroblast genes (e.g. collagens, periostin) in fibroblasts in the TAC model and inhibited hypertrophy-markers in CM groups. They subsequently identified MD2, the co-receptor for TLR4, as the molecular target of artesunate in cardiac Fbs. Although this study leveraged several models to assess artesunate's therapeutic utility and to derive mechanistic insight, the initial screen was not conducted in primary cells from donors with the relevant disease. As such, the direct translational relevance to human forms of cardiac fibrosis, in the aged and co-morbid heart, is uncertain. Similarly, artesunate, an antimalarial, is typically given acutely and therefore its safety for chronic administration presents a possible barrier to its use.

Indeed, the use of *in vitro* screening models with limited disease relevance is a common pitfall in drug screens. I intend to minimise this with the use of AF patient-derived ACFs to faithfully recapitulate human disease biology.[110] Similarly, non-superiority is a frequently cited reason for the abandonment of drug candidates but, in this instance, there are no approved therapies for the reversal of AF-associated cardiac fibrosis against which a putative therapy could be compared.[112] Conversely, the use of compound libraries and collaborative initiatives were identified as facilitators of successful repurposing.[112] Therefore, I conducted a cell-phenotyping drug screen of >3000 approved drugs, including those acting on GPCRs and structural proteins, in collaboration with A/Professor Daniel Ebner's group at Oxford's Target Discovery

Institute. The most promising hits were validated in orthogonal assays, and their possible mechanisms of action explored.

In conclusion, HTS represents a cornerstone methodology for contemporary drug repurposing efforts, particularly for complex phenotypes, which mitigates many of the risks inherent to *de novo* drug discovery. An unbiased assessment of clinically relevant compounds, with well characterised pharmacological profiles, may provide important insight into the mechanisms of loss of surface CALCR in AF and offer a pragmatic bridge between basic mechanisms and translational application. It is hoped insight into why surface CALCR expression is reduced may be gained by identifying how it can be restored.

1.6 Hypotheses, Aims and Objectives

The principal hypothesis of this thesis is that the loss of surface CALCR in AF-ACFs underlies their insensitivity to CT and the restoration of surface CALCR resensitises them to the antifibrotic effects of CT. Although many regulators of CALCR surface expression have been proposed, conclusions on their relative contributions have been conflicting and have been underexplored in native cell contexts. Given the potential therapeutic benefit of restoring CT-sensitivity to AF-ACFs, this thesis has two overarching Aims:

Aim 1 (mechanistic): Explore the mechanisms of loss of surface CALCR in AF-ACFs.

Aim 2 (therapeutic): Unbiasedly identify molecules which restore cell-surface CALCR and examine whether this resensitises AF-ACFs to the antifibrotic effects of CT.

From these overarching Aims, the specific Objectives of the following chapters evolve:

Chapter 3: Examine whether filamin A contributes to surface CALCR expression in primary human ACFs.

Chapter 4: Assess the effect of non-filamin A regulators of CALCR localisation.

Chapter 5: Optimise and conduct a high-throughput screen to characterise the effects of clinically relevant molecules on CALCR localisation.

Chapter 6: Validate the functional restoration of the CT-CALCR axis by lead hit compounds and explore their possible mechanisms of action.

CHAPTER 2: MATERIALS AND METHODS

Materials and methods relevant to results spanning multiple chapters are described here, while experimental details pertaining to specific datasets are presented at the start of the corresponding results chapters (Chapter 3-6).

2.1 Patient recruitment and cardiac fibroblast isolation

Human research was approved by the local Research Ethics Committee (South Central – Berkshire B Research Ethics Committee). Samples from the left and right atrial appendages were collected from donors undergoing elective cardiac surgery for coronary artery bypass grafting (CABG) and/or valve repair/replacement who had consented to participate in the Cardiac Fibrosis in Heart Disease study (18/SC/0404). A total of 55 donors were recruited for this study; their clinical demographics are summarised in **Table 2.1**. Donors were classified as sinus rhythm controls (SR; without history of AF and who remained in sinus rhythm until hospital discharge) or persistent AF (AF; defined by ECG-evidenced episodes of AF with episodes lasting at least 7 days). Appendage biopsies were collected in ice-cold low Ca^{2+} solution (LCS).

Atrial fibroblasts (ACFs) were isolated as described previously (**Fig 2.1**).[1] Adipose and necrotic tissue was removed from the appendage biopsies and the myocardium was cut into ~2mm^3 pieces, washed with oxygenated LCS and then enzymatically digested twice for 10 minutes at 37°C with collagenase V (0.1 g / 100 mL; C9263-1G, Sigma) and protease XIV (0.01 g / 100 mL; P5417-1G, Sigma) diluted in oxygenated LCS containing 0.1% w/v bovine serum albumin (BSA-LCS). The tissue was digested for 12-minutes in protease XIV (0.01 g / 100 mL BSA-LCS) and the supernatant discarded. The tissue was repeatedly digested with protease XIV (0.005 g / 100 mL BSA-LCS) for up to six 10-minute washes or until the tissue appeared translucent. The cell-containing supernatant was collected after each wash, cardiomyocytes were pelleted (100g) and then fibroblasts were pelleted (400g). The fibroblast pellet was resuspended in Fibroblast Basal Medium supplemented with FGM 3 SingleQuots (CC-4526, Lonza) containing 10% FBS, rhFGF,

antibiotics and insulin and anti-mycotic, transferred to a 6-well plate and incubated at 37°C and 5% CO_2. The media was replaced the following day and every 2-3 days thereafter. At 80-90% confluency, cells were trypsinised and passaged. To minimise confounding effects of prolonged culture on cell behaviour, all experiments were performed on cells within the first 5 passages, as previously validated.[1,113]

It is important to acknowledge that a limitation of this work is that SR and AF groups (**Table 2.1**) were not perfectly matched across every clinical characteristic. Notably, compared to SR, a significantly greater proportion of AF donors were (i) undergoing valve surgery, (ii) taking anticoagulants, and (iii) taking β-blockers. These differences are likely to be explained by (i) the established independent association between valvular heart disease and AF, (ii) the use of β-blockade for rate control in AF, and (iii) anticoagulation being the foundation of stroke prevention in AF patients.[11] Meanwhile, more SR donors had type II diabetes mellitus which is consistent with diabetes being a major risk factor for coronary artery disease. This constitutes a limitation of the study; however, the cohort was not designed for strict matching, and consecutive recruitment ensures that the sample reflects the real-world clinical profile of patients undergoing cardiac surgery at the John Radcliffe Hospital.

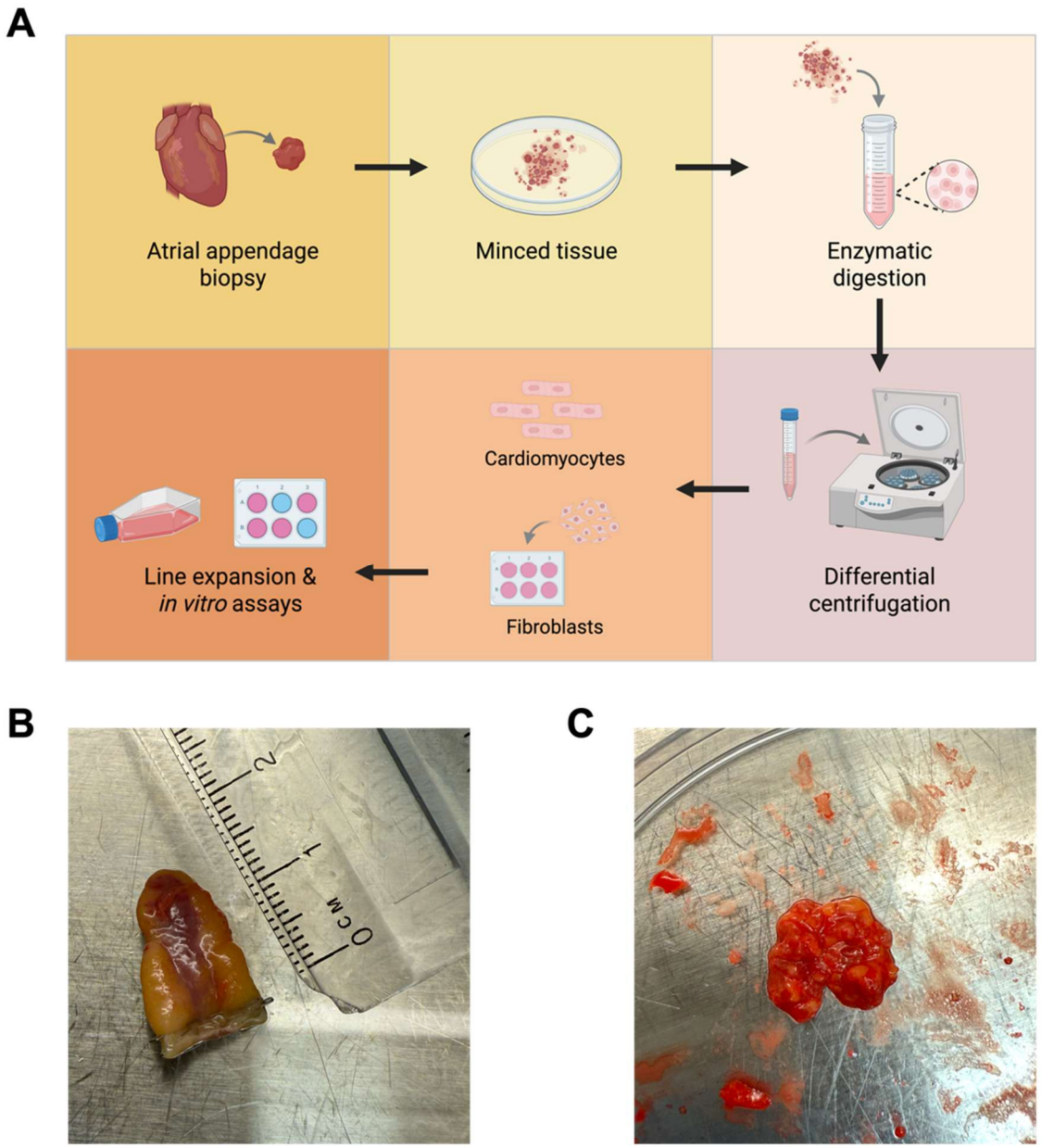


Fig 2.1 Isolation of ACFs. **(A)** Schematic depicting the protocol for fibroblast isolation from atrial appendage biopsies. **(B)** Image of a left atrial appendage biopsy. **(C)** Image of the biopsy after adipose tissue has been removed and the myocardial tissue has been minced.

Table 2.1 Clinical characteristics of study participants

ACEi, angiotensin-converting enzyme inhibitor; ARB, angiotensin II receptor blocker; AVR, aortic valve repair/replacement; CABG, coronary artery bypass grafting; COPD, chronic obstructive pulmonary disease; HFrEF, heart failure with reduced ejection fraction (<40%); MI, myocardial infarction; MVR, mitral valve repair/replacement. [a] Unpaired, two-tailed t-test, [b] χ^2 test; [c] Mann Whitney test.

Characteristic	Sinus Rhythm (SR)	Atrial Fibrillation (AF)	p-value
Number of donors, N	32	23	
Mean age, years ± SD	66.1 ± 7.5	69.5 ± 8.5	0.1241[a]
Male, N (%)	24 (75)	18 (78)	0.7789[b]
Median BMI (IQR)	27.9 (5.0)	26.0 (7.5)	0.3606[c]
Surgical Procedure, N (%)			
CABG ± AVR/MVR	15 (47)	4 (17)	0.0233[b]
AVR/MVR only	17 (53)	19 (83)	0.0233[b]
Medical history, N (%)			
COPD	1 (3)	1 (4)	0.8111[b]
Type II diabetes mellitus	8 (25)	1 (4)	0.0411[b]
HFrEF	4 (13)	6 (26)	0.1975[b]
Hypertension	21 (66)	13 (57)	0.4931[b]
Prior MI	9 (28)	3 (13)	0.2623[b]
Smoker/ex-smoker	17 (53)	8 (35)	0.1778[b]
Medications, N (%)			
ACEi and ARBs	21 (66)	16 (70)	0.7587[b]
Anticoagulants	8 (25)	22 (96)	<0.0001[b]
β-blockers	13 (41)	17 (74)	0.0145[b]
Calcium-channel blockers	8 (25)	4 (17)	0.5004[b]
Diuretics	10 (31)	12 (52)	0.1182[b]
Statins	16 (50)	13 (57)	0.6328[b]

2.2 Real-time quantitative polymerase chain reaction (RT-qPCR)

ACFs were lysed in 4°C lysis buffer and total RNA was isolated (*mir*Vana miRNA Isolation Kit, #AM1561, Invitrogen) as per the manufacturer's instructions. RNA concentration was measured using an LVis Plate (BMG Labtech). 100-500 ng of RNA was reverse transcribed using the QuantiTect Reverse Transcription Kit (205311, Qiagen), as per the manufacturer's protocol. Gene expression was determined by RT-qPCR using TaqMan Fast Advanced Master Mix (#4444557, Applied Biosystems) and TaqMan Assays (**Table 2.2**) on the QuantStudio7 Flex Real-Time PCR System (Applied Biosystems). Samples were run in technical duplicate and gene expression was quantified using the $2^{-\Delta Ct}$ method, normalised to hypoxanthine guanine phosphoribosyltransferase (*HPRT1*).[114] *HPRT1* was selected as the RT-qPCR housekeeping gene as it showed minimal inter-sample variability and no association with disease state in ACFs (**Fig 2.2**).

Table 2.2 RT-qPCR TaqMan™ Assay IDs

Gene	TaqMan™ Assay ID
Housekeeping genes	
Human *HPRT1*	Hs02800695_m1
Target genes	
Human *ARRB1*	Hs00244527_m1
Human *ARRB2*	Hs01034139_g1
Human *CACNA1C*	Hs00167681_m1
Human *CAPN1*	Hs00559804_m1
Human *CAPN2*	Hs00965097_m1
Human *FLNA*	Hs00924645_m1
Human *FLNC*	Hs00155124_m1
Human *RAMP1*	Hs00195288_m1
Human *RAMP2*	Hs00237194_m1
Human *RAMP3*	Hs00389131_m1

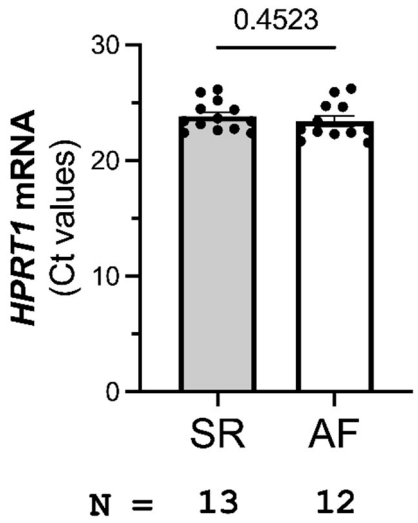


Fig 2.2: Validation of HPRT1 as an RT-qPCR housekeeping gene. Cycle threshold values of HPRT1 in SR- and AF-ACFs.

2.3 Western blot (WB)

ACFs were washed in filtered PBS before lysis with Cell Lytic M (C2978, Merck) reagent including protease (cOmplete ULTRA, 05892970001, Roche) and phosphatase (PhosSTOP, 04906837001, Roche) inhibitors. Homogenates were centrifuged at 14,000g at 4°C for 15 minutes. Protein concentration was measured by the Pierce BCA Protein Assay Kit. Equal amounts of protein (2-5 µg) were added with NuPAGE LDS Sample Buffer (NP0007, Invitrogen) and NuPAGE Sample Reducing Agent (NP0009, Invitrogen) and boiled at 95°C for 5 minutes. Proteins were resolved by molecular weight on 10-, 12- or 15-well NuPAGE 4-12% gradient 1.0mm Bis-Tris gels with 1x NuPAGE MOPS SDS Running Buffer (NP0001, Life Technologies) at 160 V for 90 minutes, unless otherwise specified. Proteins were dry transferred using an iBlot™ 2 and NC regular 0.2 µm nitrocellulose stack (IB23001, Novex) for 7 minutes at 20 V or wet transferred at 4°C at 230 mA for 1.5h to 0.2 µm nitrocellulose membrane in 1x NuPAGE transfer buffer (containing 20% methanol, NP00061, Life Technologies). Membranes were blocked for 1h with 5% milk in PBS-T (PBS containing 0.1% Tween20) and incubated on a rocker overnight at 4°C with the primary antibody (**Table 2.3**). The following day, the membranes

were washed thrice for 15 minutes with PBS-T and incubated for 2h with the appropriate HRP-conjugated secondary antibody (**Table 2.4**). Membranes were incubated with SuperSignal Chemiluminescent Substrate, exposed on a ChemiDoc Imaging System (Bio-Rad) and target protein expression was normalised to GAPDH loading control (ImageLab 6.1, Bio-Rad).

Table 2.3 Details of primary antibodies used for immunocytochemistry and Western blot

Primary Antibody	Catalogue # (Manufacturer)	Host Species	Dilution Factor	
			Immunocytochemistry	Western blot
αSMA	A5228 (Sigma-Aldrich)	Mouse	N/A	1:1000
Beta-tubulin	AC021 (Abclonal)	Mouse	1:500	1:1000
CALCR (C-terminus)	AP5688b (Abcepta)	Rabbit	1:100	1:1000
CALCR (N-terminus)	ACR-053 (Alomone labs)	Rabbit	1:100	N/A
Calpain 1	10538-1-AP (Proteintech)	Rabbit	1:100	1:1000
Calpain 2	2539S (Cell Signalling)	Rabbit	1:100	1:1000
Calpastatin	GTX23515 (GeneTex)	Mouse	1:100	1:2000
Caspase 3	9662S (Cell Signalling)	Rabbit	N/A	1:500
Collagen 1	1310-01 (SouthernBiotech)	Goat	1:500	N/A
Collagen 1	14695-1-AP (Proteintech)	Rabbit	N/A	1:1000
FLNa (N-terminus)	MAB1678 (Merck)	Mouse	1:200	1:1000
FLNa (C-terminus)	LS-C352201 (LSBio)	Rabbit	1:100	1:1000
GAPDH	MA5-15738-HRP (Invitrogen)	Mouse	N/A	1:5000
Histone 3	A17562 (Abclonal)	Rabbit	N/A	1:1000
Lamin A/C	10298-1-AP (Proteintech)	Rabbit	N/A	1:5000
MAP1LC3A	L8918 (Merck)	Rabbit	N/A	1:1000
N-cadherin	22018-1-AP (Proteintech)	Rabbit	N/A	1:2000
RAMP1	AF6428 (Bio-Techne)	Sheep	1:50	1:500
RAMP2	AF6427 (Bio-Techne)	Sheep	1:50	1:500
Ubiquitin	3936S (Cell Signalling)	Mouse	N/A	1:1000
Vimentin	A19607 (Abclonal)	Rabbit	N/A	1:250

Table 2.4 Details of secondary antibodies used for immunocytochemistry and Western blot

Secondary Antibody	Catalogue # (Manufacturer)	Dilution Factor
Western blot		
Anti-Mouse IgG (H+L), HRP Conjugate	W4021 (Promega)	1:2000
Anti-Rabbit IgG (H+L), HRP Conjugate	W4011 (Promega)	1:2000
Donkey Anti-Sheep IgG HRP Affinity Purified PAb	HAF016 (Bio-Techne)	1:2000
Immunocytochemistry		
Alexa Fluor 488 donkey anti-rabbit IgG	A21206 (Invitrogen)	1:500
Alexa Fluor 488 donkey anti-mouse IgG	A21202 (Invitrogen)	1:500 (drug screen)
Alexa Fluor 546 goat anti-mouse	A11018 (Invitrogen)	1:500
Alexa Fluor 555 donkey anti-goat	A21432 (Invitrogen)	1:500 (drug screen)
Alexa Fluor 594 chicken anti-mouse IgG	A21201 (Invitrogen)	1:500
Alexa Fluor 633 goat anti-rabbit IgG	A21070 (Invitrogen)	1:500
Alexa Fluor 647 goat anti-rabbit IgG	A32733 (Invitrogen)	1:500 (drug screen)

2.4 Immunoprecipitation of FLNa and CALCR

SR- and AF-ACFs from a T75 flask were trypsinised (and neutralised 1:1 with 10% FBS media), pelleted (300g, 5 minutes), and washed in PBS before lysis in 400 µL lysis buffer, as described in **section 2.3**. Lysates (100 µL per reaction) were pre-cleared for 1h with Protein A/G agarose beads (sc-2003, Santa Cruz) and immunoadsorbed overnight at 4°C with rotary agitation using (i) anti-CALCR (15 µL / 100 µL; AP5688B, Abcepta), (ii) anti-FLNa (15 µL / 100 µL; LS-C352201, LSBio), (iii) a rabbit IgG isotype control (3900, Cell Signalling) or, (iv) without primary antibody (beads only). The latter two conditions controlled for non-specific binding. Immune complexes were precipitated by addition of 50 µL of the bead slurry for 4h at 4°C with rotary agitation, the complexes were pelleted (1000g for 3 minutes) and washed thrice with ice-cold PBS, and proteins were eluted in 1x NuPAGE LDS Sample Buffer by boiling at 95°C for 5 minutes. Samples, and unprocessed input control, were examined by WB.

2.5 siRNA transfection of ACFs

siRNA lipotransfection was used to knockdown calpain 1 (*CAPN1)*, caspase 3 (*CASP3*), FLNa, β-arrestin 1 (*ARRB1*), β-arrestin 2 (*ARRB2*), and the pore-forming subunit of the $Ca_v1.2$ L-type calcium channel (*CACNA1C*). ON-TARGETplus siRNAs and non-targeting control pools (NC) were acquired from Horizon Discovery Biosciences Limited (**Table 2.5**). 5 nmol of each siRNA was reconstituted in RNase-free water to form 20 µM stocks. ACFs were plated in 6- or 12-well plates and cultured in 10% FBS media. At 60-80% confluency, the media was replaced with opti-MEM™ (31985070, Life Technologies Ltd) for 2h. Equal volumes of siRNA (diluted in opti-MEM) and lipofectamine RNAiMAX (3 µL lipofectamine RNAiMAX / 50 µL opti-MEM) (13778150, Life Technologies) were combined, inverted, and left at room temperature for 20 minutes. The siRNA/lipofectamine solution was added at a final [siRNA] of 50 nM. siRNA was removed after 6h and cells were recovered in antibiotic-free, 10% FBS media. Cells were lysed

for mRNA and/or protein at 24h, 48h, and 72h as outlined in the text. mRNA knockdown efficiency was quantified by the $2^{-\Delta\Delta Ct}$ method.[114]

Table 2.5 Details of ON-TARGETplus human siRNAs used in this study.

Target	Target Sequence 5' to 3'; 4 pooled sequences per target	Catalogue Number
β-arrestin 1 (ARRB1)	UGGAUAAGGAGAUCUAUUA AUGGAAAGCUCACCGUCUA GAACUGCCCUUCACCCUAA GAACGAGACGCCAGUAGAU	L-011971-00-0005
β-arrestin 2 (ARRB2)	CGAACAAGAUGACCAGGUA CGGCGUAGACUUUGAGAUU GGGCUUGUCCUUCCGCAAA UAGAUCACCUGGACAAAGU	L-007292-00-0005
Calcitonin receptor (CALCR)	CCGGUGAGCUGCAAGAUUU CCAAUGGGCCCAAUUCAAA CCACCUGGUUGAAGUAGUA GCAACCUGGUCCAACUAUA	L-003635-00-0005
Calpain 1 (CAPN1)	GGAACAACGUGGACCCAUA GUGAAGGAGUUGCGGACAA UAGAGACCAUGUUCCGAUU GAAGGGCCAUGCCUACUCU	L-005799-00-0005
Caspase 3 (CASP3)	CCGACAAGCUUGAAUUUAU CCACAGCACCUGGUUAUUA GAAUUGAUGCGUGAUGUUU GCGAAUCAAUGGACUCUGG	L-004307-00-0005
Filamin A (FLNA)	GCAGGAGGCUGGCGAGUAU GCACCCAGACCGUCAAUUA GCACAUGUUCCGUGUCCUA GAAUGGCGUUUACCUGAUU	L-012579-02-0005
L-type Ca^{2+} channel subunit α1C (CACNA1C)	GGAGGAGCACAUUCGAUAA GGAUGUUAGUCUGUAUUUA GGGUAGCAUUGUUGAUAUA GAAGAUGACUGCUUAUGGG	L-006123-00-0005
Non-targeting pool (NC)	UGGUUUACAUGUCGACUAA UGGUUUACAUGUUGUGUGA UGGUUUACAUGUUUUCUGA UGGUUUACAUGUUUUCCUA	D-001810-10-05

2.6 ACF immunostaining and confocal microscopy

To assess protein localisation, ACFs were cultured in 8-well µ-Slides with removable insert (IB-80841, Ibidi) and, at ~80% confluency, fixed for 5 minutes with methanol:acetone (1:1 v/v, -20°C), washed twice with PBS before blocking for 1h with Serum-Free Protein Block before incubation with primary antibodies (**Table 2.3**) overnight. The following day, cells were washed twice with PBS, and incubated with appropriate secondary antibodies with non-overlapping emission spectra (**Table 2.4**) for 4h and washed twice more with PBS. The insert was removed, the slide mounted with SlowFade Gold Antifade Mountant with DAPI and left for 30 minutes before imaging. The slides were imaged using a Leica DM 6000 CFS confocal microscope with a 63x (oil immersion) objective. Control slides were prepared excluding the primary antibody for all experiments, negligible background fluorescence was detected in all cases. Image analysis was performed on Fiji ImageJ2 (v2.9.0/1.54d). Co-localisation between CALCR and DAPI/FLNa was quantified using the JACoP BIOP plugin. A channel threshold was assigned using an interclass variance algorithm (Otsu) and was applied to individually outlined cells. The Overlap Coefficient was reported as an estimate of co-localisation.[115] The overlap coefficient considers the pixel intensity of each channel and returns a value for the ROI (cell) selected between 0 and 1 depending on the extent of channel co-localisation and is calculated by:

$$r = \frac{(\sum_i A_i \times B_i)}{\sqrt{\sum_i (A_i)^2 \times \sum_i (B_i)^2}}$$

For channel A (green, CALCR) and channel B (red, FLNa or blue, DAPI) where A_i and B_i represent the pixel intensity value.

2.7 Statistical analyses

All data analysis was completed using Microsoft Excel (v16.108; Microsoft, USA) and GraphPad Prism (v11.0.0, GraphPad Software Inc.; San Diego, USA). Data were assessed for normality using the Shapiro-Wilk test. For datasets with n = 3, normality

was not assumed, owing to the limited utility of formal normality testing at such small sample sizes, and these data were therefore analysed using non-parametric methods. A p-value < 0.05 was considered statistically significant.

Normally distributed data

Comparisons between two groups were performed using two-tailed paired or unpaired Student's t-tests. Comparisons involving more than two groups were analysed using one-way ANOVA (independent groups), repeated-measures one-way ANOVA (paired data), two-way ANOVA (two factors, independent groups), or repeated measures two-way ANOVA (two factors, paired data). Post hoc multiple comparisons were conducted using Tukey's test (all pairwise comparisons) and Dunnett's test (for comparisons against a single control group). Normally distributed data are expressed as mean ± standard error of the mean (SEM), unless otherwise stated.

Non-normally distributed data

For two-group comparisons in which one or both groups did not pass the normality assumption, the Mann-Whitney test (independent groups) or Wilcoxon matched-pairs signed rank test (paired data) was used. For comparisons involving more than two groups, the Kruskal-Wallis (independent groups) or Friedman test (paired data) were applied. Where appropriate, post hoc comparisons were performed using Dunn's test. Data are presented as median and interquartile range (IQR), unless otherwise stated.

Comparisons between categorical variables were assessed with the χ^2 test.

CHAPTER 3: THE ROLE OF FILAMIN A AND ITS PROTEOLYTIC FRAGMENTS IN CALCR LOCALISATION

3.1 Introduction

In this chapter, I investigate the mechanisms underlying the aberrant subcellular localisation of the calcitonin receptor (CALCR) in atrial cardiac fibroblasts (ACFs) in patients with atrial fibrillation (AF-ACFs). This phenotype, previously identified by our group, contributes – as part of a dysfunctional calcitonin signalling cascade – to impaired antifibrotic signalling in AF.[1] I begin by systematically characterising CALCR localisation across multiple sinus rhythm (SR) and atrial fibrillation (AF) donor-derived fibroblasts to establish the consistency of the increased internalisation phenotype. Prior studies, as detailed in **section 1.4.4**, have described a functional interaction between filamin A (FLNa) and the intracellular C-terminus of CALCR which facilitates receptor recycling to the cell surface following constitutive internalisation.[91] However, the relevance of this interaction in primary human cells, particularly ACFs, remains unexplored. Accordingly, this chapter examines whether alterations in FLNa abundance, proteolytic processing, or turnover contribute to CALCR's aberrant localisation in AF-ACFs.

Structurally, full-length FLNa ($FLNa^{FL}$) is a ~280 kDa protein comprised of an N-terminal actin-binding domain (ABD) followed by 24 immunoglobulin-like (Ig-like) repeats, separated by two flexible hinge regions (**Fig 3.1.1**).[116] Proteolytic cleavage at hinge regions generates N-terminal and C-terminal fragments ($FLNa^{NT}$ and $FLNa^{CT}$, respectively). $FLNa^{NT}$ contains the ABD and 15 Ig-like repeats, conferring actin cross-linking capacity and cytoskeletal integrity. In contrast, $FLNa^{CT}$ – encompassing Ig-like repeats 16-24 and typically released as a ~110 kDa fragment which is further processed to ~90 kDa – functions as a dynamic signalling hub. Through interactions with myriad binding partners – including transmembrane receptors, transcription factors, ion channels, and signalling intermediates – $FLNa^{CT}$ integrates mechanical and biomechanical cues to regulate receptor trafficking, signal compartmentalisation, transcriptional programmes, and cell fate decisions.[88,90,91,117-121] Notably, $FLNa^{CT}$ contains the reported CALCR binding region (**Fig 3.1.1**).[91]

The proteolytic processing of FLNa has been most extensively attributed to calpains, a family of Ca^{2+}-activated, neutral, cysteine proteases comprising at least 15 members.[116,122] The ubiquitously expressed conventional calpains, calpain 1 and 2, are activated by micromolar and millimolar levels of Ca^{2+} respectively, and mediate limited proteolysis of substrates.[122] Rather than recognising specific amino acid sequences, calpains preferentially target substrates based on their three-dimensional conformation.[122] Calpain activity has been previously implicated in AF pathophysiology; for instance, increased activity has been reported in right atrial appendage tissue from patients with paroxysmal and persistent AF.[123,124] Moreover, tachypacing of the mouse-derived HL-1 atrial myocyte line has been shown to increase calpain activity, suggesting a potential link between electrical stress and calpain mediated proteolysis.[125]

Although calpains are the principal proteases associated with FLNa cleavage, additional proteases have been implicated in specific biological contexts. Caspase 3 has been shown to cleave $FLNa^{FL}$ following exposure to pro-apoptotic chemical stimuli, or upon incubation with recombinant enzyme, generating $FLNa^{NT}$ and $FLNa^{CT}$.[126] However, whether caspase 3 contributes to FLNa processing in non-apoptotic, or non-transformed cells remains unclear. Similarly, FLNa has been identified as a substrate of the serine protease granzyme B, classically produced by cytotoxic T cells and natural killer cells, independently of caspase activation.[127] The contribution of these proteases to FLNa processing has not been previously explored in cardiac fibroblasts nor linked with AF.

The steady-state abundance of FLNa and its proteolytic fragments reflects the balance between their generation, via synthesis and protease-mediated cleavage, and their turnover through protein degradation pathways. A major regulator of protein turnover is the ubiquitin proteasome system (UPS), an ATP-dependent protein complex responsible for degrading ubiquitin-tagged proteins. Proteasomal degradation of FLNa has been reported, with several studies indicating that ubiquitination occurs at the N-terminal actin-binding domain in an ankyrin repeat-containing protein with a suppressor of cytokine

signalling box-2 (ASB2α)-dependent manner.[128-130] However, other reports have shown that proteasome inhibition with carboxybenzoxy-Leu-Leu-leucinal (MG-132) does not affect FLNa degradation in COS-7 cells.[131] These discrepancies suggest that FLNa turnover is governed by cell-type specific regulatory mechanisms.

Considering this existing literature, I examine:

1. The potential proteolytic or degradative pathways regulating $FLNa^{CT}$ abundance in ACFs.
2. The unresolved question of whether FLNa-CALCR binding promotes surface CALCR localisation in ACFs.
3. The FLNa-dependency of CALCR localisation in ACFs through disruption of FLNa binding or reduction of FLNa itself.

Collectively, this chapter investigates whether FLNa regulates CALCR localisation in primary human ACFs. By first interrogating the mechanisms governing FLNa's proteolytic processing and turnover, and directly testing FLNa's functional role, these results refine the understanding of CALCR trafficking in ACFs and establish a foundation for subsequent chapters exploring alternative pathways underlying receptor internalisation and antifibrotic signalling dysfunction.

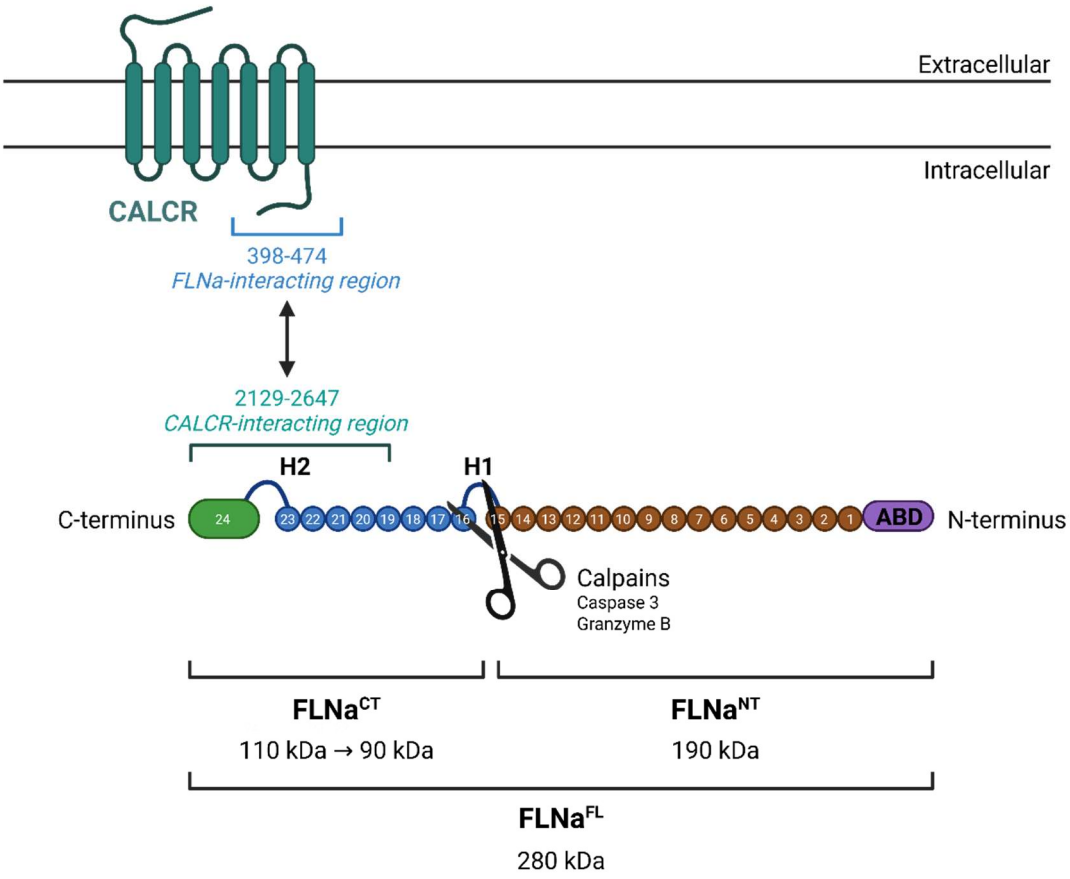


Figure 3.1.1 Schematic representation of FLNa domain organisation and interaction with the CALCR. FLNa is shown with an N-terminal actin-binding domain (ABD) followed by 24 immunoglobulin-like repeats organised into rod domains, separated by two flexible hinge regions located between repeats 15-16 (H1) and 23-24 (H2). These hinge regions are sites of regulated proteolysis and are cleaved by proteases including calpains, caspase 3, and granzyme B generating FLNa fragments, $FLNa^{NT}$ and $FLNa^{CT}$. The CALCR-interacting region of FLNa (amino acids 2129-2647) is highlighted, along with the corresponding FLNa-binding region of CALCR (amino acids 398-474). Indicated molecular weights are approximate.

3.2 Methods & Materials

3.2.1 Subcellular fractionation

The specific extraction of proteins by subcellular location was carried out using the ProteoExtract® Subcellular Proteome Extraction Kit (#539790, Calbiochem®). A total proteome is fractionated into four subcellular fractions: F1 cytosolic proteins, F2 membrane and organelle proteins, F3 nuclear proteins and F4 cytoskeletal proteins. ACFs from a T75 flask (~500,000) from the LAA of SR or AF donors were trypsinised, pelleted, resuspended in 1 mL of wash buffer and pelleted again. Subcellular fractions were sequentially solubilised with each of the four extraction buffers, as per the manufacturer's protocol. Each fraction was examined by WB, as described in **section 2.3**, and efficiency confirmed with fraction-specific markers.

3.2.2 Calpain activity assay

Calpain activity was measured, using a commercially available fluorescence-based assay (ab65308, Abcam), in ACFs from 7 SR and 6 AF donors, as per the manufacturer's instructions. Fluorescence was measured on a Clariostar Plus (BMG LABTECH) at Ex/Em 400/505. The fluorescent substrate Ac-LLY-AFC emits blue light (λ_{max}=400nm) which shifts to yellow-green (λ_{max}=505nm) when free AFC substrate is released following cleavage by calpains. Purified calpain 1 (included in the kit) was included as a positive control; lysates treated with 10 μM calpeptin were used as a negative control.

3.2.3 Calpain 1 pharmacological inhibition

The ACFs from 4 SR donors were plated at 50,000 cells per well in 12-well plates, grown to 80% confluency and serum-starved (0.5% FBS, antibiotic-free) overnight then treated, in technical duplicate, with the calpain inhibitor calpeptin (10 nM-100 μM; sc-202516, Insight Biotechnology) or DMSO vehicle control (1:500 v/v) for 24h. Target protein expression was assessed by WB.

3.2.4 Proteasome and lysosome inhibition in human ACFs

The effects of proteasome inhibition were assessed using MG-132 (HY-13259-10mg, Cambridge Bioscience), an inhibitor of the chymotrypsin-like β-subunit of the 26S proteasome, in human ACFs.[132] Specifically, ~50,000 ACFs were seeded in 12-well plates from three SR donors. The following day, cells were serum starved (0.5% FBS) for 4h and treated with MG-132 (1, 10, or 20 μM prepared in DMSO) or DMSO vehicle control for 2h, 6h, or 24h. Cell lysates were collected for evaluation of target protein expression by WB. MG-132's effect on CALCR localisation (**section 2.6**) was assessed in AF-ACFs by immunocytochemistry following a 24h treatment with MG-132 (10 μM).

Lysosome inhibition was assessed using bafilomycin A1 (b0025-0.1 mg, Cambridge Bioscience), a potent inhibitor of vacuolar-type H^+-ATPases which prevents lysosomal acidification and autophagosome-lysosome fusion. Human ACFs were treated with bafilomycin A1 (100 nM-1 μM) to inhibit lysosomal acidification and degradation of autophagolysosome contents. Autophagosome accumulation was confirmed by WB (**section 2.3**) for LC3 and calculating the ratio of autophagosomal LC3-II (phosphatidyl-ethanolamine-conjugated form) to cytoplasmic LC3-I (unmodified form).[133]

3.2.5 Tandem ubiquitin-binding entity (TUBE) pulldown assay

Ubiquitinated proteins were enriched by TUBE pulldown according to the manufacturer's protocol (2B Scientific). Briefly, ~500,000 cells in a T75 flask were starved in 0.5% FBS FBM for 2 hours before a 24h treatment with MG-132 (10μM; HY-13259-10mg, Cambridge Bioscience), bortezomib (100 nM; T2399-5 mg, Cambridge Bioscience) or vehicle (0.1% v/v DMSO). Post-treatment cells were lysed in Cell Lytic M buffer supplemented with protease inhibitors (1 tablet per 10 mL; Roche) and the deubiquitinase inhibitor PR-619 (22.3 μL per 10 mL lysis buffer). Lysates were cleared by centrifugation at 2000g for 5 minutes at 4ºC, and total protein concentration was determined using the BCA assay to ensure equal protein input across conditions.

Agarose-conjugated TUBE beads (UM0402, 2B Scientific) and agarose negative control beads (UM0400, 50% slurry, 2B Scientific) were gently resuspended by inversion prior to use. For each sample, 50 µL of 50% slurry was prepared. Beads were pelleted by centrifugation at 2000g for 5 minutes at 4ºC, and the supernatant was discarded. Beads were washed thrice with 5x resin volume of TBS-T (1x TBS with 0.1% Tween) with gentle rotation for 5 minutes at 4ºC, followed by centrifugation. After the final wash, beads were resuspended in TBS-T to generate a 50% slurry.

250 µg of protein from each treatment condition was combined with either TUBE agarose or negative control beads (50 µL of 50% slurry per 200 µL sample). A small aliquot of each lysate was retained as an input control. Pulldown reactions were incubated overnight at 4ºC with end-over-end rotation. Following incubation, samples were centrifuged at 2000g for 5 minutes at 4ºC. The supernatant was collected as the unbound fraction. Beads were washed thrice with TBS-T, rotating for 5 minutes per wash, and centrifuged at 2000g for 5 minutes at 4ºC. Bound proteins were eluted by resuspending the beads in 1x LDS sample buffer (prepared by diluting 4x LDS sample buffer 1:3 with lysis buffer) supplemented with 10x reducing agent. Samples were gently mixed, incubated on ice for 30 minutes, and then heated at 95ºC for 10 minutes to elute bound proteins. Input, unbound, and bound fractions were centrifuged at 14,000g for 10 minutes at 4ºC prior to WB analysis.

3.2.6 Cycloheximide chase assay

Protein half-life was assessed by starving SR-ACFs in 0.5% FBS for 4 hours prior to treatment with the ribosome inhibitor cycloheximide (50 µg/mL, C001-1g, Cambridge Bioscience) or DMSO vehicle control (0.1% v/v). Cells were then lysed in Cell Lytic M buffer at 2h, 4h, 6h, 24h and 48h after the start of treatment and target protein expression assessed by WB.[134]

3.2.7 Cloning and transfection of a CALCR-FLNa interaction disrupting peptide

Recombinant DNA sequences encoding a 100% match of the FLNa-interacting region of CALCR (residues: 398-474) or a scrambled negative control (using peptidenexus.com) were cloned into a pRP backbone under a CMV promoter also containing an EGFP reporter by VectorBuilder and provided as E. coli stocks. The FLNa-interacting region (targeting, TAR) and scrambled (SCR) codon-optimised DNA sequences were: 5'-ATG-GAG-GTG-CAG-ACA-ACC-GTG-AAA-AGG-CAG-TGG-GCC-CAG-TTC-AAG-ATC-CAG-TGG-AAT-CAG-AGA-TGG-GGC-AGG-AGG-CCC-AGT-AAC-CGG-TCC-GCC-AGA-GCC-GCC-GCC-GCC-GCC-GCC-GAG-GCC-GGA-GAT-ATC-CCC-ATC-TAT-ATA-TGC-CAC-CAG-GAG-CTG-CGC-AAC-GAG-CCT-GCC-AAT-AAC-CAG-GGC-GAA-GAG-AGC-GCC-GAG-ATC-ATC-CCA-CTG-AAC-ATC-ATC-GAG-CAG-GAG-TCC-TCC-GCC-GAC-TAC-AAA-GAC-GAC-GAT-GAC-AAG-TGA-3' and 5'-ATG-CGG-TAC-CGG-AAC-CAG-CCC-ATC-CAG-ATC-AAG-CAG-ATC-CAG-GGC-GAG-GAG-GCC-TGG-GAG-AGG-GCC-GAG-GCC-CTG-ATC-GCC-AAT-AGA-AAC-TGC-TTT-ATC-GAG-GCC-CTG-CCA-GCC-GCC-GTG-GAG-AGG-ACA-GGC-AAG-CCT-ACC-AGC-GAG-CCT-TGG-ATT-AAC-AGG-GCC-AAC-CAC-TGG-AGG-GCC-GCC-TCT-GAG-GAA-GTG-CAG-TCC-GAT-AAT-GCC-CAG-CAG-GGA-CAG-AGC-TCC-ATC-GCC-ATT-GAC-TAC-AAG-GAT-GAC-GAC-GAT-AAA-TGA-3', respectively. Plasmid DNA was purified with a HiSpeed Plasmid Maxi Kit (12662, Qiagen) as per the manufacturer's instructions. DNA concentration was measured and A260/A280 absorbance ratios were confirmed to be >1.8. The purified plasmid DNA sequence was confirmed by Source BioScience with custom primers. Plasmid purity was confirmed by running purified DNA on a 1% agarose gel (TAE buffer) at 50V for 1h with SYBRSafe (1:10,000) (not shown).

ACFs from 3 donors in SR were cultured for 2-3 days until 80% confluency before transfection with the targeting (TAR) and scrambled (SCR) construct expressing plasmid DNA (0.5-2µg). Initial transfection attempts using Lipofectamine 2000 were unsuccessful so nucleofection was used (4D-NucleofectorTM Core and X Unit, Lonza) with EN-150

and EO-114 protocols. Post-nucleofection, ACFs were plated in 8-well chambers with removable insert. Once EGFP expression was observed (48h), the cells were fixed for 12 minutes at 4ºC with BD Cytofix/Cytoperm™ Fixation and Permeabilization Solution (BD Biosciences) and then washed twice with 1x BD Perm/Wash Buffer (BD Biosciences). Cells were stained for CALCR (ACR-053, Alomone Labs, raised against an N-terminal epitope) and FLNa (MAB1678, Merck) overnight with rocking at 4ºC, washed thrice in Perm/Wash Buffer and the secondary antibodies (anti-mouse 546 [A-11018] and anti-rabbit 633 [A-21070], both Invitrogen) were added for 4h. The slide was prepared and imaged as described in **section 2.6**. The DAPI-CALCR overlap coefficient was calculated in SCR- or TAR-transfected EGFP+ ACFs.

3.3 Results

3.3.1 Confirmation of CALCR internalisation

Previously our group observed a greater intracellular distribution of CALCR in AF-ACFs when compared to SR-ACFs (control cells).[1] Given the importance of this phenotype to this thesis, the localisation of CALCR was systematically assessed in ACFs derived from SR and AF donors (**Fig 3.3.1A**). Primary and secondary antibody-only controls confirmed the specificity of the antibodies and staining protocol (**Fig 3.3.1B**). Co-localisation quantification revealed a consistent and significant increase in the calculated overlap coefficient between CALCR and the nuclear stain 4',6-diamidino-2-phenylindole (DAPI) in AF-ACFs, confirming a significant internalisation of the receptor (**Fig 3.3.1C-D**). Similarly, I observed a significant reduction in the overlap with the cytoplasmic and membrane marker FLNa (**Fig 3.3.1C-D**).

Given the semi-quantitative nature of immunocytochemistry, the redistribution of CALCR was corroborated biochemically with subcellular fractionation and WB (**Fig 3.3.1E**). Fraction-specific controls (calpain 1 - for the cytosol, N-cadherin - for the membrane, histone 3 - for the nucleus, vimentin - for the cytoskeleton) confirmed the efficiency of subcellular fractionation. Subcellular fractionation showed the proportion of CALCR in membrane versus cytoskeletal fractions was reduced by 70% representing a substantial redistribution, with virtually absent CALCR in nuclear compartments (**Fig 3.3.1F**). Consistent with the fractionation results, the amino acid sequences of both major splice variants of CALCR (P30988-2 and P30988-1) were not predicted to contain a nuclear localisation signal (NLS) for the importin αβ pathway, as assessed by the cNLS Mapper algorithm, shown for P30988-2 (**Fig 3.3.1G**).[135] Myc proto-oncogene protein (MYC, P01106), a protein containing a well-characterised, functional monopartite NLS, is shown as a control to confirm the validity of the analysis (**Fig 3.3.1H**).[135]

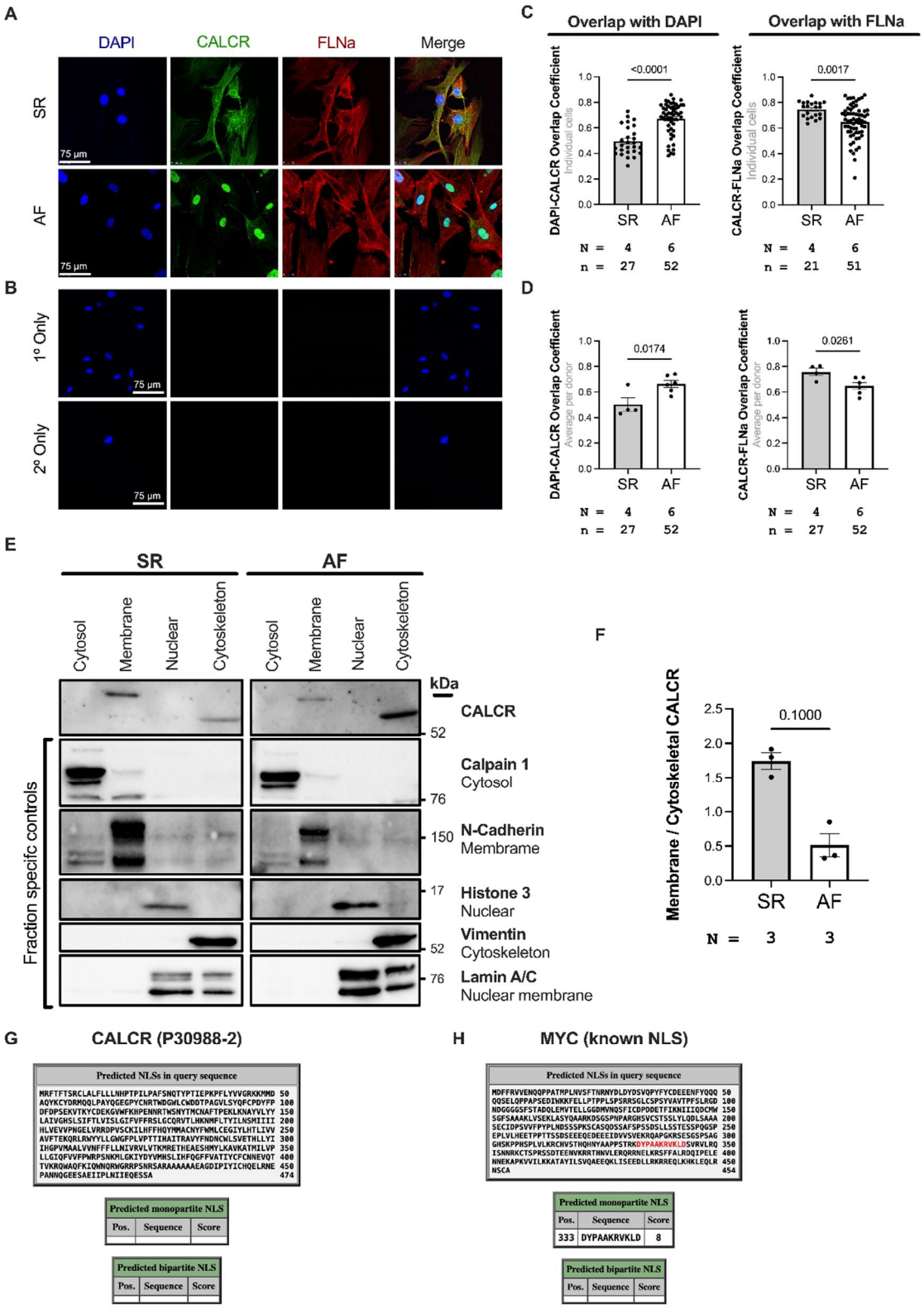


Figure 3.3.1 CALCR is aberrantly localised in AF-ACFs. (A) Representative immunofluorescence images of ACFs from sinus rhythm (SR) and atrial fibrillation (AF) donors. Scale bar: 75 µm. **(B)** Primary and secondary antibody-only controls. **(C)** Quantification of CALCR

overlap coefficients with DAPI (left) and FLNa (right), calculated using the JACoP BIOP plugin for ImageJ. Each point represents a single cell (n) from 4/5 individual donors. **(D)** Donor-averaged overlap coefficient values (≥5 cells across ≥3 frames). **(E)** WB of subcellular fractions from SR- and AF-ACFs. (**F**) Ratio of membrane to cytoskeletal CALCR signal. (**G-H**) cNLS Mapper analysis demonstrating absence of a predicted NLS for the αβ importin pathway for CALCR (insert-negative isoform), **(H)** MYC (P01106) shown as a positive control. Data expressed as mean ± SEM, *two-tailed, unpaired t-test* (C, D) or median (IQR), *Mann-Whitney test* (F).

3.3.2 Reduced expression of FLNa^{CT} in AF-ACFs

As ACFs abundantly express FLNa, and its co-localisation with CALCR is reduced in AF-ACFs (**Fig 3.3.1C-D**), the role of FLNa in regulating surface CALCR expression was examined. Firstly, FLNa mRNA and protein levels were assessed. RT-qPCR revealed a trend towards reduced FLNa mRNA expression (36% reduced, p=0.0652, **Fig 3.3.2A**).

At the protein level, while FLNa^{FL} trended towards a reduction in AF, FLNa^{CT} was significantly reduced (**Fig 3.3.2B-C**). There was no significant difference in the ratio of FLNa^{CT} to FLNa^{FL} (**Fig 3.3.2D**). If FLNa directly affected CALCR localisation, the two proteins should physically interact under physiological conditions. I confirmed an endogenous interaction by co-immunoprecipitation followed by WB (**Fig 3.3.2E**). Intriguingly, the CALCR pulldown predominantly retrieved the FLNa^{CT} fragment, which was downregulated in AF, compared to FLNa^{FL}.

A previous report found that FLNa^{CT} can localise to the nucleus which could, in turn, drive internalisation of CALCR.[117] To test this hypothesis, I co-stained AF-ACFs with antibodies raised against C- and N-termini epitopes. This revealed significant co-localisation between the two FLNa channels (*Pearson correlation coefficient*: 0.925; overlap coefficient 0.939) with no obvious nuclear localisation of FLNa^{CT} (**Fig 3.3.2F**). Subcellular fractionation similarly confirmed the absence of FLNa^{CT} in the nuclear compartment (**Fig 3.3.2G**).

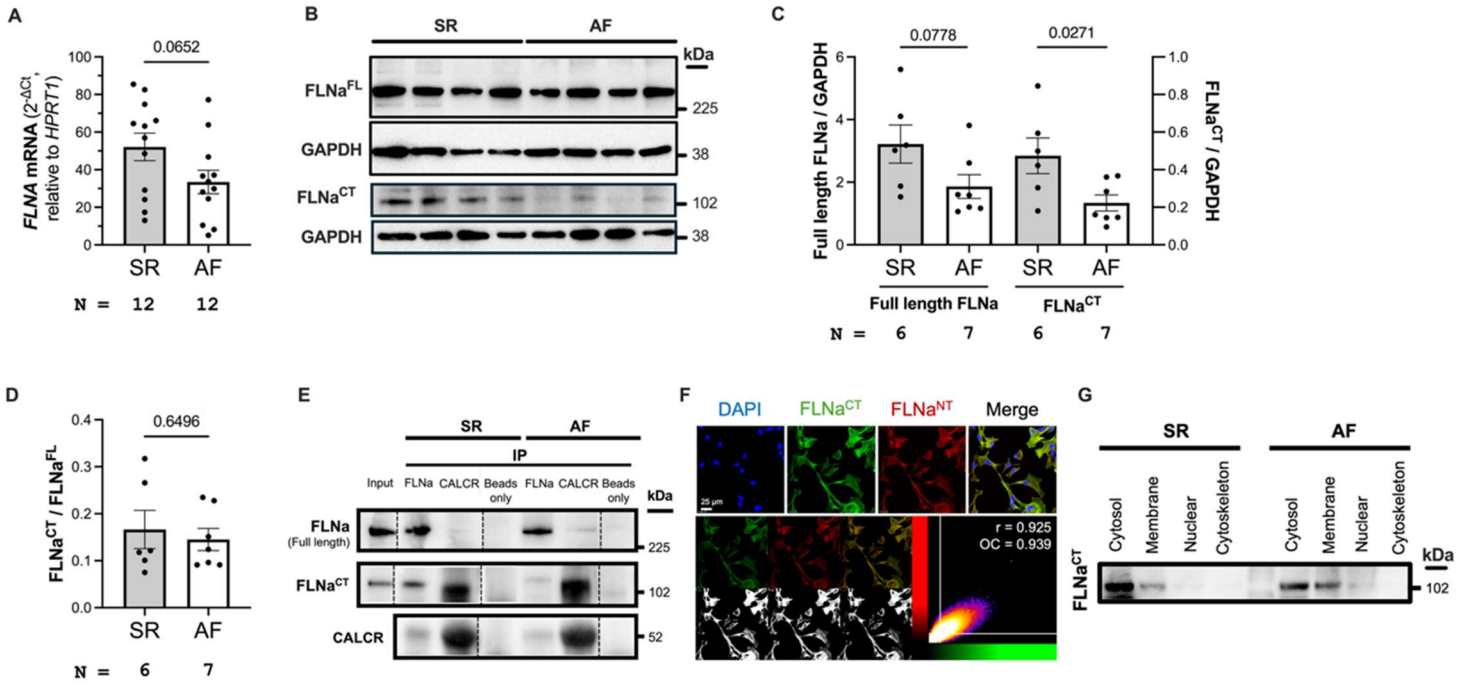


Figure 3.3.2 FLNa^{CT} interacts with CALCR and is reduced in AF-ACFs. (A) *FLNA* mRNA expression in SR- and AF-ACFs, normalised to *HPRT1*. **(B)** Representative WBs and **(C)** quantification of full-length FLNa (FLNa^{FL}) and FLNa^{CT}. **(D)** Ratio of FLNa^{CT} to FLNa^{FL} in SR- and AF-ACFs. **(E)** FLNa co-immunoprecipitation with CALCR in SR and AF-ACFs (and vice versa) assessed by WB. Dashed lines indicate non-adjacent lanes that were repositioned from the same original membrane for presentation clarity. **(F)** AF-ACFs co-stained with antibodies raised against FLNa's C- (green) and N-terminal (red). The output image from the BIOP JACoP plugin for ImageJ showing each channel, the merge image and the fluorogram. The calculated *Pearson correlation coefficient* (r) and overlap coefficient (OC) are shown. Scale bar, 25 µm. **(G)** WB for FLNa^{CT} in subcellular fractions from SR- and AF-ACFs. N, individual donors. Data expressed as mean ± SEM, *two-tailed, unpaired t-test*.

3.3.3 Unaltered calpain expression and activity in AF-ACFs

As $FLNa^{CT}$ was reduced in AF-ACFs, and it was demonstrated to be the major CALCR-interacting fragment of FLNa, I sought to investigate the mechanisms underpinning its reduction. Firstly, I hypothesised that the generation of $FLNa^{CT}$, through proteolytic cleavage of $FLNa^{FL}$, may be reduced in AF-ACFs.

Calpains are the primary proteases reported to cleave $FLNa^{FL}$ to generate $FLNa^{CT}$. The expression of calpain 1 (gene: *CAPN1*) and calpain 2 (gene: *CAPN2*) was examined. While transcript levels of both *CAPN1* and *CAPN2* were unaffected by rhythm status, calpain 1 protein – but not calpain 2 – was significantly reduced in AF-ACFs (**Fig 3.3.3A,B**). Given this reduction, calpain-like activity was assessed in human ACF lysates using a fluorometric assay based on the cleavage of the synthetic substrate Ac-LLY-AFC, which produces a shift in fluorescence emission upon release of free AFC (**Fig 3.3.3C**). This analysis revealed no significant difference in total calpain-like activity between SR- and AF-ACFs (**Fig 3.3.3D**).

To delineate the contribution of *bona fide* calpains, lysates were treated with the cell-permeable, pan-classical calpain inhibitor calpeptin (10 μM). Although calpeptin abolished the activity of purified calpain 1, it reduced calpain-like activity in ACF lysates by only ~15%, indicating the presence of additional protease(s) with overlapping substrate specificity, that are insensitive to calpeptin (**Fig 3.3.3E,F**). Yet, the calpeptin-sensitive fraction – taken to represent true calpain activity – did not differ between SR- and AF-ACFs (**Fig 3.3.3G**). Alongside protein abundance, calpain activity is modulated by its endogenous inhibitor calpastatin and by subcellular localisation (it is most active at the plasma membrane).[122,136] However, calpastatin protein expression was unchanged (**Fig 3.3.3H**) and no discernible differences in calpain 1 localisation were observed between SR- and AF-ACFs (**Fig 3.3.3I**).

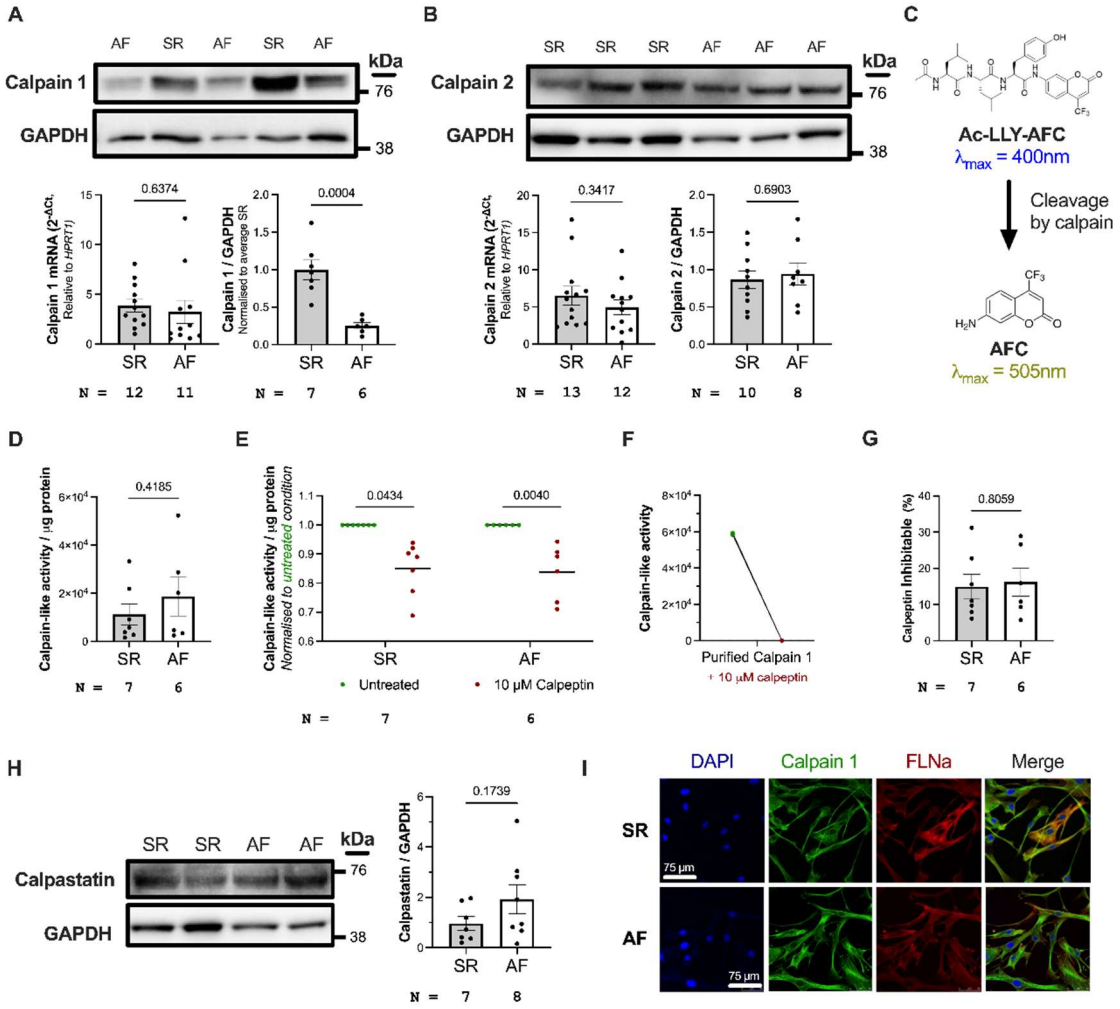


Figure 3.3.3 Calpain-like activity is not altered in AF, despite reduced calpain 1 expression. **(A)** Representative WB for calpain 1 with quantification of mRNA (bottom left) and protein (bottom right) in SR- and AF-ACFs. **(B)** as in **A**, but for calpain 2. **(C)** Structure of the fluorescent substrate Ac-Leucine-Leucine-Tyrosine-7-amino-4-trifluoromethylcoumarin (Ac-LLY-AFC) used to quantify calpain-like activity. The substrate is cleaved to liberate free AFC which emits maximally at 505 nm. **(D)** Calpain-like activity in SR- and AF-ACFs, normalised to the amount of protein loaded (µg). **(E)** Normalised calpain-like activity in SR- and AF-ACFs ± calpeptin (10 µM). **(F)** Calpain-like activity of purified calpain 1 ± calpeptin (10 µM). **(G)** Calpeptin-inhibitable activity expressed as a percentage of total calpain-like activity in SR- and AF-ACFs. **(H)** Representative WB for calpastatin with protein level quantification. **(I)** Representative images of SR- and AF-ACFs immunostained for calpain 1 and FLNa. N, individual donors. Scale bar, 75 µm. Data expressed as mean ± SEM; *two-tailed unpaired t-test* except **E**, *two-way ANOVA* with *Šídák's multiple comparisons test* (on the non-normalised data).

Given the extensive literature implicating calpains in FLNa processing, it was important to directly test their contribution to regulating FLNa^{CT} abundance in this context. Calpains were pharmacologically inhibited with calpeptin. A preliminary cytotoxicity assessment demonstrated that calpeptin was well tolerated at concentrations up to 100 µM, beyond which substantial cell death was observed (**Fig 3.3.4A**). As SR-ACFs exhibited higher basal levels of FLNa^{CT}, these cells were treated with a range of concentrations of calpeptin for 24 hours, after which FLNa^{CT} abundance was quantified by WB (**Fig 3.3.4B**). FLNa^{CT} expression was not altered by calpeptin treatment at any concentration tested (**Fig 3.3.4C**). As a control, calpain 1 protein levels were shown to remain unchanged, excluding compensatory upregulation in response to pharmacological inhibition (**Fig 3.3.4D**).

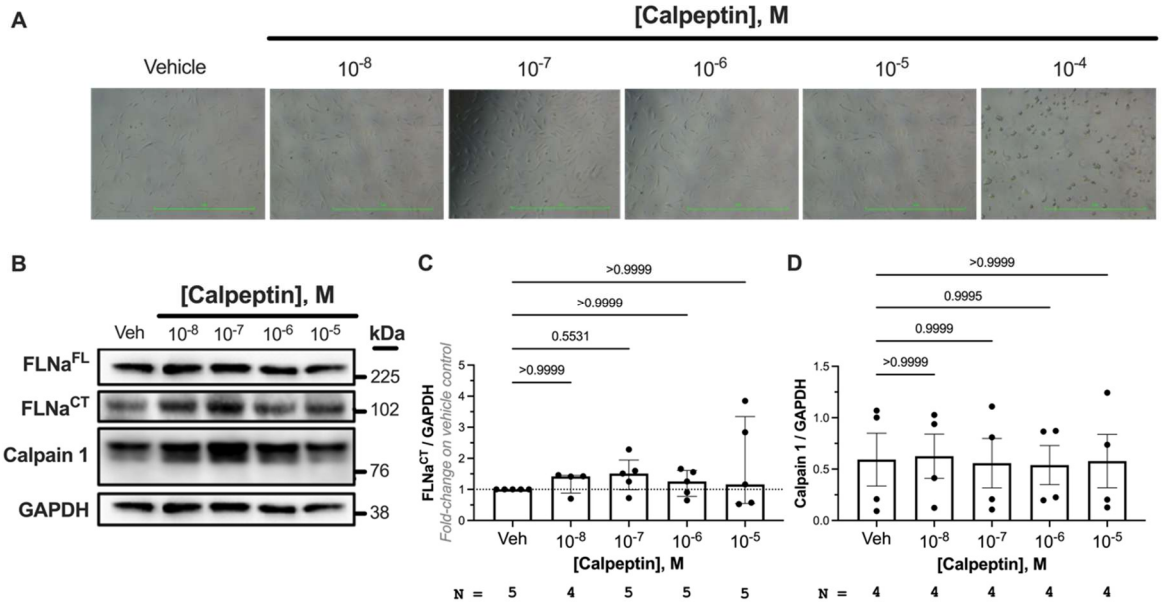


Figure 3.3.4 Pharmacological inhibition of classical calpains does not reduce FLNa^{CT} expression in SR-ACFs. (A) Representative brightfield images of SR-ACFs after 24h treatment with calpeptin or vehicle (DMSO, 1:500 v/v). **(B)** Representative WBs for FLNa^{FL}, FLNa^{CT}, calpain 1 and GAPDH (loading control) in SR-ACFs from one donor after 24h calpeptin treatment (10nM-10µM). **(C)** Quantification of FLNa^{CT} expression, normalised to vehicle (median [IQR]; *Kruskal-Wallis test with post-hoc Dunn's multiple comparisons test*). **(D)** Calpain 1 protein levels (mean ± SEM; *one-way ANOVA with Tukey's multiple comparisons test*). Each point represents the mean of technical duplicates.

To further exclude calpain 1 as a determinant of FLNa^{CT} generation, *CAPN1* was silenced using siRNA. Optimisation of transfection duration identified 48h to be the most effective for reduction in *CAPN1* mRNA (~92%, **Fig 3.3.5A**) and calpain 1 protein (~52%, **Fig 3.3.5B)**. Despite robust calpain 1 suppression, FLNa^{CT} levels were unaltered (**Fig 3.3.5B,C**). This was independent of calpain 2 expression (**Fig 3.3.5A**). In summary, although FLNa^{CT} and calpain 1 levels were decreased in AF-ACFs, comprehensive biochemical, pharmacological, and loss-of-function studies demonstrated no difference in calpain activity between SR- and AF-ACFs collectively arguing against a predominant role for classical calpains in FLNa^{CT} generation under these experimental conditions.

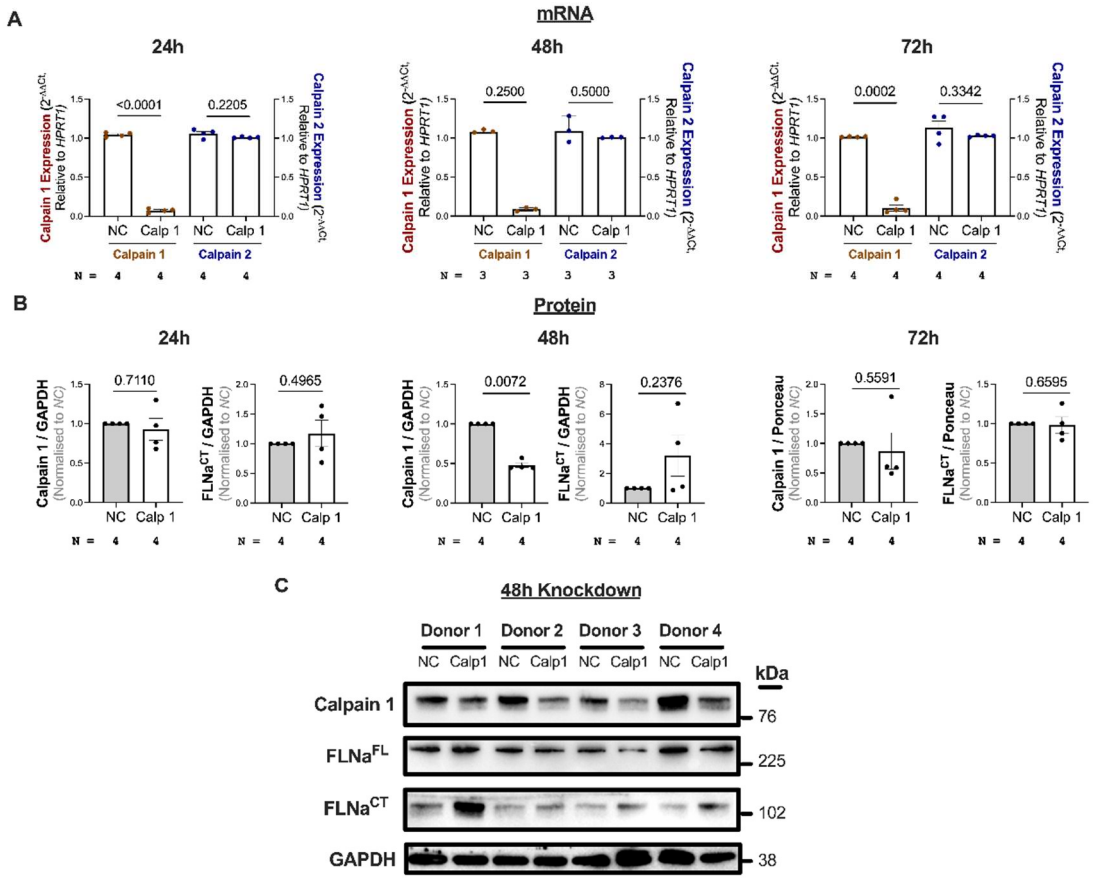


Figure 3.3.5 Calpain 1 siRNA-knockdown does not affect FLNa^{CT} in SR-ACFs. (A) Calpain 1 (brown) or calpain 2 (blue) mRNA expression after 24h, 48h and 72h siRNA lipotransfection with non-targeting control (NC) or anti-calpain 1 siRNA (Calp1). Mean ± SEM. **(B)** Quantification of calpain 1 (left) and FLNa^{CT} (right) protein expression at 24h, 48h and 72h following NC or Calp1 siRNA treatment. Median (IQR). **(C)** WB of calpain 1, FLNa^{FL}, FLNa^{CT} and GAPDH after 48h transfection. *Two-tailed paired t-test* (**B**, on non-normalised data), except the 48h timepoint in A, which is median (IQR), Wilcoxon signed-rank matched pairs.

3.3.4 Caspase 3 knockdown does not alter FLNa^{CT} abundance in ACFs

Although the existing literature predominantly implicates calpains in the proteolytic processing of FLNa, this was not apparent in the ACF context. To identify alternative candidate proteases in a systematic and unbiased manner, I interrogated a previously published SR-ACF proteomic dataset generated by our group against the MEROPS protease database, a curated resource that classifies and annotates proteases, their substrates, and endogenous inhibitors.[1,137] This analysis identified the expression of 147 proteases within human ACFs (**Table 3.1**). To refine this list, each candidate protease was subjected to a literature review to determine whether prior evidence existed linking it to FLNa cleavage. Among the proteases identified, only caspase 3 (CASP3) was previously reported to mediate FLNa proteolysis.[126] Accordingly, CASP3 protein expression was assessed; however, no difference in expression was observed between SR- and AF-ACFs (**Fig 3.3.6A-B**). When *CASP3* was knocked down by siRNA in SR-ACFs for 48h, there was no effect on FLNa^{CT} expression (**Fig 3.3.6C-E**). Therefore, caspase 3 is unlikely to be a mediator of FLNa^{CT} generation.

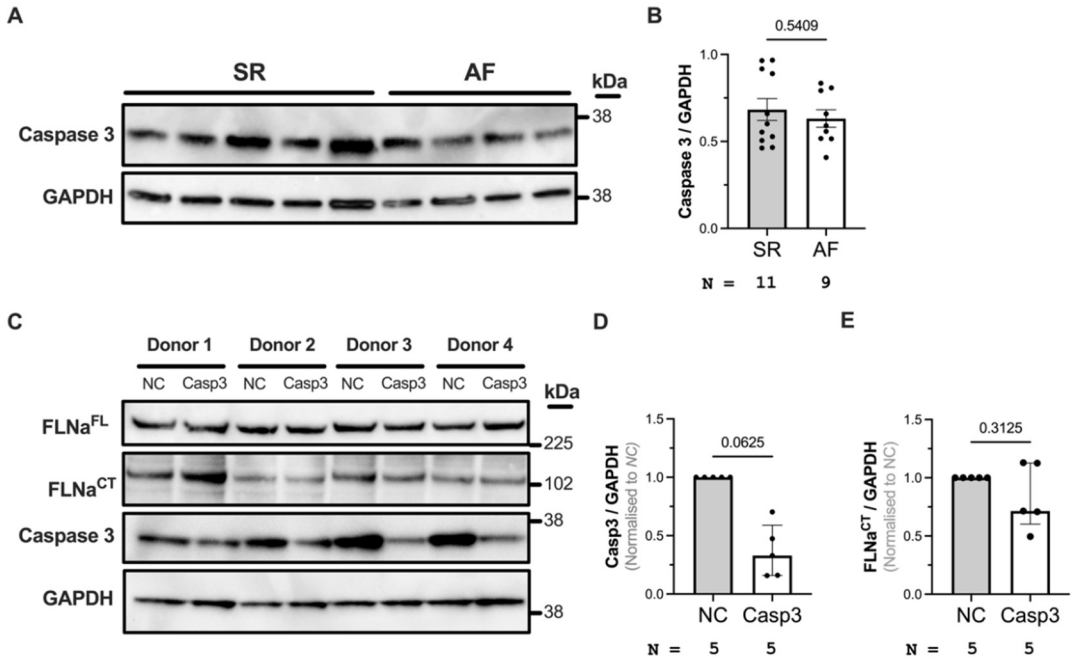


Figure 3.3.6 Caspase 3 siRNA-knockdown does not affect FLNa^{CT} expression in SR-ACFs. **(A)** WB of caspase 3 in SR- and AF-ACFs. **(B)** Quantification of caspase 3 protein expression. **(C)** WB of FLNa^{FL}, FLNa^{CT}, caspase 3 and GAPDH after non-targeting control (NC) or anti-caspase 3 siRNA treatment for 48h. **(D)** Quantification of caspase 3 and **(E)** FLNa^{CT} protein expression following siRNA treatment. N, individual donors. Expressed as mean ± SEM (B) or median (IQR) (D,E). *Two-tailed unpaired t-test* (B) and *Wilcoxon matched-pairs signed rank test* (D, E).

Table 3.1 **List of proteases (HGNC symbols) in the MEROPS database also identified in a human ACF proteomic database.** Caspase 3 (CASP3) was previously reported to cleave FLNa.

ABHD10	**CASP3**	DPYSL2	LYPLA2	PMPCB	TFRC
ABHD12	CASP4	DPYSL3	MEST	PPME1	TGM2
ABHD14B	CD97	DPYSL4	METAP1	PRCP	THOP1
ACY1	CES1	ECE1	METAP2	PREP	TPP1
ADAM10	CLPP	EIF3F	MMP14	PREPL	TPP2
ADAM17	CNDP2	EIF3H	MMP2	PSMA1	UCHL1
ADAM9	COPS5	EPHX1	NCLN	PSMA3	UCHL3
ADAMTS1	COPS6	ERAP1	NDRG1	PSMA7	UQCRC1
ADAMTS2	CPD	ERAP2	NDRG3	PSMB1	UQCRC2
AEBP1	CPE	ERMP1	NLN	PSMB2	USP10
AFG3L2	CPS1	ESD	NPEPL1	PSMB4	USP14
AGA	CTPS1	FAP	NPEPPS	PSMB5	USP15
ANPEP	CTSA	GFPT1	NRDC	PSMB6	USP16
APEH	CTSB	GFPT2	NUP98	PSMB7	USP24
ASAH1	CTSC	GGH	OTUB1	PSMB8	USP39
ASNS	CTSD	GMPS	PA2G4	PSMB9	USP47
BLMH	CTSF	HM13	PAMR1	PSMD14	USP5
C1R	CTSK	HTRA2	PAPPA	PSMD7	USP7
C1S	CTSZ	IDE	PARK7	SCPEP1	USP8
CAD	DAG1	LACTB	PEPD	SCRN1	USP9X
CAPN1	DNPEP	LAP3	PFAS	SCRN2	XPNPEP1
CAPN2	DPP3	LGMN	PIGK	SCRN3	ZMPSTE24
CAPN5	DPP4	LNPEP	PITRM1	SPPL2A	
CAPN7	DPP7	LONP1	PLBD2	STAMBP	
CASP1	DPP9	LTA4H	PMPCA	SUPT16H	

3.3.5 Proteasome, but not lysosome, inhibition reduces FLNa^{CT} expression

Subsequent analyses focused on pathways that may promote the enhanced degradation of FLNa^{CT}. Accordingly, the contribution of proteasomal and lysosomal degradation pathways was examined. Initially, I assessed the contribution of the ubiquitin proteasome system (UPS) with MG-132, a cell-permeable reversible inhibitor of the 20S and 26S proteasome. After 24h, but not 2h or 6h, there was a consistent accumulation of a larger protein (~10 kDa) fragment detected by the FLNa^{CT} antibody, with no change in FLNa^{CT} *per se* (**Fig 3.3.7A-E**). Of note, the abundance of FLNa^{FL} showed a trend towards an increase (**Fig 3.3.7F**) and a significant decrease in the FLNa^{CT} to FLNa^{FL} ratio after 10 μM MG-132 treatment (**Fig 3.3.7G**). Importantly, the ratio of FLNa^{CT} to FLNa^{FL} was independent of GAPDH which appears to have also been reduced by treatment, as has been reported previously, which may affect normalisation.[138] Future studies should aim to find a more stable housekeeping protein following MG-132 treatment.

These results indicate that MG-132 negatively affects the production of FLNa^{CT} from the cleavage of FLNa^{FL} rather than preventing the degradation of FLNa^{CT} by the UPS. A cycloheximide chase assay, to assess protein turnover, revealed a FLNa^{CT} half-life of approximately 2-4h, therefore the 6h duration of proteasome inhibition, which should encompass at least 1 round of protein turnover, should have shown an increase in FLNa^{CT} if it was being degraded by the UPS (**Fig 3.3.8**).

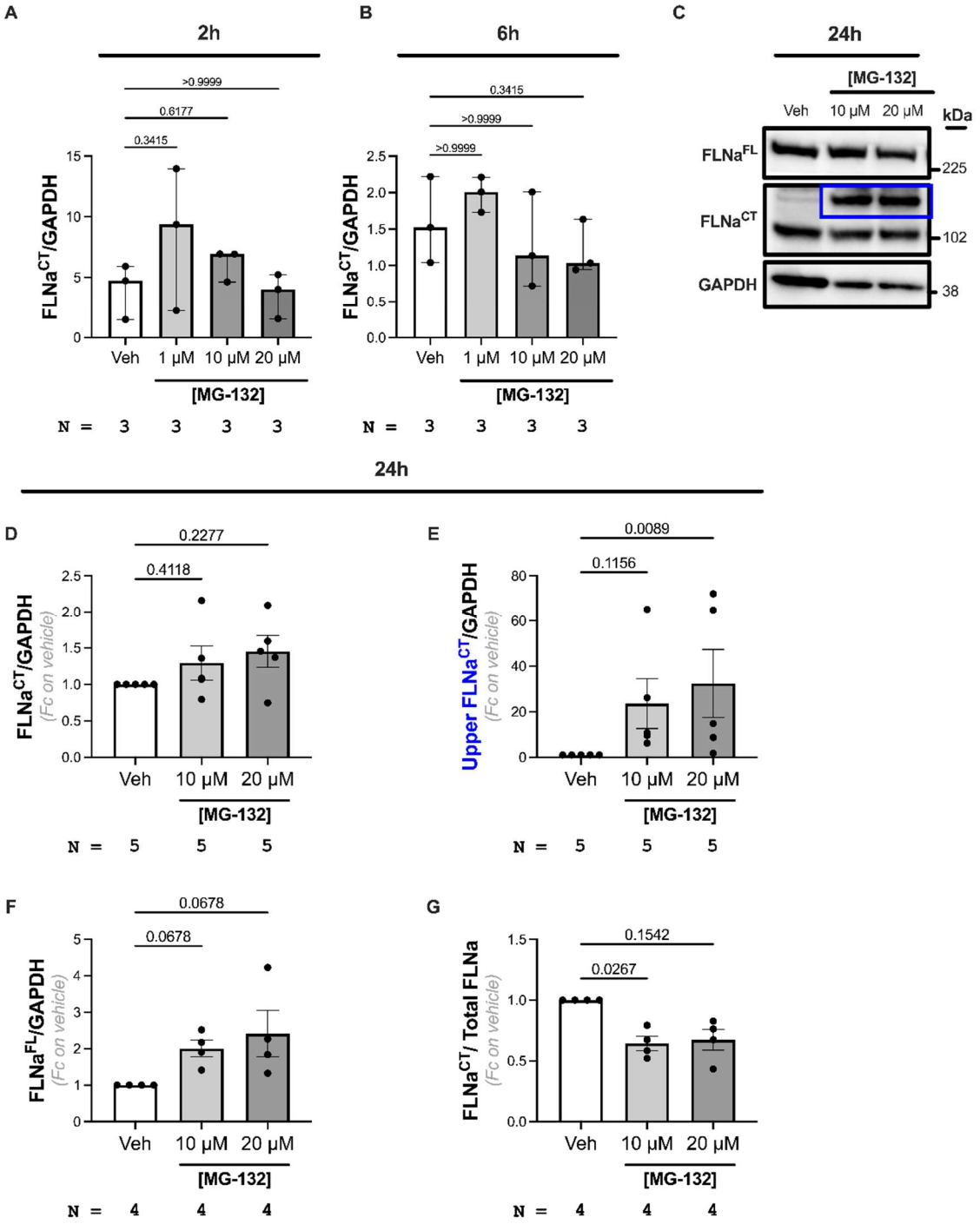


Figure 3.3.7 Effects of MG-132 on FLNa species. Effect of MG-132 (10 and 20 µM) on FLNa^{CT} protein levels after 2h **(A)** or 6h **(B)** treatment in SR-ACFs. **(C)** Representative WB showing the accumulation of a larger FLNa^{CT} fragment after 24h of MG-132 treatment. **(D)** Quantification of FLNa^{CT}, **(E)** the upper fragment, **(F)** FLNa^{FL} and **(G)** the ratio of FLNa^{CT} to FLNa^{FL}. Veh, 0.1% v/v DMSO. Median (IQR), *Friedman test* with post-hoc Dunn's test.

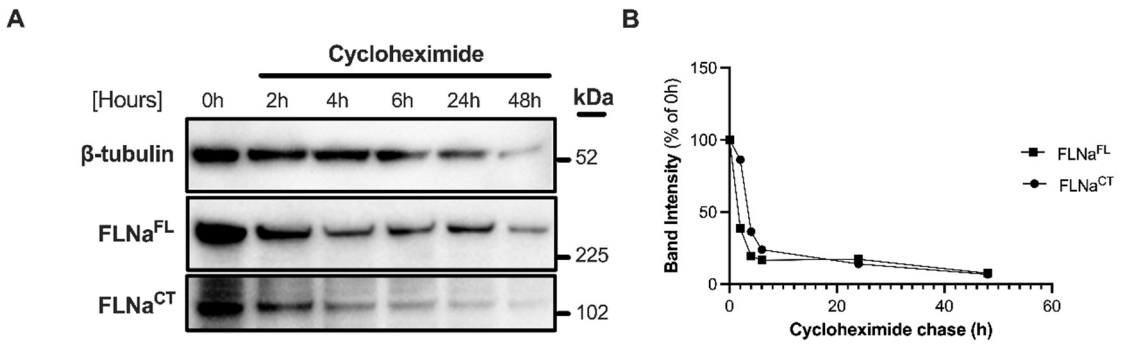


Figure 3.3.8 Cycloheximide chase assay to assess turnover of FLNa species. (A) WB probed for $FLNa^{FL}$, $FLNa^{CT}$ and β-tubulin after SR-ACFs from one donor were treated with cycloheximide (50 µg/mL) for 2h, 4h, 6h, 24h, and 48h. **(B)** Densitometric analysis of time-dependent degradation of $FLNa^{FL}$ (squares) and $FLNa^{CT}$ (circles), expressed as a percentage of the 0h value.

I aimed to exclude the possibility that the larger fragment, which ran ~10kDa higher than $FLNa^{CT}$, may be a (poly)ubiquitinated form of $FLNa^{CT}$ which is not ordinarily observed when the UPS is operational. Cells were treated with MG-132 or the clinically approved, and more potent, proteasome inhibitor bortezomib for 24h (or a DMSO loading control).[132] Ubiquitinated proteins were enriched using a tandem ubiquitin-binding entity (TUBE) assay prior to immunoblot analysis (**Fig 3.3.9A**). Immunoblotting with an anti-ubiquitin antibody demonstrated enrichment of ubiquitinated species in the TUBE pulldown, particularly following MG-132 or bortezomib treatment, compared with input and flow-through fractions, confirming efficient capture of ubiquitinated proteins. Non-specific control beads (NC) were included to show the enrichment of polyubiquitinated proteins was specific to the TUBE beads. In contrast, neither $FLNa^{CT}$ nor $FLNa^{FL}$ were detectably enriched in the TUBE-bound fraction and remained predominantly in the unbound fraction, despite treatment with MG-132 (**Fig 3.3.9C**) or bortezomib (**Fig 3.3.9D**). These results indicate that $FLNa^{CT}$ is not appreciably ubiquitinated under basal conditions or following proteasome inhibition.

As the functional significance of the larger $FLNa^{CT}$ species – that appeared following MG-132 treatment – is unclear, the effect of 24h MG-132 (10 μM) treatment on CALCR localisation was assessed by immunocytochemistry. This did not alter CALCR's co-localisation with DAPI in AF-ACFs (**Fig 3.3.10A, B**).

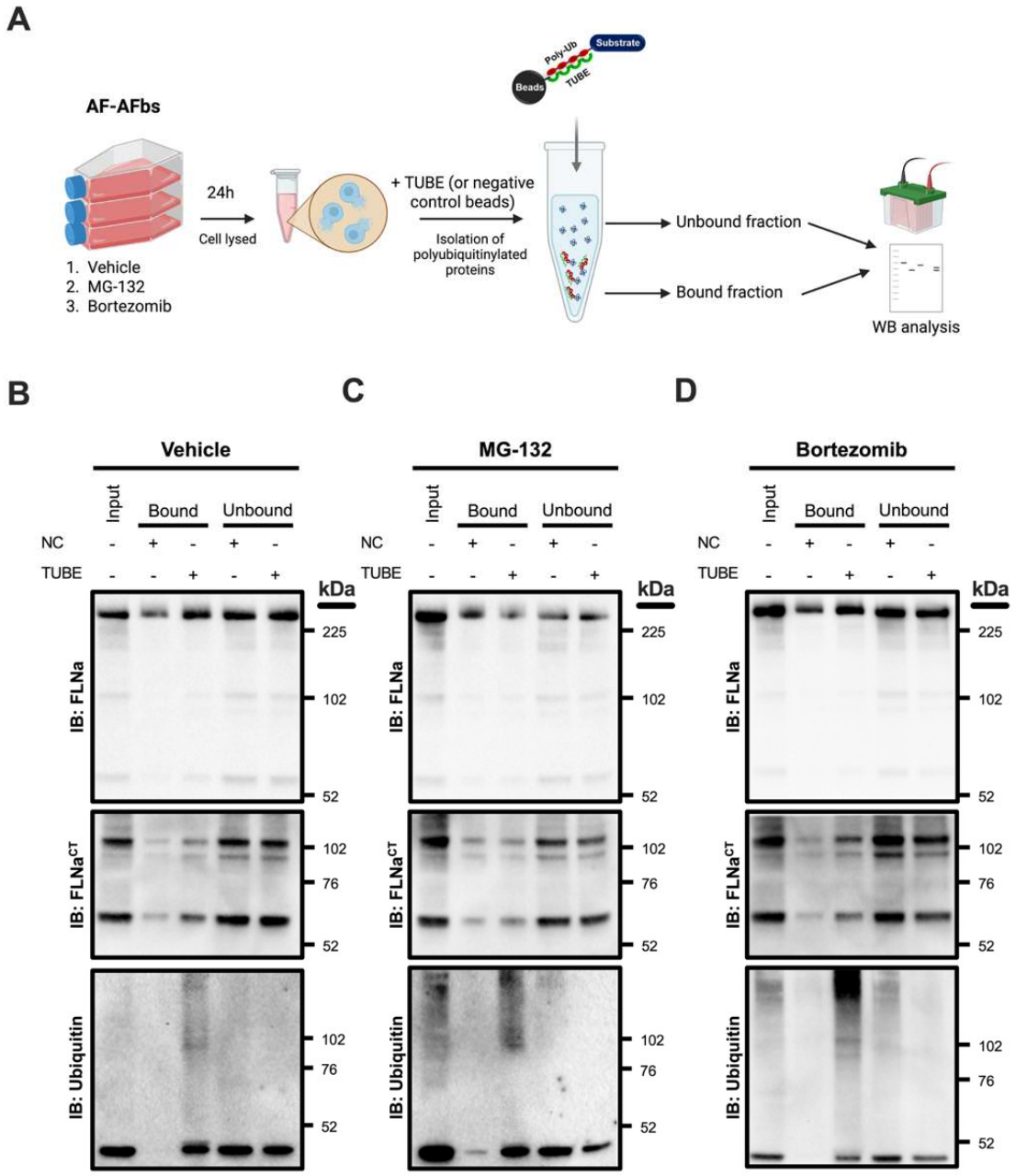


Figure 3.3.9 Assessment of FLNa^{CT} ubiquitination using tandem ubiquitin-binding entity (TUBE) pulldown assays. (A) Schematic of the experimental workflow. ACFs were treated for 24h with vehicle (DMSO, 0.1% v/v), MG-132 (10 μM), or bortezomib (100 nM) prior to cell lysis and enrichment of polyubiquitinated proteins using TUBE agarose beads or negative control (NC) beads. Bound and unbound fractions were analysed by WB. **(B-D)** Representative immunoblots of input, bound, and unbound fractions following TUBE pulldown in ACFs treated with vehicle (B), MG-132 (C), or bortezomib (D). Blots were probed for FLNa^{FL}, FLNa^{CT} and ubiquitin.

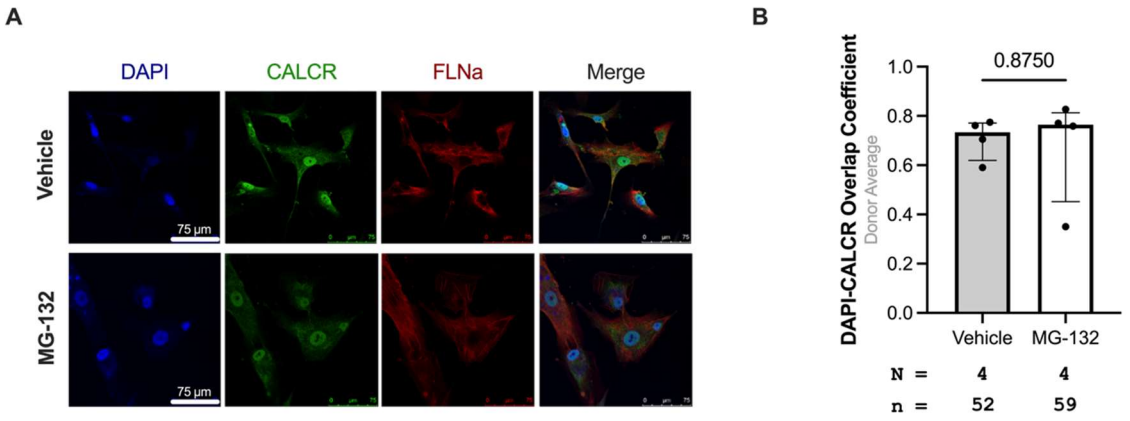


Figure 3.3.10 Effect of MG-132 on CALCR localisation. (A) Representative images of AF-ACFs treated with vehicle (0.1% v/v DMSO) or MG-132 (10 µM) for 24h. Scale bar: 75 µm. **(B)** Quantification of the CALCR overlap coefficient with DAPI, calculated using the JACoP BIOP plugin for ImageJ. Each point represents the donor-averaged coefficient (calculated from ≥10 cells across at least 3 frames). n, individual cells. N, individual donors. Data expressed as median (IQR), *Wilcoxon matched-pairs signed rank test.*

3.3.6 FLNa^{CT} is not degraded by the lysosomal pathway

Having found no evidence that the UPS is a major determinant of FLNa^{CT} degradation and, ultimately, the regulation of CALCR localisation, I next investigated whether lysosomal pathways contributed to its turnover. To this end, ACFs were treated with the lysosomal inhibitor bafilomycin A1 for 6h (**Fig 3.3.11A-C**) or 24h (**Fig 3.3.11D-F**), which blocks autophagosome and lysosome acidification by binding the V_0 subunit of the vacuolar-type H^+-ATPase. Inhibition was confirmed by an increased LC3-II to LC3-I ratio, consistent with impaired autophagic flux (**Fig 3.3.11C, F**). Despite effective lysosomal inhibition, FLNa^{CT} abundance was unchanged following bafilomycin A1 treatment at both time points, indicating that lysosomal degradation is unlikely to be a dominant degradative mechanism for FLNa^{FL} or FLNa^{CT} and therefore is unlikely to account for the reduced FLNa^{CT} levels observed in AF-ACFs.

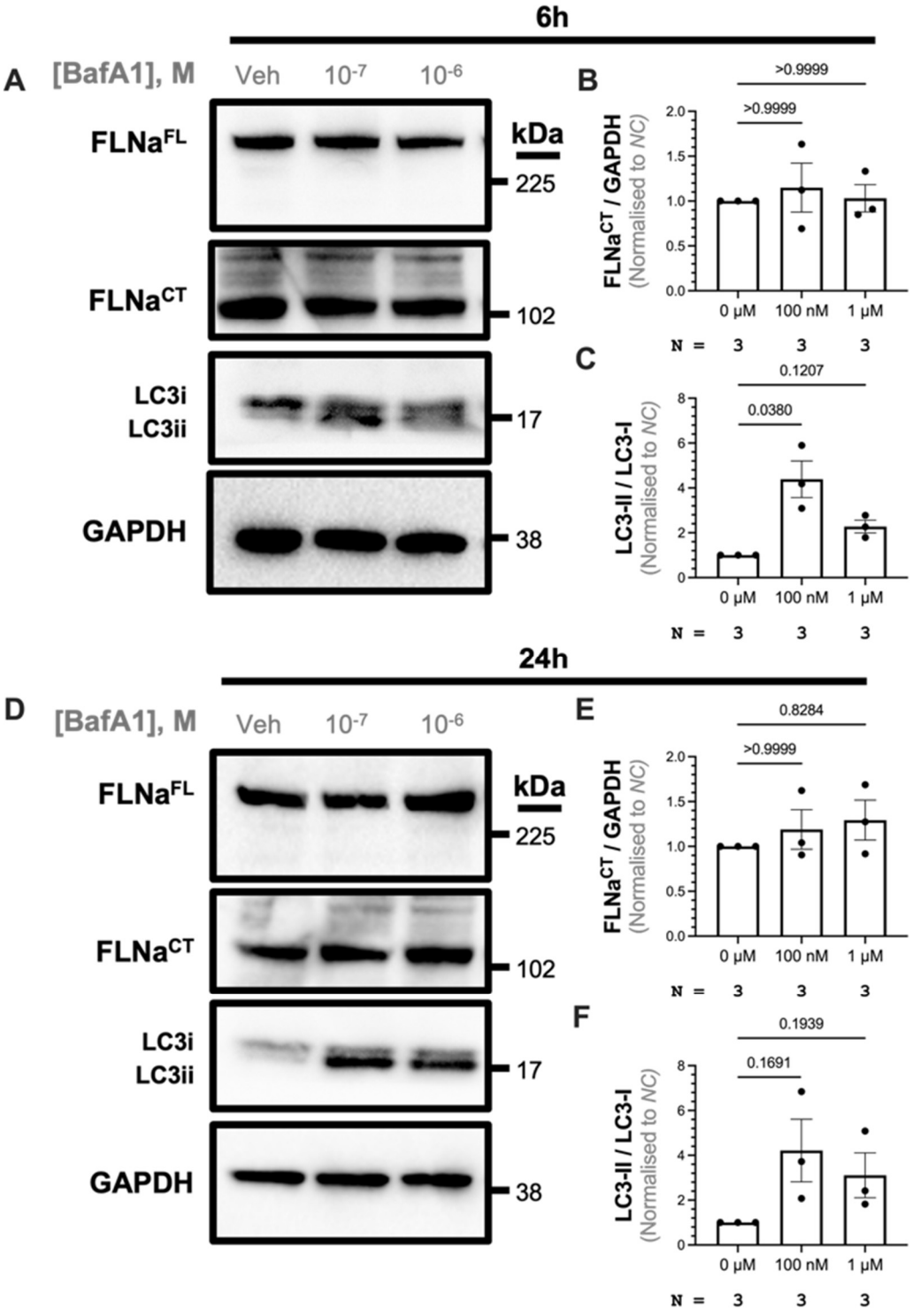


Figure 3.3.11 Effect of bafilomycin A1 (BafA1) on FLNa^{CT}. (A) Representative WB following 6h of treatment with BafA1 for FLNa^{FL}, FLNa^{CT}, microtubule-associated protein 1 light chain 3 (LC3i and lipidated LC3ii) and GAPDH. **(B)** Quantification of FLNa^{CT} and **(C)** the ratio of LC3-II to LC3-I. **(D-F)** as for A-C but for a 24h BafA1 treatment. Veh, 0.1% v/v DMSO. Data expressed as median (IQR). *Friedman test.*

3.3.7 FLNa is not a major regulator of CALCR localisation in ACFs

Irrespective of the upstream mechanisms responsible for reduced $FLNa^{CT}$, it was important to directly interrogate the functional relevance of the FLNa-CALCR interaction in regulating CALCR subcellular localisation. To this end, two complementary, but mechanistically distinct, strategies were employed to disrupt the endogenous FLNa-CALCR interaction, thereby allowing assessment of whether this interaction is required for maintenance of CALCR surface expression under physiological conditions.

First, a competitive disrupting peptide was designed to competitively disrupt endogenous FLNa-CALCR interactions without altering overall FLNa expression. A peptide corresponding to the C-terminal region of CALCR (residues 398-474), encompassing CALCR's previously reported FLNa-interacting domain, was cloned into a plasmid for expression (**Fig 3.3.12A**). An enhanced green fluorescent protein (EGFP) reporter was incorporated to identify successfully transfected cells. A scrambled version (SCR), lacking FLNa-binding capacity, was generated as a negative control.

Significant efforts were dedicated to optimising plasmid delivery into primary ACFs, which are resistant to conventional transfection approaches.[139] Lipotransfection with lipofectamine 2000 resulted in negligible EGFP expression (**Fig 3.3.12B**), indicating limited transfection success. Consequently, a nucleofection-based strategy was adopted to identify conditions that maximised transgene expression while preserving cell viability. This optimisation identified the EO-114 protocol with 2 µg plasmid DNA as yielding the highest transfection efficiency, although still modest (~10%, **Fig 3.3.12C, D**).

Following optimisation, human SR-ACFs were nucleofected with either the targeting (TAR) or scrambled (SCR) plasmids and cultured for 48h to allow sufficient expression of the disrupting peptide. Under the working hypothesis that FLNa contributes to CALCR's surface expression, it was predicted that disrupting this interaction would promote CALCR internalisation. To assess receptor localisation, cells were

immunostained for CALCR using an antibody raised against the N-terminal extracellular domain, thereby avoiding potential cross-reactivity with the expressed C-terminal TAR peptide (**Fig 3.3.13A**). Co-localisation analysis revealed no significant difference in the DAPI-CALCR overlap coefficient between EGFP-positive cells expressing the TAR peptide and those expressing the SCR control (**Fig 3.3.13B, C**). These findings indicate that competitive disruption of the FLNa-CALCR interaction is insufficient to alter CALCR localisation in SR-ACFs.

As I observed a reduction in $FLNa^{CT}$ abundance in AF-ACFs, I next assessed whether loss of FLNa itself, using siRNA-mediated knockdown, was sufficient to alter CALCR's subcellular distribution. After a 48h siRNA transfection period, there was a robust reduction in *FLNA* mRNA (~90%) and $FLNa^{CT}$ (28%) and $FLNa^{FL}$ protein (44%) suggesting successful knockdown of FLNa (**Fig 3.3.14A-D**). These results fell short of statistical significance due to the limited sample size (N=3). However, in both SR- and AF-ACFs (N=3 per group) there was no effect on CALCR's localisation as assessed by the DAPI-CALCR overlap coefficient (**Fig 3.3.14E-H**).

These data suggest that FLNa binding to CALCR is not a major determinant of physiological CALCR surface expression and that disruption of this interaction, either through the targeted construct or with a cruder FLNa knockdown approach, alone does not recapitulate the CALCR internalisation observed in AF.

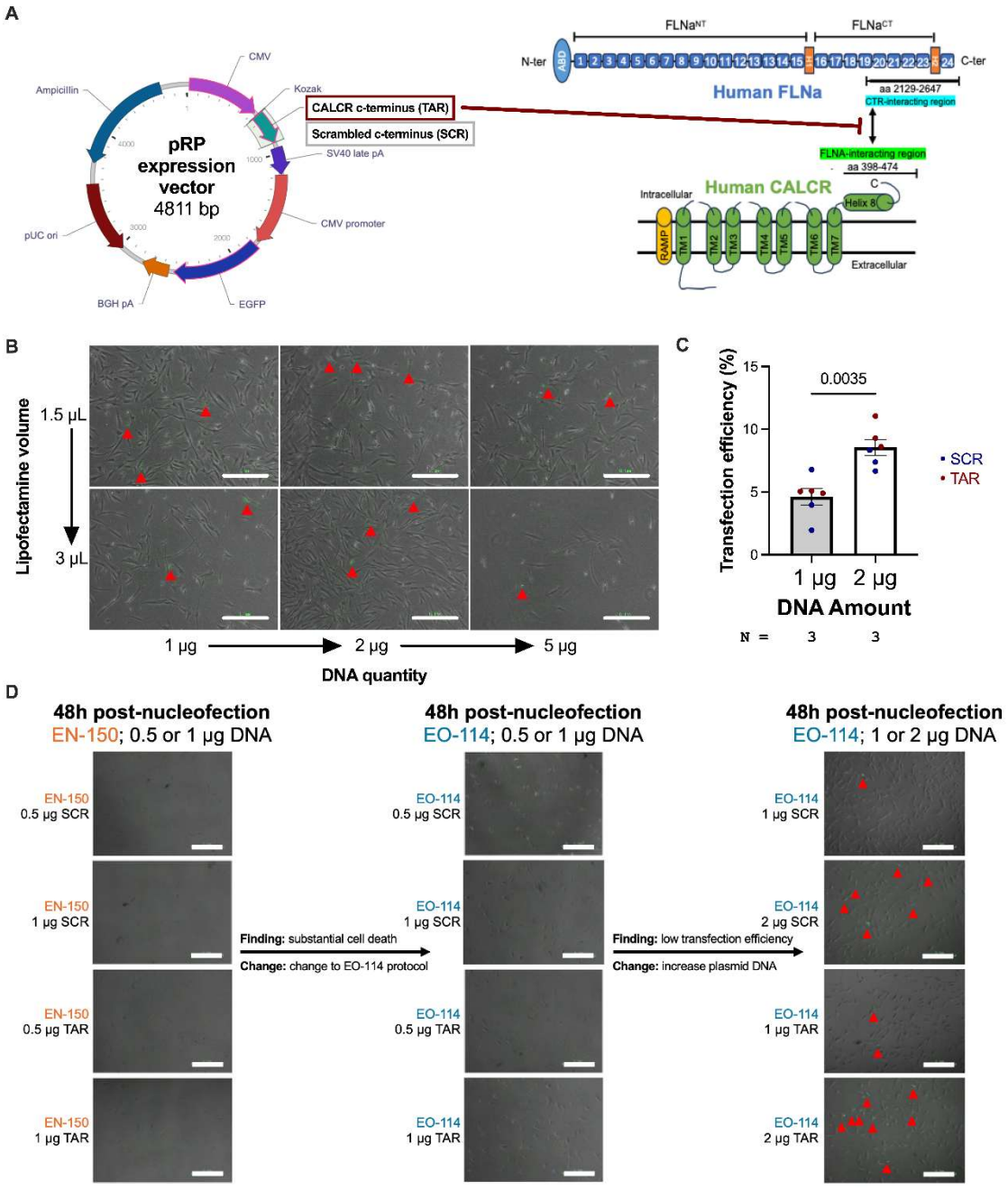

A
pRP expression vector 4811 bp
CMV
Kozak
CALCR c-terminus (TAR)
Scrambled c-terminus (SCR)
SV40 late pA
CMV promoter
EGFP
BGH pA
pUC ori
Ampicillin
FLNaNT
FLNaCT
N-ter
C-ter
Human FLNa
aa 2129-2647
CTR-interacting region
FLNA-interacting region
aa 398-474
Human CALCR
Intracellular
Extracellular
Helix 8
RAMP
TM1
TM2
TM3
TM4
TM5
TM6
TM7
B
Lipofectamine volume
1.5 µL
3 µL
1 µg
2 µg
5 µg
DNA quantity
C
Transfection efficiency (%)
0.0035
SCR
TAR
1 µg
2 µg
DNA Amount
N = 3 3
D
48h post-nucleofection
EN-150; 0.5 or 1 µg DNA
EN-150 0.5 µg SCR
EN-150 1 µg SCR
EN-150 0.5 µg TAR
EN-150 1 µg TAR
Finding: substantial cell death
Change: change to EO-114 protocol
48h post-nucleofection
EO-114; 0.5 or 1 µg DNA
EO-114 0.5 µg SCR
EO-114 1 µg SCR
EO-114 0.5 µg TAR
EO-114 1 µg TAR
Finding: low transfection efficiency
Change: increase plasmid DNA
48h post-nucleofection
EO-114; 1 or 2 µg DNA
EO-114 1 µg SCR
EO-114 2 µg SCR
EO-114 1 µg TAR
EO-114 2 µg TAR

Figure 3.3.12 Design and optimisation of a CALCR C-terminal disrupting peptide to interfere with FLNa-CALCR interactions. (A) Schematic of the plasmid encoding a peptide corresponding to the C-terminal FLNa-interacting region of CALCR (CALCR C-term [TAR]), or scrambled sequence control (SCR) cloned into a pRP expression vector under a CMV promoter with an EGFP reporter. **(B)** Representative merged phase-contrast and fluorescence images demonstrating attempted plasmid delivery into ACFs by lipotransfection, which resulted in minimal EGFP expression (red arrowheads). **(C)** Comparison of nucleofection transfection efficiency using 1 versus 2 µg plasmid DNA under the optimal program (EO-114), SCR and TAR transfections pooled from 3 donors. **(D)** Optimisation of plasmid delivery by nucleofection using multiple electroporation programs and conditions (EN-150, EO-114). Scale bar, 100 µm. Data expressed as mean ± SEM, *two-tailed paired t-test*.

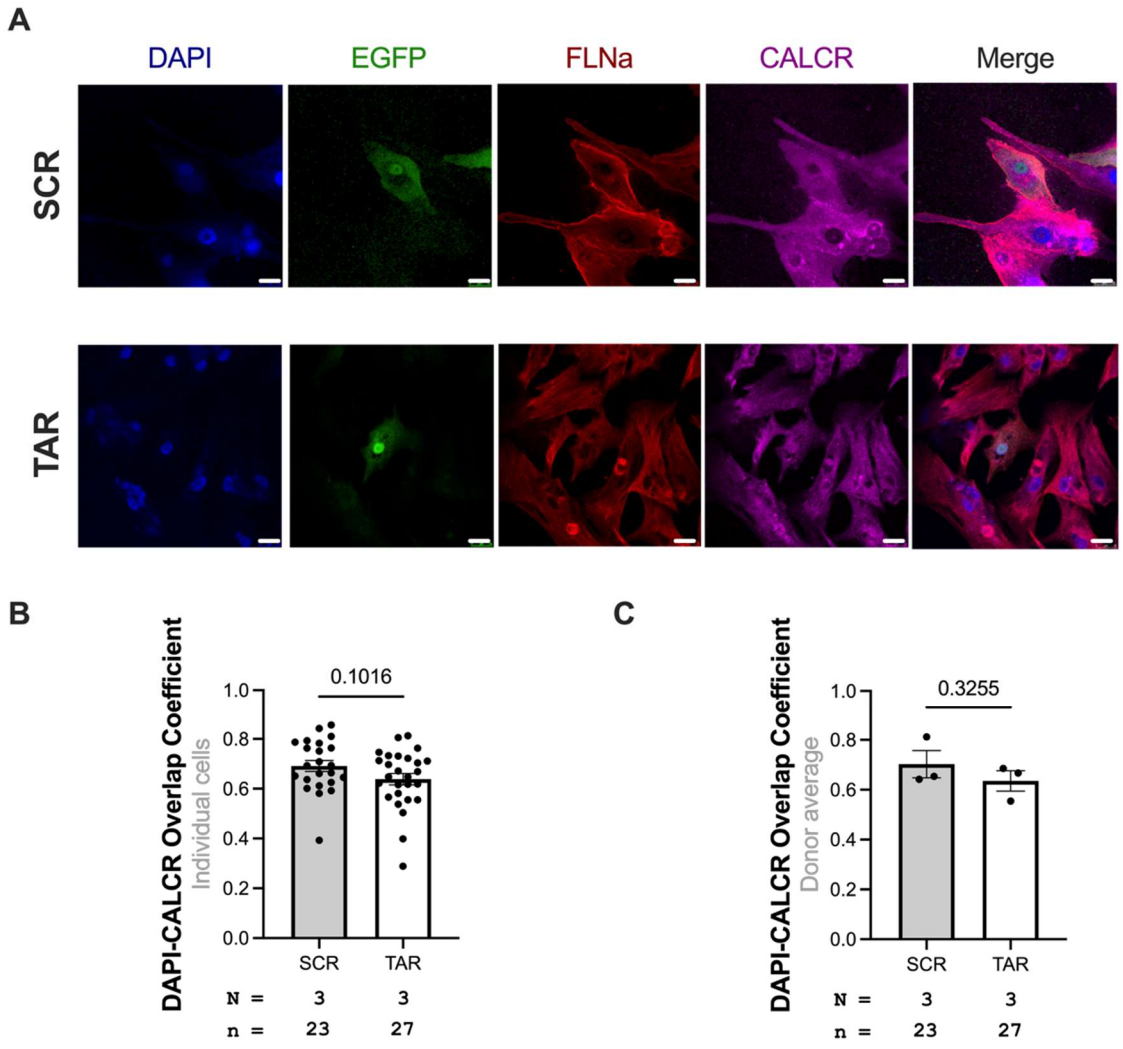


Figure 3.3.13 Expression of a FLNa-CALCR disrupting peptide does not affect CALCR localisation. (A) Representative immunofluorescence images of SR-ACFs following transfection with a scrambled control (SCR) peptide or a FLNa-CALCR targeting (TAR) peptide. Cells were immunostained for FLNa (red) and CALCR (N-terminus, green), with nuclei counterstained using DAPI (blue). EGFP expression (green) identified successfully transfected cells. Scale bar, 25 μm. **(B)** Quantification of the DAPI-CALCR overlap coefficient for single EGFP-positive cells from ≥3 fields per condition across N=3 independent SR donors. Mean ± SEM, *two-tailed unpaired t-test* **(C)** Donor-averaged DAPI-CALCR overlap coefficients. Median (IQR), *Wilcoxon signed-rank matched pairs test*.

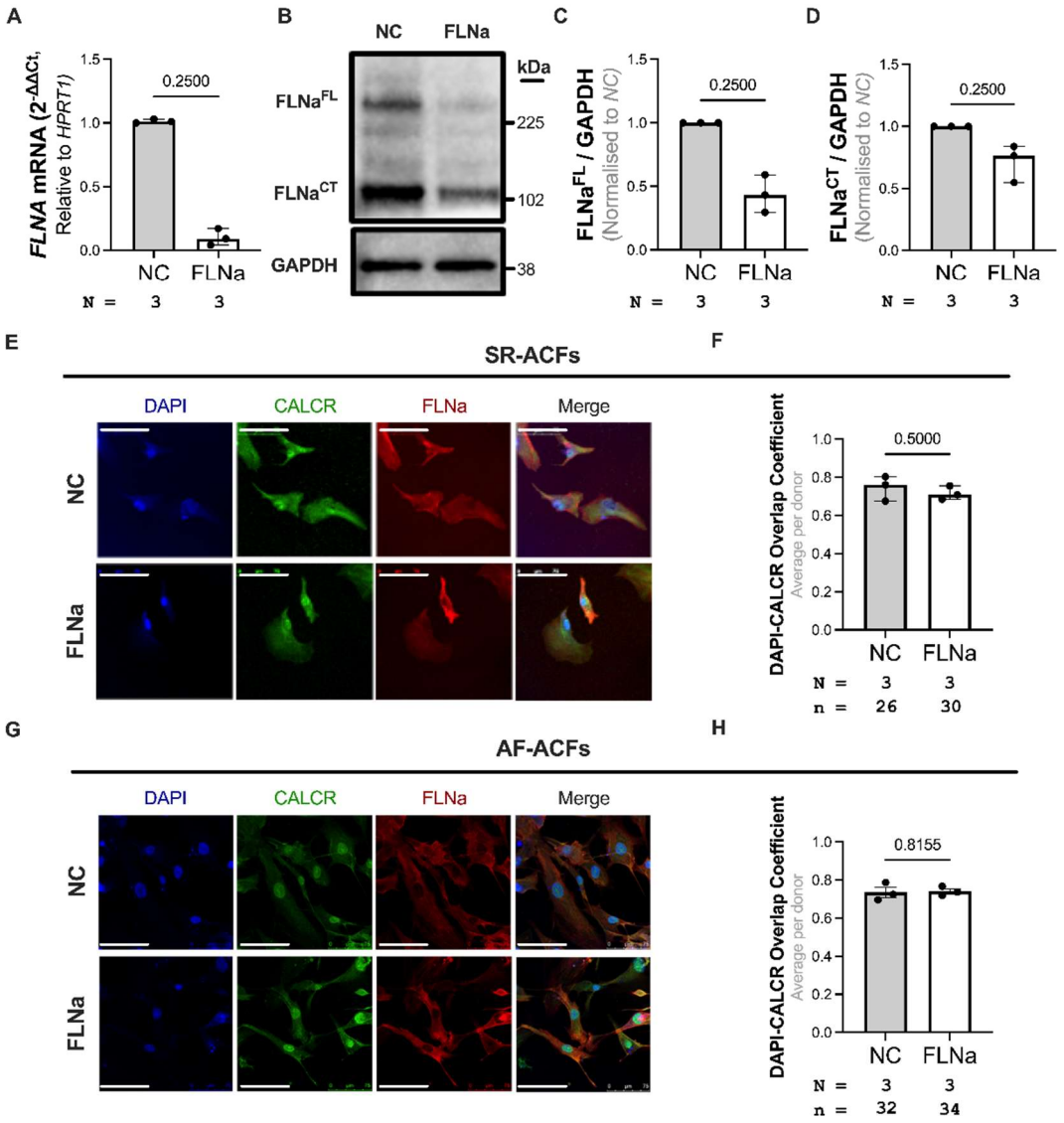


Figure 3.3.14 FLNa siRNA-knockdown does not affect CALCR localisation. (A) Quantification of *FLNA* mRNA after non-targeting control (NC) or anti-FLNa (FLNa) siRNA treatment for 48h. **(B)** Representative WB for $FLNa^{FL}$ and $FLNa^{CT}$ after siRNA-mediated knockdown, with GAPDH as a loading control. **(C)** Quantification of $FLNa^{FL}$ protein and **(D)** $FLNa^{CT}$ protein in 3 independent donors. **(E)** Representative immunofluorescence images of SR-ACFs treated with NC or FLNa targeting siRNA. **(F)** DAPI-CALCR overlap coefficient averaged for each donor with ≥3 fields per condition across N=3 independent SR donors and ≥5 cells per donor. **(G)** As in E, but with AF-ACFs. **(H)** As for F, but with AF-ACFs. Scale bar, 75 μm. Data expressed as median (IQR) with *Wilcoxon matched-pairs signed rank test.*

3.4 Discussion

This chapter investigated whether altered FLNa expression, proteolytic processing, or turnover contribute to aberrant CALCR localisation in AF-ACFs. Building on prior studies in heterologous systems implicating FLNa-CALCR interactions in receptor recycling,[91] this work provides the first systematic evaluation of these mechanisms in primary ACFs. Collectively these findings demonstrate that although CALCR internalisation and reduced $FLNa^{CT}$ abundance co-exist in AF-ACFs, FLNa-CALCR binding is unlikely to be a primary determinant of CALCR localisation in this context. Furthermore, they reveal that the mechanisms governing FLNa proteolysis and turnover in human ACFs differ substantially from those described in transformed cell lines.

3.4.1 CALCR internalisation in AF-ACFs reflects redistribution to cytoskeletal compartments

Consistent with our previous observations, CALCR in AF-ACFs exhibited reduced membrane localisation and increased association with intracellular, cytoskeletal fractions.[1] However, confocal microscopy did not precisely pinpoint the compartment in which CALCR was internalised. Hence, subcellular fractionation demonstrated that CALCR was redistributed to cytoskeletal compartments, excluding true nuclear compartmentalisation, consistent with the lack of predicted NLS signal. Imaging flattened adherent fibroblasts has limited axial resolution and can cause perinuclear signal to project into the nuclear plane. Even with confocal z-stacks, axial displacement as small as 1 µm (the minimal axial increment on the microscope used) markedly reduced cellular definition.

The distinction between CALCR being in a *bona fide* nuclear versus perinuclear or cytoskeletal compartment is mechanistically important as it alludes to defects in membrane anchoring, cytoskeletal retention, or receptor trafficking rather than nuclear import. Together, these findings do not exclude the possibility of CALCR accumulation

within the perinuclear space (PNS), a region closely integrated with the cytoskeleton and implicated in protein trafficking.[140] Detection of lamin A/C – structural components of the nuclear lamina (the internal border of the PNS) in both nuclear and cytoskeletal fractions further supports this interpretation. Future studies using super-resolution microscopy, electron microscopy, or proximity-based assays (e.g. proximity ligation assay or Förster resonance energy transfer) with established nuclear envelope or cytoskeletal markers could refine CALCR localisation. Furthermore, an unbiased interactome analysis, as presented in Chapter 4, identified clues for novel potential regulators of CALCR redistribution in human AF-ACFs.

3.4.2 FLNa processing is altered in ACFs in patients with AF

A key observation was the reduction of $FLNa^{CT}$ in AF-ACFs, despite relatively preserved $FLNa^{FL}$ levels. This is notable because $FLNa^{CT}$ contains the reported CALCR-binding domain and has a distinct functional profile.[91] Consistent with the report by Seck *et al* (2003), I observed preferential co-immunoprecipitation of CALCR with $FLNa^{CT}$, rather than $FLNa^{FL}$, which suggests that this interaction does not directly anchor CALCR to the actin cytoskeleton, as the ABD is contained within $FLNa^{NT}$. While technical limitations may have reduced recovery of $FLNa^{FL}$ during co-immunoprecipitation, preferential binding of CALCR to $FLNa^{CT}$ is consistent with prior mapping studies which identified residues 2129-2330 as the CALCR-binding region, with enhanced interaction when compared with longer C-terminal constructs.[91]

However, $FLNa^{CT}$ did not accumulate in nuclear or cytoskeletal compartments in AF-ACFs, contrasting with reports of nuclear $FLNa^{CT}$ localisation in transformed cells and underscoring the importance of studying FLNa biology in primary human cells.[88,117] These data suggest that $FLNa^{CT}$-CALCR interactions are confined to membrane or immediate perimembrane pools and are disrupted upon CALCR internalisation in AF-ACFs. Although $FLNa^{CT}$ may contribute to limited receptor recycling from submembrane

compartments, this mechanism is unlikely to explain the pronounced CALCR internalisation observed in AF-ACFs. Surface biotinylation assays could directly test this possibility by resolving true surface receptors from those internalised but retained near the membrane.

3.4.3 Calpains and caspase 3 are not the predominant proteases responsible for $FLNa^{CT}$ generation in human ACFs

Although calpains are widely reported as mediators of FLNa cleavage and exhibit increased activity in AF atrial tissue, they did not account for $FLNa^{CT}$ generation in ACFs.[123,125] Despite reduced calpain 1 expression in AF-ACFs, total and calpeptin-sensitive calpain activity was unchanged, possibly reflecting regulation by local Ca^{2+} concentration, subcellular localisation, and substrate proximity in human ACFs.[122] Differences from tissue-level studies likely reflect contributions from other cell types, such as cardiomyocytes. Crucially, neither pharmacological inhibition nor siRNA-mediated knockdown of calpain 1 (similar to the reduction observed in AF-ACFs) reduced $FLNa^{CT}$ abundance, providing strong evidence that calpains do not mediate basal FLNa processing in ACFs. Similarly, although caspase 3 can cleave FLNa during apoptosis, its genetic suppression did not affect $FLNa^{CT}$ levels, consistent with the absence of apoptotic signalling in these cells.[126] Although CASP3 knockdown did not alter $FLNa^{CT}$ abundance, this experiment does not exclude redundancy among caspase family members. Future studies using a pan-caspase inhibitor could determine whether broader caspase activity contributes to basal FLNa processing in ACFs. Together, these findings indicate that FLNa proteolysis in human ACFs differs fundamentally from stress-induced or transformed cell models and is likely to be regulated in a cell-specific manner.

3.4.4 $FLNa^{CT}$ is not degraded by proteasomal or lysosomal pathways

To determine whether enhanced degradation contributes to reduced $FLNa^{CT}$ abundance, I examined potential involvement of proteasomal and lysosomal pathways. Firstly,

proteasome inhibition, over intervals encompassing the $FLNa^{CT}$ half-life, did not increase $FLNa^{CT}$ abundance, arguing against direct proteasomal turnover. Instead, prolonged inhibition resulted in accumulation of a higher-molecular-weight FLNa species that was neither detectably ubiquitinated nor associated with the characteristic polyubiquitin smear on WB. On this basis, I hypothesise the larger fragment is the ~110 kDa precursor to mature $FLNa^{CT}$, consistent with a reduction in the $FLNa^{CT}$ to $FLNa^{FL}$ ratio following proteasome inhibition.[116] In this model, proteasome inhibition indirectly impairs terminal FLNa processing driving precursor accumulation and reduced mature $FLNa^{CT}$. Mass spectrometric analysis of the accumulated band could directly test this hypothesis.

Similarly, lysosomal inhibition with bafilomycin A1 did not alter $FLNa^{CT}$ abundance, despite effective blockade of autophagic flux. Together, these data indicate that neither proteasomal nor lysosomal pathways are dominant regulators of $FLNa^{CT}$ turnover in ACFs. A limitation is that degradation inhibitors were not combined with translational blockade, and therefore compensatory reductions in $FLNa^{CT}$ synthesis may mask modest effects on degradation.

Overall, reduced $FLNa^{CT}$ (~53%) in AF-ACFs is unlikely to reflect impaired proteolytic cleavage of $FLNa^{FL}$ or $FLNa^{CT}$'s enhanced degradation. Closer examination of the original quantifications (**Fig 3.3.2**) revealed parallel, albeit non-significant, reductions in *FLNA* mRNA (~36%) and $FLNa^{FL}$ protein (~42%) in AF-ACFs, while the $FLNa^{CT}/FLNa^{FL}$ ratio remained preserved. If $FLNa^{FL}$ cleavage was reduced or $FLNa^{CT}$ degradation were to be enhanced, a reduction in the $FLNa^{CT}/FLNa^{FL}$ ratio would be expected, either through relative accumulation of $FLNa^{FL}$ or disproportionate loss of $FLNa^{CT}$. The preservation of this ratio instead supports the interpretation that the $FLNa^{CT}$ reduction may reflect an overall decrease in FLNa expression at the transcriptional and translational level, rather than altered post-translational processing. Increasing donor numbers would improve statistical power and clarify whether the apparent reductions in *FLNA* transcript and $FLNa^{FL}$ are significant.

3.4.5 FLNa-CALCR interaction is not a major determinant of CALCR localisation in ACFs

The central functional conclusion of this chapter is that disruption of FLNa-CALCR binding – either via a competitive CALCR C-terminal peptide or by siRNA-mediated FLNa knockdown – was insufficient to alter CALCR subcellular localisation in human ACFs. This contrasts with prior findings in heterologous systems and indicates that FLNa-CALCR interactions are not a major determinant of CALCR surface expression in this cell type.[91] On this basis, further in-depth characterisation of FLNa biology in ACFs was not pursued.

Competitive peptide strategies are well established in FLNa research, with dominant-negative fragments, encompassing Ig-like repeats 20-21, previously reported to successfully disrupt FLNa-receptor interactions.[141] The optimisation of non-viral transfections in ACFs, a notoriously difficult cell type to transfer, may prove useful for future studies.[142] However, expression and functional competition of the peptide could not be definitively confirmed: although EGFP fluorescence verified plasmid uptake, the FLAG-tagged peptide was not detected by immunoblotting, likely due to low transfection efficiency. Alternative explanations, including promoter competition and limited construct expression, cannot be excluded. As expression and functional competition of the TAR peptide could not be directly confirmed, this experiment alone cannot establish that disruption of the FLNa-CALCR interaction is without effect. Fusion directly with EGFP was avoided due to the likelihood of steric interference, given the size disparity between EGFP (239 amino acids) and SCR/TAR peptide (76 amino acids). A lentiviral approach could overcome these limitations.[143] Importantly, the concordant negative results obtained with FLNa knockdown independently supported the conclusion that FLNa does not play a major contributing role in CALCR localisation.

The experiments confirming gene knockdown following siRNA treatment were performed in a limited number of independent donors and, despite demonstrating substantial and consistent effect sizes, were underpowered to confirm the effect statistically. Similarly, the negative results for experiments with MG-132 (2h and 6h), bafilomycin A1, the disrupting peptide, and FLNa-knockdown were similarly underpowered and may have missed modest effects. Future studies should aim to repeat these experiments in more donors.

3.4.6 Conclusions and implications

In summary, this chapter delineates which aspects of FLNa biology are unlikely to underlie CALCR mislocalisation in human AF-ACFs and highlights the existence of FLNa-independent mechanisms regulating GPCR trafficking in ACFs. By systematically testing altered FLNa proteolysis, degradation, and FLNa-CALCR binding, and finding no evidence that these represent primary mechanisms, these findings narrow the mechanistic landscape governing CALCR trafficking in AF. They also highlight the fundamental differences between immortalised cell lines and primary ACFs, cautioning against direct extrapolation across systems. Finally, these results provide a foundation for subsequent chapters investigating alternative pathways driving CALCR mislocalisation and antifibrotic signalling dysfunction in AF.

CHAPTER 4: MECHANISTIC INTERROGATION OF ALTERNATIVE REGULATORS OF CALCR LOCALISATION

4.1 Introduction

The surface expression of CALCR in ACFs is theorised to be central to the integrity of the CT-CALCR antifibrotic axis.[1] Although FLNa has been proposed as a key regulator of CALCR surface recycling in heterologous cell systems, the data presented in Chapter 3 suggest that FLNa's association with CALCR is not a major regulator of CALCR's surface expression under these conditions.[91] The mechanistic basis of CALCR internalisation in AF-ACFs therefore remains unresolved.

As reviewed in **section 1.4**, GPCR surface expression is a complex, multifaceted process orchestrated by the coordinated action of numerous molecular regulators. Several processes have been studied specifically in the context of CALCR, or class B GPCRs more broadly, and include alternative splicing of the CALCR gene, co-expression of RAMPs, β-arrestin-dependent internalisation, and post-translational modifications, including N-linked glycosylation.[75,79,97,144]

I, therefore, hypothesised the internal redistribution of CALCR in ACFs in patients with AF may be due to disease-associated alterations in the receptor's molecular environment. To investigate this possibility, I characterised the CALCR interactome in human SR- and AF-derived ACFs using immunoprecipitation (IP) coupled with mass spectrometry (MS), enabling characterisation of the disease-state-specific CALCR interactome and hypothesis-generating KEGG pathway analysis of putative interactors. Guided by the interactome findings, I then assessed the functional contribution of clathrin-mediated endocytosis (CME) and actin-dependent trafficking to CALCR localisation using selective inhibitors. In parallel, the previously described regulators of CALCR surface expression were systematically evaluated in primary human ACFs for the first time. The overarching aim of these experiments was to narrow the mechanistic field and identify the most tractable molecular determinants of the AF-associated CALCR trafficking defect.

4.2 Methods & Materials

4.2.1 Sample preparation, mass spectrometry (MS) & data analysis of the CALCR interactome

To explore the interactome of FLNa and CALCR in SR- and AF-ACFs, FLNa and CALCR were immunoprecipitated (along with an IgG isotype control) in passage 2-3 ACFs from 4 SR and 4 AF donors as described in **section 2.4**. The enrichment of CALCR is demonstrated in **Fig 3.3.2E**. Immunoprecipitates, prior to elution, were sent for MS analysis to the Technical University of Denmark's Proteomics Core and the following methods and analyses were contributed by Biogenity, Denmark.

20 µL of lysis buffer (6M Guanidinium Hydrochloride, 10 mM TCEP, 40 mM CAA, 50 mM HEPES pH 8.5) was added to each immunoprecipitated sample, followed by sonication on high for three cycles of 30s on and 30s off in a Bioruptor Pico sonication water bath (Diagenode) at 4°C. Samples were diluted 3x with digestion buffer (10% Acetonitrile in 50 mM HEPES pH 8.5) and 200 ng of LysC (MS-grade Wako) was added. Samples were incubated for 3 hours at 37°C, shaking at 1000 RPM. After LysC digestion, samples were diluted to a final 10x in digestion buffer and digested with 100 ng Trypsin (MS-Grade, Sigma Aldrich) for 16 hours at 37°C, shaking at 1000 RPM. Digestion was stopped by adding 2% trifluoroacetic acid (TFA) to a final concentration of 1%. Samples were centrifuged for 1 minute at 1500 RCF to pellet the beads, and supernatants were desalted on a SOLAµ SPE plate (HRP, Thermo). Between each application, the solvent was spun through by centrifugation at 350 RCF. For each sample, the filters were activated with 200 µL of 100% Methanol, then 200 µL of 80% Acetonitrile, 0.1% formic acid. The filters were equilibrated twice with 200 µL of 1% TFA, 3% Acetonitrile, after which the sample was loaded. After washing the tips twice with 200 µL of 0.1% formic acid, the peptides were eluted into clean Eppendorf Protein LoBind tubes using 40% Acetonitrile, 0.1% formic acid. The eluted peptides were concentrated in an Eppendorf

Speedvac and subsequently reconstituted in A* buffer (2% Acetonitrile, 1% TFA) with iRT peptides (Biognosys).

Peptides were loaded onto a 2cm C18 trap column (ThermoFisher 164946), connected in-line to a 15cm C18 reverse-phase analytical column (Thermo EasySpray ES904) using 100% Buffer A (0.1% Formic acid in water) at 750 bar, using the Thermo EasyLC 1200 HPLC system, and the column oven operating at 30°C. Peptides were eluted over a 70 minute gradient ranging from 10% to 60% of Buffer B (80% acetonitrile, 0.1% formic acid) at 250 nl/min, and the Orbitrap Exploris instrument (Thermo Fisher Scientific) was run in data-independent acquisition (DIA) mode with FAIMS ProTM Interface (ThermoFisher Scientific) with CV of -45 V. Full MS spectra were collected at a resolution of 120,000, with an AGC target of 300% or maximum injection time set to 'auto' and a scan range of 400–1000 m/z. The MS2 spectra were obtained in DIA mode in the orbitrap operating at a resolution of 60,000, with an AGC target 1000% or maximum injection time set to 'auto', a normalised HCD collision energy of 32. The isolation window was set to 6 m/z with a 1 m/z overlap and window placement on. Each DIA experiment covered a range of 200 m/z resulting in three DIA experiments (400-600 m/z, 600-800 m/z and 800-1000 m/z). Between the DIA experiments a full MS scan was performed. MS performance was verified for consistency by running complex cell lysate quality control standards, and chromatography was monitored to check for reproducibility.

The raw files were analysed using SpectronautTM (version 19.0). Spectra were matched against the human reviewed UniProt database. The data were searched with the BGS workflow with Oxidation (M) and Acetyl on protein N-termini as dynamic modifications. Cysteine carbamidomethyl was set as a static modification. The proteotypicity filter was turned on, MS quantity level to MS1 and local normalization was turned on. For statistical enrichment analyses, the data was filtered so only proteins with 2 unique peptides and at least 60% valid values across all samples, or at least 75% within an experimental group were used in the downstream data analysis. Expression data were $\log_2$

transformed as this substantially improved normality. Statistical significance was assessed by either limma (normal) or Wilcoxon signed-rank (non-normal) test depending on whether the proteins demonstrated a normal distribution or not.[145] Filtration and statistical analysis were performed in the R programming language. Interaction scores were calculated using the MIST R scripts based on the log transformed Intensity.[146]

4.2.2 Data Analysis and KEGG pathway analysis

For unique interactor analysis, unfiltered log_2 transformed intensity data were analysed. Disease-state unique interactors were defined as those proteins identified in ≥3/4 biological replicates for the CALCR pulldown, and absent in ≥3/4 of the donor-matched IgG negative control pulldown. Unique interactors were subjected to Kyoto Encyclopedia of Genes and Genomes (KEGG) pathway analysis using ShinyGO 0.85.1, with the list of all human protein-coding genes set as background.[147]

4.2.3 Endocytosis and N-glycosylation inhibition

Human AF-ACFs were seeded at a density of 5,000 per well in 8-well µ-Slides. At 70% confluency, cells were serum starved (0.5% FBS) for 4h prior to treatment with Dyngo4A (10 µM, ab120689-5mg, Abcam), chlorpromazine (10 µM, C8138-5G, Merck), and cytochalasin D (100 nM, sc-201442, Insight Biotechnology) for the durations indicated. After treatment, cells were fixed and stained for CALCR and FLNa, as described in Chapter 2. N-glycosylation was also inhibited using tunicamycin (1 µg/mL, T7765-10MG, Merck) during a 24h treatment before assessment of CALCR localisation or CALCR expression by WB (as described in **section 2.3**).

4.2.4 RT-qPCR for CALCR splice variants

To assess the presence of CALCR splice variants, differing by a 48 bp insert, total RNA was isolated from SR- and AF-ACFs (*mirVana* miRNA Isolation Kit, #AM1561, Invitrogen), as per the manufacturer's protocol. RNA concentration was measured using

an LVis plate (BMG Labtech) and 200 ng of RNA was reverse transcribed using the QuantiTect Reverse Transcription Kit (205311, Qiagen), as per the manufacturer's protocol. PCR amplification was carried out using custom-designed primers flanking either side of the 48bp insert region (Forward: 5'-CACACCGGCTGGAGTATTGT-3'; Reverse: 5'-CTTCGCACGAGCTCTCCATT-3') using the Q5 High-Fidelity polymerase (M0492S, New England Biolabs). Reactions were performed under the following cycling conditions: initial denaturation at 98ºC for 30s; followed by 35 cycles of denaturation at 98ºC for 8 seconds, annealing at 62ºC for 30s, and elongation at 72ºC for 30s; with a final extension step at 72ºC for 120 seconds. Samples were then held at 10ºC. PCR products were separated on 2% (w/v) agarose gel containing SYBR Safe DNA stain (1:40,000 v/v) and electrophoresed in SB buffer. A 100 bp HyperLadder DNA marker was included to determine amplicon size and distinguish splice variants based on the expected 48 bp size difference. Bands were imaged using a Bio-Rad ChemiDoc system. PCR products were sent to Source Bioscience for Sanger sequencing to confirm sequence.

4.3 Results

4.3.1 Quality assessment and global overview of the CALCR interactome

To explore the interactome of CALCR, CALCR (or IgG isotype control) was immunoprecipitated from 4 unique SR- and AF-donor derived ACFs. The efficiency of the pulldown was confirmed by WB (**Fig 3.3.2E**). Mass spectrometry identified more unique proteins in the CALCR IPs than in the IgG controls, whereas total protein abundance was higher in the IgG controls (CALCR vs IgG, **Fig 4.3.1A**, **B**). Principal component analysis (PCA) revealed separation of CALCR and IgG IP samples (**Fig 4.3.1C**). Together, these analyses confirm the quality of the dataset and the effective enrichment of a CALCR interactome, that is distinguishable from the species-specific isotype control, prior to downstream pathway interrogation. Across all groups, 1162 quantifiable proteins were detected after filtering. Differential expression analysis, across all groups, considered 3157 comparisons of which 503 were nominally significant ($p<0.05$) (**Table 4.1**). However, only 1 comparison, the enrichment of peroxiredoxin 4 (PRDX4) in AF-ACFs compared to AF-ACF IgG controls, remained significant after Benjamini-Hochberg adjustment for multiple comparisons (**Fig 4.3.1D-E**, **Table 4.1**).[148]

Figure 4.3.1 Quality assessment and overview of the CALCR interactome from 4 unique SR- and AF-ACFs. (A) Number of proteins identified per sample group. **(B)** Total summed protein abundance per sample group. **(C)** Principal component analysis (PCA) of log_2-transformed protein intensities (PC1: 38%; PC2: 13%). **(D)** Volcano plot of CALCR_AF versus IgG_AF. Vertical dashed lines indicate $|log_2(FoldChange)| = 1$ and horizontal lines indicate unadjusted p-values (bottom) or adjusted p-values (top) = 0.05. The one significant protein (PRDX4) is indicated in red. **(E)** Log_2-transformed expression of PRDX4 in CALCR_AF and IgG_AF groups. Mean ± SEM; *limma test after Benjamini-Hochberg correction*.

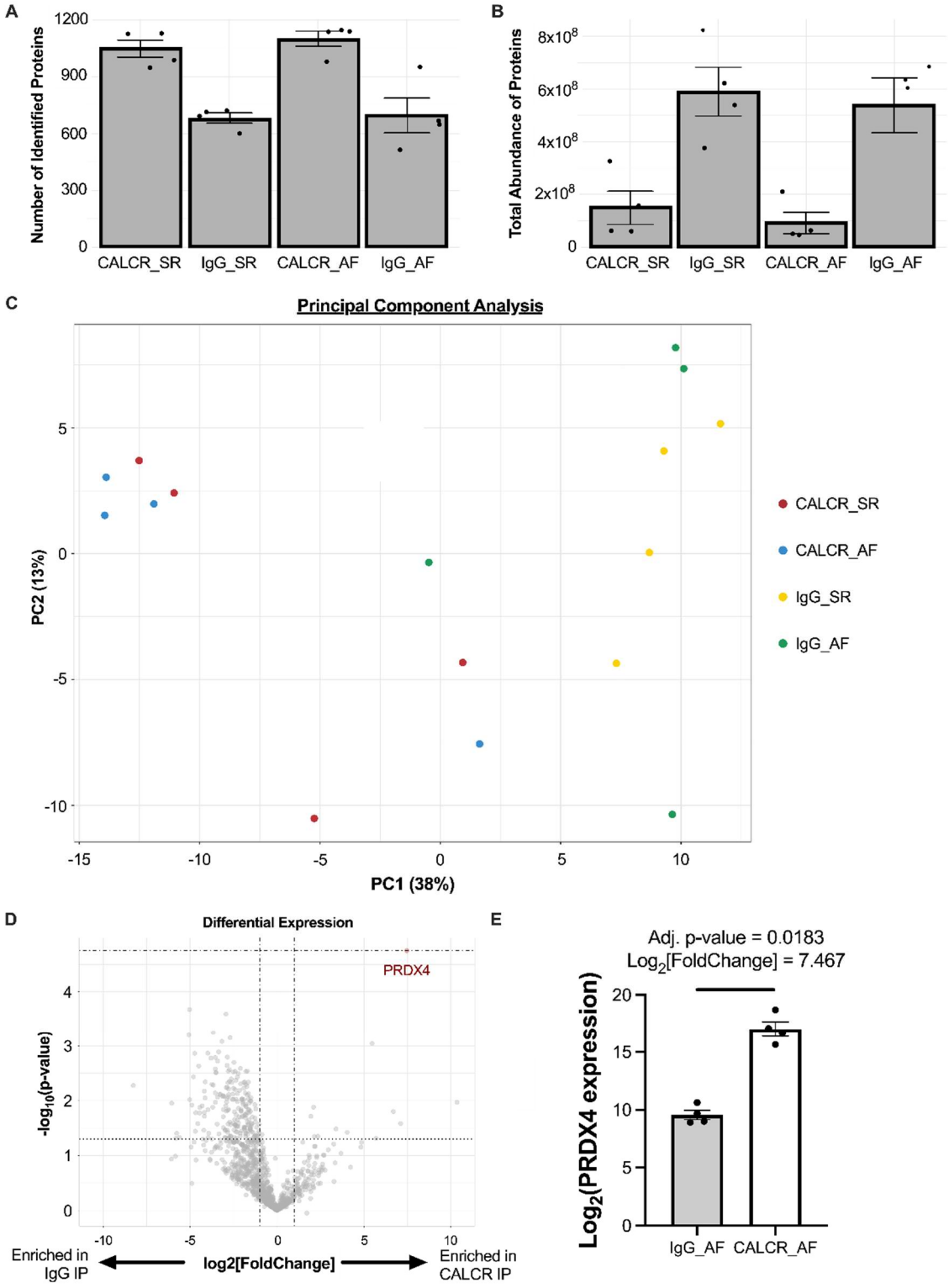

A
Number of Identified Proteins
1200
900
600
300
0
CALCR_SR
IgG_SR
CALCR_AF
IgG_AF
B
Total Abundance of Proteins
8x10^8
6x10^8
4x10^8
2x10^8
0
CALCR_SR
IgG_SR
CALCR_AF
IgG_AF
C
Principal Component Analysis
PC2 (13%)
PC1 (38%)
CALCR_SR
CALCR_AF
IgG_SR
IgG_AF
D
Differential Expression
PRDX4
-log10(p-value)
Enriched in IgG IP
log2[FoldChange]
Enriched in CALCR IP
E
Adj. p-value = 0.0183
Log2[FoldChange] = 7.467
Log2(PRDX4 expression)
IgG_AF
CALCR_AF

Table 4.1: Summary of differential protein enrichment across comparisons in the CALCR interactome dataset.

Comparisons:	Number of proteins with p-value ≤ 0.05	Number of proteins with adjusted p-value ≤ 0.05	Number of proteins with |log2 (fold change)| ≥ 1 and adjusted p-value ≤ 0.05:
CALCR SR vs CALCR AF	48 (40 enriched in CALCR SR)	0	0
CALCR SR vs IgG SR	234 (31 enriched in CALCR)	0	0
CALCR AF vs IgG AF	221 (12 enriched in CALCR)	1	1

4.3.2 KEGG pathway analysis of unique interactors

As few proteins passed statistical thresholds, and those that did in the unadjusted analyses were mostly enriched in the IgG pulldown, I complemented the study with a qualitative, unique-interactor analysis to identify disease-specific, candidate binding partners. Unique interactors were defined as proteins observed in ≥3/4 donors after CALCR pulldown and not detected in ≥3/4 IgG pulldowns. This hypothesis-generating approach identified 169 proteins unique to the SR-ACF CALCR pulldown and 427 unique to the AF-ACF CALCR pulldown suggesting AF-specific remodelling of the receptor-associated complex (**Appendices 1** and **2**). On these putative disease-specific CALCR interactors, I performed a KEGG pathway analysis and ranked enriched pathways by fold enrichment (**Fig 4.3.2A,B** and **Tables 4.2** and **4.3**).[147,149] This analysis identified pathways commonly enriched in affinity purification mass spectrometry approaches (e.g. Ribosome, Spliceosome, Proteasome) due to the frequent interactions between bait proteins and some of the proteins in these pathways, but it also identified candidate pathways that may contribute to CALCR surface trafficking in SR-ACFs (e.g. Nucleocytoplasmic transport, **Fig 4.3.2C**) or internalisation in AF-ACFs (e.g. Endocytosis, **Fig 4.3.2D**).

Despite the absence of these proteins in the donor-matched IgG pulldowns, I further interrogated the proteins within enriched pathways by cross-referencing them with the

CRAPome (Contaminant Repository for Affinity Purification) database.[150] The CRAPome aggregates negative control data from many affinity purification mass spectrometry experiments to identify, and score, likely nonspecific interactors that may not have been identified in my own negative-control dataset due to undetected variations (at any experimental step) or unreliable detection of low-abundance peptides.[150] Genes encoding proteins that are common (appearing in >50% of negative control datasets) are highlighted in red in **Tables 4.2** and **4.3**. This additional annotation of likely non-specific interactors provides additional stringency and indicated enriched pathways that may be contributed to by likely non-specific contaminants (e.g. Spliceosome).

Table 4.2: **Significantly enriched KEGG pathways (ranked by fold enrichment) among putative CALCR interactors in SR-ACFs.** Genes in red text indicate those genes identified in ≥50% of negative control experiments performed in Homo sapiens in the CRAPome database.[150] Analysis performed using ShinyGO 0.85.1.[147]

KEGG Pathway	# Proteins / # Proteins in Pathway	Fold Enrichment (FDR)	Genes
hsa03040 Spliceosome	9/185	6.7 (0.001344)	DDX5, DHX15, HNRNPA3, PUF60, HNRNPA1, SNU13, PRPF40A, SRSF7, U2AF1
hsa03013 Nucleocytoplasmic transport	5/107	6.4 (0.042271)	UPF2, KPNA2, UPF1, NUP93, NUP58
hsa03010 Ribosome	6/158	5.2 (0.042271)	MRPL13, MRPL22, RPSA, RPL22, RPL36AL, RPLP0
hsa05168 Herpes simplex virus 1 infection	6/181	4.6 (0.046456)	JAK1, EIF2AK2, ZC3HAV1, SRSF7, TAP2, C3
hsa04820 Cytoskeleton in muscle cells	7/232	4.2 (0.042271)	COL1A2, COL5A2, LMNA, BGN, SNTB2, PDLIM4, PDLIM7
hsa05171 Coronavirus disease-COVID-19	7/234	4.1 (0.042271)	JAK1, RPSA, EIF2AK2, RPL22, RPL36AL, RPLP0, C3
hsa05014 Amyotrophic lateral sclerosis	10/367	3.7 (0.028144)	ADRM1, DCTN3, HNRNPA3, HNRNPA1, MAP2K3, PSMA2, PSMB7, SRSF7, NUP93, NUP58

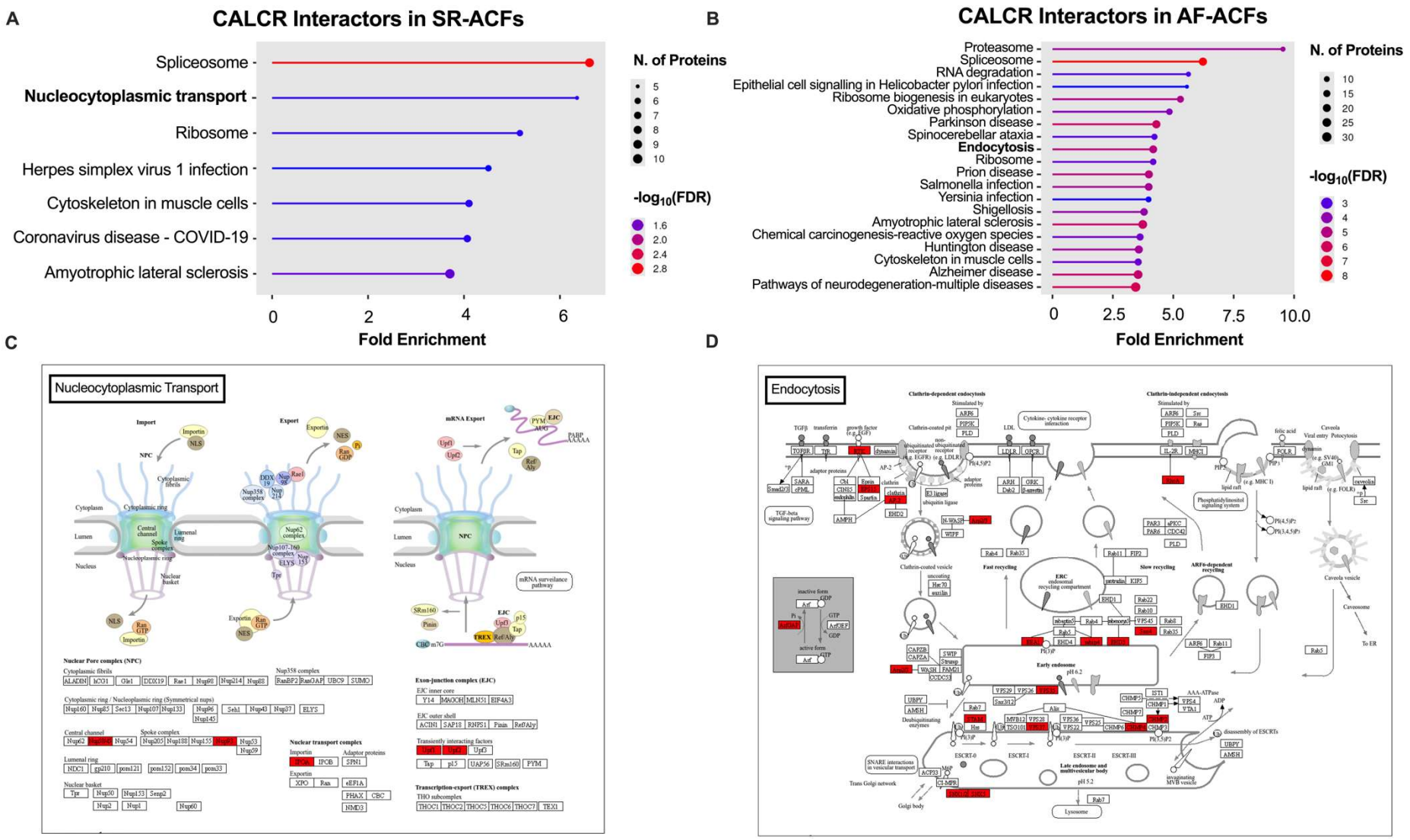


Figure 4.3.2 KEGG pathway analysis of unique CALCR interactors in SR- and AF-ACFs. KEGG pathway analysis for unique CALCR interactors in SR-ACFs **(A)** and AF-ACFs **(B)**, ranked by fold enrichment. Dot size represents the number of genes mapped to each pathway, and colour indicates log10(FDR). **(C-D)** KEGG Nucleocytoplasmic transport (C) and Endocytosis (D) pathway maps. Identified interactors are highlighted in red.

Table 4.3: **Top 20 enriched KEGG pathways (ranked by fold enrichment) among putative CALCR interactors in AF-ACFs.** Genes in red text indicate those genes identified in ≥ 50% of negative control experiments performed in Homo sapiens in the CRAPome database.[150] Analysis performed using ShinyGO 0.85.1.[147]

KEGG Pathway	# Proteins / # Proteins in Pathway	Fold Enrichment (FDR)	Genes
hsa03050 Proteasome	8/46	9.5 (4.18E-05)	PSMA1, PSMA3, PSMB4, PSMC6, PSMD4, PSMD12, PSME2, PSMF1
hsa03040 Spliceosome	21/185	6.2 (8.21E-09)	SF3B4, CHERP, SRSF10, SF3B2, SNW1, ACIN1, SF3B1, PRPF31, PRPF19, PLRG1, RBM25, SRSF1, SRSF5, TRA2B, SNRPA1, SNRPC, SNRPD1, SNRPE, PHF5A, SRSF9, SNRNP40
hsa03018 RNA degradation	8/78	5.6 (0.0013811)	XRN2, DIS3, EDC4, CNOT3, EXOSC10, XRN1, SKIC8, CNOT9
hsa05120 Epithelial cell signalling in Helicobacter pylori infection	7/69	5.6 (0.0036379)	TCIRG1, CSK, ATP6V1D, ATP6V1B2, PTPN11, RELA, MAP2K4
hsa03008 Ribosome biogenesis in eukaryotes	14/145	5.3 (1.59E-05)	NXF1, RPP38, UTP14A, POP1, CSNK2B, DKC1, XRN2, MDN1, GNL3, SBDS, XRN1, NAT10, RIOK2, UTP4
hsa00190 Oxidative phosphorylation	12/136	4.8 (0.0001663)	TCIRG1, COX4I1, COX5B, NDUFA5, NDUFB10, NDUFS1, NDUFV2, ATP6V1D, ATP5ME, ATP6V1B2, SDHB, UQCRC2
hsa05012 Parkinson disease	21/268	4.3 (1.79E-06)	TRAP1, COX4I1, COX5B, GNAI2, SLC25A4, KLC1, NDUFA5, NDUFB10, NDUFS1, NDUFV2, PSMA1, PSMA3, PSMB4, PSMC6, PSMD4, PSMD12, RPS27A, SDHB, TUBA4A, UQCRC2, CAMK2G
hsa05017 Spinocerebellar ataxia	11/143	4.2 (0.0010835)	ATXN2L, SLC25A4, ATP2A2, OPA1, PSMA1, PSMA3, PSMB4, PSMC6, PSMD4, PSMD12, TBPL1
hsa04144 Endocytosis	19/250	4.2 (7.67E-06)	ARPC4, ACTR2, ARPC2, AP2S1, CHMP4B, VPS37A, CHMP2A, EHD3, RHOA, PDGFRA, VPS35, EPS15L1, SNX6, SNX2, RUFY1, STAM, EEA1, SNX4, ASAP2
hsa03010 Ribosome	12/158	4.2 (0.0006127)	MRPL3, RPL22L1, MRPL15, MRPL2, MRPS17, MRPL16, RPLP1, RPS26, RPS27A, MRPS9, MRPL24, MRPL33
hsa05020 Prion disease	20/275	4.0 (7.67E-06)	COX4I1, COX5B, CSNK2B, SLC25A4, KLC1, NDUFA5, NDUFB10, NDUFS1, NDUFV2, PPP3R1, MAPK3, PSMA1, PSMA3, PSMB4, PSMC6, PSMD4, PSMD12, SDHB, TUBA4A, UQCRC2

hsa05132 Salmonella infection	18/248	4.0 (2.46E-05)	ARPC4, ACTR2, ARPC2, ACTR1B, EXOC5, CSE1L, CTNNB1, KLC1, RHOA, PFN2, PIK3C2A, ARL8B, MAPK3, RELA, MAP2K4, ACBD3, SKP1, TUBA4A
hsa05135 Yersinia infection	10/138	4.0 (0.0033782)	ARPC4, ACTR2, ARPC2, IL2, RHOA, MAPK3, PXN, RELA, MAP2K4, ARHGEF7
hsa05131 Shigellosis	17/246	3.8 (7.27E-05)	ARPC4, ACTR2, ARPC2, H3C14, DIAPH1, H3C15, RHOA, PFN2, PPID, ATG16L1, MAPK3, PXN, RELA, RPS27A, SKP1, H3C13, SQSTM1
hsa05014 Amyotrophic lateral sclerosis	25/367	3.7 (1.79E-06)	ACTR1B, NXF1, ATXN2L, COX4I1, COX5B, ANXA11, KLC1, NDUFA5, NDUFB10, NDUFS1, NDUFV2, PFN2, PPP3R1, PSMA1, PSMA3, PSMB4, PSMC6, PSMD4, PSMD12, RANBP2, SDHB, TUBA4A, UQCRC2, SQSTM1, NUP153
hsa05208 Chemical carcinogenesis-reactive oxygen species	15/227	3.6 (0.0004014)	COX4I1, COX5B, SLC25A4, GSTM3, GSTT1, NDUFA5. NDUFB10, NDUFS1, NDUFV2, MAPK3, PTPN11, RELA, SDHB, MAP2K4, UQCRC2
hsa05016 Huntington disease	20/307	3.6 (2.99E-05)	ACTR1B, AP2S1, COX4I1, COX5B, SLC25A4, KLC1, NDUFA5, NDUFB10, NDUFS1, NDUFV2, PSMA1, PSMA3, PSMB4, PSMC6, PSMD4, PSMD12, SDHB, TUBA4A, UQCRC2, TBPL1
hsa04820 Cytoskeleton in muscle cells	15/232	3.5 (0.0004833)	FMNL2, COL4A2, COL5A1, COL6A2, DIAPH1, DSP, EMD, NID2, DAAM1, SUN2, AMPD2, HSPG2, THBS2, ZYX, TMEM43
hsa05010 Alzheimer disease	25/387	3.5 (3.16E-06)	COX4I, COX5B, CSNK2B, CTNNB1, NCSTN, SLC25A4, KLC1, NDUFA5, NDUFB10, NDUFS1, NDUFV2, ATP2A2, PPID, PPP3R1, MAPK3, PSMA1, PSMA3, PSMB4, PSMC6, PSMD4, PSMD12, RELA, SDHB, TUBA4A, UQCRC2
hsa05022 Pathways of neurodegeneration-multiple diseases	30/478	3.4 (7.02E-07)	ACTR1B, TRAP1, ATXN2L, COX4I1, COX5B, CSNK2B, CTNNB1, SLC25A4, KLC1, NDUFA5, NDUFB10, NDUFS1, NDUFV2, ATP2A2, PPID, PPP3R1, MAPK3, PSMA1, PSMA3, PSMB4, PSMC6, PSMD4, PSMD12, RELA, RPS27A, SDHB, TUBA4A, UQCRC2, CAMK2G, SQSTM1

4.3.3 Inhibition of endocytosis does not affect CALCR localisation

Notably, endocytosis emerged as a significantly enriched KEGG pathway in the AF CALCR interactome, demonstrating a 4.2-fold enrichment with 19 contributing proteins. Importantly, none of these proteins were reported as non-specific contaminants in the CRAPome database, supporting the specificity of this enrichment.[150] The overrepresentation of endocytosis-associated proteins indicates increased recruitment of trafficking machinery to CALCR in AF-ACFs, consistent with a mechanistic role in receptor internalisation.

Several interactors mapped directly to CME, the principal pathway governing GPCR internalisation following phosphorylation.[75] Adaptor Related Protein Complex 2 Subunit Sigma 1 (AP2S1) encodes the σ subunit of the heterotetrameric AP-2 adaptor complex, which participates in cargo selection and clathrin coat assembly during vesicle formation.[151] Epidermal growth factor receptor pathway substrate 15 like 1 (EPS15L1) is a well-characterised component of clathrin-coated pits which interacts with AP-2 to facilitate membrane protein internalisation.[152] Their detection supports engagement of CALCR with canonical clathrin adaptor machinery in AF-ACFs. Additional interactors support this interpretation: ArfGAP with SHR domain (ASAP2) functions as an Arf-GTPase activating protein regulating membrane curvature, while Ras homolog family member A (RHOA) coordinates actin cytoskeletal dynamics required for efficient endocytic vesicle formation.[153,154] Together, these findings indicate coordinated recruitment of clathrin and actin regulatory elements of the CALCR complex in AF-ACFs.[153,155]

To functionally interrogate CME involvement, dynamin-dependent vesicle scission was selectively inhibited using Dyngo4A (**Fig 4.3.3A**). Dyngo4A is a potent and selective inhibitor of dynamin GTPase activity, with improved potency, reduced detergent binding, and greater selectivity for helical dynamin compared to its predecessor Dynasore.[156,157]

AF-ACFs were treated with Dyngo4A for 2h, 6h or 24h prior to immunostaining to determine whether blockade of vesicle fission would restore peripheral receptor localisation (**Fig 4.3.3B,C**). Dyngo4A treatment resulted in the appearance of discrete CALCR puncta within the submembrane region, consistent with accumulation of CALCR within stalled clathrin-coated pits. Despite this redistribution, no significant change in the DAPI-CALCR overlap coefficient was observed, and overall receptor distribution remained broadly comparable to vehicle-treated cells.

Endocytosis was further inhibited at the level of clathrin coat assembly using chlorpromazine (10 μM) which disrupts AP-2-clathrin interactions.[158] However, similar to Dyngo4A, chlorpromazine treatment did not significantly alter the DAPI-CALCR overlap coefficient and did not produce prominent submembrane puncta indicative of receptor trapping within coated pits at 1h, 2h, or 24h (**Fig 4.3.3D-F**). Collectively, these findings indicate that while components of CME are enriched within the AF-ACF CALCR interactome and pharmacological inhibition alters receptor microdistribution, acute blockade of CME does not substantially rescue the global receptor localisation in AF-ACFs.

Given the enrichment of Actin Related Protein 2/3 complex (ARPC2/3) subunits (e.g. ARPC2, ARPC4, ACTR2) and RHOA within the AF-ACF CALCR interactome, inhibition of actin assembly was hypothesised to attenuate receptor internalisation or redistribution. Cytochalasin D, an inhibitor of F-actin polymerisation, did not significantly increase the DAPI-CALCR overlap coefficient (**Fig 4.3.3G-I**). Although there was a non-significant trend towards an increase in overlap coefficient, visual inspection did not appear to show obvious differences in CALCR localisation (**Fig 4.3.3G-I**). These results suggest acute disruption of actin polymerisation may promote CALCR internalisation in AF-ACFs.

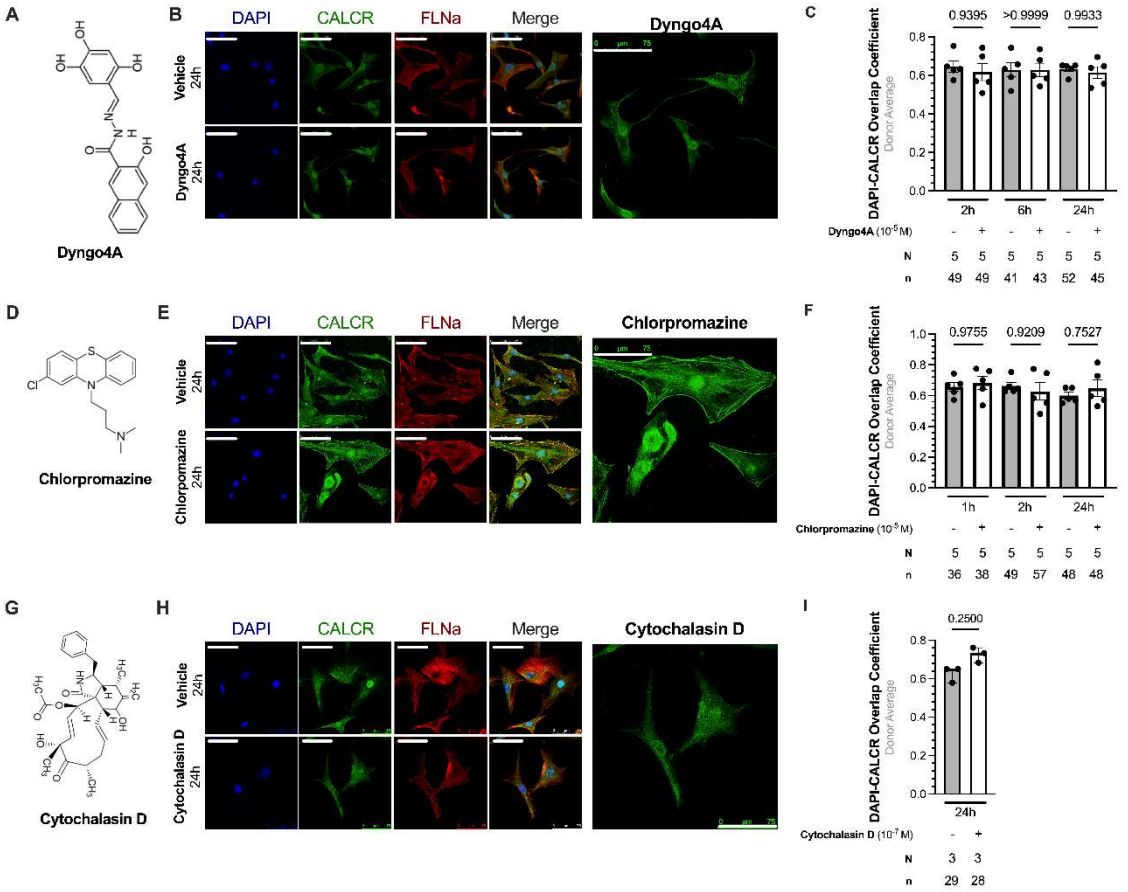


Figure 4.3.3 Effect of endocytosis inhibition on CALCR localisation in AF-ACFs. (A) Chemical structure of Dyngo4A. **(B)** Representative images of AF-ACFs treated with vehicle (0.1% v/v DMSO) or Dyngo4A (10 μM) for 24h. Right, enlarged image of CALCR staining showing submembrane puncta. **(C)** Quantification of the CALCR overlap coefficient with DAPI, calculated using the JACoP BIOP plugin for ImageJ, at 2h, 6h and 24h Dyngo4A treatment. **(D)** Chemical structure of chlorpromazine. **(E)** Representative images of AF-ACFs treated with vehicle (0.1% v/v DMSO) or chlorpromazine (10 μM) for 24h. Right, enlarged image of CALCR staining. **(F)** Quantification of the CALCR overlap coefficient with DAPI at 1h, 2h, and 24h. **(G)** Chemical structure of cytochalasin D. **(H)** Representative images of AF-ACFs treated with cytochalasin D (100 nM) for 24h. Right, enlarged image of CALCR staining. **(I)** Quantification of the CALCR overlap coefficient with DAPI at 24h. n, individual cells. N, individual donors. Data expressed as mean ± SEM, *repeated measures one-way ANOVA with post-hoc Tukey's test* (C, F) or median (IQR), Wilcoxon signed-rank matched pairs test (I). Scale bar, 75 μm.

4.3.4 CALCR isoform expression in human ACFs

To determine whether differential expression of CALCR splice variants contributes to altered receptor localisation in AF-ACFs, primers flanking the 48 bp insert, which distinguishes $CALCR_a$ from $CALCR_b$, based on amplicon size were designed (**Fig 4.3.4A**). Analysis of RT-PCR products by agarose gel electrophoresis revealed a single band of identical size in the majority of SR- and AF-derived ACFs (**Fig 4.3.4B**). In contrast, in TT cells – a cell line derived from a human medullary thyroid carcinoma – there was a distinct double band pattern, consistent with expression of both splice variants and confirmation that the assay could resolve isoforms differing by 48 bp. To confirm the DNA sequence, the PCR product from one of the samples (indicated in **Fig 4.3.4B**) was analysed by Sanger sequencing which confirmed 100% alignment with $CALCR_a$ (ENST00000426151) and the absence of the insert-positive ($CALCR_b$) variant (**Fig 4.3.4C**). Therefore, differential isoform expression is unlikely to account for the altered CALCR localisation observed in AF-ACFs.

4.3.5 Assessment of RAMP1-3 expression in human ACFs

Given that the RAMP family of proteins have been reported to regulate calcitonin receptor trafficking, surface expression, and ligand specificity (**section 1.4.3**), their expression was examined as a potential contributor to altered CALCR localisation in AF-ACFs. At the transcript level, *RAMP1* and *RAMP2* were detected by RT-qPCR in both SR- and AF-derived ACFs, whereas RAMP3 mRNA was not. Compared to SR-ACFs, AF-ACFs demonstrated a trend towards and a significant reduction in *RAMP1* and *RAMP2* mRNA, respectively (**Fig 4.3.5A-B**). At the protein level, despite detection of RAMP1 and 2 in myocardial tissue (positive control), neither RAMP1 nor RAMP2 proteins were detected in SR- or AF-ACF lysates under the same experimental conditions (**Fig 4.3.5C**). Consistently, RAMP1-3 were not identified in any experimental group within the CALCR interactome dataset. Collectively, these results suggest that

RAMP expression at the protein level is minimal, or below detection, in ACFs and that differential RAMP expression is unlikely to account for the altered CALCR localisation observed in AF-ACFs.

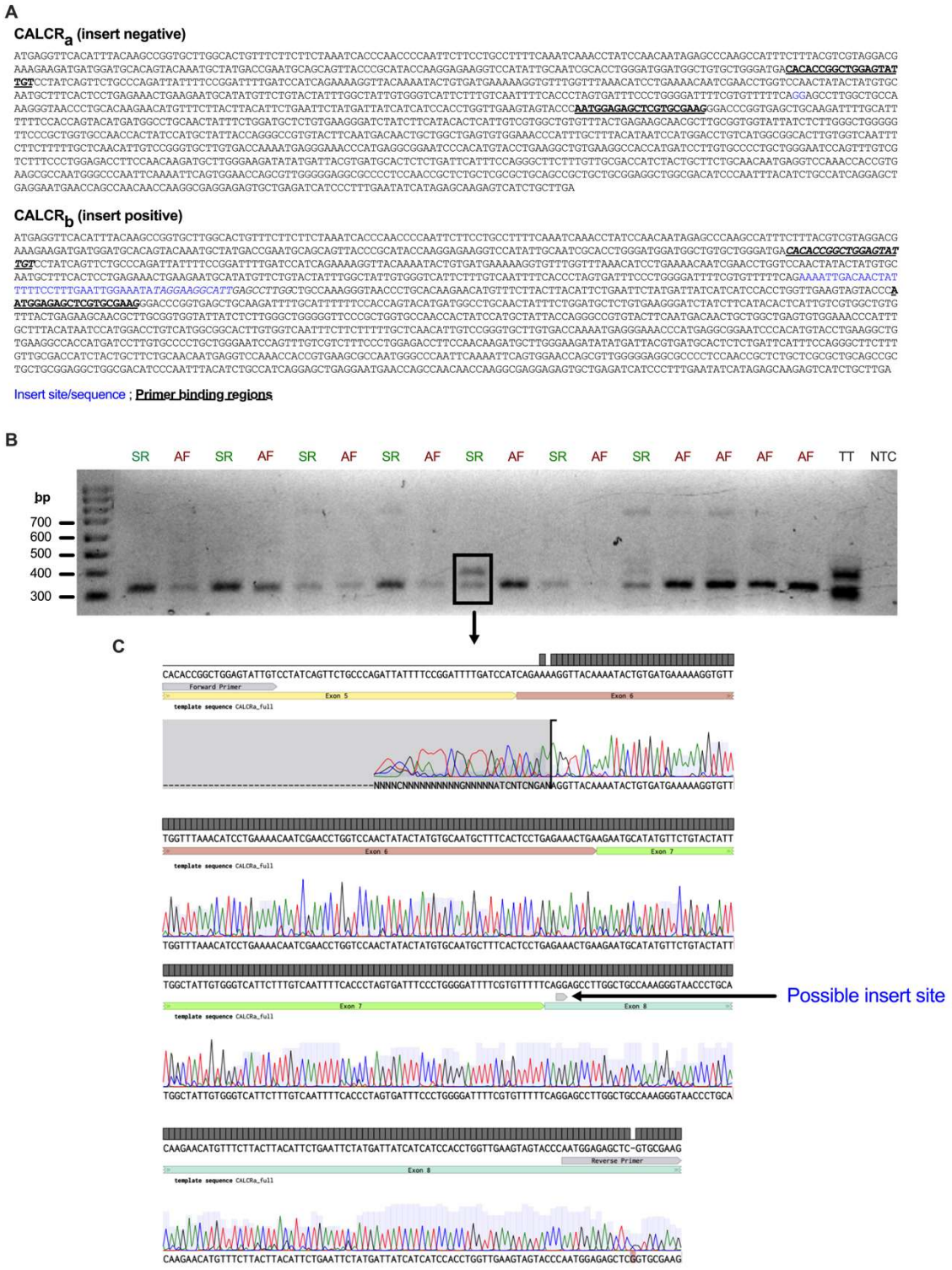


Figure 4.3.4 Analysis of CALCR splice variant expression in SR- and AF-ACFs. (A) Sequences of the insert-negative ($CALCR_a$) and insert-positive ($CALCR_b$), with the 48bp insert highlighted in blue and primer binding regions underlined and emboldened. Primers flanked the insert to enable isoform discrimination by PCR product size (390 vs 438 bp). **(B)** Agarose gel electrophoresis of PCR products from SR- and AF-derived ACFs. TT control samples displayed a double band consistent with expression of both splice variants. NTC, no-template control. (C) Sanger sequencing results of the sample indicated with the box in (B) using the forward primer. Alignment of the PCR product (bottom) with $CALCR_a$ (top) is shown.

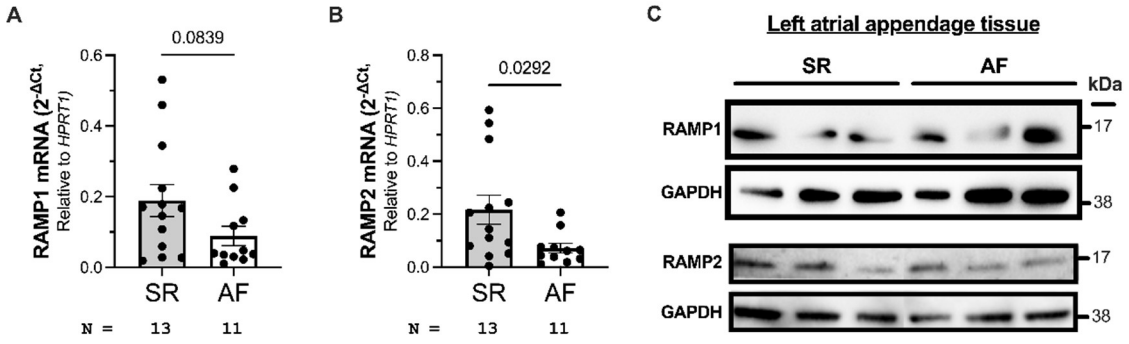


Figure 4.3.5 Expression of RAMP1-2. (A) *RAMP1* and **(B)** *RAMP2* mRNA expression in SR- and AF-ACFs, normalised to *HPRT1*. **(C)** WB of RAMP1 (top) and RAMP2 (bottom) in left atrial appendage tissue from SR and AF donors (N=3 per group). Data expressed as mean ± SEM, *two-tailed, unpaired t-test*.

4.3.6 Assessment of β-arrestin expression and function in human ACFs

β-arrestin recruitment is considered a major mechanism of GPCR desensitisation and internalisation and it was explored for a possible role in AF-related CALCR internalisation.[75] mRNA expression of β-arrestin 1 (*ARRB1*) and β-arrestin 2 (*ARRB2*) was comparable between SR- and AF-ACFs (**Fig 4.3.6A-B**). To investigate whether β-arrestin-mediated trafficking contributes to CALCR internalisation in AF-ACFs, siRNA-mediated knockdown of *ARRB1*, *ARRB2*, and combined knockdown of both isoforms was performed. Efficient mRNA knockdown was confirmed by RT-qPCR, with the most consistent and pronounced reduction observed at 48h post-transfection (**Fig 4.3.6C-D**). Efficient knockdown of ARRB1 at 48h was confirmed at the protein level by WB which revealed a mean protein reduction of 70% **(Fig 4.3.6E)**. Despite knockdown, image analysis revealed no detectable change in the DAPI-CALCR overlap coefficient in any condition when compared with negative control siRNA **(Fig 4.3.6F-G)**. These findings suggest that β-arrestin-dependent internalisation is not a major determinant of basal CALCR subcellular localisation in AF-ACFs.

4.3.7 Assessment of CALCR N-glycosylation

To determine whether altered N-linked glycosylation contributes to differences in CALCR localisation between SR- and AF-ACFs, cells were treated with tunicamycin to block N-linked glycosylation. Immunostaining following a 24h treatment with tunicamycin (1 μg/mL) in AF-ACFs did not result in a clear change in CALCR localisation although the DAPI-CALCR overlap coefficient did trend towards an increase (**Fig 4.3.7A-B**). These data suggest that inhibition of N-glycosylation may augment the internalised phenotype in AF-ACFs. To test the hypothesis that CALCR may be N-glycosylated in SR-ACFs, I examined whether a molecular weight shift was evident for CALCR after tunicamycin treatment. However, there was no detectable shift when assessed by WB suggesting that CALCR is unlikely to be substantially glycosylated (**Fig 4.3.7C**). To confirm effective

inhibition of N-glycosylation, lysosome-associated protein 1 (LAMP1), a protein that is heavily glycosylated, was probed which showed a clear reduction in the glycosylated species at ~100 kDa (**Fig 4.3.7D**).

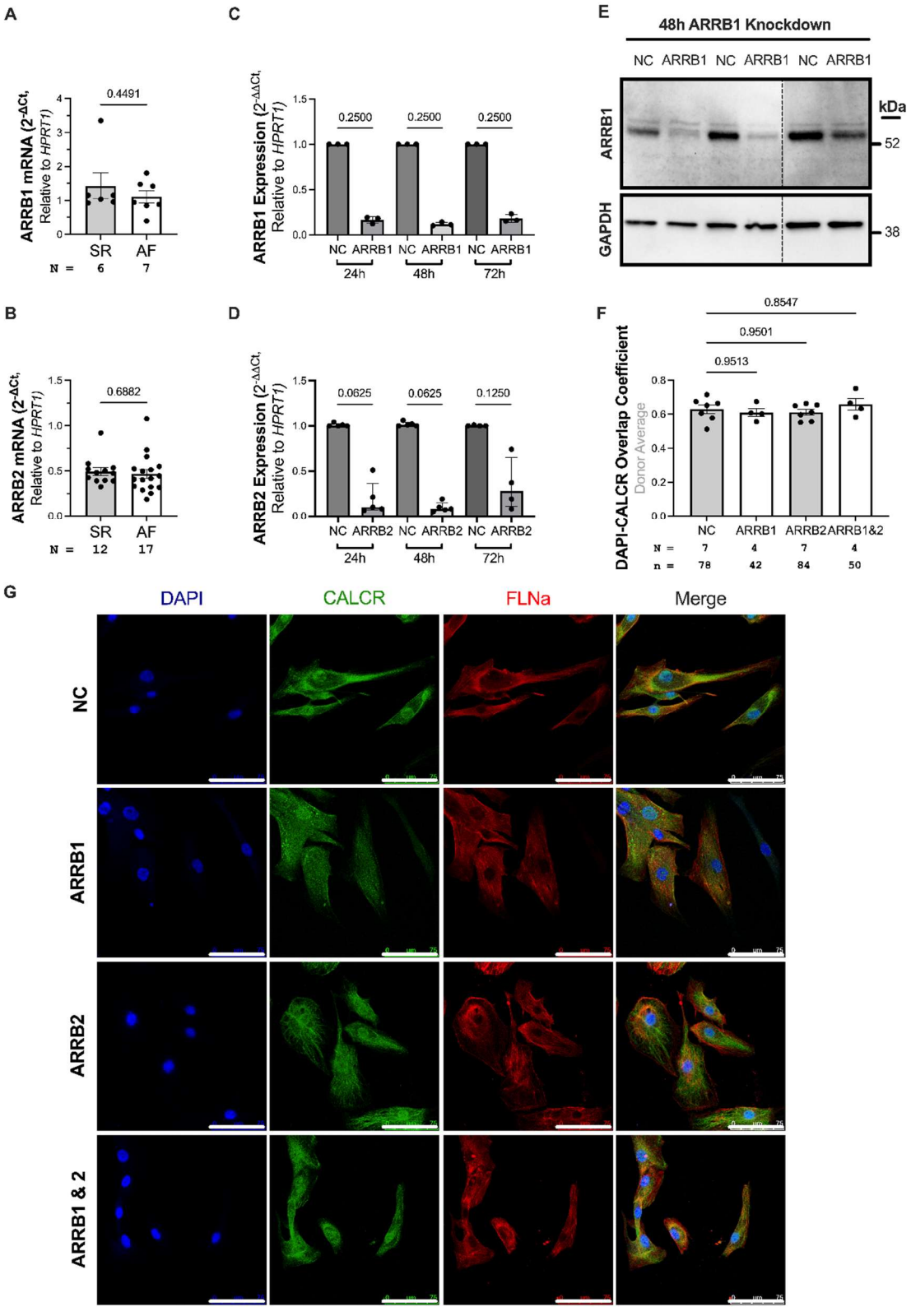


Figure 4.3.6 β-arrestin expression and effect on CALCR localisation in AF-ACFs. (A) *ARRB1* and **(B)** *ARRB2* mRNA expression in SR- and AF-ACFs, normalised to *HPRT1*. *Two-tailed unpaired t-test.* **(C)** *ARRB1* and **(D)** *ARRB2* expression following siRNA-mediated knockdown at 24h, 48h, and 72h compared to non-targeting siRNA (NC). *Wilcoxon matched-pairs signed rank test*. **(E)** WB of ARRB1 and GAPDH after non-targeting control (NC) or anti-ARRB1 siRNA treatment for 48h in 3 donors. Dashed lines indicate non-adjacent lanes that were repositioned from the same original membrane for presentation clarity. **(F)** Quantification of DAPI-CALCR overlap for each knockdown condition, each point represents a donor-averaged coefficient (N, donors; n, individual cells). **(G)** Representative images of AF-ACFs after each *NC*, *ARRB1*, *ARRB2* and *ARRB1&2* dual knockdown. Scale bar, 75 μm. *One-way ANOVA with post-hoc Tukey's test*. Data expressed as mean ± SEM (A-B, E-F) and median (IQR) (C-D).

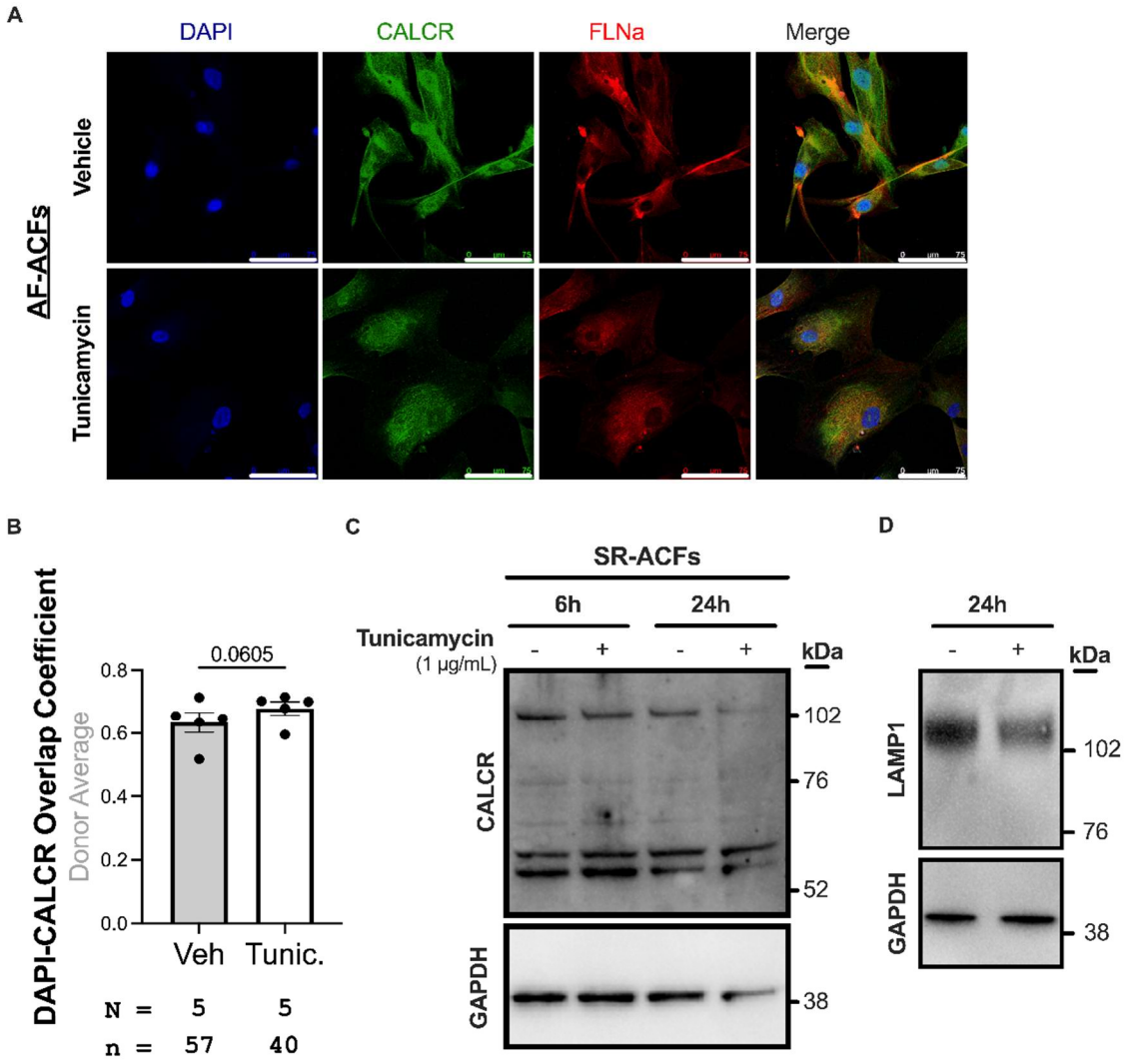


Figure 4.3.7 Effect of N-glycosylation inhibition in ACFs. (A) Representative images of AF-ACFs after 24h tunicamycin (1 µg/mL) treatment. Scale bar, 75 µm. **(B)** Quantification of DAPI-CALCR overlap coefficient for vehicle (0.1% DMSO) and tunicamycin treatment, each point represents a donor-averaged coefficient. Data expressed as mean ± SEM, *two-tailed paired t-test*. **(C)** Representative WB for CALCR and GAPDH after 6h and 24h tunicamycin treatment. **(D)** Representative WB for LAMP1 and GAPDH after 24h tunicamycin treatment.

4.4 Discussion

In this chapter, I systematically investigated six candidate mechanisms for the AF-associated loss of CALCR surface localisation in ACFs:

1. Disease-specific remodelling of the CALCR interactome, with particular focus on endocytic machinery
2. Clathrin-mediated endocytosis and actin-dependent trafficking
3. Differential CALCR splice variant expression
4. Potential involvement of receptor-activity modifying proteins (RAMPs)
5. β-arrestin-dependent internalisation
6. N-linked glycosylation

Despite extensive interrogation, no single mechanism was identified as the definitive driver of the CALCR redistribution in AF-ACFs. However, the work substantially narrows the mechanistic field and generates testable hypotheses for future studies.

4.4.1 CALCR interactome profiling reveals AF-specific remodelling

The immunoprecipitation-mass spectrometry (IP-MS) approach successfully enriched a CALCR interactome distinguishable from the IgG isotype control, as demonstrated by PCA separation, differential protein abundance, and the identification of a greater number of unique proteins in CALCR, compared with IgG, pulldowns. The only differential expression result after Benjamini-Hochberg correction was the significant enrichment of peroxiredoxin 4 (PRDX4) in the CALCR interactome of AF-ACFs vs IgG controls.

PRDX4 is an ER-resident and secreted member of the peroxiredoxin antioxidant family and is abundantly expressed in the heart, its primary biological roles include H_2O_2 scavenging, thereby protecting proteins from oxidative damage, and oxidative protein folding.[159] Defects in post-translational modification or disulfide bond formation, which

are conserved in class B GPCRs, could plausibly dysregulate protein folding and trafficking.[63] PRDX4's presence in the CALCR interactome is also biologically intriguing given that AF is associated with heightened oxidative stress in cardiac fibroblasts.[160,161] It also indicates CALCR in AF-ACFs may be localised to ER endomembranes. In cardiac fibroblasts, in the context of aortic stenosis, PRDX4 expression is reduced due to galectin-3 upregulation. This parallels rises in oxidative stress markers indicating PRDX4 is an important defence against oxidative stress in cardiac fibroblasts.[162] Although only hypothesis-generating, its identification points towards a connection between ER redox regulation and CALCR trafficking that has not previously been explored in cardiac fibroblasts.

However, it is important to note that this enrichment was observed in the CALCR-AF versus IgG-AF comparison rather than as a direct CALCR-AF versus CALCR-SR comparison, and so it is not yet established whether the PRDX4-CALCR association is disease-specific or simply more readily detected in AF-ACFs due to differential abundance. Functional studies testing whether PRDX4 overexpression or knockdown alters CALCR localisation would be needed to evaluate causality. Similarly, the small sample size (N=4), inherent heterogeneity of different donor cells, and challenges of deep quantification in IP-MS experiments, mean these approaches, although valuable, are primarily hypothesis generating. Moreover, it is important to acknowledge that CALCR itself was not identified in any IP-MS sample. Examination of online repositories of MS data revealed CALCR is seldom observed suggesting it may be resistant LysC or trypsin cleavage or the resulting peptides are poorly ionised.[163] However, WB validation (**Fig 3.3.2E**) confirmed CALCR enrichment and the PCA revealed separation of IgG and CALCR IP-MS samples. Future work could also orthogonally validate interactors using co-immunoprecipitation.

One of the more compelling hypotheses, informed by the enrichment of the endocytosis pathway amongst AF-specific CALCR interactors, is that enhanced endocytosis of

CALCR in AF-ACFs drives disease-specific, constitutive CALCR internalisation. The contributing interactors included those involved in CME (AP2S1, ASAP2, EPS15L1), Arp2/3-mediated actin remodelling (ARPC2, ARPC4, ACTR2), retromer-mediated recycling (VPS35, SNX2, SNX6), and Rab-effector proteins (EHD3, RUFY1, EEA1).[164] The simultaneous enrichment of retromer components – which mediate retrograde recycling from endosomes to the trans-Golgi network – and early endosome markers (EEA1, RUFY1) may indicate that internalised CALCR is not efficiently recycled to the plasma membrane but instead accumulates within the endosomal system, consistent with the perinuclear localisation observed by immunofluorescence.[164]

The enrichment of the nucleocytoplasmic transport pathway in SR-ACFs is similarly intriguing. Although CALCR is not predicted to contain a classical bipartite NLS, the identification of importin-α1 (KPNA2) and other nucleopore complex components (e.g. NUP93, NUP58) raises the possibility that nucleocytoplasmic translocation of CALCR-associated proteins may contribute to its surface delivery in SR-ACFs. It is notable that mutations in NUP155, a component of the inner ring of the nuclear pore complex alongside NUP93, have been linked with familial AF demonstrating that defective nucleocytoplasmic transport is a mechanism of AF pathogenesis.[165,166]

4.4.2 Pharmacological inhibition of CME and actin polymerisation does not rescue CALCR surface expression

Despite the compelling interactome-derived evidence for CME engagement in AF-ACFs, pharmacological blockade of two mechanistically distinct steps of endocytosis – dynamin-dependent vesicle scission (Dyngo4A) and clathrin coat assembly via AP-2 disruption (chlorpromazine) – did not significantly alter CALCR localisation, as measured by the DAPI-CALCR overlap coefficient. Unexpectedly, inhibition of F-actin polymerisation with cytochalasin D produced a non-significant trend towards increased

DAPI-CALCR overlap coefficient. This apparent paradox between the interactome and pharmacological data merits careful consideration.

Firstly, it is important to emphasise that these results do not support the conclusion that CALCR is not internalised by CME-dependent pathways, as was reported previously.[91] Indeed, the appearance of submembrane CALCR puncta following Dyngo4A treatment is consistent with its accumulation in halted clathrin-coated vesicles and suggests the effective engagement of Dyngo4A with its target. However, this subtle redistribution did not translate into a statistically significant change in the DAPI-CALCR overlap. This may be because CME accounts for only a fraction of the internalised receptor pool or the treatment duration/concentration were insufficient to reverse the chronic redistribution. Although Dyngo4A is a selective and potent inhibitor of dynamin GTPases, and is often used at 10 μM (with an IC_{50} of around 5.7 μM), it is possible residual dynamin activity remained.[156,157] Likewise, the DAPI-CALCR overlap coefficient may lack the sensitivity to detect subtle redistribution of a small proportion of CALCR molecules; however, the readout's use is justified on the grounds that it is significantly different in SR- versus AF-ACFs and therefore distinguishes disease-relevant differences. It is important to acknowledge that this metric does not inform on the precise location of accumulation which would be better examined with co-localisation assays with markers for specific organelles, i.e. ER (calnexin), Golgi (GM130), early endosomes (Rab5), lysosomes (LAMP1), and slow recycling endosomes (Rab11).[167]

Other, non-mutually exclusive, explanations may also account for the discrepancy. It is possible that CALCR is internalised by CME-independent pathways and the enrichment of CME components reflects the composition of the endosomal compartments in which CALCR resides, rather than the primary mechanisms through which it is internalised. Furthermore, the internalisation phenotype may represent a chronic, steady-state redistribution or a failure of a CALCR pool to ever reach the plasma membrane rather than an active internalisation of the surface pool (**Fig 4.4.1**). In this model, acute inhibition

of endocytosis would not restore surface expression, especially if the recycling arm of the pathway is also impaired. The endocytic internalisation and recycling capacity in SR- and AF-ACFs could be examined using a labelled transferrin uptake assay which is widely used to study endosome recycling.[168] Future experiments should focus on the recycling, rather than internalisation, arm.

The non-significant increase in the DAPI-CALCR overlap with cytochalasin D, alongside the enrichment of Arp2/3 complex subunits and RHOA in the AF-ACF CALCR interactome, suggests that actin dynamics may contribute to CALCR surface expression. Notably, cytochalasin D disrupts actin barbed-end polymerisation broadly and may not selectively target the Arp2/3-dependent branched actin nucleation in endocytic vesicle formation (or trafficking within and from the Golgi apparatus), without also affecting the cortical actin cytoskeleton that supports membrane receptor residence.[169] The N=3 for this experiment was underpowered to detect a significant effect. Nevertheless, the results obtained with cytochalasin D could point towards a role for actin-dependent transport but the exact nature and location of this interaction is unclear. Therefore, future studies could increase the sample size and use more selective tools, e.g. CK-666 (a potent Arp2/3 inhibitor), to provide a more direct mechanistic answer.[170] It is possible that actin may directly engage CALCR in ACFs to promote surface recycling, independently of FLNa, which is consistent with the negative results presented in Chapter 3.[91]

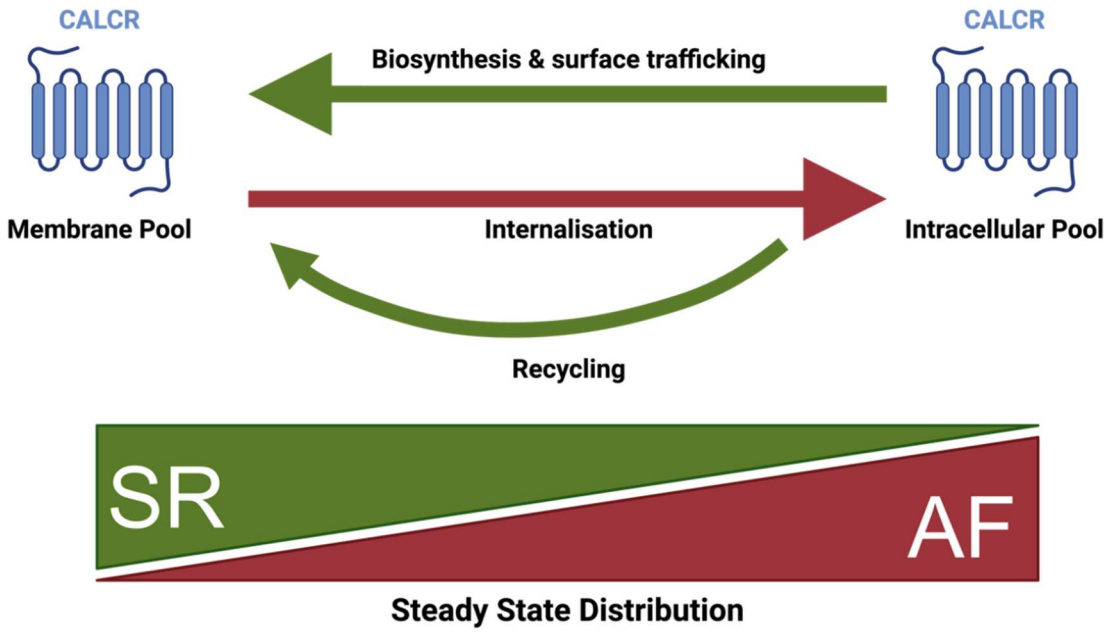


Figure 4.4.1 Schematic of CALCR trafficking dynamics and dysregulation in AF. Steady-state CALCR distribution is governed by opposing fluxes between the plasma membrane and intracellular compartments, including CALCR delivery via biosynthetic trafficking and recycling, and removal via endocytosis and degradation. In AF, the balance is chronically disrupted, favouring receptor internalisation, leading to reduced surface CALCR.

4.4.3 CALCR splice variant expression is conserved between SR- and AF-ACFs

The detection of a single amplicon, corresponding to the insert-negative $CALCR_a$ isoform in the vast majority of SR- and AF-ACFs, confirmed by Sanger sequencing to align with ENST00000426151, effectively excludes differential alternative splicing as a contributor to the altered receptor localisation in AF. As reviewed in Introduction, earlier work in immortalised cell lines suggested the insert-positive $CALCR_b$ isoform exhibits lower surface expression and substantially reduced cAMP signalling relative to $CALCR_a$, and differential splicing could have presented a simple explanation for the AF-associated CALCR trafficking phenotype.[69] The TT cell positive control, exhibiting a double-band pattern consistent with expression of both isoforms, validates the assay's sensitivity to resolve the 48 bp size difference. This result narrowed the mechanistic landscape to altered trafficking, internalisation, or post-translational regulation of a single isoform.

4.4.4 RAMP proteins are not detectable at the protein level in human ACFs

The inability to detect RAMP1 and RAMP2 protein expression in SR- and AF-ACF lysates under conditions that detected both proteins in atrial myocardial tissues, combined with the absence of any RAMP peptides in the CALCR interactome dataset, suggests that RAMPs are not physiologically relevant modulators of CALCR surface expression or ligand specificity in the primary human ACF context. This finding is consistent with the cell-type-specific expression of RAMP family members and with prior reports that, unlike CALCRL, CALCR does not require RAMP co-expression for surface delivery in immortalised cell lines.[79] The detection of *RAMP1* and *RAMP2* mRNA in ACFs, with evidence of reduced expression in AF, indicates the genes are transcribed but the proteins are either absent, post-transcriptionally silenced, or below the antibody detection limit.[79,83] Future siRNA knockdown or proximity labelling approaches might resolve whether trace RAMP expression exerts a biologically meaningful effect on a

subset of CALCR molecules, but the balance of evidence presented here argues against a major contributory role.

4.4.5 β-arrestins are unlikely to promote CALCR internalisation

Comparable *ARRB1* and *ARRB2* mRNA levels between SR- and AF-ACFs argue against differential β-arrestin expression as a driver of enhanced CALCR internalisation. The siRNA knockdown experiments, which achieved consistent and pronounced mRNA (and protein in the case of ARRB1) reduction at 48h for both isoforms, failed to detectably alter the DAPI-CALCR overlap. This finding is consistent with an emerging consensus in the GPCR field that β-arrestins are not universally required for GPCR internalisation, and that Class B GPCRs in particular directly engage AP-2 and undergo β-arrestin-independent internalisation.[75,171,172] This is consistent with investigations by Dal Maso and coworkers that concluded β-arrestin was not recruited to CALCR following ligand stimulation in the transformed COS-7 cell line.[69] Although CALCR was not directly included in the study by Liu *et al* (2025), that systematically explored the β-arrestin dependence of internalisation of 60 GPCRs, the current data, in a physiologically relevant primary human cell system, does not support a β-arrestin dependence for constitutive CALCR internalisation.[75]

Current studies are confirming the protein-level knockdown for ARRB2 by WB. Additionally, the role of GRK-mediated CALCR phosphorylation – upstream of β-arrestin recruitment and an independent regulator of receptor trafficking – has not been directly assessed and remains a potentially relevant mechanism. An important limitation is that β-arrestin knockdown was assessed in the absence of exogenous calcitonin. These experiments therefore principally address the β-arrestin dependence of basal or constitutive CALCR localisation and do not exclude a role for β-arrestins in agonist-induced receptor internalisation. Future experiments should assess CALCR trafficking following defined hCT stimulation in the presence and absence of ARRB1/2 depletion.

4.4.6 Inhibition of N-glycosylation does not significantly alter CALCR localisation

Tunicamycin-mediated inhibition of N-linked glycosylation in AF-ACFs produced a non-significant trend towards increased CALCR internalisation (as measured by the overlap coefficient), indicating that N-glycosylation may contribute to surface delivery of CALCR. However, the absence of a molecular weight shift on WB analysis following tunicamycin treatments suggests that the receptor may not be (detectably) N-glycosylated in primary patient ACFs, in contrast to findings from recombinant expression systems where N-glycosylation of asparagine-130 in the CALCR extracellular domain has been shown to enhance ligand affinity.[96] This discrepancy may reflect the different cellular context, post-translational processing capacity of ACFs versus HEK293 cells, or the sensitivity of the WB system to detect the relatively subtle mass shift expected from glycosylation of a single residue on a ~60 kDa protein. Possible N-glycosylation of CALCR could be further studied using PNGase F to hydrolyse N-linked oligosaccharides.[96,97]

The trend towards increased CALCR internalisation warrants follow-up. Broad inhibition of N-glycosylation with tunicamycin induces ER stress and activates the unfolded protein response (UPR), which could exacerbate receptor misfolding and perinuclear accumulation through mechanisms independent of site-specific CALCR glycosylation. Future experiments using CALCR N130A or N130Q point mutants to selectively abolish the specific glycosylation site, rather than global glycosylation inhibition, could provide a more mechanistically precise assessment of whether N-glycosylation at this residue regulates CALCR surface trafficking in ACFs. Given the extensive internalisation present in AF-ACFs at baseline, these experiments would be best conducted in SR-ACFs.

4.4.7 Conclusions and implications

This chapter presents the first systematic evaluation of candidate mechanisms underlying CALCR surface loss in native patient AF-ACFs. Through interactome

profiling, targeted pharmacological inhibition, splice variant analysis, RAMP characterisation, β-arrestin functional studies, and N-glycosylation perturbation, six distinct mechanistic hypotheses were examined. The interactome data revealed an AF-associated remodelling of the CALCR protein interaction network, characterised by enrichment of endocytic machinery alongside the emergence of PRDX4 as a candidate AF-specific CALCR interactor linking ER oxidative stress to receptor biology. Despite this, acute pharmacological inhibition of endocytosis, at different levels, did not restore CALCR surface expression, suggesting either that constitutive steady-state redistribution rather than active internalisation underlies the AF-ACF phenotype, or that redundant and parallel endocytic pathways together mediate the receptor's intracellular accumulation. Of note was the enhanced internalisation of CALCR in AF-ACFs by cytochalasin D. Future studies should directly investigate the FLNa-independent role of actin in CALCR recycling. Alternative splice variant expression, RAMP co-expression, β-arrestin-dependent trafficking, and detectable N-glycosylation were evaluated and no evidence was found that these were major determinants of CALCR mislocalisation in primary human ACFs.

These findings refine the list of possible mechanisms and point towards the recycling axis and surface delivery – rather than enhanced internalisation – as the most likely determinant of the AF-associated CALCR internalisation. While a definitive causal mechanism remains to be identified, the systematic exploration of multiple previously hypothesised regulators represents important progress towards understanding a disease-specific trafficking defect. These investigations highlight that the mechanisms governing GPCR localisation in primary, patient-derived cells may differ from those that are dominant in immortalised cell lines and artificial over-expression systems.

CHAPTER 5: DEVELOPMENT OF A HIGH-THROUGHPUT DRUG SCREENING PLATFORM IN AF-ACFs TO ASSESS CALCR LOCALISATION

5.1 Introduction

Despite extensive mechanistic interrogation of previously reported mechanisms, no single pathway appeared to account for altered CALCR localisation in AF-ACFs. The results in preceding chapters suggested that aberrant CALCR localisation in AF-ACFs is unlikely to be caused by disruption of a single canonical trafficking/internalisation pathway. Instead, a model of complex, potentially redundant or converging pathways emerges to explain CALCR internalisation.

In this context, hypothesis-driven approaches targeting individual, discrete molecular nodes may fail to unmask the complex, network-level alterations underlying the AF-associated CALCR phenotype. Therefore, an unbiased, hypothesis-free, functional strategy was pursued. I sought to identify compounds capable of restoring surface CALCR localisation in AF-ACFs without presupposing underlying mechanism. To maximise translational potential, a chemically diverse, cell permeable, 3091 compound library (HY-L066, MedChemExpress) was screened containing drugs approved by the world's leading pharmaceutical regulatory agencies - e.g. U.S. Food and Drug Administration (FDA), European Medicines Agency (EMA), China's National Medical Products Administration (NMPA), and Japan's Pharmaceuticals and Medical Devices Agency (PMDA) – and other pharmacopeial agents. Such a strategy, while potentially identifying pathways underlying aberrant CALCR localisation, may also reveal candidates for drug repurposing. Repurposing licensed agents offers several advantages, including established safety profiles, well-characterised pharmacokinetics, and accelerated paths to clinical translation.

Accordingly, I built a quantitative, unbiased, high-throughput screening (HTS) platform to measure CALCR localisation using primary donor-derived ACFs from patients with long-standing AF. HTS has become established as a powerful tool for the simultaneous interrogation of the effects of thousands of interventions on an objective, quantifiable

biological readout (e.g. intracellular CALCR accumulation) in disease-relevant *in vitro* models.[173] It presents a convenient and systematic approach to screen potential molecules that can then be subsequently validated and optimised as drug candidates. This chapter describes the development, validation, and implementation of this HTS platform, and presents the identification of candidate compounds capable of restoring physiological CALCR localisation in AF-ACFs. Advantageously, and in the context of AF-associated atrial fibrotic remodelling, the same HTS model enabled, as an orthogonal readout to CALCR localisation, the identification of compounds capable of suppressing collagen I protein production independently of CALCR surface restoration.

5.2 Methods & Materials

5.2.1 Seeding density and antibody optimisation

To determine optimal seeding density for high-content imaging, ACFs were plated in PhenoPlate 384-well microplates (6057302, Revvity) using a Combi Reagent Dispenser at densities from 1000-2000 cells per well. DMSO tolerance was assessed by treating cells with 0.1% or 0.5% (v/v) DMSO, or media alone, for 24h. Cell viability was assessed using SYTOX Green (1:20,000, S7020, Invitrogen). The proportion of dead cells was calculated as the ratio of SYTOX Green-positive cells to total Hoechst33342-positive nuclei.

For optimisation of immunostaining conditions, cells were fixed 48h after seeding using ice-cold BD Cytofix/Cytoperm™ (BD Biosciences) for 12 min, followed by three washes in BD Perm/Wash™ (BD Biosciences). Cells were then incubated overnight at 4ºC with primary antibodies against FLNa (MAB1678, Merck, 1:500), CALCR (AP5688b, Abcepta, 1:200), and collagen I (1310-01, SouthernBiotech, 1:500), diluted in Perm/Wash™ buffer. After washing, cells were incubated with appropriate secondary antibodies (at 1:500 or 1:1000 dilutions) and Hoechst33342 (H3570, Invitrogen, 1:2500) for 1h at room temperature, followed by two additional washes and storage in PBS prior to imaging. All liquid handling steps were automated using a Janus MDT Workstation (Revvity). The plates were imaged on the Opera Phenix High Content Imager (Revvity). Given the reliance of the screen on the CALCR antibody, it was validated by siRNA knockdown of CALCR and Western blot (**Fig 5.2.1**).

5.2.2 High-throughput drug screening assay

ACFs derived from three donors with persistent AF (≥1 year duration) were isolated as described in Chapter 2 and expanded to passage 4 (clinical demographics are shown in **Table 5.2**). ACFs from the same control SR donor were used in each screen. Cells were

cultured in T175 flasks, and surplus cells were cryopreserved in liquid nitrogen using freezing medium comprising 50% foetal bovine serum (FBS), 40% DMEM, and 10% dimethyl sulfoxide (DMSO). For HTS, ACFs were seeded at a density of 1250 cells per well across 24 assay plates with edge wells left cell-free to prevent edge-effects. Cells were counted using a LUNA II Automated Cell Counter (Logos Biosystems). Plates were left at room temperature for 45 min to facilitate uniform cell settling prior to incubation overnight in standard culture conditions (10% FBS-containing medium supplemented with antibiotics). The following day, cells were serum-starved in 45 µL of 0.5% FBS-containing media (without antibiotics) for 4h prior to compound treatment. A total of 3,091 compounds from an FDA-approved and pharmacopeial drug library (HY-L066, MedChemExpress) were screened (**Table 5.1**). Using an Echo 555 acoustic liquid handler, compounds were transferred into intermediate plates and diluted in 0.5% FBS-containing medium to generate 10x working stocks. A subsequent 1:10 dilution (5 µL into 45 µL) into assay plates yielded final treatment concentrations, typically 10 µM.

Table 5.1 Summary of FDA Approved & Pharmacopeial Drug Library (HY-L066).

Plate ID	Solvent	Stock Concentration	Number of Compounds	Final Treatment Concentration
HYCPK34133	DMSO	2mM	48	10µM
HYCPK34134	Water	2mM	7	10µM
HYCPK34135	DMSO	3mg/mL	9	3 µg/mL
HYCPK34136	Water	3mg/mL	9	3 µg/mL
HYCPK34137	DMSO	10mM	320	10µM
HYCPK34138	DMSO	10mM	320	10µM
HYCPK34139	DMSO	10mM	320	10µM
HYCPK34140	DMSO	10mM	320	10µM
HYCPK34141	DMSO	10mM	320	10µM
HYCPK34142	DMSO	10mM	320	10µM
HYCPK34143	DMSO	10mM	320	10µM
HYCPK34144	DMSO	10mM	289	10µM
HYCPK34145	DMSO	10mM	320	10µM
HYCPK34146	Water	10mM	169	10µM
		Total:	3091	

Each assay plate included vehicle control wells (0.1% and 0.5% v/v DMSO) and a column of internal control SR-ACFs for calculation of assay performance metrics, including Z'-factor. All screening plates were processed in technical duplicate. Following 24h compound treatment, cells were fixed and immunostained as in **section 5.2.1**. HTS experiments were carried out in collaboration with the Ebner group at the Target Discovery Institute, University of Oxford, with particular assistance from Dr Val Millar.

5.2.3 High content imaging and image analysis

Imaging was performed on an Opera Phenix High Content Screening System (Revvity) with a 40x water immersion objective (numerical aperture: 1.1). Four fluorescence channels were acquired sequentially to minimise spectral overlap: Hoechst 33342 (405 nm excitation / 435-480 nm emission; 100ms, 100% power), FLNa (488 nm / 500-550 nm; 100ms, 100% power), collagen I (561 nm / 570-630 nm; 400 ms, 100% power), and CALCR (640 nm / 650-760 nm; 440ms, 100% power). For each well, 15-25 fields were captured, corresponding to approximately 20-30% well coverage. Image analysis was conducted using Harmony® High-Content Imaging and Analysis Software (v4.9, Revvity). Nuclei were identified in the Hoechst channel with size (50-500μm^2) and roundness (>0.7) filters applied. A concentric perinuclear region was defined by inward resizing of the nuclear mask (by -12 µm/px), and cytoplasmic regions were identified using the FLNa channel (as this was shown previously and in preceding chapters to consistently delineate ACFs),[1] excluding both nuclear and perinuclear compartments. CALCR localisation was quantified by measuring fluorescence intensity within defined subcellular regions and calculating a perinuclear-to-cytoplasmic intensity ratio (P/C, **Fig 5.2.2A**).

Collagen I protein content and accumulation were assessed by measuring mean fluorescence intensity within the cytoplasm and by calculating the proportion of cell area occupied by a thresholded collagen mask (threshold intensity = 1000) (**Fig 5.2.2B**). For

all readouts, single cell-level data were averaged to generate a well-level summary for downstream analysis.

5.2.4 Definition of toxic and hit compounds

Consistent with previous studies, compounds were classified as toxic if they reduced cell number by more than two standard deviations (SD) below the mean cell count across all treatment wells, corresponding to an approximate 50% reduction relative to the 0.1% DMSO control.[174] Toxic compounds were excluded from primary analysis.

Among non-toxic compounds, hits were defined based on the primary CALCR localisation readout. Specifically, compounds that reduced the CALCR P/C ratio by more than two standard deviations (Z-score ≤ -2) from the mean of all non-toxic compound-treated wells were classified as *primary hits*. Secondary analyses identified compounds that reduced collagen I protein expression, defined as a decrease in either mean staining intensity or cell area coverage exceeding two standard deviations (Z-score ≤ -2). Compounds identified as toxic at 10 μM were re-evaluated in each donor in secondary screens at lower concentrations (0.25, 1, and 5 μM) using an identical assay pipeline.

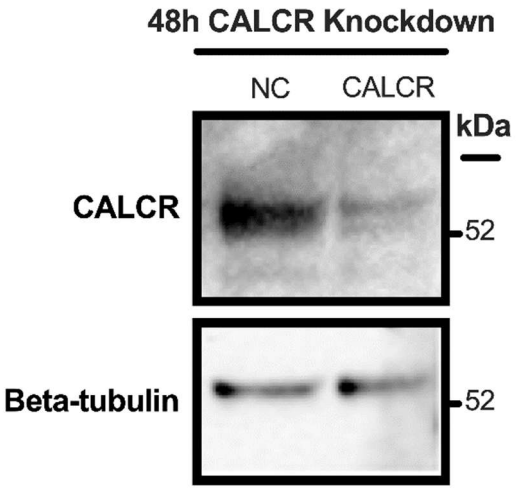


Figure 5.2.1 Knockdown validation for the confirmation of the CALCR antibody's specificity. WB of CALCR and beta-tubulin after non-targeting control (NC) or anti-CALCR siRNA treatment for 48h.

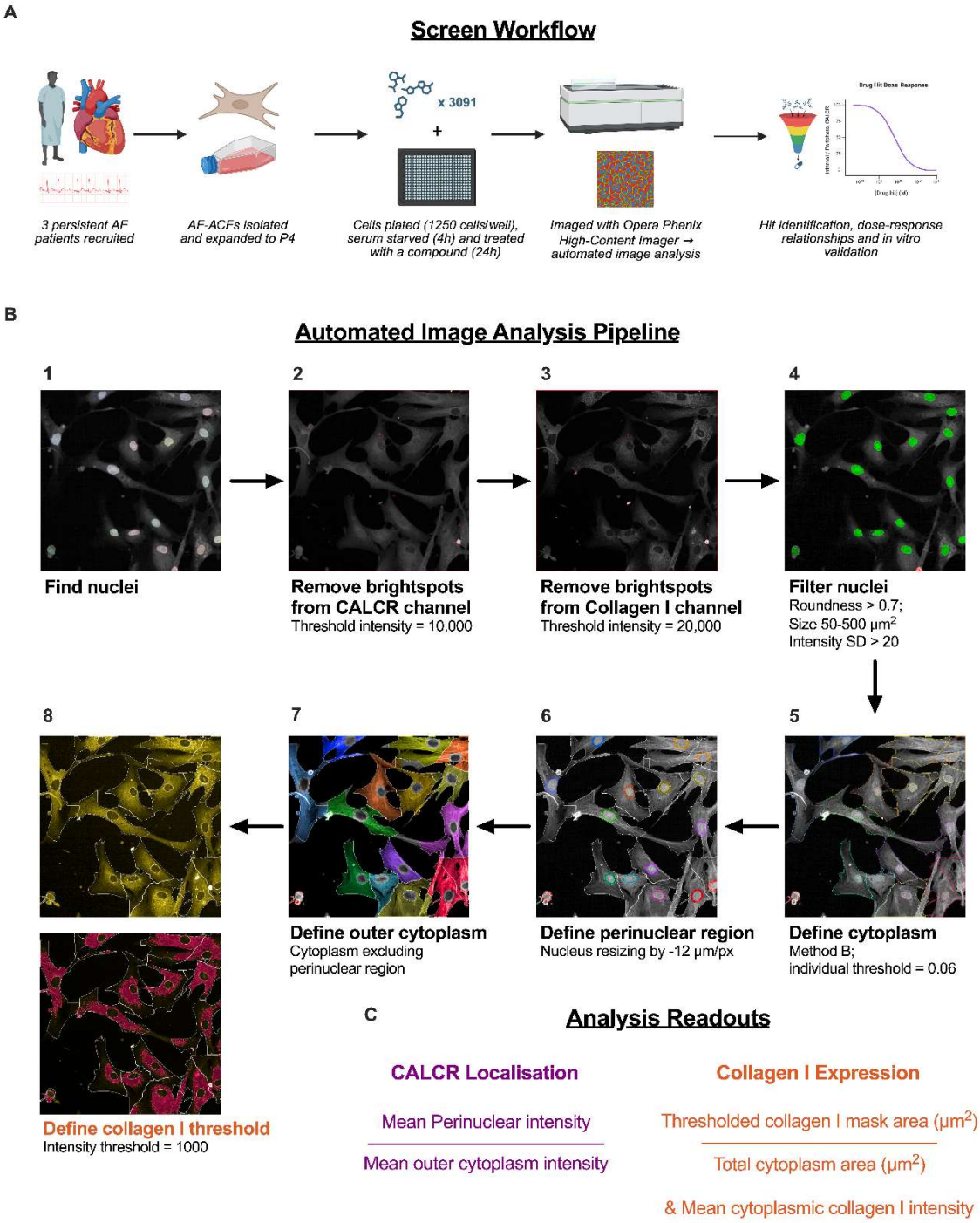


Figure 5.2.2 Schematic overview of the high-content screening workflow and automated image analysis. (A) Experimental workflow: AF-ACFs from 3 patients with persAF were expanded, plated, serum-starved, and treated with a library of 3091 compounds for 24h, followed by high-content imaging and automated analysis. **(B)** Image analysis pipeline: nuclei were identified using a preset algorithm, high-intensity artefacts removed from CALCR and collagen I channels, and cell segmentation performed to define nuclear, perinuclear, and cytoplasmic regions. **(C)** Calculation of primary readouts for CALCR localisation and collagen I expression.

5.3 Results

5.3.1 Optimisation of HTS conditions

To establish robust assay conditions for the HTS, key parameters including cell density, antibody dilution, vehicle tolerance, and assay readout robustness were systematically optimised. Cells were seeded at densities of 1000-1750 cells per well and, following overnight attachment, subjected to serum starvation (4h) before a subset of control wells were treated with DMSO (0.1% and 0.5% v/v) for 24h to assess vehicle tolerance. A seeding density of 1250 cells/well was identified as optimal, providing an appropriate balance between confluency and single-cell resolution over the ~48h assay window (**Fig 5.3.1A**). Post-assay automated image analysis demonstrated that final cell counts closely reflected initial seeding densities, indicating minimal proliferation during the assay period and confirming the accuracy of the automated segmentation pipeline for cell identification (**Fig 5.2.2B** and **5.3.1B**).

Cell viability was quantified using SYTOX Green staining. Treatment with 0.1% (v/v) DMSO did not result in a significant increase in dead cell percentage in either SR- or AF-ACFs, whereas 0.5% (v/v) DMSO induced a modest, but statistically significant, increase in cell death in AF-ACFs (**Fig 5.3.1C-D**). These experiments confirmed tolerance to the final DMSO exposure (0.1% v/v) for most library compounds in both SR- and AF-ACFs.

To optimise reagent usage while maintaining signal quality, secondary antibody concentrations of 1:500 and 1:1000 were evaluated in SR- and AF-ACFs. Staining quality was appreciably better at 1:500 so this dilution was selected for the full screens (**Fig 5.3.1E**).

Table 5.2 Clinical characteristics of the three AF donors and common SR control used in each HTS.

ACEi, angiotensin-converting enzyme inhibitor; ARB, angiotensin II receptor blocker; AVR, aortic valve repair/replacement; BMI, body mass index; CABG, coronary artery bypass grafting; COPD, chronic obstructive pulmonary disease; HFrEF, heart failure with reduced ejection fraction (<40%); MI, myocardial infarction; MVR, mitral valve repair/replacement.

Characteristic	AF Donor 1	AF Donor 2	AF Donor 3	SR Control
Age	51	69	74	70
Sex	Male	Male	Female	Male
BMI	31.9	22.6	24.2	31.2
Surgical Procedure	MVR + AVR	AVR + ascending aorta replacement	MVR	AVR + CABG
Medical history				
COPD	No	No	No	No
Diabetes mellitus	No	No	No	No
HFrEF	No	Yes	No	Yes
Hypertension	No	Yes	No	Yes
Chronic kidney disease	No	No	No	No
Prior MI	No	No	No	No
Prior stroke	No	No	No	No
Smoker/ex-smoker	Current	Never	Never	Ex
AF family history	Yes	No	Yes	No
Medications				
ACEi or ARB	Yes	Yes	Yes	Yes
Direct oral anticoagulant	Yes	Yes	Yes	No
Antiplatelet	No	No	No	No
Beta-blocker	Yes	No	Yes	Yes
Calcium-channel blockers	No	No	No	No
Diuretics	Yes	No	Yes	No
Statins	Yes	Yes	No	Yes

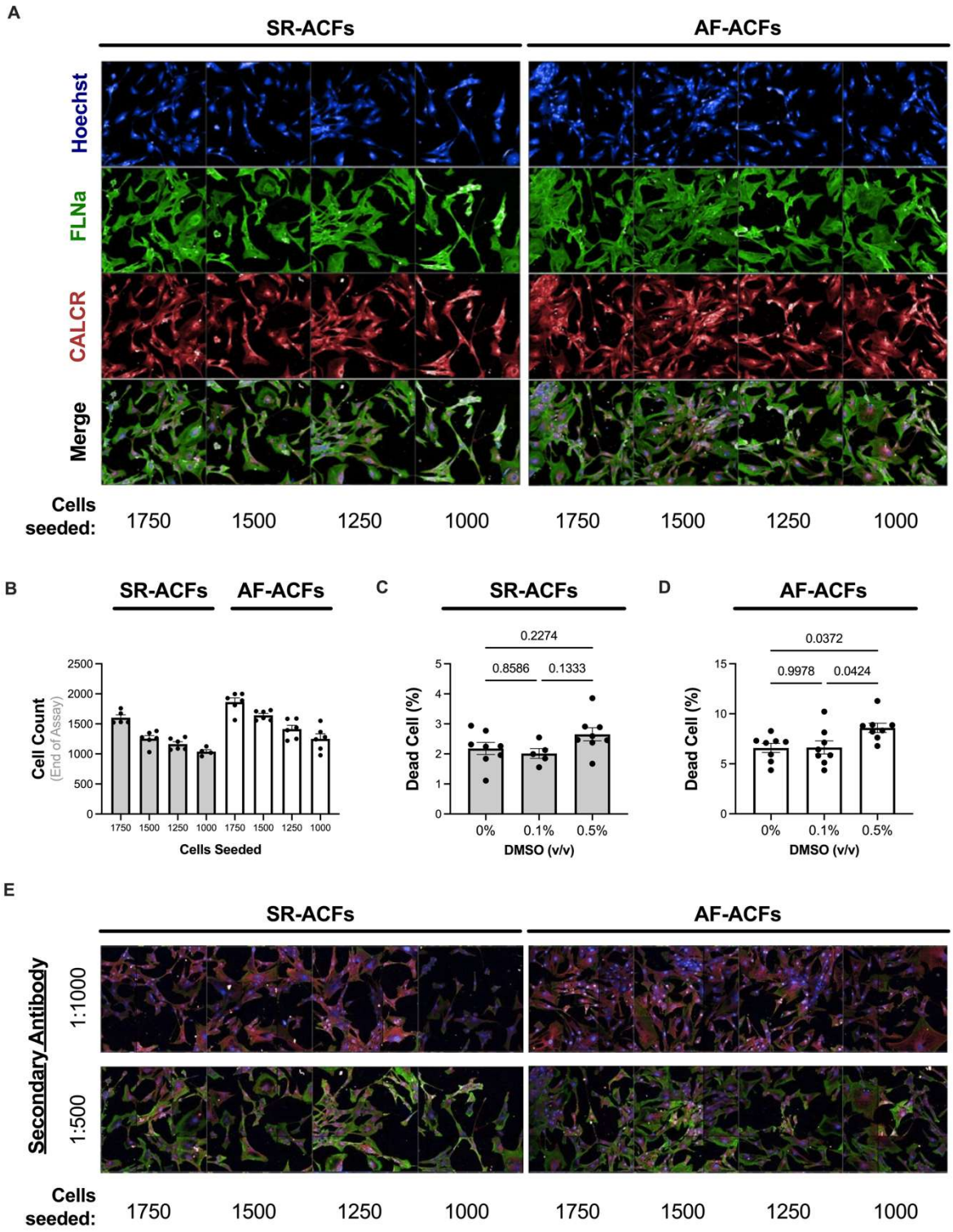

A
SR-ACFs
AF-ACFs
Hoechst
FLNa
CALCR
Merge
Cells seeded:
1750
1500
1250
1000
1750
1500
1250
1000
B
SR-ACFs
AF-ACFs
Cell Count
(End of Assay)
2500
2000
1500
1000
500
0
1750 1500 1250 1000 1750 1500 1250 1000
Cells Seeded
C
SR-ACFs
0.2274
0.8586
0.1333
Dead Cell (%)
5
4
3
2
1
0
0%
0.1%
0.5%
DMSO (v/v)
D
AF-ACFs
0.0372
0.9978
0.0424
Dead Cell (%)
15
10
5
0
0%
0.1%
0.5%
DMSO (v/v)
E
SR-ACFs
AF-ACFs
Secondary Antibody
1:1000
1:500
Cells seeded:
1750
1500
1250
1000
1750
1500
1250
1000

Figure 5.3.1 Optimisation of seeding density and DMSO tolerance in control (SR-) and AF-ACFs. (A) Representative immunofluorescence images of SR- and AF-ACFs seeded at 1000-1750 cells/well and fixed at 48h and stained with Hoechst 33342 (blue), FLNa (green), and CALCR (red). **(B)** Automated quantification of cell number at 48h. (**C-D**) SYTOX Green-based viability assessment in SR- (C) and AF-ACFs (D) following 24h treatment with DMSO (0, 0.1% and 0.5% v/v). **(E)** Representative merged channel images showing staining with secondary antibodies at 1:500 and 1:1000 (identical acquisition settings). Data are presented as mean ± SEM; each point represents an individual well (with cells derived from the same donor). p-values calculated by *one-way ANOVA* with *Tukey's post hoc test*.

5.3.2 Selection of an assay readout for CALCR localisation

To ensure robust and reproducible performance of the HTS platform, selection of an appropriate single-cell level assay readout was guided by quantitative assessment of assay quality using the Z'-factor.[175] The Z'-factor (Z') is a dimensionless metric that considers both the dynamic range of the assay signal and the variability of positive (AF-ACFs) and negative (SR-ACFs) controls, providing a standardised measure of assay suitability for HTS applications:

$$Z' = 1 - \frac{3(\sigma_p + \sigma_n)}{|\mu_p - \mu_n|} \qquad \sigma_p = SD\ of\ positive\ controls; \quad \sigma_n = SD\ of\ negative\ controls;$$
$$\mu_p = mean\ of\ positive\ controls; \ \mu_n = mean\ of\ negative\ controls$$

Z'-factors >0.5 indicate an excellent assay, whereas values between 0 and 0.5 reflect moderate assay performance.

Consistent with the observations in Chapter 3 and previous work, immunostaining suggested CALCR was enriched in the perinuclear region in AF-ACFs.[1] To objectively evaluate and quantify this localisation as a potential screening readout, multiple candidate metrics were derived from the analysis pipeline including raw intensity measurements and intensity ratios between subcellular compartments (**Fig 5.2.2B**; **Fig**

5.3.2A). Z'-factors were calculated using DMSO-treated SR-ACFs and AF-ACFs, with the mean signal from four wells per plate used for analysis; each plate was treated as an independent replicate (n=24 plates). The candidate metrics assessed included (i) outer cytoplasmic CALCR intensity (Z' = -0.09), (ii) average nuclear and perinuclear intensity normalised to outer cytoplasmic CALCR intensity (Z'=-0.485), and (iii) perinuclear-to-cytoplasmic CALCR intensity ratio (P/C; Z'=0.31) (**Fig 5.3.2B**). The P/C CALCR intensity ratio emerged as the best metric to separate SR- and AF-ACFs. The Z' value of 0.31 indicates a moderate assay performance and reflects a reproducible and biologically meaningful shift in CALCR localisation, despite the biological heterogeneity inherent in working with primary patient-derived cells, supporting its selection as the primary readout for subsequent CALCR localisation screening. The use of a ratiometric measure also mitigates intra- and inter-screen well-to-well variability in staining intensity and cell density, further enhancing assay robustness. Meanwhile, collagen I-based readouts yielded substantially lower Z'-factors (-0.44 for cytoplasm staining intensity and 0.12 for percentage cell coverage by the thresholded collagen mask) (**Fig 5.3.2B**). This indicates intracellular collagen I staining does not provide an adequate dynamic range to reliably distinguish SR- from AF-ACFs in this assay format.

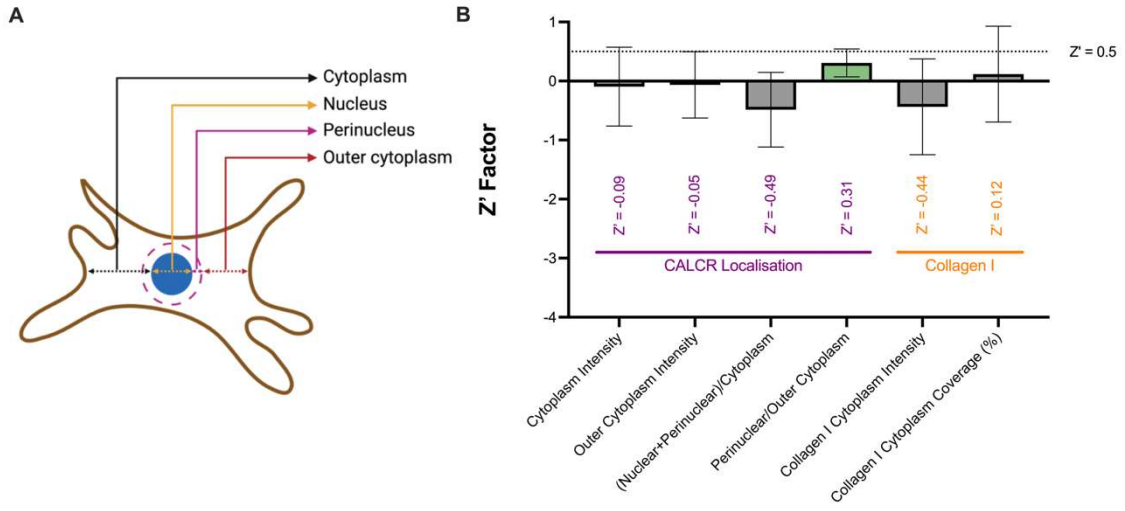


Figure 5.3.2 Selection of assay readout based on Z'-factor analysis. (A) Schematic illustrating the subcellular regions assigned by automated cell segmentation. **(B)** Z'-factor analysis of candidate assay readouts derived from CALCR and collagen I channels in DMSO-treated SR- and AF-ACFs, bars represent the mean of Z'-factor from 24 plates (± SD). The dashed line indicates the conventional threshold for an excellent HTS assay (Z' = 0.5); our assay showed sufficient robustness for screening.

5.3.3 Comparative analysis of screen-level performance metrics

Following optimisation of assay conditions, I independently screened AF-ACFs derived from three donors against a library of 3,091 compounds, at a single concentration (10 μM for 99.4% of compounds) (clinical characteristics summary **Table 5.2**). Compounds were distributed across twelve 384-well plates (≤280 compounds per plate), each plate was run in technical replicate and included a column of SR-ACFs, the same control donor was used in each screen (**Fig 5.3.3A,B, Table 5.2**). After image-based quality control and filtering, the mean number of identified cells per well in the fields imaged ranged from 189 to 302 across the three screens (**Fig 5.3.3C**). Cytotoxic compounds were defined as those reducing cell number by ≥2 SD beneath the mean of all conditions which corresponded to threshold values ranging from 89 to 119 cells per well, representing reductions of 61%, 53%, and 59% (**Fig 5.3.3C**). Wells with cell counts below these thresholds were excluded from downstream analysis of CALCR localisation or collagen I abundance; these compounds were all re-screened at 5, 1, and 0.25 μM in methodologically identical screens. Strong concordance in cell count was observed between technical replicate plates, demonstrating good intra-plate reproducibility and assay stability (**Fig 5.3.3D-F**).

Consistent with the Z'-factor, the three screens exhibited a robust dynamic range, evidenced by the consistently higher P/C ratio in AF-ACFs versus the SR-ACF line across all plates (**Fig 5.3.3G**). This confirmed the sensitivity and suitability of the P/C readout for detecting compound-induced modulation of CALCR localisation in AF-ACFs.

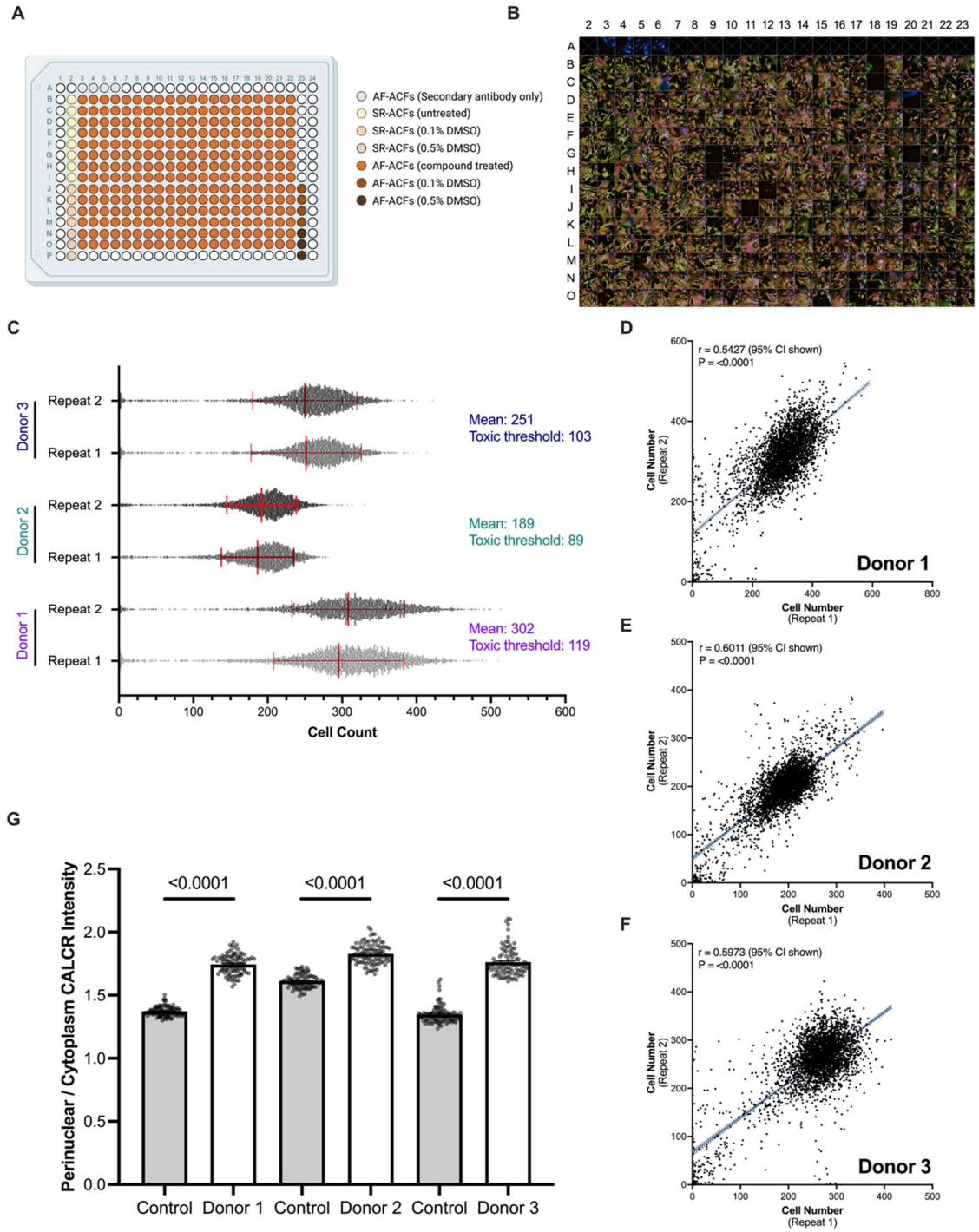


Figure 5.3.3 Full screen assay performance and reproducibility. (A) Representative 384-well plate layout showing distribution of test compounds and control wells. **(B)** Representative whole-plate imaging output (all channels merged). **(C)** Distribution of well cell counts for each donor, indicating mean cell number and toxicity thresholds. **(D-F)** Correlation plots of cell count across each replicate; *Pearson correlation coefficients* are shown. **(G)** Comparison of perinuclear-outer cytoplasmic ratio (P/C) in 0.1% DMSO treated control (SR-) and AF-ACFs. *Two-tailed unpaired t-test.* For all graphs, each point represents the result from a single well.

5.3.4 Identification of CALCR Localisation Hits

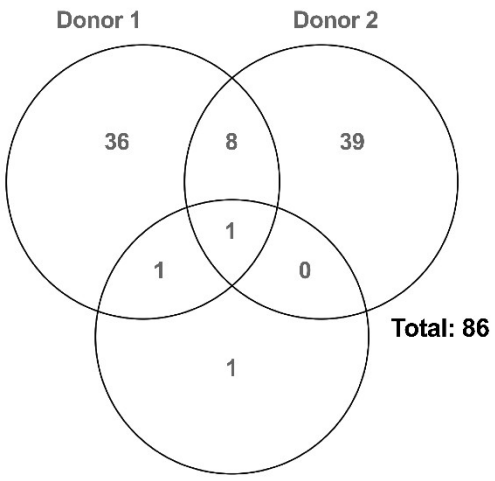
Each HTS identified a discrete set of compounds that favourably altered CALCR localisation in AF-ACFs, defined as a reduction in the P/C ratio by ≥2 SD from the mean of all conditions in that screen. Specifically, 46 (hit rate: 1.5%), 48 (1.6%), and 3 (0.1%) were identified as hits in donor 1, 2, and 3, respectively (**Table 5.3**, **Fig 5.3.4A**). These compounds were distributed across a range of cell counts, indicating that the observed effects were not confined to compounds that approached the predefined toxicity threshold (**Fig 5.3.4B**). Notably, levamlodipine besylate, the stereoselective preparation of racemic amlodipine, was the only compound identified as a hit across all three donors (**Fig 5.3.4C**). The racemic formulation, amlodipine (maleate), was identified in two of the three donors. Nine compounds were mutually identified in two donors: amlodipine (maleate), chlorprothixene, cyclo(RGDyK) (trifluoroacetate), docetaxel (trihydrate), gilteritinib (hemifumarate), niclosamide, pimethixene (maleate), temoporfin, and perphenazine.

Visual inspection of CALCR staining for these drugs indicated temoporfin was a false positive due to the intrinsic fluorescence of the compound itself. Furthermore, docetaxel, gilteritinib (hemifumarate), and niclosamide profoundly altered cell morphology, consistent with cytostatic or cytotoxic effects suggesting their unsuitability as repurposing candidates (**Fig 5.3.4D**). These compounds were deprioritised for further analysis.

Table 5.3 CALCR localisation compound hits in each donor, ranked by Z-score.

Donor 1	Donor 2	Donor 3
Temoporfin	Temoporfin	Levamlodipine besylate
Amantadine	Mitoxantrone	Lapatinib ditosylate
Tilorone (dihydrochloride)	L-Cysteine (hydrochloride)	Perphenazine
Vinorelbine (ditartrate)	Sorafenib	
Cabazitaxel	Mitoxantrone (dihydrochloride)	
Amlodipine (besylate)	Fenbendazole	
Docetaxel (Trihydrate)	Quercitrin	
Levamlodipine besylate	Cyclo(RGDyK) (trifluoroacetate)	
Halofantrine (hydrochloride)	Siponimod	
Tolbutamide	Gilteritinib hemifumarate	
Amlodipine (maleate)	Erdafitinib	
Loperamide (hydrochloride)	Gilteritinib	
Vandetanib	Berbamine	
Vincamine	Levamlodipine besylate	
Niclosamide	Pexidartinib	
Pimethixene maleate	Niclosamide	
Rucaparib	Chlorprothixene	
Benfluorex (hydrochloride)	Tocofersolan	
Ciclopirox	Carcainium (chloride)	
Urea	Amlodipine (maleate)	
Lovastatin	Ceftezole (sodium)	
Perphenazine	Regorafenib (Hydrochloride)	
Gilteritinib hemifumarate	Lanatoside C	
Chlorprothixene	Neotame	
Clomipramine (hydrochloride)	Cilengitide	
Nalidixic acid	Encorafenib	
Lumefantrine	Anisodamine	
Cyclo(RGDyK) (trifluoroacetate)	Parecoxib (Sodium)	
Triacetin	Umbralisib	
Loxapine (succinate)	Docetaxel (Trihydrate)	
Tetramisole (hydrochloride)	Pexidartinib (hydrochloride)	
Nilotinib (monohydrochloride monohydrate)	Doxazosin (mesylate)	
Zotepine	Pizotifen	
Mibefradil (dihydrochloride)	Digitoxin	
Rimantadine (hydrochloride)	Mitotane	
Vincristine (sulfate)	Cyproheptadine (hydrochloride)	
Oxantel (pamoate)	Vinpocetine	
Abemaciclib	Miglitol	
Aristolochic acid A	Selpercatinib	
Ambroxol	Tianeptine	
Vitexin-2"-O-rhamnoside	Fludrocortisone acetate	
Mirtazapine	Bacitracin	
Vildagliptin	Fangchinoline	
Alverine (citrate)	Rifaximin	
Phenothrin	Pimethixene maleate	
Vinblastine (sulfate)	Vinburnine	
	Naproxen	
	Salmeterol	

A

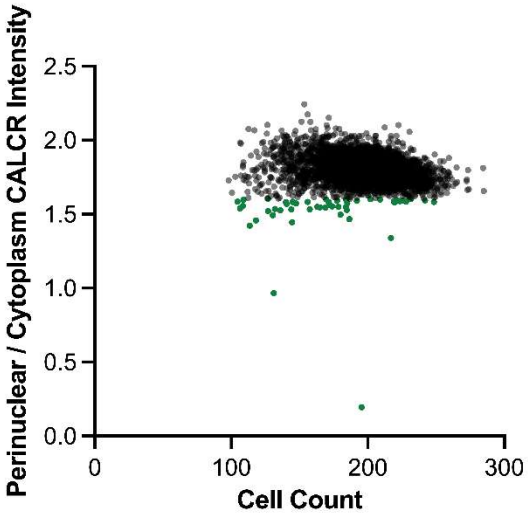


Donor 1 ∩ Donor 2 ∩ Donor 3:
Levamlodipine (besylate)

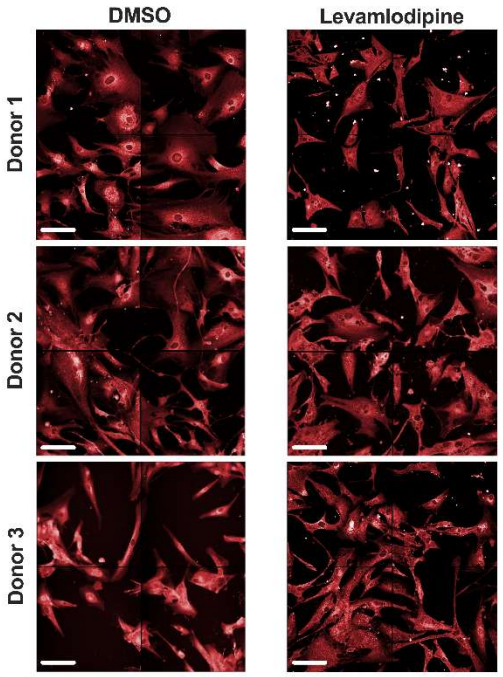
Donor 1 ∩ Donor 2:
Amlodipine (maleate)
Chlorprothixene
Cyclo(RGDyK) (trifluoroacetate)
Docetaxel (trihydrate)
Gilteritinib (hemifumarate)
Niclosamide
Pimethixene (maleate)
Temoporfin

Donor 1 ∩ Donor 3:
Perphenazine

B



C



D

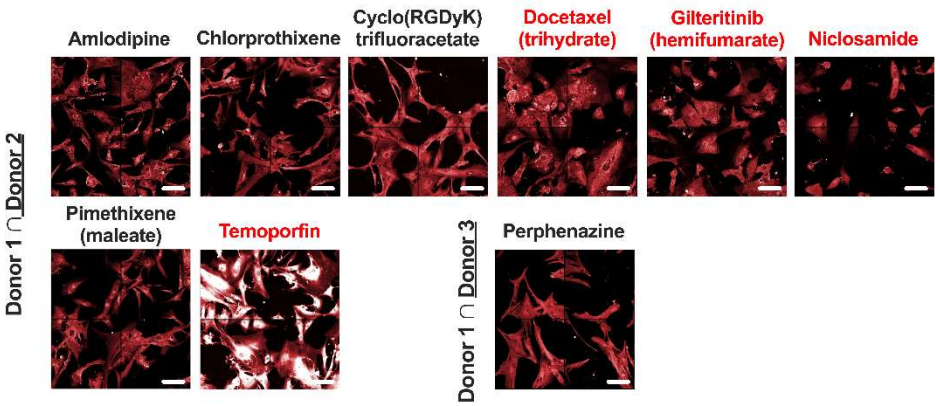


Figure 5.3.4 Identification of CALCR localisation hits. (A) Venn diagram showing overlap of the 86 hit compounds across three screens. **(B)** Distribution of hit compounds across cell counts after toxic conditions were removed for donor 2, the donor with the most identified hits. **(C)** CALCR immunofluorescence images (red) after 10 μM levamlodipine besylate or 0.1% v/v DMSO treatment in each of the donor ACFs. **(D)** Representative CALCR immunofluorescence images of hit compounds identified in 2 of 3 donors. Red text: compounds that were deprioritised due to intrinsic fluorescence or profound morphological change. Representative images of ACFs from the underlined donor. Scale bar, 100 μm.

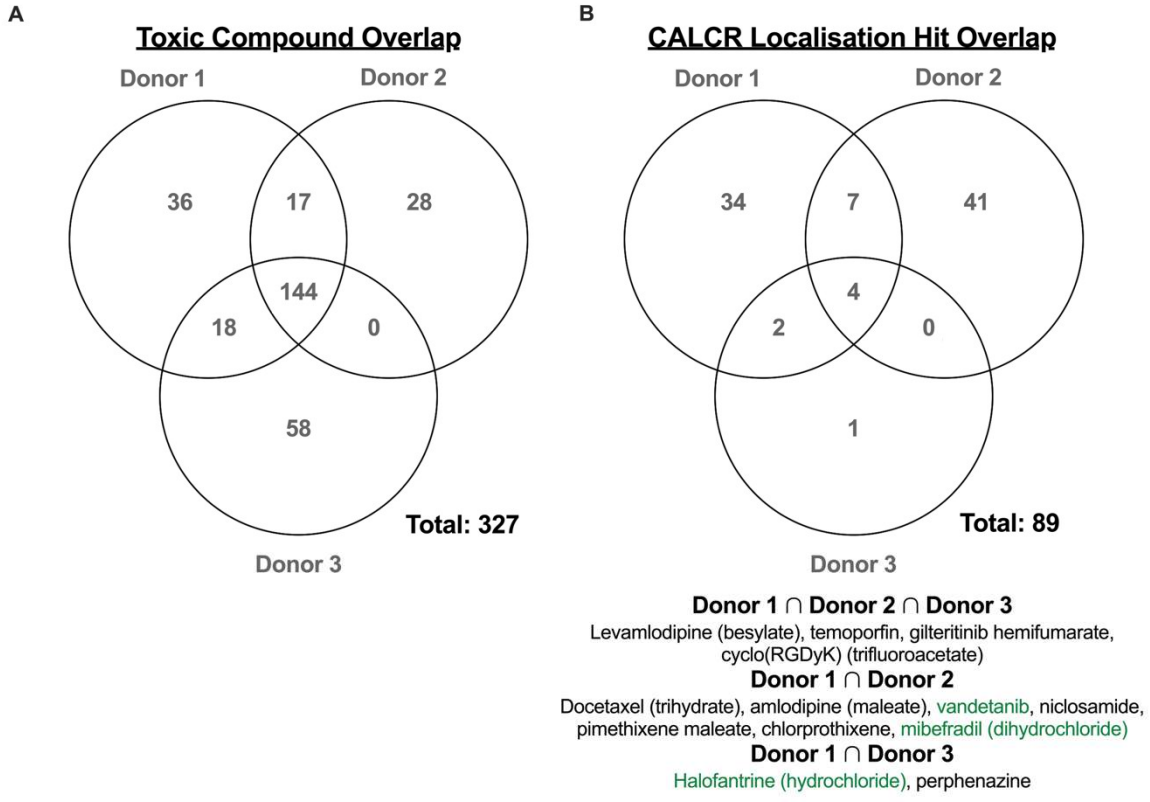
5.3.5 Secondary screening of the effects of cytotoxic compounds on CALCR localisation

As the primary HTS was conducted at 10 μM, it is possible compounds exhibiting cytotoxicity at this dose may have been prematurely excluded despite potential activity at lower, non-toxic concentrations. To address this, compounds previously classified as toxic were re-evaluated in an identical assay format at reduced concentrations (0.25, 1, and 5 μM). There was substantial concordance in the compounds identified as toxic across donors: of the 327 toxic compounds across the three primary screens, 144 (44%) were consistently classified as toxic in all donors (**Fig 5.3.5A**). A complete list of toxic compounds for each donor is provided in **Appendix 3** which may serve as a useful reference for dose selection in primary ACFs in future work. Application of the same hit-defining P/C threshold identified an additional 1 (donor 1), 4 (donor 2), and 4 (donor 3) hit compounds (**Table 5.4**). Three of the new hits identified in donor 3 were previously identified as hits in the other two donors at 10 μM. To include hits identified at any dose, I constructed a new Venn diagram summarising the updated inter-donor overlap (**Fig 5.3.5B**). This identified three additional compounds that were identified as hits in ≥2 donors (**Fig 5.3.5C**).

Table 5.4 CALCR localisation compound hits identified after re-screening compounds previously identified as toxic at lower concentrations.

Donor 1	Donor 2	Donor 3
Verteporfin	Vandetanib	Temoporfin*
	Cinobufotalin	Gilteritinib hemifumarate
	Mibefradil (dihydrochloride)	Halofantrine (hydrochloride)
	Atorvastatin	Cyclo(RGDyK) (trifluoroacetate)

*All compounds were identified as hits at 5 µM, except for temoporfin in donor 3 which emerged as a hit at both 5 and 1 µM



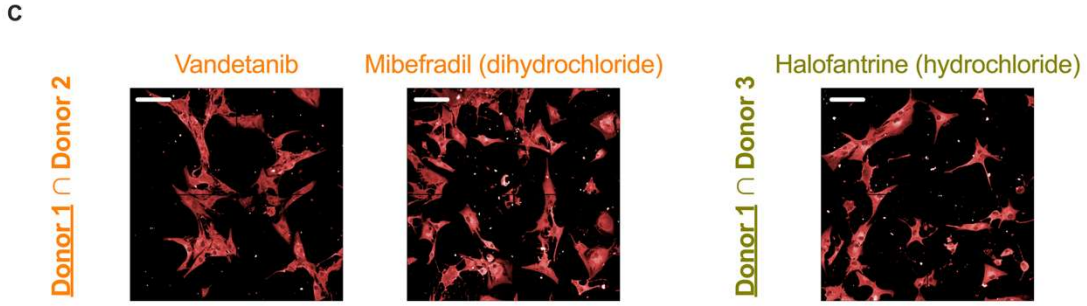


Figure 5.3.5 Re-evaluation of cytotoxic compounds at lower concentrations identifies additional CALCR localisation hits. (A) Venn diagram showing overlap of compounds classified as toxic across the three donor screens. **(B)** Venn diagram summarising overlap of CALCR localisation hits across donors following inclusion of compounds identified at any dose (10 μM primary screen and 0.25-5 μM secondary screen). Green text indicates new overlapping hits. **(C)** Representative CALCR immunofluorescence images of additional hit compounds identified in ≥2 donors. Images are taken from donor 1 (underlined) at 10 μM, a concentration at which these compounds were not classified as toxic. Scale bar, 100 μm.

5.3.6 Identification of Collagen I hits

To assess the effects of library compounds on the production of collagen I by AF-ACFs, two complementary readouts were employed: (i) mean cytoplasmic collagen I fluorescence intensity, and (ii) a metric in which fluorescence intensity was thresholded to generate a binary mask, from which the proportion of cytoplasmic area occupied by this collagen I mask was calculated (**Fig 5.2.2B-C**). The latter was designed to reduce sensitivity to variation in absolute intensity.

Using the intensiometric readout, 42 unique compounds were identified as hits across the three donors in primary screening (**Table 5.5**, **Fig 5.3.6A**), with ixazomib and copanlisib (dihydrochloride) identified in all donors. Re-evaluation of compounds initially classified as toxic at lower concentrations (0.25, 1, and 5 μM; **Appendix 3** and **section 5.3.5**) yielded an additional three hits in donor 3 – homoharringtonine, halofuginone, and harringtonine (all at 5 μM) – each of which had been identified in the other donors at 10 μM. Inclusion of these compounds increased the number of hits consistently identified across all donors to five (**Fig 5.3.6B-C**).

Using the thresholded collagen I coverage metric, 130 unique compounds were identified across the primary screens (**Table 5.6**; **Fig 5.3.7A**). No additional hits were identified following re-evaluation of toxic compounds at lower concentrations. Three compounds –

5-azacytidine, ixazomib, and ixazomib citrate – were consistently identified across all donors, with a further 30 compounds identified in two of three donors (**Fig 5.3.7A-B**). Notably, all compounds identified as hits in ≥2 donors using the intensiometric readout were also captured by the coverage-based metric, indicating strong concordance between the two approaches.

Table 5.5 Collagen I compound hits in each donor, ranked by Z-score, as defined by mean collagen I cytoplasmic staining intensity.

Donor 1	Donor 2	Donor 3
Tetrandrine	Homoharringtonine	Bortezomib
Lanatoside C	Halofuginone (hydrobromide)	Copanlisib (dihydrochloride)
Estradiol	Mitoxantrone (dihydrochloride)	Rilpivirine
9-Aminoacridine	Harringtonine	Progesterone
5-Azacytidine	Mitoxantrone	Montelukast (sodium)
Ouabain (Octahydrate)	5-Azacytidine	Ixazomib
Berberine (chloride)	Halofuginone	Masitinib
Methylene blue (trihydrate)	Copanlisib (dihydrochloride)	
Cinobufotalin	Lanatoside C	
Halofuginone	Halofuginone (hydrobromide)	
Homoharringtonine	Deslanoside	
Ciclesonide	Digitoxin	
Copanlisib (dihydrochloride)	Ixazomib citrate	
Harringtonine	Ixazomib	
Amantadine	9-Aminoacridine	
Deslanoside	Octenidine (dihydrochloride)	
Digitoxin	Bortezomib	
Rubitecan	CB-5083	
Ixazomib	Vitamin K4	
Quercetin	Sanguinarine (chloride)	
Flucytosine	Quercitrin	
Nitroxoline	Visomitin	
Triclocarban	Sofalcone	
Pyrotinib dimaleate	Berberine (chloride)	
Toceranib (phosphate)	Brexpiprazole	

Table 5.6 Collagen I compound hits in each donor, ranked by Z-score, as defined by proportion of the cytoplasm covered by a binary collagen I mask

Donor 1	Donor 2	Donor 3
Halofuginone	Harringtonine	Bortezomib
Lanatoside C	Homoharringtonine	Rilpivirine
Methylene blue (trihydrate)	Mitoxantrone (dihydrochloride)	Sofalcone
Ouabain (Octahydrate)	Mitoxantrone	Sanguinarine (chloride)
Cinobufotalin	Halofuginone (hydrobromide)	Copanlisib (dihydrochloride)
Estradiol	Halofuginone	Benidipine (hydrochloride)
Topotecan (Hydrochloride)	Digitoxin	Mitoxantrone
Homoharringtonine	Halofuginone (hydrobromide)	Ixazomib
Ciclesonide	Lanatoside C	Montelukast (sodium)
Pyrotinib dimaleate	Deslanoside	Progesterone
9-Aminoacridine	5-Azacytidine	CB-5083
Digitoxin	Copanlisib (dihydrochloride)	CP21R7
Atorvastatin	Vitamin K4	Tilorone (dihydrochloride)
Berberine (chloride)	Ixazomib citrate	Proflavine (hemisulfate)
Ixazomib	Bortezomib	Gilteritinib
Triptolide	9-Aminoacridine	Danazol
Harringtonine	Ixazomib	Amonafide
Rubitecan	Brexpiprazole	Atorvastatin
Tivozanib	Ethacridine (lactate monohydrate)	Masitinib (mesylate)
Ruxolitinib	Sofalcone	Melflufen (hydrochloride)
Ixazomib citrate	Sanguinarine (chloride)	Masitinib
L-Ornithine	CB-5083	Ixazomib citrate
Pitavastatin (Calcium)	Rifamycin (sodium)	Aclacinomycin A hydrochloride
Prednisone	Avermectin B1	Norethindrone
Betamethasone valerate	Progesterone	Dasatinib
Isavuconazole	Proflavine (hemisulfate)	Fluvastatin (sodium)
5-Azacytidine	Quercetin	Brexpiprazole
Deslanoside	Octenidine (dihydrochloride)	Midostaurin
CP21R7	Quercetin (dihydrate)	Trifarotene
2-Naphthol	Ethacrynic acid	5-Azacytidine
2-Methoxyestradiol	Prazosin (hydrochloride)	Rucaparib (monocamsylate)
Bleomycin (sulfate)	Rimonabant (Hydrochloride)	Mitoxantrone (dihydrochloride)
Ancitabine (hydrochloride)	Venetoclax	Nitazoxanide
Bifemelane (hydrochloride)	(-)-Securinine	Buclizine (dihydrochloride)
Mozavaptan (hydrochloride)	Pazopanib	Menadione
Desoximetasone	Morin	Chloroxine
Triclocarban	Abemaciclib	Ruboxistaurin
Medrysone	Ethidium (bromide)	Cabozantinib
Teneligliptin (hydrobromide)	Asunaprevir	Estradiol benzoate
Ethacrynic acid	Mitoxantrone (dihydrochloride)	Baricitinib
Duloxetine (hydrochloride)	Clioquinol	Quercetin (dihydrate)
Nilotinib (monohydrochloride monohydrate)	Pitavastatin (Calcium)	Ethacridine (lactate monohydrate)
Dexamethasone	Berberine (chloride)	Betulin
Ibrutinib	Nifedipine	Rubitecan

Isoeugenol	Methylene blue (trihydrate)	Ripasudil
Santonin	Fumagillin	Lomerizine dihydrochloride
Rosiglitazone (maleate)	Quercitrin	Wedelolactone
Azvudine (hydrochloride)	Testosterone propionate	Nitroxoline
	Raloxifene (hydrochloride)	Zofenopril (calcium)
	Triptolide	Adefovir dipivoxil
	Dasabuvir	Lercanidipine (hydrochloride)
	Deferiprone	Testosterone propionate
	Cerivastatin (sodium)	Morin
	Lappaconitine (hydrobromide)	Visomitin
	Irinotecan (hydrochloride)	
	Ponesimod	
	Peficitinib	
	Rucaparib	
	Niclosamide	
	Fidaxomicin	
	Remdesivir	
	Bedaquiline (fumarate)	
	Pyrotinib dimaleate	
	Baicalein	
	Fangchinoline	
	Tipranavir	

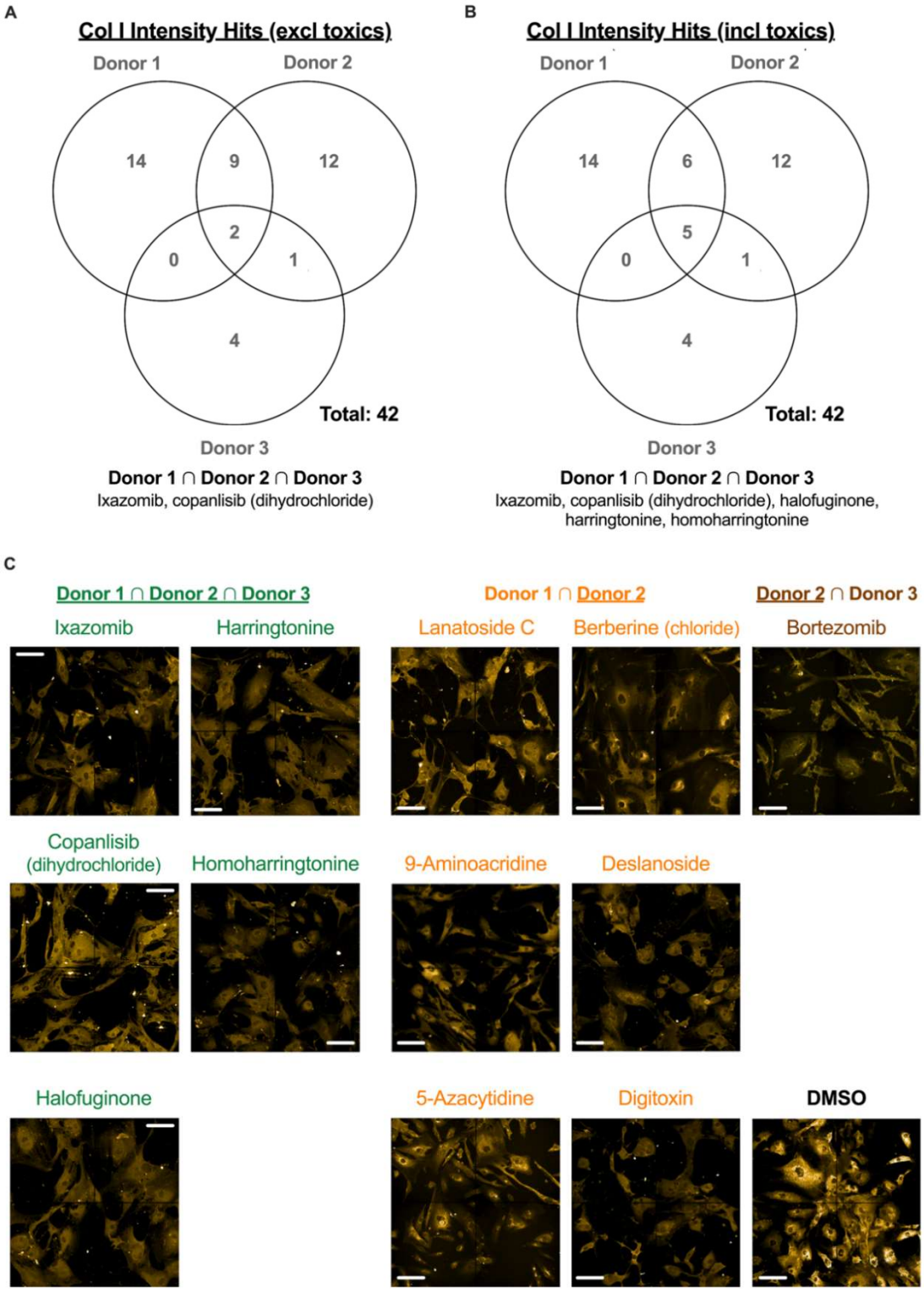


Figure 5.3.6 Identification of collagen I hits assessed by cytoplasmic staining intensity. (A) Venn diagram summarising overlap of hits across the three screens. **(B)** As A, but including compounds identified as hits at any dose (10 μM primary screen and 0.25-5 μM secondary screen). **(C)** Representative collagen I (yellow) immunofluorescence images from donor 2 (underlined) of compounds identified in ≥2 donors. DMSO treated well shown as a control. Scale bar, 100 μm.

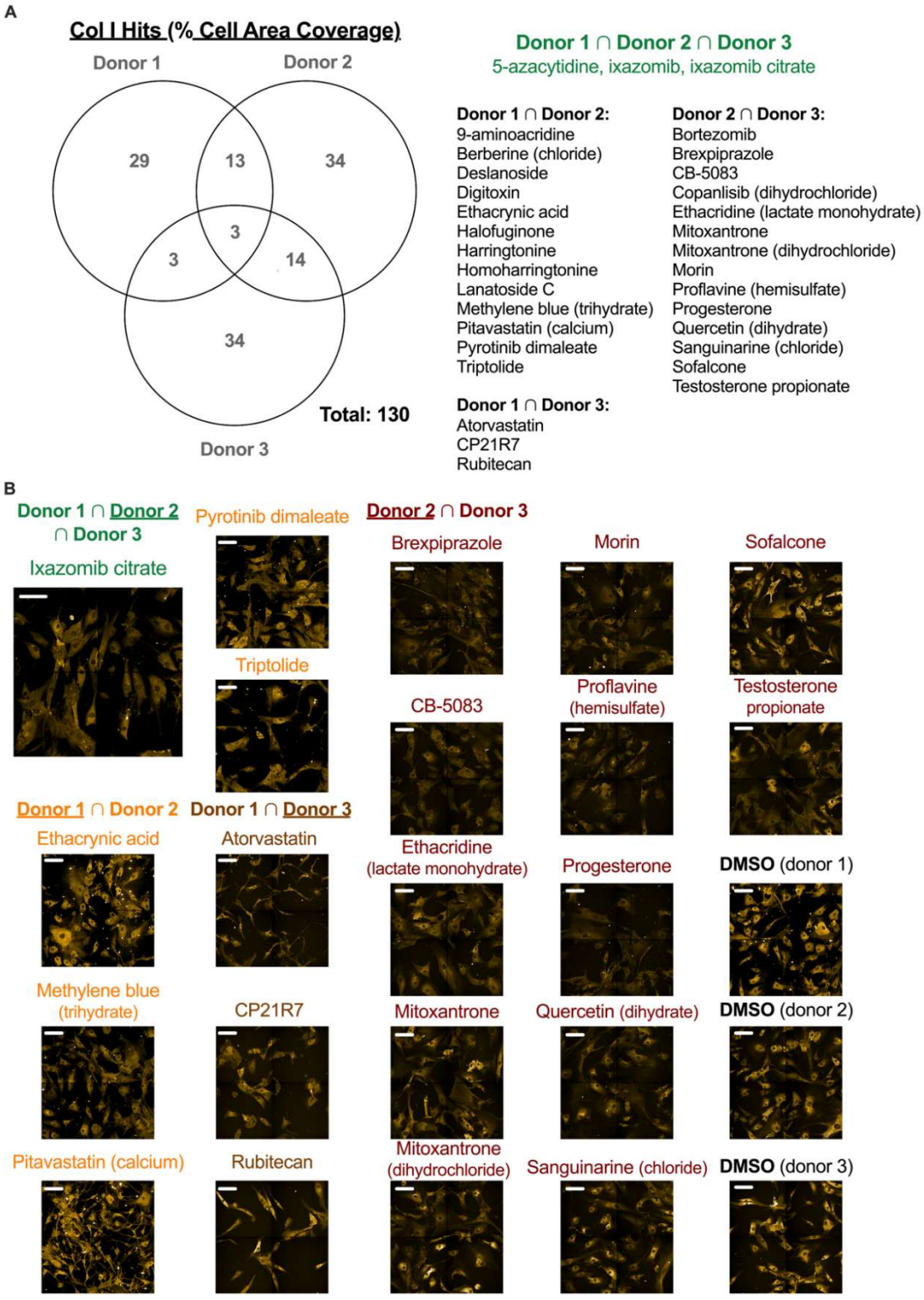


Figure 5.3.7 Identification of collagen I hits assessed by thresholded cytoplasmic area coverage. (A) Venn diagram summarising hit overlap across the three screens. **(B)** Representative collagen I (yellow) immunofluorescence images of compounds identified in ≥2 donors, excluding those shown in **Fig 5.3.6**. Representative images of ACFs from the underlined donor. DMSO treated wells for each donor shown as a control. Scale bar, 100 μm.

5.4 Discussion

In this chapter, I developed and implemented a high-content, phenotypic screening pipeline to identify clinically tractable compounds capable of restoring CALCR localisation in AF-ACFs. This approach was motivated by evidence from previous reductionist studies suggesting that CALCR internalisation in AF-ACFs is unlikely to be driven by a single dominant mechanism. The adoption of an unbiased screening strategy therefore represented a shift from mechanistic dissection to direct identification of pharmacological interventions that normalise receptor localisation irrespective of the underlying molecular mechanism. To my knowledge, this is the first high-throughput drug screen in AF-ACFs.

5.4.1 Assay development and performance

The screening assay exhibited important features required for robust high-throughput screening. First, optimisation of seeding density, antibody conditions, and vehicle tolerance ensured reproducible cell morphology and staining quality over the assay period enabling single-cell resolution. Second, the use of a ratiometric readout (perinuclear-to-outer cytoplasmic CALCR intensity ratio; P/C) improved robustness by mitigating variability in absolute fluorescence intensity and cell density. However, the P/C ratio serves only as a surrogate measure of CALCR localisation and does not directly confirm restoration of a functional surface receptor. This requires further validation assays presented in Chapter 6.

Thirdly, the assay demonstrated a good dynamic range between AF-ACFs and the internal control SR-ACFs (**Fig 5.3.3G**), with a Z'-factor of 0.31 for the P/C ratio indicating good, and widely acceptable, assay performance though falling below the threshold typically considered "excellent" (>0.5).[175,176] It is important to note that this Z'-factor was derived in primary ACFs from distinct donors; a model in which biological variability is

inherently greater than in immortalised cell lines or ACFs treated with artificial, and often extreme, activation protocols.[177,178]

A similar study by Gomes and colleagues (2025), which adopted a similar HTS assay format in commercially available human ACFs, reported a Z'-factor of 0.3 when distinguishing ACFs treated for 3 days with or without TGF-β1 with their assay readout, αSMA expression.[178] Despite their artificial activation protocol, their Z'-factor was comparable to ours highlighting the strength of our assay which did not require experimental perturbation but rather distinguished groups by their native disease background. Furthermore, as expounded by Bar and Zweifach (2020), the HTS field's attachment to Z' > 0.5 may hinder detection of useful compounds by promoting the use of extreme positive control conditions or suppressing the advance of useful phenotypic assays to HTS that capture important disease-relevant biology.[176] To enhance confidence in the robustness and reproducibility of the assay's results, I have 'retested' the most promising compounds in two subsequent donor screens, and validated them in more (independent) donors (Chapter 6).

The use of primary AF-ACFs consequently presents both a significant strength and a limitation. This model, unlike recent large compound library screens which have used iPSC-derived cardiac fibroblasts,[177] captures human-relevant disease-specific biology and has obvious clinical relevance, but introduces variability related to donor background, including age, sex, disease burden, and prior treatments. Although I aimed to limit this variation by including only donors with long-standing (>1 year) persistent AF and excluding donors with type II diabetes or previous stroke, this variability was likely reflected in cell numbers, cell morphology, and in the number of hits identified between donors, most notably the reduced hit rate observed in donor 3. Notably, donor 3 was the only female included in the primary screen and those ACFs were visibly smaller and there were fewer cells per well at the end of the assay. This most likely reflects biological heterogeneity and perhaps sex-specific variation in pharmacological responsiveness,

although technical factors such as differences in attachment efficiency or plate handling cannot be excluded. Another important consideration is the lack of positive control (e.g. a compound which could restore surface CALCR localisation), as it does not exist, against which the performance of hits could be benchmarked. Nevertheless, the preservation of a consistent AF versus SR phenotype across all plates supported the overall validity of the assay.

5.4.2 CALCR localisation hit identification and reproducibility

Application of the automated, objective analysis pipeline identified a relatively small subset of compounds capable of reducing the CALCR P/C ratio, with hit rates ranging from 0.1-1.6% across donors. This low hit frequency is consistent with phenotypic screening approaches employing stringent statistical thresholds and highlights the specificity of this assay. However, concordance between donors was limited, with only a single compound – levamlodipine besylate – identified as a hit across all three donor screens. This may reflect confounding donor-specific characteristics and inter-individual variability in cellular responsiveness, highlighting the importance of considering personalised therapeutic approaches.[179]

The markedly reduced number of hits identified in donor 3 appeared to be driven by a narrow distribution and reduced standard deviation of P/C ratios among non-toxic conditions. This was largely attributable to the exclusion of temoporfin, an intrinsically fluorescent compound that contributed to increased variance in donors 1 and 2, where it was not classified as toxic at 10 μM. Although exclusion of intrinsically fluorescent compounds could reduce assay variability, such an approach risks introducing subjectivity into an otherwise fully automated and unbiased screening pipeline. Given that reproducible hits were identified despite the inclusion of such compounds, this strategy was not adopted. These observations highlight the limitation of artefactual signal arising from compound-specific properties in imaging-based screens.

5.4.3 CALCR hits: L-type calcium channel blockers

The identification of levamlodipine besylate, together with its racemic counterpart amlodipine (in two of three donors), is of particular interest. Amlodipine is a widely prescribed dihydropyridine (DHP) calcium channel blocker (CCB) used as a first-line therapy for hypertension, particularly in non-diabetic patients over 55 years of age and in individuals of Black African or African-Caribbean ancestry, and angina pectoris. Its established clinical use in CVDs, favourable pharmacokinetic profile, and safety record make it an attractive candidate for drug repurposing in CVD (NICE guideline NG136, 2026). Importantly, none of the donors were taking amlodipine or another calcium channel blocker at the time of surgery. While amlodipine is commonly administered as different salt formulations (e.g. besylate, maleate, mesylate), they are generally considered bioequivalent.[180,181] In contrast, the stereoselective S-enantiomer (levamlodipine) possesses distinct pharmacodynamic properties, with 1000-fold greater potency at the L-type calcium channel than the R-enantiomer.[181-183] Compared with racemic formulations, levamlodipine is equally effective at half-dose and has been reported to be better tolerated with lower incidence of peripheral oedema, an important adverse event associated with DHP CCB use.[184,185]

Notably, other DHP CCBs (including azelnidipine, benidipine, clevidipine, cilnidipine, felodipine, isradipine, lacidipine, lercanidipine, manidipine, nifedipine, nimodipine, nitrendipine) or non-DHP CCBs (e.g. verapamil or diltiazem) were included in the library but did not emerge as hits. This suggests that the observed effect of levamlodipine on CALCR localisation is unlikely to reflect a simple inhibition of calcium influx in ACFs. Instead, these findings point towards a more specific or off-target mechanism, potentially related to stereoselective effects on cytoskeletal or trafficking pathways. Amlodipine has previously been reported to modify actin cytoskeleton dynamics in the fenestrations of liver sinusoidal cells and disrupt cytoskeletal organisation in oocytes.[186,187]

5.4.4 CALCR hits: integrin inhibitors

Several additional compounds were identified in two of three donors. Specifically, cyclo(RGDyK) (trifluoroacetate) (an inhibitor of the $\alpha_v\beta_3$ arginine-glycine-aspartic acid (RGD)-binding integrin family) and cilengitide (a dual $\alpha_v\beta_3$ and $\alpha_v\beta_5$ inhibitor) were identified as hits at 10 μM in one donor and approached the hit threshold in the other two donors when screened at lower concentrations. Integrins are heterodimeric transmembrane receptors that mediate bidirectional ('inside-out' and 'outside-in') signalling.[188] In fibrogenesis, α_v-containing integrins expressed by myofibroblasts bind RGD motifs with the latency-associated peptide (LAP) of TGF-β, thereby facilitating activation of latent TGF-β.[188-190] Consistently, pharmacological inhibition or genetic ablation of α_v integrins suppresses fibrosis across multiple organs, including lung, liver, skeletal muscle, and heart.[191,192] It is therefore plausible that the anti-fibrotic effects of α_v-integrin inhibition extend beyond attenuation of pro-fibrotic signalling (e.g. TGF-β), and may involve restoration of responsiveness to anti-fibrotic cues, such as CT.

Moreover, the integrins form extensive interactions with components of the actin, intermediate filament and microtubule components of the cytoskeleton which regulate cell migration, force transduction and cytoskeletal organisation.[193,194] This dynamic crosstalk may explain how integrin inhibition influences CALCR localisation through changes in cytoskeletal organisation and function.

In the context of CVD, small molecule and antibody antagonists of $\alpha_{IIb}\beta_3$ integrins have been approved for the management of acute coronary syndrome and thrombotic disorders as inhibitors of platelet aggregation. However, their clinical use has declined due to the availability of P2Y12 and PAR1 antagonists, which have lower bleeding risk.[195] Given the elevated haemorrhagic risk associated with combining antiplatelet agents with oral anticoagulation – the mainstay of stroke prevention in AF – careful consideration of

integrin subtype specificity will be essential when evaluating the repurposing of anti-integrin therapies in patient populations with indication for antiplatelet therapy.[196]

5.4.5 CALCR hits: deprioritised compounds

Image inspection also revealed a proportion of the identified hits represented false positive results or had significant off-target effects. For example, temoporfin and verteporfin exhibited strong intrinsic fluorescence, leading to artefactual signal detection. Similarly, compounds such as docetaxel, gilteritinib, and niclosamide induced marked morphological changes, consistent with cytotoxic or cytostatic effects, which confound interpretation of localisation metrics. These findings underscore the importance of integrating automated analysis with manual inspection in high-content screening workflows. Future work may also study the compounds that enhanced CALCR internalisation, as these may yield mechanistic insight into the pathways governing receptor trafficking in ACFs.

5.4.6 Secondary collagen I readouts

Alongside the CALCR localisation readout, collagen I expression was assessed as a surrogate measure of direct antifibrotic activity to identify hits that may serve as a foundation for future studies. Two independent metrics – cytoplasmic intensity and thresholded cytoplasmic coverage – generated largely consistent lists of hits. The identification of ixazomib, copanlisib (dihydrochloride), and 5-azacytidine across donors suggests that pathways regulating protein degradation, kinase signalling, and epigenetic modulation may influence fibroblast activation and production of important ECM components. Ixazomib, an oral 20S proteasome inhibitor approved for multiple myeloma, is associated with a side-effect profile that is unlikely to be acceptable to patients with AF, who typically have a relatively low symptom burden.[197] Similarly, copanlisib, a PI3-kinase inhibitor previously used as a treatment for relapsed follicular lymphoma, was recently withdrawn by Bayer due to limited efficacy when combined with existing

chemoimmunotherapies.[198] Moreover, its use was associated with poor tolerability and significant adverse events including hyperglycaemia and hypertension which similarly makes it unacceptable for patients with AF.[198] Therefore, these therapies represent unattractive candidates for therapeutic repurposing in this indication but their identification may reveal insight into ACF biology and the mechanisms of fibrogenesis.

Some of the identified hits were consistent with the existing literature. Comparison of the hits that were identified in ≥2 donors, across either readout, with those identified in the study by Gomes *et al* (2025) which used the smaller Prestwick compound library (1280 compounds), identified mutual hits: mitoxantrone [dihydrochloride], pitavastatin [chloride], and lanatoside C. The co-identification of these molecules in HTS assays using different primary readouts to assess fibroblast activation enhances confidence in their potential anti-fibrotic capabilities. The further study of these hits is currently underway by another doctoral student in the group.

However, and consistent with the study by Gomes and colleagues, metrics based exclusively on collagen I staining produced unsatisfactory Z'-factors suggesting they are unsuitable as primary readouts in this assay format.[178] Furthermore, these readouts do not inform on the extracellular deposition of mature collagen which is of more direct relevance to cardiac fibrosis. In future screens, alternative approaches – such as secreted collagen I or extracellular matrix deposition assays – may provide more sensitive antifibrotic readouts.

5.4.7 Conclusions and implications

This chapter describes the development and implementation of a robust, high-content phenotypic screening platform to identify therapeutically promising compounds capable of restoring CALCR localisation in AF-ACFs. By screening over 3000 compounds in three independent donors, I identified levamlodipine besylate as a reproducibly effective compound. Additional candidate compounds, including integrin inhibitors, suggest

potential links between cytoskeletal signalling and receptor trafficking and align with the existing corpus of literature that has studied integrin signalling in the setting of fibrosis biology. Collectively, these findings establish a scalable, disease-relevant screening platform that identified attractive compounds which narrowed the therapeutic landscape and closed the gap towards clinical translation. Crucially, as CALCR localisation is only a proxy for functional receptor signalling, the next chapter directly assesses these candidate compounds *in vitro* to determine whether they restore cellular responsiveness to CT to rescue antifibrotic signalling in AF-ACFs. I will also begin to explore the possible mechanisms underpinning the observed effect of levamlodipine on CALCR localisation.

CHAPTER 6: MECHANISTIC INVESTIGATIONS INTO THE ANTIFIBROTIC EFFECTS OF SELECTED HIT COMPOUNDS

6.1 Introduction

While the previous chapter's findings establish a framework for pharmacological restoration of receptor localisation, they do not establish whether such changes translate to restoration of functional CALCR signalling and thus reinstate the antifibrotic CT-CALCR axis in AF-ACFs.[1] Accordingly, this chapter aims to functionally validate the most promising screening hit, levamlodipine. Moreover, preliminary studies into the mechanism by which levamlodipine influences CALCR localisation are presented. The potency of prioritised lead compounds on CALCR localisation is also presented.

Given the identification of a dihydropyridine L-type calcium channel (specifically $Ca_V1.2$) antagonist as a lead compound, but not other LTCC antagonists, experiments explored whether the observed effects reflect a compound-specific – rather than a target-specific – mechanism. The mRNA expression of the LTCC in fibroblasts was first reported in foetal dermal fibroblasts, and subsequently in cardiac fibroblasts.[199,200] However, direct functional interrogation of LTCCs in cardiac fibroblasts have been conflicting. Chen *et al* (2010) concluded LTCCs play a subtle role in regulating Ca^{2+} oscillations in ventricular fibroblasts, yet Poulet *et al* (2016) could not detect a voltage-gated Ca^{2+} channel current in right atrial appendage-derived ACFs by voltage-clamp.[113,200] Intriguingly, the latter study did report upregulation of *CACNA1C* (the pore-forming subunit of $Ca_V1.2$) in AF-ACFs when compared with SR-ACFs.[113] Contrastingly, in pulmonary fibroblasts, $Ca_V1.2$ antagonism with nifedipine attenuated fibrogenesis in a bleomycin-induced model of pulmonary fibrosis.[201] These studies illustrate that the mechanisms, and downstream consequences, of Ca^{2+} influx into fibroblasts may vary across species, tissue, and disease state.

The importance of Ca^{2+} influx in ACF activation is increasingly recognised; particularly, inward currents carried by transient receptor potential canonical (TRPC) channels which have emerged as dominant mediators of Ca^{2+} influx in cardiac fibroblasts.[202-204] In

tachypaced dogs, TRPC3 channel inhibition reduced left atrial ACF proliferation, ECM gene expression, and, importantly, reduced AF burden *in vivo*. Leveraging novel computational approaches, a recent study by Khorasani *et al* (2025) established the first atrial-informed, AF-associated fibrosis signalling network, and uncovered a key role for TRPC-mediated Ca^{2+} influx in profibrotic response activation.[205] However, this model was informed using existing literature and did not include a node representing Ca^{2+} influx through $Ca_V1.2$, so a contribution of this pathway to ACF biology may have been overlooked.[205,206] Moreover, the majority of inter-node connections were informed by data generated in non-human fibroblast models which may have limited relevance to human AF-ACFs. Reciprocally, TRPC-channel inhibitors did not feature in the compound library presented in Chapter 5 and, therefore, whether TRPC channel antagonists can restore CALCR localisation is unknown. If the effect of levamlodipine on CALCR localisation was accounted for by solely reducing Ca^{2+} influx, antagonists of other, ostensibly more sizeable Ca^{2+} influx pathways, would be predicted to similarly modify CALCR localisation.

TRPC channels are also contributing components to store-operate Ca^{2+} entry (SOCE), a ubiquitous mechanism whereby Ca^{2+} entry is activated in response to depletion of intracellular Ca^{2+} stores.[207] It was recently shown SOCE is implicated in the cardiac fibroblast profibrotic response to TGFβ1 *in vitro*.[208] Another key molecular component of SOCE is the *Orai1* protein, which forms a hexameric complex and carries the Ca^{2+}-release activated Ca^{2+} current (CRAC) when stimulated by the endoplasmic reticulum-localised Ca^{2+} sensor Stromal interaction molecule 1 (Stim1).[207] Pharmacological inhibition of *Orai1* or siRNA-mediated silencing attenuated the profibrotic response of cardiac fibroblasts to angiotensin II.[209]

This chapter then explores the molecular mechanisms of levamlodipine's effects by knocking down its canonical target (*CACNA1C*), performing RNA sequencing (RNAseq) following levamlodipine treatment, and establishing the consistency of the CALCR localisation phenotype in an *in vivo* model of persistent AF.

The prevalence of AF among small mammals is perishingly low and, therefore, supraphysiological perturbation (either anatomical, genetic, or pharmacological) is required to establish sustained AF.[210] Accordingly, animal models typically recapitulate specific pathogenic processes (e.g. ectopy, structural remodelling, inflammation) but largely fail to recapitulate the heterogenous and multi-faceted processes that culminate in human AF. One model that captures processes relevant to this work is the cAMP-Response Element Modulator-IbΔC-X isoform overexpressing transgenic (CREM-Tg) mouse under the control of the cardiomyocyte-specific α myosin heavy chain (αMHC) promoter which is characterised by progressive atrial remodelling, cardiomyocyte Ca^{2+} mishandling, and the gradual progression of atrial ectopy to chronic AF.[211,212] CREM is a member of the cAMP-dependent transcription factor family which transduces cAMP signalling to transcriptional regulation; the CREM-IbΔC-X isoform is a repressor of cAMP-mediated gene transcription.[213] At 3 months of age these mice begin to exhibit signs of atrial ectopy which progresses to permanent AF by 9 months, concurrent with severe atrial dilation and fibrosis (with only mildly reduced left ventricular function).[214] Therefore, these mice recapitulate the progressive evolution of structural remodelling observed in AF patients.

Collectively, this chapter integrates functional, pharmacological, transcriptomic, and cross-species approaches to determine whether compounds identified in the high-throughput screen can restore CALCR-dependent antifibrotic signalling and begins the process of defining the mechanisms by which these effects are mediated.

6.2 Methods & Materials

6.2.1 *In silico* prediction of protein targets of CALCR hits

The BindingDB database is an experimental molecular recognition database encompassing 2.9 million unique binding measurements between 1.3 million compounds and thousands of protein targets. Compounds were queried with the "Find My Compound's Targets" tool and the maximum similarity filter was set to 1 (to include only compounds identical to that being queried).[215,216]

For SwissTargetPrediction, Simplified Molecular Input Line Entry System (SMILES) identifiers for the bioactive component of the compound (i.e. excluding the counterion) were imported into the online webtool (http://www.swisstargetprediction.ch/) and predictions with >50% probability of being a target for that molecule were recorded.[217] This model uses a ligand-based approach to predict the targets of compounds using 2D and 3D structural similarities between the queried molecule and the known ligands of a specific protein (2092 human proteins are included, this does not include $Ca_V1.2$). [c]

6.2.2 Determination of concentration-response relationships

Prioritised hits (levamlodipine besylate, amlodipine (maleate), chlorprothixene, cyclo(RGDyK) (trifluoroacetate), pimethixene (maleate), and perphenazine) were added to ACFs in ten serial dilutions by 3-fold from 10 μM to 0.5 nM. Similarly, the concentration-response relationships for antagonists of TRPC channels or activators/inhibitors of store-operate Ca^{2+} entry (SOCE) were determined using the same concentration range (**Table 6.2**); compounds were provided as a generous gift from Dr Tryfon Zarganis-Tzitzikas of the Target Discovery Institute, University of Oxford. All screening and data analysis was conducted blinded to the compound identity. The same three donors included in the

[c] A complete list of the proteins included in the training set for the model was provided in personal correspondence with the SwissDrugDesign team. However, at their request, this information remains confidential.

primary screen were included in this follow-up study (**Table 5.2**). The assay protocol and image analyses were identical to the primary screens, with each condition performed in technical duplicate (**section 5.2.2-3**). Concentration-response curves were modelled by nonlinear regression using a four-parameter logistic (4PL) equation (log[inhibitor] vs response, variable slope) in GraphPad Prism (v11).

6.2.3 *In vitro* validation of levamlodipine besylate

The AF-ACFs derived from donors not included in the primary screen were seeded into 6-well plates at a density of 100,000 cells/well. ACFs were serum starved (0.5% FBS) for 4h prior to a 24h pre-treatment with either levamlodipine besylate (10 μM, HY-14744A, MedChemExpress) or vehicle (0.1% v/v DMSO) control. Following pre-treatment, the media was replaced with 0.5% FBS medium containing 100 μM ascorbic acid (a co-factor for prolyl hydroxylase), ± levamlodipine besylate, ± human calcitonin (hCT, 100 nM, 4014409.0001, Cambridge Bioscience), ± the selective CALCR antagonist sCT8-32 (100 nM; Cambridge Bioscience, 4037182.0500), and incubated for an additional 48h (**Fig 6.2.1**). At the end of the treatment period, conditioned media (secretome) and cell lysates were collected, as described in **section 2.3**.

Conditioned media was concentrated 10-fold using Concentration Solution (90626, Chondrex), as per the manufacturer's protocol. Total secreted collagen in the cell culture supernatant was quantified using a Sirius Red total collagen detection kit (9062, Chondrex) as per the manufacturer's protocol and as described previously.[1] Collagen concentration was normalised to the corresponding protein concentration of the cell lysate and expressed as a fold-change on vehicle treatment. Cell lysates were subjected to WB analysis of pro-fibrotic markers including collagen I (1:1000, 14695-1-AP, Proteintech) and αSMA (1:1000, A5228, Merck). The role of $Ca_v1.2$ was studied by

CACNA1C siRNA-mediated knockdown (as described in Chapter 2) and cell lysates were collected and analysed by WB.

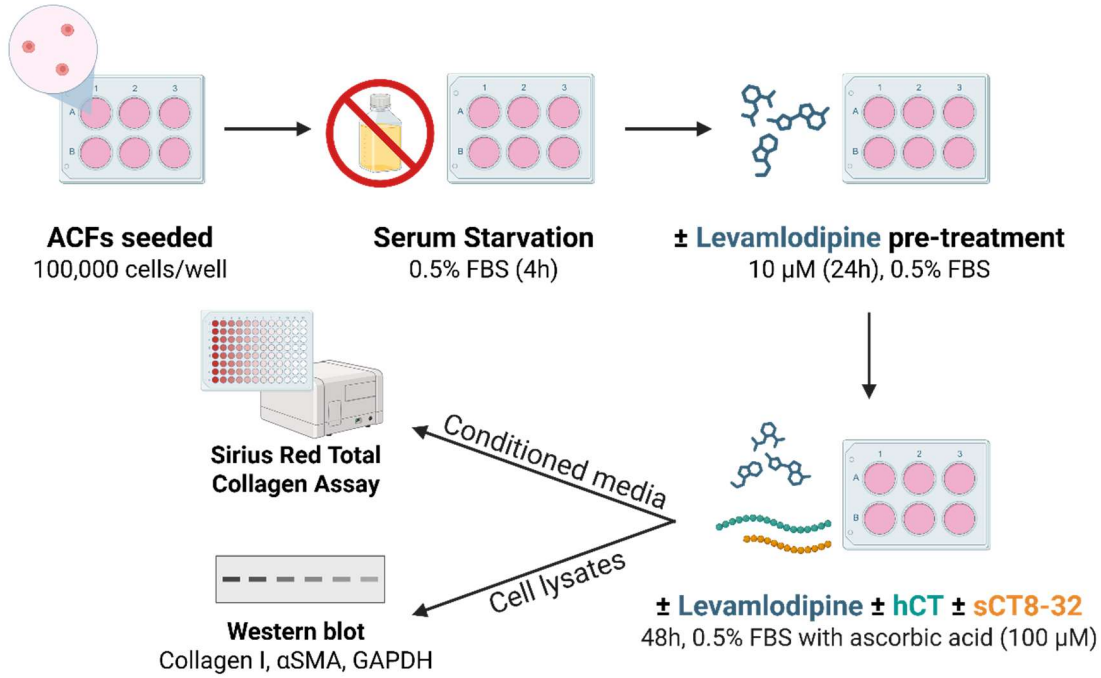


Figure 6.2.1 Experimental workflow for assessing restoration of calcitonin responsiveness in independent AF-ACFs. αSMA, α smooth muscle actin; FBS, foetal bovine serum; hCT, human calcitonin; sCT8-32, salmon calcitonin 8-32.

6.2.4 RNA sequencing (RNAseq) analysis

RNAseq was performed in human AF-ACFs derived from 4 donors, unique from those included in the primary screen, treated with 0.1% v/v DMSO (vehicle) or levamlodipine besylate (levamlodipine, 10 µM) for 24h. At the end of treatment, RNA was collected and isolated as described in **section 2.2.** 100 ng of RNA was sent for sequencing. RNAseq and differentially expressed gene (DEG) analysis were performed by Azenta Life Sciences, U.K. who provided the following technical details. RNA samples were assessed using Qubit 4.0 Fluorometer (Life Technologies, Carlsbad, CA, USA) and RNA integrity was checked with an RNA Kit using an Agilent 5300 Fragment Analyser (Agilent Technologies, Palo Alto, CA, USA). RNA libraries were prepared using the NEBNext Ultra

II RNA Library Prep Kit for Illumina following manufacturer's instructions (NEB, Ipswich, MA, USA). mRNAs were enriched with Oligo(dT) beads and fragmented for 15 minutes at 94ºC. First strand and second strand cDNAs were synthesised and cDNA fragments were end repaired and adenylated at 3' ends. Universal adapters were ligated to cDNA fragments followed by index addition and library enrichment by limited-cycle PCR. Sequencing libraries were validated using NGS Kit on the Agilent 5300 Fragment Analyser (Agilent Technologies, Palo Alto, CA, USA), and quantified by using Qubit 4.0 Fluorometer (Invitrogen, Carlsbad, CA). Quality control data are presented in **Appendix 4**.

For sequencing, libraries were multiplexed and loaded on the flowcell of the Illumina NovaSeq instrument. The samples were sequenced using a 2x150 bp paired-end configuration v1.5. Image analysis and base calling were conducted by the NovaSeq Control Software v1.7 on the NovaSeq instrument. Raw sequence data (.bcl files) generated from Illumina NovaSeq was converted into FASTQ files and de-multiplexed using Illumina bcl2fastq program v2.2μ. One mismatch was allowed for index sequence identification.

For data analysis, raw data quality was assessed, and sequence reads were trimmed to remove adapter sequences. Nucleotides with poor quality were removed using Trimmomatic v0.36. The trimmed reads were mapped to the *Homo sapiens* reference genome available on ENSEMBL using the STAR aligner v2.5.2b which detects splice junctions and incorporates them to help align the entire read sequences; this generated BAM files. Unique gene hit counts were calculated by using the Counts feature from the Subread package v1.5.2. Only unique reads that fell within exon regions were counted.

Gene hit counts were then used for downstream differential expression analysis. Using DESeq2, a comparison of gene expression between the groups of samples (vehicle vs levamlodipine) was performed.[218] The Wald test was used to determine p-values and

log_2 fold changes (Log_2[FC]). Log_2 fold change of the normalised hit counts was defined as:

$$Log_2 FoldChange = log_2(\frac{Levamlodipine\ group\ mean\ normalised\ counts}{Vehicle\ group\ mean\ normalised\ counts})$$

Global false discovery rate (FDR) was controlled for by adjusting p-values using the Benjamini-Hochberg procedure. Genes with adjusted p-values < 0.05 and absolute log_2FoldChanges > 1 were called as differentially expressed genes (DEGs). A principal component analysis (PCA) plot was constructed using the "plotPCA" function within the DESeq2 R package using the top 500 genes, selected by highest row variance.

KEGG pathways analysis of DEGs was performed using ShinyGO 0.85.1 with the background set as all the identified genes (N=19,687) during sequencing. FDR cutoff was set at 0.05 and the pathway sizes were filtered between 2-5000.

6.2.5 Assessment of CALCR localisation in ACFs from CREM-IBΔC-X-Tg mice

Animal studies were performed by our collaborators (laboratory of Professor Xander Wehrens) at the Baylor College of Medicine conforming to the Guide for the Care and Use of Laboratory Animals published by the U.S. National Institutes of Health. The atria from 3-month or 9-month-old CREM-IbΔC-X (CREM) transgenic mice on a FVB/N background were enzymatically digested to isolate ACFs as described previously.[211,219] ACFs at passage 2 from 9-month-old CREM mice were seeded on chamber slides (Nunc Lab-Tek II Chamber Slide), serum starved (0.5% FBS) overnight before a 24h treatment with levamlodipine (10 μM) or vehicle (0.1% DMSO). ACFs were fixed with 4% PFA followed by glycine quenching and permeabilization with triton x-100 and blocked using normal goat serum. They were stained for CALCR (BS-0124R, ThermoFisher) overnight at 4ºC and incubated with rabbit secondary antibody (A11008, Invitrogen) and anti-phalloidin (R415, ThermoFisher) at room temperature for 1h. The chamber was then removed, and the slide was mounted with VECTASHIELD Antifade Mounting Medium

with DAPI (H-1200-10, Vector Labs). Imaging was performed using a 20X objective on a Zeiss AXIO Observer 7. This work was performed by Mr Shuai Zhao, to whom I am very grateful. Image analysis was performed by me using the JACoP BIOP plugin for FIJI (v2.9.0 1.54d) as described in Chapter 2.

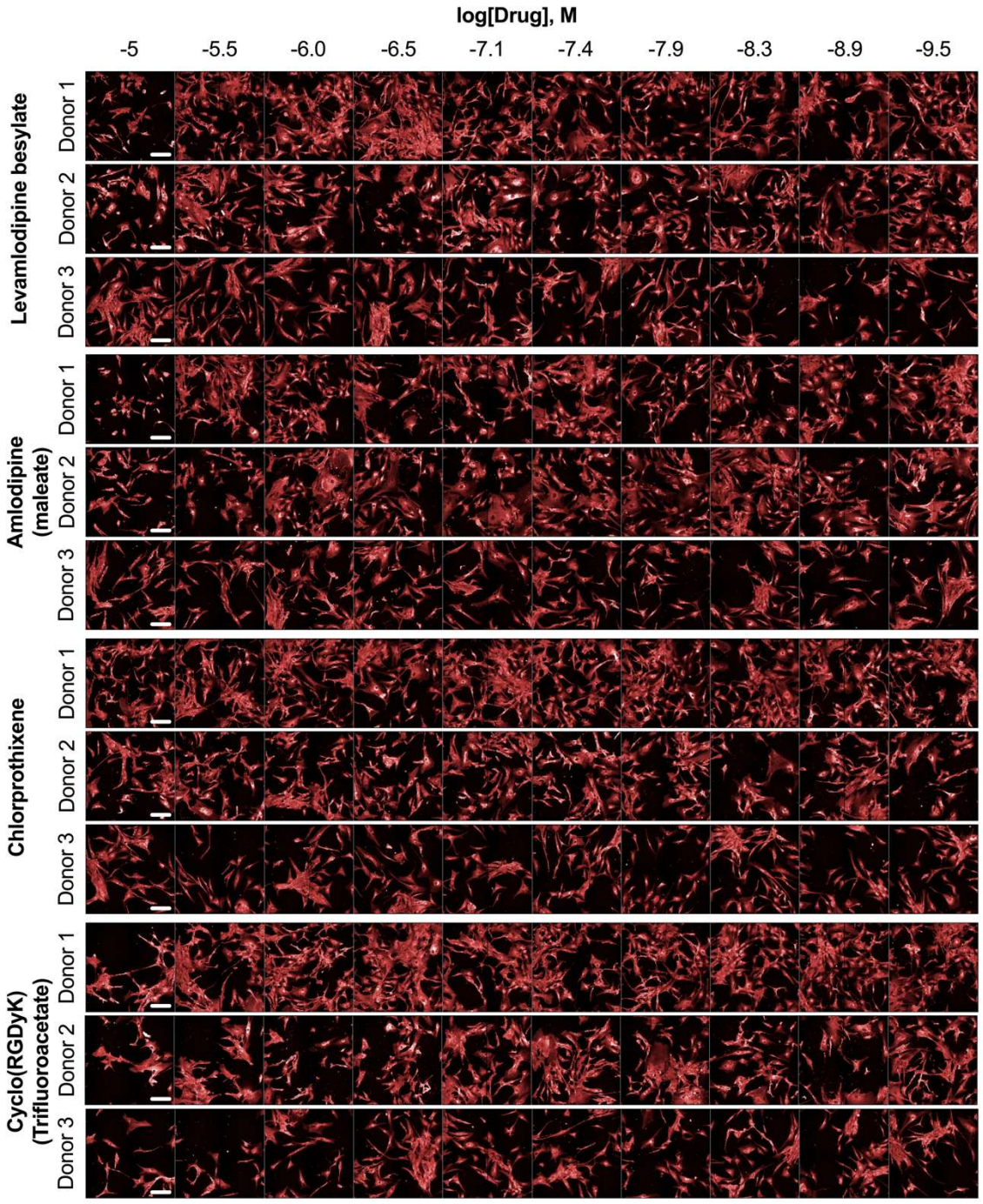
6.3 Results

6.3.1 Further characterisation of CALCR hits identified in ≥2 donors

To identify potential shared targets of the ten molecules identified as having capacity to normalise the CALCR P/C ratio, the BindingDB database of protein-ligand interactions and SwissTargetPrediction tool were interrogated (**Table 6.1**).[215,216,220] The complementary combination of the BindingDB database and the SwissTargetPrediction tool enabled integration of experimentally validated ligand-target interactions with *in silico* target prediction. Common target classes included 5-hydroxytryptamine (5-HT) receptors (specifically 2a, 6, and 7) and dopamine receptors (specifically 2, 3, and 4). Collectively, these findings suggest that restoration of CALCR localisation could arise from modulation of a limited number of shared signalling pathways.

Furthermore, 10-point concentration-response curves (CRCs, 0.5 nM-10 μM) were recorded for prioritised hits in the same three donors as used in the primary HTS (**Fig 6.3.1**). The effects on the average cell counts and P/C ratios for each donor are shown in **Fig 6.3.2A-B**. These analyses revealed evidence of a modest, donor-dependent toxicity at 10 μM for several compounds, including levamlodipine besylate, amlodipine (maleate), cyclo(RGDyK) (trifluoroacetate), and perphenazine. ACFs derived from donor 3, the only female, appeared comparatively less sensitive to these cytotoxic effects than those from the other donors, highlighting inter-donor variability.

Analyses of the CRCs demonstrate that, although a concentration-dependent effect was evident, a stable, saturating response was not achieved within the tested range, as indicated by the absence of a lower asymptote. Consequently, reliable estimation of EC_{50} values was not possible.


log[Drug], M
-5
-5.5
-6.0
-6.5
-7.1
-7.4
-7.9
-8.3
-8.9
-9.5
Levamlodipine besylate
Amlodipine (maleate)
Chlorprothixene
Cyclo(RGDyK) (Trifluoroacetate)
Donor 1
Donor 2
Donor 3

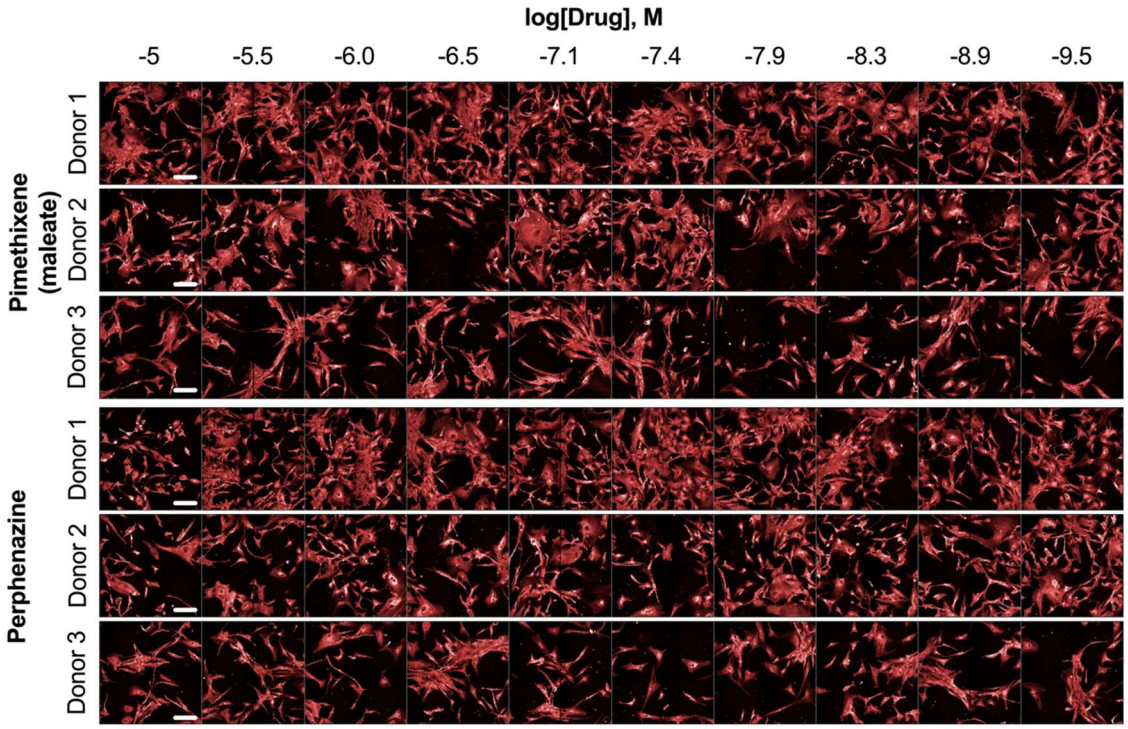


Figure 6.3.1 Concentration-dependent effects of prioritised compounds on CALCR localisation in AF-ACFs across each donor. Representative immunofluorescence images of CALCR (red) in ACFs derived from the same three donors as used in the primary screen (Chapter 5). ACFs were treated across a 10-point concentration range (log[drug], M, as indicated) with levamlodipine besylate, amlodipine (maleate), chlorprothixene, and cyclo(RGDyK) (trifluoroacetate), pimethixene (maleate), and perphenazine. Scale bar, 100 μm.

Table 6.1: Protein target prediction for mutual CALCR hit compounds by two *in silico* ligand-target prediction tools. Green text indicates proteins identified by both prediction tools for that compound.

Compound	SMILES	BindingDB Predictions	SwissTargetPrediction Predictions
Levamlodipine besylate	O=C(C1=C(COCCN)NC(C)=C(C(OC)=O)[C@@H]1C2=CC=CC=C2Cl)OCC.OS(C3=CC=CC=C3)(=O)=O	Potassium channel subfamily K member 2; Potassium two pore domain channel subfamily K member 2; Voltage-dependent L-type calcium channel subunit alpha-1C	Alpha-2a adrenergic receptor; Adrenergic receptor alpha-2; Alpha-1d adrenergic receptor; Potassium channel subfamily K member 2; Alpha-1b adrenergic receptor; Dopamine transporter; 5-hydroxytryptamine receptor 6
Amlodipine (maleate)	O=C(C1=C(COCCN)NC(C)=C(C(OC)=O)C1C2=CC=CC=C2Cl)OCC.OC(/C=C\C(O)=O)=O	Potassium channel subfamily K member 2; Potassium two pore domain channel subfamily K member 2; Voltage-dependent L-type calcium channel subunit alpha-1C	Alpha-2a adrenergic receptor; Adrenergic receptor alpha-2; Alpha-1d adrenergic receptor; Potassium channel subfamily K member 2; Alpha-1b adrenergic receptor; Dopamine transporter; 5-hydroxytryptamine receptor 6
Chlorprothixene	CN(C)CC/C=C1C2=C(SC3=C\1C=CC= C3)C=CC(Cl)=C2	5-hydroxytryptamine receptor 2A; 5-hydroxytryptamine receptor 6; 5-hydroxytryptamine receptor 7; D1A dopamine receptor; D1B dopamine receptor; D2 dopamine receptor; D3 dopamine receptor; D4 dopamine receptor; Histamine H1 receptor; Histamine H3 receptor; Muscarinic acetylcholine receptor M1; Muscarinic acetylcholine receptor M2; Muscarinic acetylcholine receptor M3; Muscarinic acetylcholine receptor M4; Muscarinic acetylcholine receptor M5	D1 dopamine receptor; D2 dopamine receptor; D3 dopamine receptor; D5 dopamine receptor; Histamine H1 receptor; 5 hydroxytryptamine receptor 6
Cyclo(RGDyK) (trifluoroacetate)	O=C(N[C@H](C(N[C@H]1CCCNC(N)=N)=O)CCCCN)[C	None identified	Integrin αIIb/β3; Integrin αv/β3; Integrin αv/β5; Integrin αv/β6

	@H](NC([C@@H](NC(CNC 1=O)=O)CC(O)=O)=O)CC2= CC=C(O)C=C2.O=C(O)C(F)(F)F.O=C(O)C(F)(F)F		
Docetaxel (trihydrate)	O=C(OC(C)(C)C)N[C@H]([C @H](C(O[C@@H]1C(C)=C([C@@H](O)C([C@@]2(C)[C @](C[C@@](CO3)(OC(C)=O)[C@@]3([H])C[C@@H]2O)([H])[C@@H]4OC(C5=CC=C C=C5)=O)=O)C(C)(C)[C@@]4(O)C1)=O)O)C6=CC=CC= C6.O.O.O	Epidermal growth factor receptor; Growth hormone releasing hormone receptor; Kinesin-like protein KIF11	Epidermal growth factor receptor; Growth hormone-releasing hormone receptor; Neurokinin 2 receptor
Gilteritinib hemifumarate	CCC1=C(N=C(C(=N1)C(=O) N)NC2=CC(=C(C=C2)N3CC C(CC3)N4CCN(CC4)C)OC)N C5CCOCC5.CCC1=C(N=C(C (=N1)C(=O)N)NC2=CC(=C(C=C2)N3CCC(CC3)N4CCN(CC4)C)OC)NC5CCOCC5.C(=CC(=O)O)C(=O)O	ALK tyrosine kinase receptor; Dimer of Receptor-type tyrosine-protein kinase FLT3; Leukocyte tyrosine kinase receptor; Proto-oncogene tyrosine-protein kinase Ret; Proto-oncogene tyrosine-protein kinase FLT3; Receptor type tyrosine-protein kinase FLT3; Transcription factor ETV6/Tyrosine-protein kinase receptor UFO; Tyrosine protein kinase JAK2; Tyrosine-protein kinase JAK2; Tyrosine-protein kinase JAK2; Tyrosine-protein kinase receptor; Tyrosine-protein kinase receptor UFO	Proto-oncogene tyrosine-protein kinase FLT3; Proto-oncogene tyrosine-protein kinase Ret; ALK tyrosine kinase receptor; Proto oncogene tyrosine-protein kinase ROS
Niclosamide	O=C(NC1=CC=C([N+]([O])= O)C=C1Cl)C2=CC(Cl)=CC= C2O	Anoctamin-1; Replicase polyprotein 1ab; Signal transducer and activator of transcription 3	Signal transducer and activator of transcription 3
Temoporfin	OC1=CC=CC(/C2=C3CCC(/ C(C4=CC(O)=CC=C4)=C5C= C/C(N/5)=C(C6=CC(O)=CC= C6)/C(C=C/7)=NC7=C(C8=C C(O)=CC=C8)/C9=CC=C2N9)=N\3)=C1	None identified	None identified

Perphenazine	OCCN1CCN(CCCN2C3=C(C=CC=C3)SC4=CC=C(Cl)C=C24)CC1	5-hydroxytryptamine receptor 1A; 5-hydroxytryptamine receptor 2A; 5-hydroxytryptamine receptor 2C; 5 hydroxytryptamine receptor 6; 5-hydroxytryptamine receptor 7; Aldehyde dehydrogenase 1A1; Aldehyde oxidase; Aldehyde oxidase 1; Alpha-1A adrenergic receptor; Alpha-2B adrenergic receptor; Alpha-2C adrenergic receptor; Cytochrome P450 2D6; D1A dopamine receptor; D2 dopamine receptor; D3 dopamine receptor; D4 dopamine receptor; Histamine H1 receptor; Sigma non-opioid intracellular receptor 1	D2 dopamine receptor; HERG; 5 hydroxytryptamine receptor 7; Sigma non opioid intracellular receptor 1

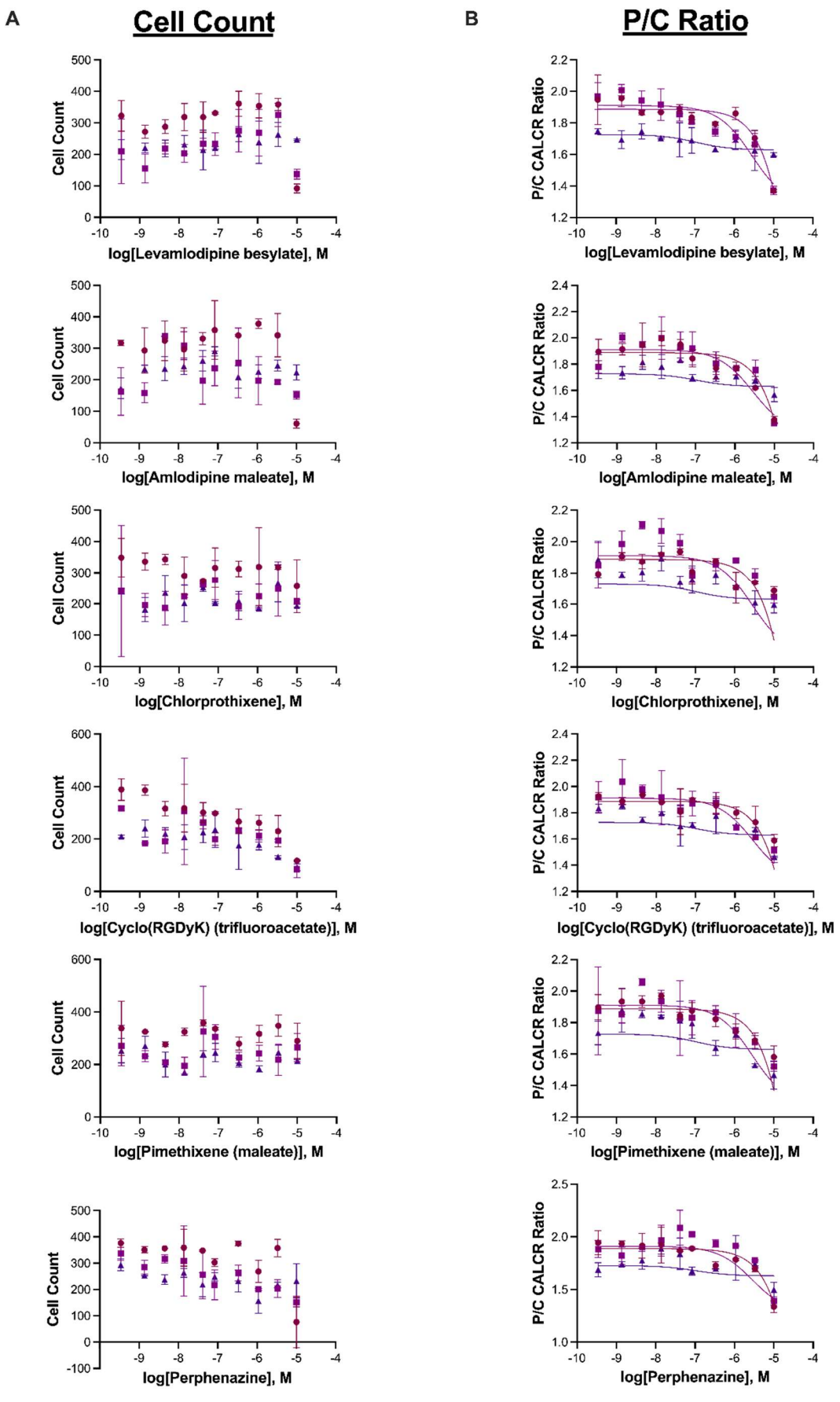

A
Cell Count
B
P/C Ratio
Cell Count
P/C CALCR Ratio
log[Levamlodipine besylate], M
log[Amlodipine maleate], M
log[Chlorprothixene], M
log[Cyclo(RGDyK) (trifluoroacetate)], M
log[Pimethixene (maleate)], M
log[Perphenazine], M
Donor 1
Donor 2
Donor 3

Figure 6.3.2 Concentration-response relationships of prioritised compounds on cell number and CALCR localisation in AF-ACFs. Concentration-response curves for the effect on cell count **(A)** and P/C CALCR ratio **(B)** for prioritised compounds in AF-ACFs from the same three donors as used in the primary screen. Each point represents the mean of technical replicates, with error bars indicating standard deviation.

6.3.2 Assessment of TRPC channel antagonists on CALCR localisation

Given the existing literature demonstrating the dominant role of TRPC channels in carrying Ca^{2+} currents in ACFs, and their association with fibrotic responses, I examined the potential effect of nine inhibitors (and one activator) of TRPC and SOCE channels. I arbitrarily named them TRPC_1-10 (**Table 6.2**). The ten molecules included potent and selective TRPC3 (TRPC_3, TRPC_4 [JW-65], TRPC_10),[221,222] TRPC6 (TRPC_1 and TRPC_2 [BI-749327], TRPC_7, and TRPC_8),[223-225] dual, non-selective TRPC3/6 antagonists (TRPC_9),[226] as well as a SOCE inhibitor and activator (**Table 6.2**).[227] All compounds were well tolerated at the maximal concentration of 10 μM (**Fig 6.3.3A**). Most of the compounds displayed no concentration-response effect on the P/C ratio (**Fig 6.3.3B**). Those that potentially demonstrated modest responses (e.g. TRPC_3 or TRPC_10) had concentration-response relationships which were variable, contained outliers, and were not observed in all three donors (cf. **Fig 6.3.2**). Similarly, there was no concentration-response relationship for these compounds when considering their effect on the collagen 1 cell coverage metric introduced in Chapter 5 (**Fig 6.3.3C**).

T**able 6.2: Summary of TRPC antagonists and SOCE modifiers**, including their SMILES structures, common name (or those they were assigned in the primary publication), the relative potency at each channel with IC_{50} (in nM) values when known. SOCE, store-operated Ca^{2+} entry through stromal interaction molecules (STIM) and Orai containing systems.

Identifier	SMILES	Name	Target (IC50, nM)	Literature
TRPC_1	N[C@H]1CN([C@@H]2CC3=CC=CC=C3[C@H]2OC4=CC=C(C=C4Cl)C#N)CCC1.Cl.Cl	SAR7334	TRPC6 (9.5) > TRPC3 (282) ≈ TRPC7 (226)	Maier *et al* (2015)[223]
TRPC_2	NC1=NN=C(C=C1)C2CCN(CC2)C(C3=CC=C(C=C3)OC4=CC=C(C=C4)C(F)(F)F)=O	BI-749327	TRPC6 (19) >> TRPC7 (550) > TRPC3 (1100)	Lin *et al* (2019)[224]
TRPC_3	O=C(NCC)C1=C(C(F)(F)F)N(C2=CC=C(N3C=CC(C)=CC3=O)C=C2)N=C1	(Compound 17)	TRPC3 >> TRPC6/7	Zhang *et al* (2021)[221]
TRPC_4	O=C(NCC)C1=C(C(F)(F)F)N(C2=CC=C(N3C=CC(Cl)=C(Cl)C3=O)C=C2)N=C1	JW-65 (Compound 20)	TRPC3 (370) >> TRPC6/7 (>10 μM)	Zhang *et al* (2021)[221]
TRPC_5	CC1=NOC(C2=C(C(F)(F)F)N(C3=CC=C(NC(C4=C(F)C=CC=C4F)=O)C=C3)N=C2)=N1	(Compound 22)	SOCE (3100)	Aprile *et al* (2021)[227]
TRPC_6	CC1=NOC(C2=C(C(F)(F)F)N(C3=CC=C(NC(CCCCC)=O)C=C3)N=C2)=N1	(Compound 37)	SOCE activator	Aprile *et al* (2021)[227]
TRPC_7	O=C(N1C(C)C(C)CCC1)C2=C(Cl)SC(NC3=C(F)C=C(OCO4)C4=C3)=N2	(Compound 17)	TRPC6 (4) > TRPC3 (32)	Washburn *et al* (2013)[225]
TRPC_8	O=C(N1C(C)C(C)CCC1)C2=C(C)SC(NC3=C(F)C=C(Cl)C=C3)=N2	(Compound 18)	TRPC6 (50) > TRPC3 (250)	Washburn *et al* (2013)[225]
TRPC_9	CN(C)CCN(C(C1=CC(CCCC2)=C2C=C1)=O)C3=NC4=C(OC)C=CC=C4S3	(Compound 1s)	TRPC3 (3300) ≈ TRPC6 (4200) >> TRPC7 (no inhibition at 10 μM)	Wei *et al* (2021)[226]
TRPC_10	CCNCC1=C(N(N=C1)C2=CC=C(C=C2)N3C=CC(Cl)=C(C3=O)Cl)C(F)(F)F	(Compound 60a)	TRPC3 (90) >> TRPC6/7 (no inhibition at 10 μM)	Wang *et al* (2025)[222]

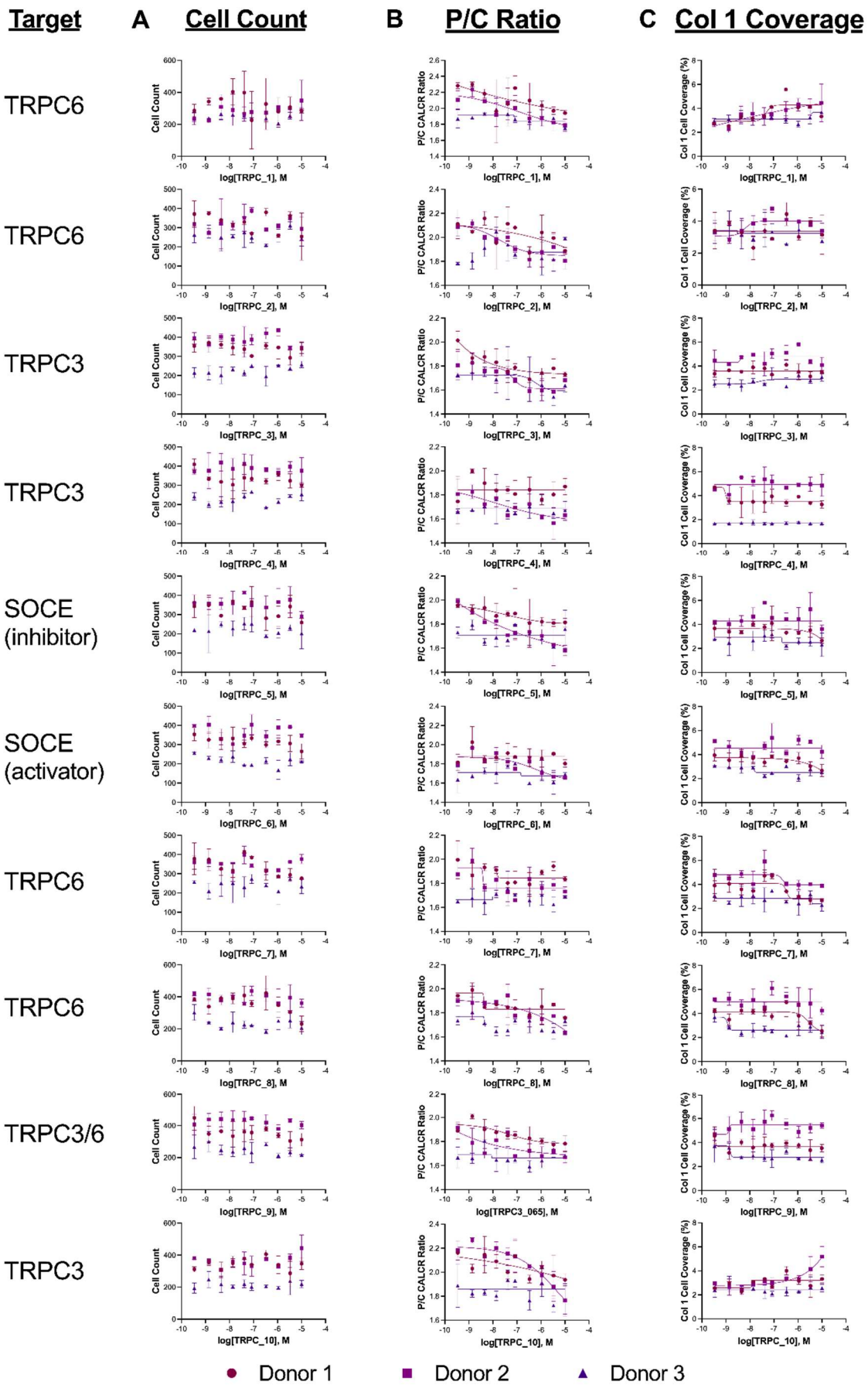

Target
A Cell Count
B P/C Ratio
C Col 1 Coverage
TRPC6
TRPC6
TRPC3
TRPC3
SOCE (inhibitor)
SOCE (activator)
TRPC6
TRPC6
TRPC3/6
TRPC3
Cell Count
P/C CALCR Ratio
Col 1 Cell Coverage (%)
log[TRPC_1], M
log[TRPC_2], M
log[TRPC_3], M
log[TRPC_4], M
log[TRPC_5], M
log[TRPC_6], M
log[TRPC_7], M
log[TRPC_8], M
log[TRPC_9], M
log[TRPC3_065], M
log[TRPC_10], M
Donor 1
Donor 2
Donor 3

Figure 6.3.3 Concentration-response relationships of TRPC3/6 or store-operated calcium entry (SOCE) modulators on cell number, CALCR localisation, and collagen 1. Concentration-response curves for cell count **(A)**, P/C CALCR ratio **(B)**, and thresholded cytoplasmic collagen 1 coverage **(C)** for the ten experimental compounds in AF-ACFs from the same three donors as used in the primary screen. Each data point represents the mean of technical replicates, with error bars indicating standard deviation.

6.3.3 Functional validation of levamlodipine on CALCR localisation and antifibrotic signalling

Given that levamlodipine was uniquely identified as a hit in all three donors, it exhibited a concentration-response relationship, and its racemic formulation is commonly used in CVD, this compound was carried forwards for *in vitro* validation. AF-ACFs from independent donors (not included in the primary screen) were treated with levamlodipine in combination with the endogenous CALCR agonist hCT (100 nM) to determine whether levamlodipine restores functional CALCR receptors to re-establish the CT-CALCR antifibrotic axis (**Fig 6.3.4A**).

Consistent with previous reports and with the epitope recognised by the particular antibody used, WB for collagen I revealed multiple bands (major bands were observed at ~76 kDa and ~102 kDa), in keeping with its extensive post-translational processing (**Fig 6.3.4B**).[228,229] Specifically, procollagen I α1 (COL1a1) and α2 (COL1a2) chains are ~140-200 kDa with subsequent N- and C-terminal cleavage yielding mature collagen chains (~100-140 kDa). These mature collagens are further processed to ~50-80kDa products which are components of secreted collagen fibrils. Levamlodipine and hCT co-treatment reduced expression of the major collagen I bands (**Fig 6.3.4C-D**) and trended to decrease total secreted collagen (**Fig 6.3.4F**), while levamlodipine alone had no effect. sCT8-32, a selective CALCR antagonist, abrogated the response, demonstrating CALCR dependence. Co-treatment did not affect αSMA expression suggesting the co-

treatment does not significantly influence fibroblast-to-myofibroblast differentiation within the assay duration (**Fig 6.3.4E**).

6.3.4 Knockdown of the canonical molecular target of levamlodipine

To determine whether inhibition of $Ca_V1.2$ underlies the effects of levamlodipine on CALCR localisation, the pore-forming α1C subunit (encoded by *CACNA1C*) was targeted using siRNA-mediated knockdown. RT-qPCR showed an 87% reduction in *CACNA1C* mRNA expression after 24h (**Fig 6.3.5A**). AF-ACFs were therefore transfected with either *CACNA1C*-targeting siRNA or a non-targeting negative control (NC) for 24h, followed by a further 48h treatment with levamlodipine ± hCT ± sCT8-32 (as in **section 6.3.3**).

CACNA1C encodes the pore-forming subunit of the $Ca_v1.2$ channel. Structurally, *CACNA1C* comprises four homologous domains (I-IV), each with six transmembrane helices (S1-S6); (lev)amlodipine binds at transmembrane segments IIIS5, IIIS6, and IVS6.[230] If inhibition of $Ca_V1.2$ were the primary mechanism by which levamlodipine restores CALCR function, I hypothesised that *CACNA1C* knockdown would enhance the antifibrotic response to hCT. However, this was not observed. WB analysis showed no change in collagen I or αSMA expression following *CACNA1C* knockdown in the presence of hCT (**Fig 6.3.5B**). Furthermore, *CACNA1C* knockdown did not augment the reduction in collagen I expression observed with levamlodipine and hCT co-treatment (**Fig 6.3.5C**). Consistent with **section 6.3.3**, in both *NC* and *CACNA1C*-siRNA treated AF-ACFs, co-treatment with levamlodipine and hCT resulted in a visible reduction in collagen I protein, which was abrogated by sCT8-32 (**Fig 6.3.5D**). Collectively, these findings indicate that the effect of levamlodipine on CALCR localisation is unlikely to be mediated primarily through LTCC inhibition and instead may involve an alternative molecular target(s). Ongoing work aims to extend these findings in additional donors and to confirm Cav1.2 knockdown at the protein level.

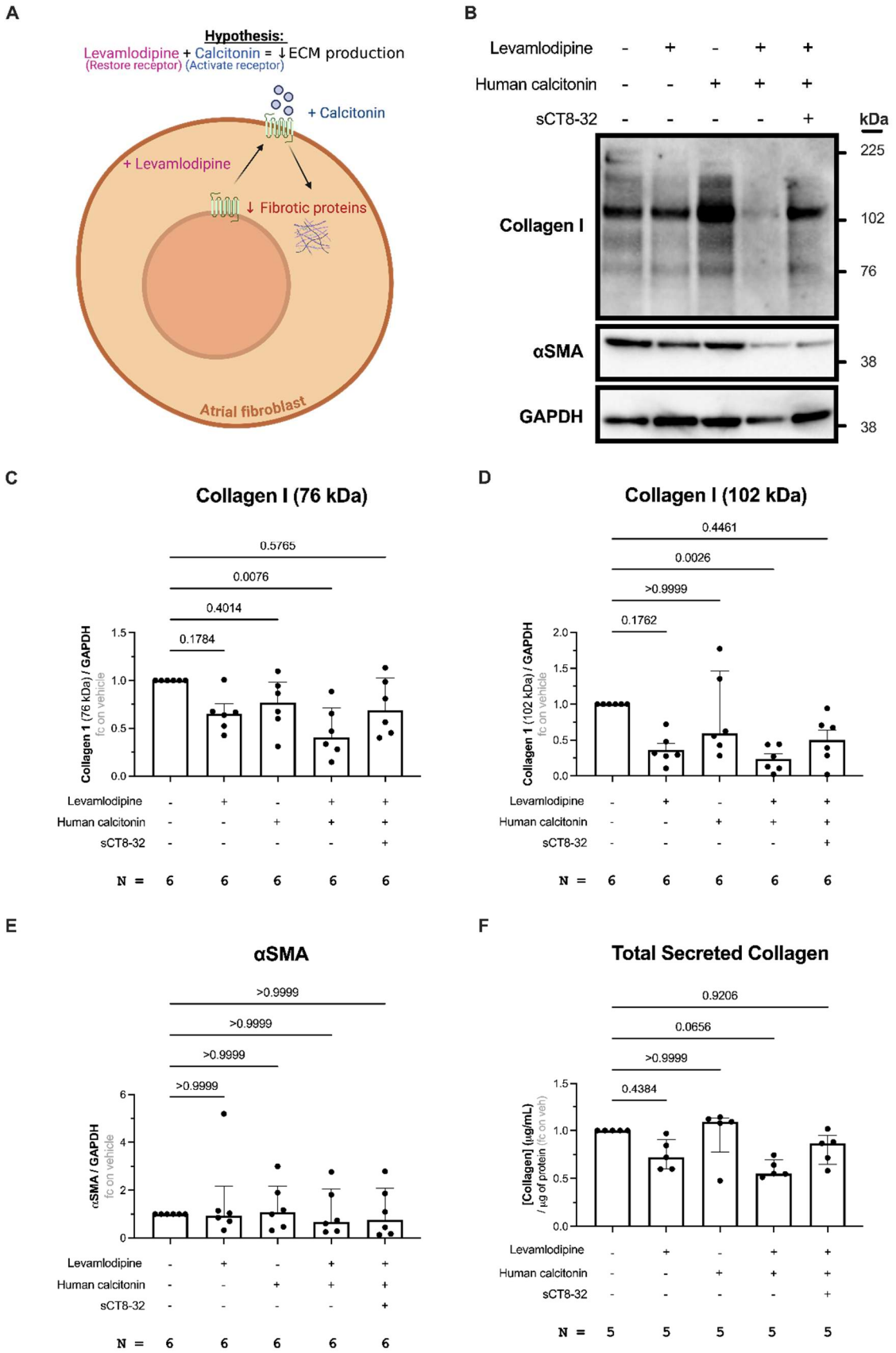

A
Hypothesis:
Levamlodipine + Calcitonin = ↓ECM production
(Restore receptor) (Activate receptor)
+ Calcitonin
+ Levamlodipine
↓ Fibrotic proteins
Atrial fibroblast
B
Levamlodipine - + - + +
Human calcitonin - - + + +
sCT8-32 - - - - +
kDa
225
102
76
Collagen I
αSMA
38
GAPDH
38
C
Collagen I (76 kDa)
0.5765
0.0076
0.4014
0.1784
Collagen 1 (76 kDa) / GAPDH
fc on vehicle
Levamlodipine - + - + +
Human calcitonin - - + + +
sCT8-32 - - - - +
N = 6 6 6 6 6
D
Collagen I (102 kDa)
0.4461
0.0026
>0.9999
0.1762
Collagen 1 (102 kDa) / GAPDH
fc on vehicle
Levamlodipine - + - + +
Human calcitonin - - + + +
sCT8-32 - - - - +
N = 6 6 6 6 6
E
αSMA
>0.9999
>0.9999
>0.9999
>0.9999
αSMA / GAPDH
fc on vehicle
Levamlodipine - + - + +
Human calcitonin - - + + +
sCT8-32 - - - - +
N = 6 6 6 6 6
F
Total Secreted Collagen
0.9206
0.0656
>0.9999
0.4384
[Collagen] (µg/mL)
/ µg of protein (fc on ven)
Levamlodipine - + - + +
Human calcitonin - - + + +
sCT8-32 - - - - +
N = 5 5 5 5 5

Figure 6.3.4 Levamlodipine restores CALCR-dependent antifibrotic signalling in human AF-ACFs. (A) Schematic illustrating the proposed antifibrotic mechanism whereby levamlodipine restores surface CALCR localisation, enabling activation by calcitonin (CT) and suppression of fibrotic protein production. AF-ACFs from N=5-6 biological donors were treated with levamlodipine (10μM) ± hCT (100 nM) ± sCT8-32 (100 nM). **(B)** Representative WBs showing collagen I and αSMA expression under the indicated conditions. **(C-E)** Quantification of major collagen I bands at 76 kDa (C), 102 kDa (D) and αSMA (E), normalised to GAPDH. **(F)** Total secreted collagen normalised to μg of protein in the cell lysate and expressed as a fold-change on the vehicle condition (0.1% v/v DMSO). Data expressed as median (IQR), *Friedman test* with post-hoc Dunn's test.

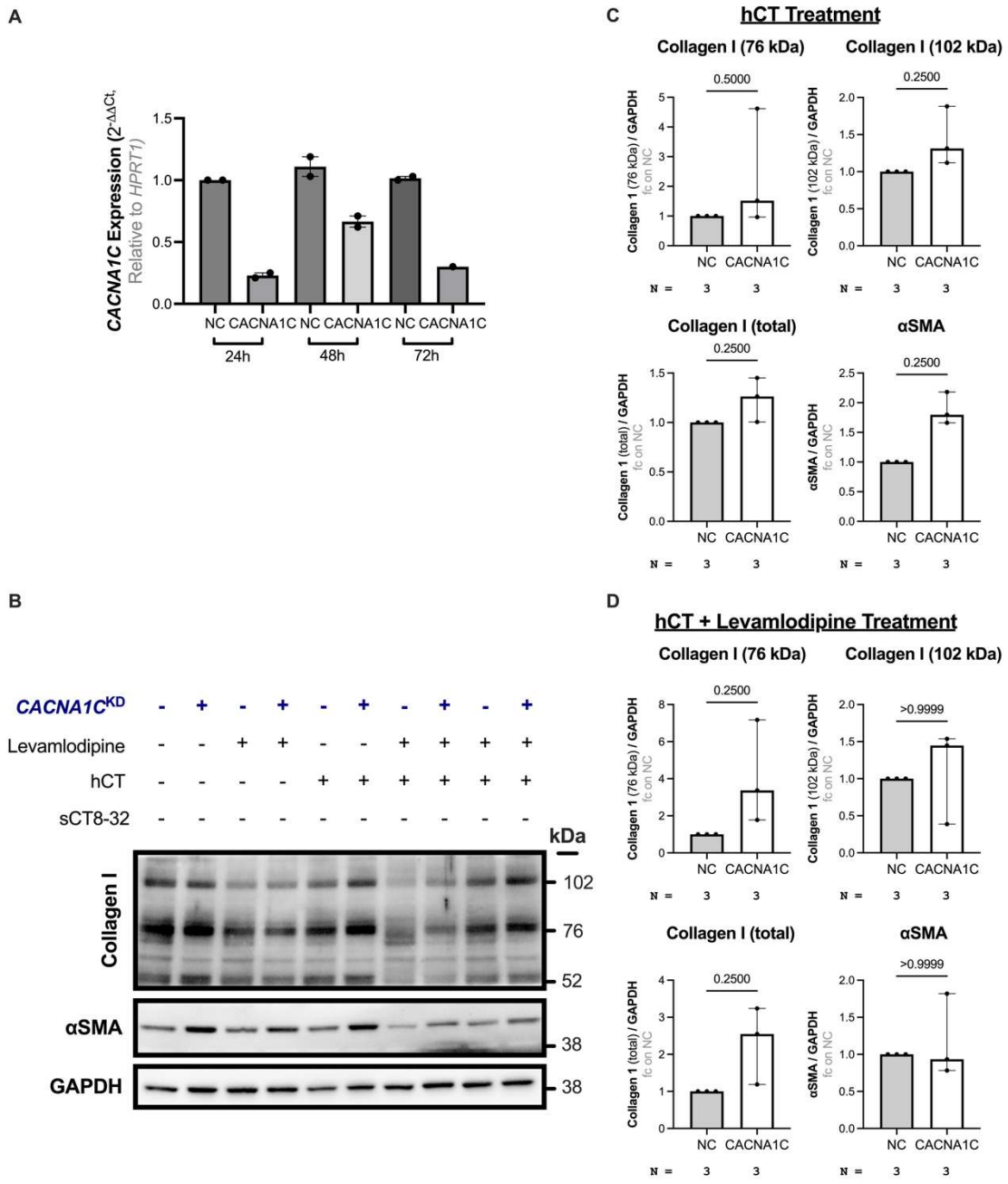


Figure 6.3.5 Effect of CACNA1C siRNA-knockdown on the antifibrotic response to human calcitonin (hCT). (A) *CACNA1C* mRNA expression following siRNA-mediated knockdown at 24, 48, and 72h relative to *HPRT1*. **(B)** Representative immunoblots showing collagen I, αSMA, and GAPDH under the indicated treatment conditions (± *CACNA1C* knockdown, ± hCT, ± sCT8-32). **(C-D)** Quantification of collagen I (76 kDa and 102 kDa major bands and total lane intensity) and αSMA expression by WB following treatment with hCT alone (C) or hCT and levamlodipine (D). hCT, human calcitonin. Data expressed as median (IQR), *Wilcoxon matched-pairs signed-rank test*.

6.3.5 Transcriptomic changes induced by levamlodipine treatment in AF-ACFs

To generate insight into alternative mechanisms through which levamlodipine may exert an effect on CALCR localisation, I performed RNAseq on vehicle- and levamlodipine-treated (10 μM, 24h) AF-ACFs derived from 4 donors not included in the primary screens. Distribution of both unnormalised and normalised read counts were comparable across donors and treatment conditions supporting the suitability of the dataset for downstream differential expression analysis (**Fig 6.3.6A**). PCA demonstrated samples primarily clustered by donor rather than treatment condition, indicating that donor-specific transcriptional differences represent the dominant source of variation (**Fig 6.3.6B**). Despite this, a consistent separation between levamlodipine-treated and vehicle-treated samples was observed within each donor, particularly in PC2. This suggests that, while smaller in magnitude than donor effects, levamlodipine treatment induces reproducible transcriptional changes.

DEG analysis identified 241 upregulated and 142 downregulated genes after FDR correction (adjusted p-value < 0.05 and absolute $\log_2$FC > 1; **Fig 6.3.6C, Appendix 5** and **6**). KEGG pathway analysis of genes upregulated following levamlodipine treatment identified significant over-representation of pathways related to lipid and cholesterol metabolism, inflammatory signalling, and immune responses (**Fig 6.3.6D**). A full list of the top 20 enriched pathways, together with contributing genes, is provided in **Table 6.3**. KEGG pathway analysis of the 142 genes downregulated following levamlodipine treatment did not identify any significantly enriched pathways so I instead considered the 258 genes which had a $\log_2$FoldChange < -1 and an unadjusted p-value < 0.05 (**Appendix 6**). This analysis identified three enriched KEGG pathways, including motor proteins (**Fig 6.3.6E** and **Table 6.4**).

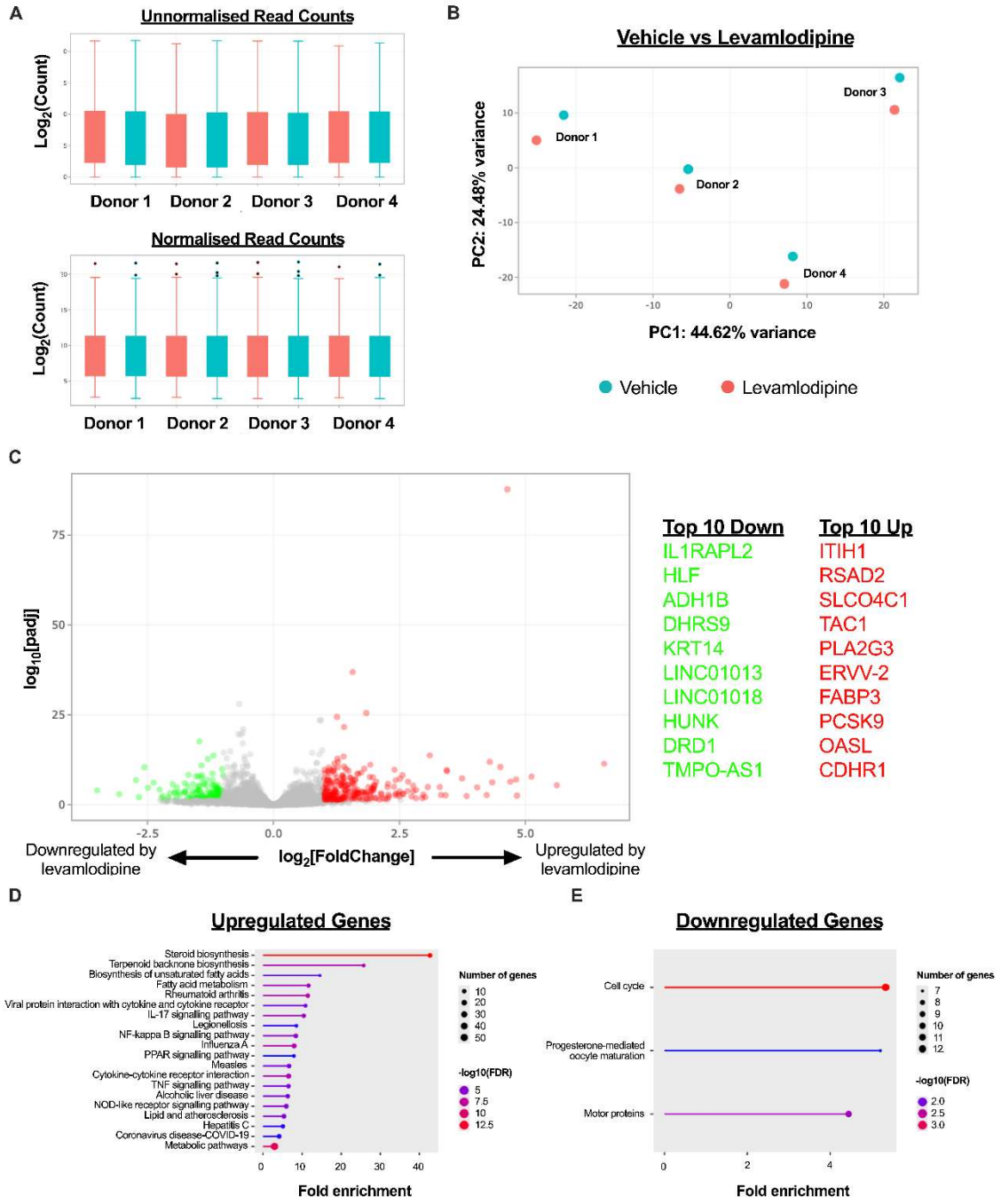


Figure 6.3.6 Transcriptomic profiling of AF-ACFs following levamlodipine treatment. (A) Boxplot of unnormalised (top) and normalised (bottom) log_2 gene counts across AF-ACFs from four donors treated with vehicle or levamlodipine. **(B)** Principal component analysis (PCA) of vehicle- and levamlodipine-treated samples. **(C)** Volcano plot of differentially expressed genes (DEGs) following levamlodipine treatment, identifying 241 upregulated (red) and 142 downregulated (green) genes. Top 10 downregulated and upregulated genes by log_2(FoldChange) indicated. **(D-E)** KEGG pathway analysis of the 241 upregulated (D) and 258 downregulated (E, using unadjusted p-values) genes ordered by fold enrichment.

Table 6.3: Top 20 enriched KEGG pathways (ranked by fold enrichment) among genes upregulated in levamlodipine-treated AF-ACFs. Analysis performed using ShinyGO 0.85.1.[147]

KEGG Pathway	# Genes / # Genes in Pathway	Fold Enrichment (FDR)	Genes
hsa00100 Steroid biosynthesis	11/20	42.7	EBP, CYP51A1, DHCR7, DHCR24, FDFT1, LSS, NSDHL, HSD17B7, MSMO1, SQLE, TM7SF2
hsa00900 Terpenoid backbone biosynthesis	7/23	25.7	FDPS, HMGCR, HMGCS1, IDI1, ACAT2, MVD, MVK
hsa01040 Biosynthesis of unsaturated fatty acids	5/27	14.6	FADS1, HSD17B12, SCD, ELOVL6, FADS2
hsa01212 Fatty acid metabolism	9/57	11.6	ACSL3, FASN, ACACA, ACAT2, FADS1, HSD17B12, SCD, ELOVL6, FADS2
hsa05323 Rheumatoid arthritis	11/93	11.5	ATP6V0D2, CXCL1, CXCL2, CXCL3, ICAM1, IL1A, IL1B, CXCL8, MMP1, CCL5, CXCL5
hsa04061 Viral protein interaction with cytokine and cytokine receptor	7/99	10.9	CXCL1, CXCL2, CXCL3, CXCL8, CCL5, CCL7, CXCL5
hsa04657 IL-17 signalling pathway	10/93	10.4	CSF3, CXCL1, CXCL2, CXCL3, IL1B, CXCL8, MMP1, PTGS2, CCL7, CXCL5
hsa05134 Legionellosis	6/56	8.6	CXCL1, CXCL2, CXCL3, HSPA6, IL1B, CXCL8
hsa04064 NF-kappa B signalling pathway	10/103	8.4	RIGI, CXCL1, CXCL2, CXCL3, BIRC3, ICAM1, IL1B, CXCL8, PTGS2, RELB
hsa05164 Influenza A	14/171	8.0	FDPS, RIGI, ICAM1, IL1A, IL1B, CXCL8, IRF7, MX1, MX2, OAS1, OAS2, CCL5, IFIH1, RSAD2
hsa03320 PPAR signalling pathway	6/76	7.9	FABP3, ACSL3, HMGCS1, MMP1, SCD, FADS2
hsa05162 Measles	10/139	6.7	RIGI, HSPA6, IL1A, IL1B, IRF7, MX1, MX2, OAS1, OAS2, IFIH1
hsa04060 Cytokine-cytokine receptor interaction	15/297	6.5	CSF3, CXCL1, CXCL2, CXCL3, IL1A, IL1B, CXCL8, TNFRSF9, LIF, IL21R, CCL5, CCL7, CXCL5, INHBE, GDF15
hsa04668 TNF signalling pathway	10/119	6.5	CXCL1, CXCL2, CXCL3, BIRC3, ICAM1, IL1B, LIF, PTGS2, CCL5, CXCL5
hsa04936 Alcoholic liver disease	10/143	6.3	FASN, LPIN1, CXCL1, CXCL2, CXCL3, ACACA, IL1B, CXCL8, SCD, SREBF1
hsa04621 NOD-like receptor signalling pathway	12/183	6.0	NAMPT, GBP5, CXCL1, CXCL2, CXCL3, BIRC3, IL1B, CXCL8, IRF7, OAS1, OAS2, CCL5
hsa05417 Lipid and atherosclerosis	13/215	5.3	CXCL1, CXCL2, CXCL3, HSPA6, ICAM1, IL1B, CXCL8, IRF7, LDLR, MMP1, NCF2, CCL5, ABCG1

hsa05160 Hepatitis C	9/159	5.1	RIGI, IRF7, LDLR, MX1, MX2, OAS1, OAS2, RSAD2, SCARB1
hsa05171 Coronavirus disease-COVID-19	11/234	4.1	CSF3, RIGI, IL1B, CXCL8, MMP1, MX1, MX2, OAS1, OAS2, IFIH1, ISG15
hsa01100 Metabolic pathways	53/1556	3.0	NAMPT, EBP, CKMT2, AK7, CMPK2, CYP51A1, DBH, DHCR7, DHCR24, TYMP, ACSL3, FASN, FDFT1, FDPS, ALDOC, LPIN1, QPRT, ATP6V0D2, IL4I1, GCH1, ACACA, HMGCR, HMGCS1, MMAB, HSD11B1, IDI1, ACAT2, FADS1, LSS, MVD, MVK, ACLY, PLA2G3, NSDHL, HSD17B12, PDE4D, HSD17B7, PFKFB4, ACSS2, PTGS2, PCYT2, MSMO1, SCD, SHMT1, SQLE, TM7SF2, ELOVL6, GALNT12, PNPLA3, B3GNT5, DHRS3, FADS2, PTGES

Table 6.4: Enriched KEGG pathways (ranked by fold enrichment) among genes downregulated (based on unadjusted p-value) in levamlodipine-treated AF-ACFs. Analysis performed using ShinyGO 0.85.1.[147]

KEGG Pathway	# Genes / # Genes in Pathway	Fold Enrichment (FDR)	Genes
hsa04110 Cell cycle	12/158	5.3	PLK1, KNL1, BUB1, BUB1B, TTK, CDC45, CCNA2, CCNB1, CCNB2, TRIP13, CDC20, CDC25C
hsa04914 Progesterone-mediated oocyte maturation	7/110	5.2	PLK1, AURKA, BUB1, CCNA2, CCNB1, CCNB2, CDC25C
hsa04814 Motor proteins	10/194	4.4	TUBA1B, CENPE, KIF2C, KIF4A, KIFC1, MYO7B, ACTA2, TNNT2, ACTG2, KIF23

6.3.6 Establishing the reproducibility of the levamlodipine-mediated effects on CALCR localisation

Preliminary studies, in collaboration with the group of Professor Xander Wehrens, sought to assess the inter-species reproducibility of the CALCR internalisation phenotype and its responsiveness to levamlodipine in the CREM-Tg mouse model of sustained AF. Comparison of the CALCR localisation in ACFs from 3-month-old mice, which exhibit minimal atrial fibrosis, and 9-month-old mice, characterised by persistent AF, atrial dilatation, and pronounced fibrosis, revealed a similar pattern of perinuclear CALCR accumulation in the older cohort (**Fig 6.3.7A**). Quantitative analysis of CALCR and DAPI overlap demonstrated a trend towards increased DAPI-CALCR colocalisation in 9-month-old animals (**Fig 6.3.7B**).

To explore whether this phenotype is pharmacologically modifiable by levamlodipine, ACFs isolated from a 9-month-old CREM-Tg mouse were treated with levamlodipine (10 μM, 24h). Levamlodipine treatment was associated with an apparent increase in surface CALCR, consistent with observations in human AF-ACFs (**Fig 6.3.7C-D**). Although these findings are derived from a single animal, and therefore require validation in additional biological replicates, they provide initial evidence that the CALCR internalisation phenomenon is a feature of murine models of AF and that the effects of levamlodipine on CALCR trafficking may be conserved in an *in vivo* model of AF. Ongoing work aims to establish whether early combination therapy of levamlodipine and salmon calcitonin (sCT), starting from 1 month, can attenuate the development of atrial fibrosis and reduce AF burden (a preliminary study timeline is outlined in **Fig 6.3.7E**).

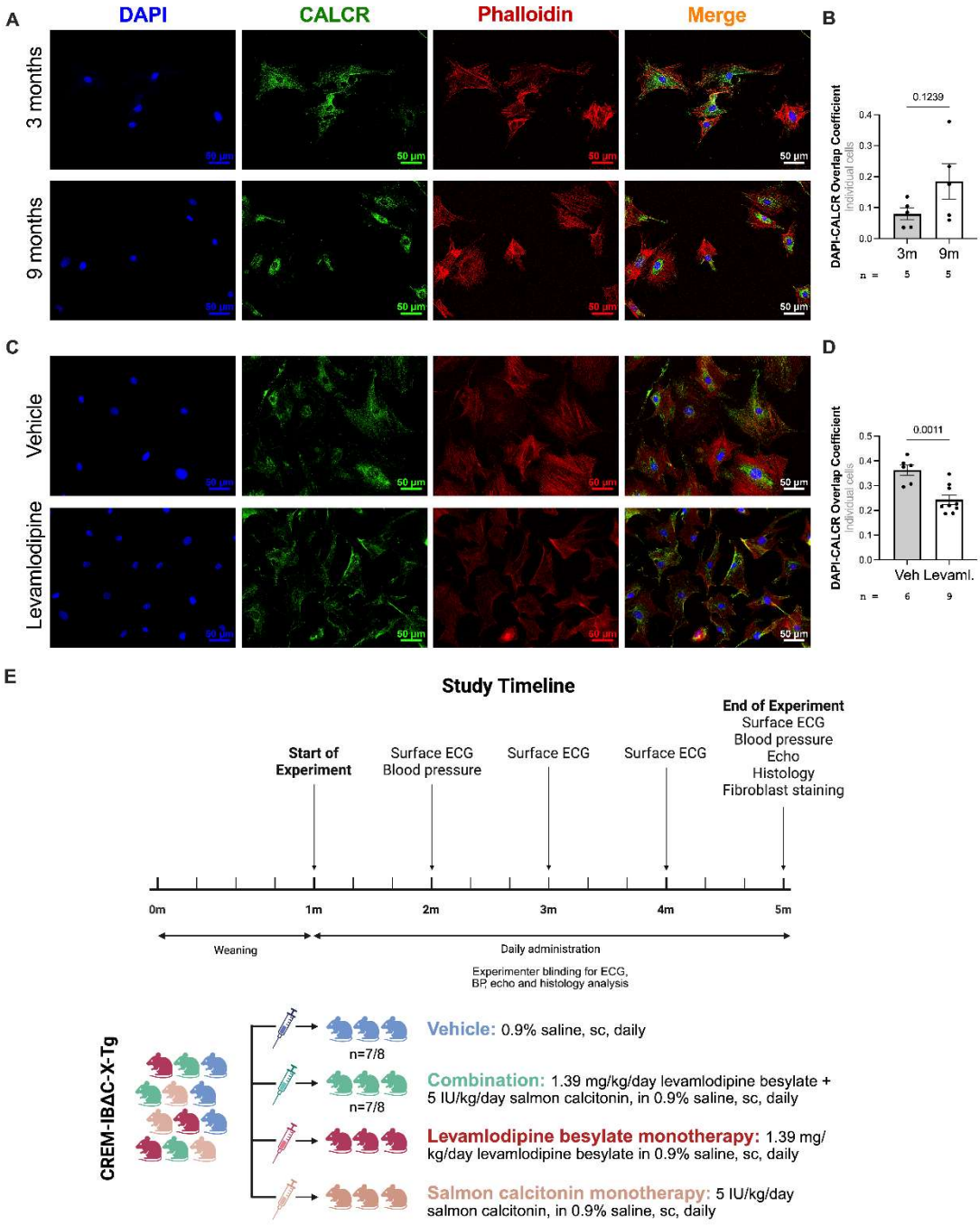


Figure 6.3.7 CALCR internalisation and pharmacological rescue in ACFs from CREM-Tg mice. (A) Immunostained ACFs from 3- and 9-month-old CREM-Tg mice. CALCR (green), DAPI (blue), and phalloidin (red). **(B)** Quantification of DAPI-CALCR overlap coefficients. **(C)** ACFs from a 9-month-old CREM-Tg mouse following vehicle or levamlodipine treatment (10 µM, 24h). **(D)** Quantification of DAPI-CALCR overlap coefficients in vehicle- or levamlodipine-treated ACFs. **(E)** Proposed design of an *in vivo* study to assess the effects of levamlodipine and salmon calcitonin on atrial remodelling and AF burden in CREM-Tg mice. Scale bar, 50 µm. Points represent single cells, data expressed as mean ± SEM, *unpaired t-test*. sc, subcutaneous. IU, international units.

6.4 Discussion

The work presented in this chapter builds upon the HTS and begins the mechanistic and functional characterisation of prioritised CALCR restoring compounds. The central findings are:

1. Levamlodipine reproducibly restores CALCR-dependent antifibrotic signalling in donor-derived AF-ACFs, demonstrated by suppression of one of the key ECM components - collagen I, an effect abrogated by CALCR antagonist sCT8-32.
2. Levamlodipine likely acts through a non-canonical mechanism independent of its canonical target $Ca_V1.2$, since siRNA-mediated knockdown of *CACNA1C* failed to phenocopy the effect of levamlodipine, or augment levamlodipine's effect when co-administered with CT.
3. Transcriptomic profiling reveals broad levamlodipine-mediated transcriptional changes in human fibroblasts, including coordinated upregulation of lipid metabolism and inflammatory signalling pathways and downregulation of cell cycle progression and cytoskeletal motor activity – a transcriptional landscape which suggests a pleiotropic, non-canonical mechanism of action that has been little explored previously.

6.4.1 Shared pharmacological targets among CALCR-restoring compounds

In silico ligand-target prediction, using previously validated interactions (BindingDB) and those predicted probabilistically based on chemical similarity with known ligand-protein interactions (SwissTargetPrediction), identified several recurring target classes among the hit compounds.[215,217] These included 5-HT receptor subtypes (particularly 5-HT_{2A}, 5-HT_6, and 5-HT_7) and dopamine receptors (D2, D3, D4). The convergence of structurally diverse compounds on a common set of receptor families suggests that modulation of one or more of these pathways may represent a shared mechanism by which CALCR surface localisation is rescued in AF-ACFs. Moreover, the consistent identification of

GPCR targets raises the possibility that persistent GPCR activation (or basal agonist-independent activation) may promote generalised (constitutive) internalisation of co-expressed GPCRs, including CALCR.[231]

The role of serotonergic and dopaminergic GPCRs in cardiac fibroblast biology is an emerging area of interest. Kisling *et al* (2021) demonstrated the expression of D1 and D3 receptors in murine left ventricular fibroblasts and showed genetic or pharmacological suppression of the D3 receptor suppressed proliferation, migration, and collagen I (but enhanced collagen III) expression.[232] This contrasted with an earlier report which found D3 receptor knockout elevated systemic blood pressure and interstitial fibrosis compared to age-matched wild-type animals.[233]

5-HT signalling has also been implicated in the regulation of cardiac development, electrophysiology and valve disease in patients with carcinoid tumours.[234] Electrophysiologically, 5-HT, acting via 5-HT_4 receptors expressed by cardiomyocytes, is considered to be positively chronotropic and inotropic in the atrium.[234,235] In myocardial and valvular fibrogenesis, signalling mediated by 5-HT_2 receptors is the dominant mode of action.[236,237] Serotonergic signalling has been shown to be increased during myofibroblast transdifferentiation, to enhance collagen I expression, and contribute to ventricular hypertrophy and fibrosis.[236,238,239] Notably, the isoprenaline-induced cytokine response in cardiac fibroblast cultures required both 5-HT_{2B} and angiotensin II receptor 1 (AT1R), which co-immunoprecipitated.[239] Whether the cardiac 5-HT system could similarly crosstalk with CALCR and promote its internalisation is an intriguing possibility and may add an additional facet to how 5-HT receptor inhibition suppresses fibrogenesis. Future studies could explore this by establishing whether CALCR and 5-HT receptors co-localise and interact.

Important limitations of the ligand-target predictions must be acknowledged. Firstly, the BindingDB database and the SwissTargetPrediction model are informed by previously

identified interactions or incomplete training datasets which therefore preclude the identification of entirely novel interactions. This is evidenced by the failure of SwissTargetPrediction to identify $Ca_V1.2$ as a target for (lev)amlodipine which is due to *CACNA1C* protein's (Q13936) absence in the training dataset. Secondly, *in silico* prediction of an interaction does not mean it occurs in ACFs, the expression of targets would need to be confirmed. Similarly, a physicochemically favourable interaction is not obligatorily physiologically meaningful. Future work should aim to unbiasedly detect ligand-target interactions empirically using on-bead affinity matrix or label-free techniques.[240] Finally, it is conceivable that identified CALCR rescuing hits act via independent pathways, or pathways that converge distal to the drug's molecular target. Nevertheless, the therapeutic value of a drug ultimately resides in its efficacy and safety profile, rather than in a comprehensive account of its molecular target(s).

6.4.2 Concentration-response relationships and potency considerations

The inability to determine reliable EC_{50} values represents a pragmatic limitation and made it difficult to compare the potencies of 89 levamlodipine structural analogues I tested as part of a structure-activity relationship study (data not presented). The absence of a clearly defined lower asymptote across the tested range is consistent with partial efficacy and competing cytotoxic effects at the higher doses within the concentration window. Future studies could extend the assay duration and include endpoint viability assays to tease apart pharmacodynamic from cytotoxic contributions. It is also notable that there was substantial inter-donor variability, particularly evidenced by the relatively shallower CRCs for donor 3. Inter-donor variability is unavoidable in primary human fibroblast studies but reflects the biological heterogeneity of the human population and the spectrum of disease.[241] This demonstrated the importance of confirming potential antifibrotic effects of levamlodipine and hCT in independent donors.

6.4.3 Levamlodipine restores functional CALCR-dependent antifibrotic signalling

The demonstration that levamlodipine and hCT co-treatment reduced collagen I expression, and trended towards decreased secreted collagen, in independent AF-ACFs constitutes the primary functional finding of this chapter. The CALCR dependence of this effect, confirmed by its abrogation with the competitive antagonist sCT8-32, directly validated the hypothesis that pharmacological restoration of CALCR surface localisation is sufficient to re-engage the antifibrotic CT-CALCR axis.[1] Similarly, the absence of an effect with levamlodipine alone is informative as it demonstrated that levamlodipine contributes to receptor sensitisation, rather than exerting a direct antifibrotic effect.

Consistent with the 'spare receptor theory' of GPCR signalling, limited restoration of the surface CALCR pool could lead to substantial antifibrotic responses owing to the large signal amplification characteristic of GPCRs.[242,243] Expressed in pharmacokinetic terms, the ligand's dissociation constant (K_d) value can be higher than the EC_{50} for the measured response.[242,243] Although collagen I is an important ECM component and marker of the activated ACF phenotype, it is only one marker of fibrosis and future work should more comprehensively establish the co-treatment effect on other fibrotic markers e.g. fibronectin, collagen III, and periostin.

6.4.4 The effects of levamlodipine on CALCR localisation are possibly independent of $Ca_V1.2$ inhibition

The finding that *CACNA1C* siRNA-mediated knockdown (achieving a mean ~87% reduction in mRNA) did not phenocopy the effect of levamlodipine on restoring CALCR responsiveness is an important mechanistic result. It provides evidence that inhibition of $Ca_V1.2$ – the canonical target of dihydropyridine CCBs – is unlikely to be the primary driver of the observed effects. This is consistent with the reported nanomolar IC_{50} values of levamlodipine at *CACNA1C*, concentrations at which there was little/no effect on

CALCR localisation.[230] It is important to note a limitation of this experiment was that protein-level knockdown was not confirmed and current studies aim to assess this as robust mRNA reductions do not always result in functional protein level reductions. Similarly, functional verification of channel inhibition (e.g. by voltage-clamp) was not performed.

The mechanism's independence from Ca^{2+}-influx is reinforced by the lack of response to TRPC3/6 and SOCE inhibitors (or activators). Moreover, none of the ten compounds appeared to exert a dose-dependent effect on the collagen I cell coverage metric which contrasts prior studies which have positioned TRPC-mediated Ca^{2+} influx as a mediator of profibrotic activity in ACFs.[205] A contribution of impaired Ca^{2+} influx to CALCR internalisation could be more definitively excluded using cell-impermeant Ca^{2+} chelators.

There is increasingly an appreciation that (lev)amlodipine exerts pleiotropic effects distinct from $Ca_V1.2$ antagonism. Across a diverse range of pre-clinical and clinical models, amlodipine (which in its racemic form will be 50% levamlodipine) treatment has been shown to reduce the expression of pro-inflammatory cytokines (e.g. TNF-α, IL-1β, IL-6) and ameliorate oxidative stress states.[244-249] Large-scale cardiovascular outcome trials have also indicated that amlodipine's protective effects exceed those predicted from blood pressure reduction alone. The CAMELOT trial reported a reduction in adverse cardiovascular events in normotensive patients with coronary artery disease that was not significantly correlated with blood pressure reduction.[250] Meanwhile, the ASCOT-BPLA trial found amlodipine and perindopril combination therapy, compared to atenolol and bendroflumethiazide, in untreated or uncontrolled hypertension had an effect on cardiovascular events that seemed to exceed that which would be expected solely from its superior blood pressure lowering effects.[251]

6.4.5 Transcriptomic profiling reveals levamlodipine affects lipid metabolic and inflammatory pathways

Pathway analysis following identification of DEGs after levamlodipine treatment in AF-ACFs identified a striking enrichment of sterol and fatty acid metabolic pathways. The transcriptional induction of the mevalonate and cholesterol biosynthesis pathway - evidenced by upregulation of genes at several stages of the biosynthetic route e.g. *HMGCR*, *HMGCS1*, *FDFT1*, *LSS*, *SQLE*, *DHCR7*, and *DHCR24* - is informative and potentially relevant to CALCR trafficking. Membrane cholesterol content is a critical determinant of GPCR localisation and signalling, with cholesterol-rich lipid raft microdomains serving as a major site of receptor clustering and signal transduction.[252] Although speculative, the possibility that levamlodipine-induced cholesterol biosynthesis increases the availability of membrane cholesterol, thereby promoting the incorporation of internalised CALCR into recycling endosomes and its return to the plasma membrane, represents a mechanistically plausible hypothesis. An initial step in testing this hypothesis would be to assess the plasma membrane cholesterol content following levamlodipine treatment e.g. using filipin III staining or mass spectrometry techniques.[253]

Owing to its unique structural properties, authors have proposed that amlodipine directly influences plasma membrane dynamics.[246] The positive charge carried by amlodipine's basic aminoethoxymethyl side chain (pK_a 8.7), which is not present in other DHP CCBs, at physiological pH accounts for its electrostatically-driven concentration at the membrane (at levels >10,000-fold higher than in the surrounding milieu).[246,254,255] Furthermore, owing to its lipid affinity, amlodipine has been reported to directly modulate membrane structure and dynamics particularly through its interference with cholesterol, which might contribute to amlodipine's antiatherogenic effects.[246,256,257]

A broader effect of (lev)amlodipine on other metabolic pathways has also been reported. Amlodipine was found to reduce triglyceride accumulation and stimulate lipolysis in white

adipose tissue exposed to high fructose conditions and attenuate the rise in PU.1 protein, a transcription factor that regulates myeloid haematopoiesis, lipid metabolism, and has recently been recognised as a regulator of profibrotic gene expression in fibroblasts.[258,259]

The upregulation of inflammatory signalling pathways – including IL-17 signalling, NF-κB, TNF signalling, and multiple chemokine networks – contrasts with some earlier reports that have reported anti-inflammatory effects of amlodipine.[247] This possibly reflects species- and cell type-specific responses to levamlodipine. Whether these changes are mechanistically linked to CALCR trafficking or represent parallel, independent effects of levamlodipine cannot be determined from the current dataset and warrant further investigation.

6.4.6 Mechanistic insight provided by genes downregulated by levamlodipine

Pathway analysis of the downregulated gene set (using unadjusted p-values due to limited identifications after FDR correction) identified enrichment of cell cycle progression pathways, oocyte maturation, and motor proteins. The downregulated genes include a striking array of mitotic regulators: *PLK1*, *AURKA*, *BUB1*, *BUB1B*, *CCNA2*, *CCNB1*, *CDC20*, *CDC25C*, *KIF2C*, *KIF4A*, *KIFC1*, *KIF23*, and *CENPE*. This signature suggests a broad anti-proliferative transcriptional response in levamlodipine-treated AF-ACFs, consistent with the known anti-proliferative properties of amlodipine in vascular smooth cells and cancer cell lines.[249,260,261]

The suppression of tubulin, kinesin, and myosin family genes is noteworthy in the context of intracellular trafficking, since these proteins contribute substantially to vesicular transport along cytoskeletal highways.[262] Notably, kinesin-like protein 23 (KIF23) has been linked with fibroblast proliferation, lipid accumulation and myocardial fibrosis post-MI.[263] It is also notable that kinesin-like proteins were also a predicted target of the hit docetaxel. Although speculative, the levamlodipine-induced disruption of intracellular

transport pathways could plausibly contribute to the restoration of CALCR surface expression and function.

Moreover, among the most significantly downregulated genes, several genes have strong links with AF biology. For example, the transcription factor paired-like homeodomain 2 (*PITX2*) was downregulated; *PITX2* variants are the most strongly associated AF variants and mechanistic studies have revealed *PITX2* regulates mitochondrial function.[18,264] Although WB did not show a reduction in αSMA protein following co-treatment of levamlodipine and hCT, its gene *ACTA2* was also significantly downregulated by levamlodipine. This discrepancy may be due to an insufficient timeframe for the reduction in *ACTA2* mRNA to reflect in αSMA protein abundance. Junctophillin-2 (JPH2), also significantly downregulated, has been associated with AF; in cardiomyocytes JPH2 regulates ryanodine receptor activity and its downregulation exacerbates atrial dysfunction during pressure-overload.[265,266] The transcriptional changes following levamlodipine treatment, and how these interact with CALCR trafficking and the broader AF substrate, are thus complex and will be investigated by a new doctoral student.

The dominant contribution of donor identity to transcriptional variance is consistent with substantial inter-donor heterogeneity compared to a relatively smaller transcriptional effect of levamlodipine. Despite this, a reproducible treatment-associated transcriptional signature was detectable across donors, particularly in PC2, providing confidence that the observed DEGs represent genuine levamlodipine-induced effects rather than noise. Transcriptional changes following levamlodipine treatment have been studied. For instance, in iPSC-CMs amlodipine, compared with other dihydropyridine and non-dihydropyridine CCBs, induced a greater transcriptomic effect.[267] Another study, using a microarray-based approach to study the transcriptome, examined the response to amlodipine in the heart and kidney of Wistar Kyoto and stroke-prone spontaneously hypertensive rats.[268] Comparison of the genes they identified to be significantly

dysregulated in the heart (total: 54 [with p-value < 5 x 10^{-5}]) with my dataset (total: 383), identified 6 genes mutually dysregulated with the same direction of effect: PRC1, PLK1, CEP55, SPAG5, TOP2A, and SHCBP1.[268] This could be due to technical differences in the methods used to assess the transcriptome (microarray versus RNAseq), species (rat versus human), and tissue (whole heart versus ACF cultures).

The use of four donors for RNAseq is acknowledged as a limitation; larger cohorts would improve statistical power and enable more confident identification of downregulated genes after FDR correction, where the current analysis required relaxation to unadjusted p-values for downregulated DEG pathway analysis.

6.4.7 Conservation of the CALCR internalisation phenotype in the CREM-Tg mouse model

The preliminary observation that CALCR perinuclear accumulation is evident in ACFs from 9-month-old CREM-Tg mice (characterised by permanent AF and severe atrial fibrosis) but not 3-month-old mice (with less extensive atrial pathology) provides important cross-species validation of the AF associated CALCR internalisation phenotype. Similarly, the phenotype's apparent sensitivity to levamlodipine is an intriguing preliminary finding. However, it is essential to interpret these data with caution given the N=1 biological replicate. Nevertheless, early evidence indicates the CREM-Tg model is well-suited for a proof-of-principle validation study to test the hypothesis that early intervention with a combination of levamlodipine and CT attenuates the progression of atrial pathology and, ultimately, AF.

6.4.8 Conclusions and implications

This chapter presents the first functional and mechanistic characterisation of a pharmacological strategy to partially restore CALCR surface expression and antifibrotic signalling in human AF-ACFs. The principal finding is that levamlodipine rescues

CALCR-dependent suppression of collagen I production, likely via a mechanism independent of its canonical target. Transcriptomic data implicate induction of sterol biosynthetic pathways and downregulation of cytoskeletal motor proteins as candidate mechanisms of CALCR surface restoration. These findings form the foundation for a dedicated doctoral project. The conservation of CALCR internalisation in the aged CREM-Tg mouse, while requiring further validation, provides the scientific rationale for a planned *in vivo* study. Collectively, this body of work advances the field towards a pharmacological approach to atrial fibrosis management in persistent AF, which remains an unsolved clinical challenge, that leverages the restoration of an endogenous paracrine antifibrotic signalling axis – a mechanistically distinct and potentially complementary strategy to existing AF therapies.

CHAPTER 7: CONCLUSIONS AND FUTURE DIRECTIONS

7.1 Overview

Atrial fibrosis is a pathological hallmark of AF and a major determinant of its progression, perpetuation, and resistance to therapy.[269] The calcitonin-CALCR antifibrotic signalling axis, in which paracrine CT, produced by cardiomyocytes, acts on CALCR-expressing ACFs, was established by our group as a physiologically important regulator of atrial fibrotic homeostasis.[1] Critically, both components of this axis – atrial CT secretion and CALCR surface expression in ACFs – are disrupted in persistent AF.[1] This may contribute to the pathological accumulation of atrial fibrosis that characterises structural remodelling in AF. The work presented in this thesis aimed to investigate two overarching questions:

1. What are the molecular mechanisms underlying the AF-associated loss of CALCR surface localisation in ACFs?
2. Can surface CALCR and, ultimately, antifibrotic signalling be rescued pharmacologically in AF-ACFs?

Addressing these questions required a multi-strategy approach. The thesis began with hypothesis-driven mechanistic interrogation guided by the existing literature on the mechanisms governing CALCR localisation (Chapters 3 and 4), pivoted to an unbiased high-throughput pharmacological screen when no single canonical mechanism could be demonstrated to account for the phenotype (Chapter 5), and concluded with functional and translational characterisation of the most promising pharmacological hit (Chapter 6). This chapter synthesises the principal findings (**Fig 7.1**), appraises the limitations of the work, and identifies the most important future directions.

7.2 Principal findings

7.2.1 FLNa is not a major regulator of CALCR localisation in primary human ACFs

Chapter 3 was predicated on the hypothesis, derived from a study in immortalised cell lines, that FLNa – specifically its proteolytically generated C-terminal fragment ($FLNa^{CT}$) – promotes CALCR recycling to the plasma membrane, and that loss of $FLNa^{CT}$ in AF might therefore account for CALCR internalisation.[91] I methodologically tested this hypothesis and concluded that, although $FLNa^{CT}$ is reduced in AF-ACFs and preferentially co-immunoprecipitates with CALCR, neither disruption of the FLNa-CALCR interaction nor loss of FLNa itself is sufficient to reproduce the CALCR internalisation phenotype observed in AF-ACFs. This is a significant negative finding: it demonstrates that the biology of CALCR trafficking in primary human ACFs diverges from that in heterologous cell systems and that translating mechanisms identified in immortalised lines to disease-relevant primary cells requires careful validation. This cautionary lesson is applicable broadly to the GPCR trafficking field, where a large proportion of mechanistic data derives from overexpression studies in immortalised lines.[270]

The investigation of FLNa proteolysis also yielded an important secondary finding: neither calpain 1 (the protease most widely implicated in FLNa cleavage) nor caspase 3, when individually inhibited or silenced by siRNA, altered $FLNa^{CT}$ abundance in human ACFs.[119,126] This indicates that FLNa proteolysis is governed by cell-type-specific mechanisms not captured by the existing literature. An interrogation of the ACF proteome identified 147 proteases expressed in human ACFs, of which only caspase 3 had prior evidence of FLNa cleavage – and I did not find evidence for its involvement in FLNa cleavage in ACFs.[126] The identity of the protease(s) responsible for $FLNa^{CT}$ generation in ACFs, and whether their activity is altered in AF, remains an open question.

7.2.2 Systematic exploration of six candidate trafficking mechanisms narrows the mechanistic field and identifies CALCR interactome remodelling in AF

Chapter 4 systematically evaluated six additional candidate mechanisms for CALCR internalisation: interactome remodelling, clathrin-mediated endocytosis and actin-dependent trafficking, alternative CALCR splicing, RAMP co-expression, β-arrestin-dependent internalisation, and N-linked glycosylation. Each was assessed in primary ACFs, and four were deemed unlikely to be major contributors: the insert-positive $CALCR_b$ splice variant was not detected in human ACFs; RAMP1 and RAMP2 proteins were not detectable in human ACFs, despite mRNA expression; β-arrestin 1 and 2 knockdown did not alter CALCR localisation; and tunicamycin-mediated inhibition of N-glycosylation did not associate with a detectable CALCR molecular weight shift nor significant changes in CALCR internalisation.

The pharmacological inhibition data (Dyngo4A, chlorpromazine, cytochalasin D) produced negative results despite the interactome analysis identifying substantial AF-specific enrichment of endocytic machinery co-immunoprecipitating with CALCR. This apparent paradox likely reflects a constitutive, steady-state redistribution of CALCR in AF-ACFs, rather than ongoing active internalisation that could be blocked acutely. If CALCR has reached a new trafficking equilibrium in AF, driven by impaired recycling or failure of surface delivery, rather than enhanced internalisation, acute blockade of internalisation pathways would not be expected to restore surface expression. The simultaneous enrichment of retromer and early endosome markers (EEA1, RUFY1) in the AF-ACF CALCR interactome supports this interpretation, suggesting that internalised CALCR accumulates within the endosomal recycling system rather than being efficiently recycled to the plasma membrane.

7.2.3 CALCR internalisation in AF-ACFs: a complex, potentially redundant, aetiology

Considered together, Chapters 3 and 4 constitute the most systematic and comprehensive mechanistic investigation of CALCR trafficking in a primary human cell system to date. The negative results across multiple independent mechanistic hypotheses – often examined by complementary approaches – collectively argue against a simple, single-gene/protein explanation for the AF-associated internalisation phenotype. The implication is that the CALCR trafficking defect in AF-ACFs likely arises from the convergent effect of multiple, partially redundant alterations in the receptor's molecular environment, rather than from a single dominant change. Such complexity is coherent with the increasingly appreciated concept of co-ordinated transcriptional and post-translational reprogramming in ACFs in AF, as we reported recently in a single-nucleus multi-omics study.[43] Strategically, this conclusion also suggests that the hypothesis-driven approach, which targets individual molecular nodes, was unlikely to identify the causal mechanism and thus provided the motivation for the unbiased phenotypic screening approach adopted in Chapter 5.

7.2.4 A high-throughput phenotypic screen identified levamlodipine as a reproducible restorer of surface CALCR localisation

In Chapter 5, I developed, validated, and implemented the first high-throughput screen (HTS) in primary donor-derived AF-ACFs. The P/C CALCR intensity ratio, quantifying the enrichment of CALCR fluorescence in the perinuclear zone relative to the cytoplasm, was identified as the optimal ratiometric readout (Z' = 0.31), despite the inherent biological variability of primary human cells. The screen of 3,091 small molecules identified levamlodipine besylate as the only compound to reduce the P/C ratio by more than 2 SDs from the mean of all compounds across all three AF donors screened. Its

racemic formulation, which is widely used clinically in the management of angina and hypertension, was a hit in two of three donors.

The identification of a clinically approved compound confers immediate translational relevance: established human safety and pharmacokinetic profiles and accelerated regulatory pathways compared with *de novo* drug candidates. Furthermore, the finding of structurally diverse compounds with shared pharmacological target classes – including 5-$HT_{2A/6/7}$ receptors and D2/3/4 dopamine receptors – raises the possibility that modulation of convergent signalling pathways mediates CALCR rescue across multiple hits and points towards specific GPCRs as candidate regulators of CALCR surface expression in AF-ACFs.

7.2.5 Levamlodipine rescues CALCR-dependent antifibrotic signalling possibly via a $Ca_v1.2$-independent mechanism

Chapter 6 moved from hit identification to functional and mechanistic characterisation of levamlodipine. The demonstration that pre-treatment with levamlodipine sensitises AF-ACFs to human calcitonin – producing a CALCR-dependent reduction in collagen I protein expression that is not observed with levamlodipine or calcitonin alone and is reversed by a CALCR antagonist – constitutes the most translationally important finding of this thesis. It provides direct evidence that pharmacological restoration of CALCR surface expression is sufficient to re-engage the endogenous antifibrotic axis in a disease-relevant human cell system.

Mechanistic interrogation of levamlodipine's action suggested that LTCC inhibition may not be the primary driver of the observed effects. This is consistent with broader literature that has demonstrated pleiotropic, LTCC-independent effects of amlodipine, and with the clinical evidence from the CAMELOT and ASCOT-BPLA trials that suggested amlodipine's cardiovascular benefits exceed those attributable to blood pressure reduction alone.[250,251] The negative results with an extensive panel of TRPC channel

antagonists and SOCE inhibitors further argued against a general role for Ca^{2+} influx modulation in governing CALCR surface expression, despite TRPC3's recent identification as a predicted profibrotic signalling node in ACFs.[205]

We aimed to leverage large population datasets to investigate whether (lev)amlodipine in combination with exogenous calcitonin, is associated with reduced AF incidence or markers of atrial remodelling, such as echocardiographic left atrial volume. Such analyses would provide supportive, real-world evidence for the antifibrotic potential of this combination therapy and may inform the design of a prospective randomised trial. However, although approximately 4.3% of participants in the UK Biobank cohort (n ≈ 500,000) reported amlodipine use, only 11 individuals reported use of clinical calcitonin formulations (e.g. Miacalcin), and just one participant reported concurrent use of both. These small numbers precluded meaningful exploratory analyses. Given the reduction in myocardial CT production in AF, amlodipine *per se* would not necessarily be expected to prevent atrial structural remodelling.

RNA sequencing of levamlodipine-treated AF-ACFs identified 241 upregulated and 142 downregulated genes, with the transcriptional signature dominated by co-ordinated induction of mevalonate/cholesterol biosynthesis pathways and downregulation of cell cycle regulators and motor proteins. The cholesterol biosynthesis is mechanistically compelling given the established role of membrane cholesterol and lipid raft integrity in GPCR surface expression and endosomal recycling.[252] The downregulation of kinesin-family members, which facilitate ATP-dependent plus-end directed transport along microtubular tracks, provides another candidate mechanism connecting levamlodipine's transcriptional effects to CALCR surface trafficking. These data, in sum, argue for a pleiotropic, membrane- or trafficking-level mechanism of action that may be distinct from LTCC blockade that is largely unexplored in prior literature.

Finally, preliminary evidence from the CREM-Tg mouse model demonstrated that the CALCR internalisation is apparently conserved across species and is evident in 9-month-old mice (with permanent AF and atrial fibrosis) but not 3-month-old mice (with much less atrial pathology).[212] Furthermore, levamlodipine treatment of CREM-Tg ACFs is associated with an apparent CALCR surface redistribution. Although derived from a single biological replicate and requiring validation, these data support the utility and relevance of this model for a preclinical *in vivo* study.

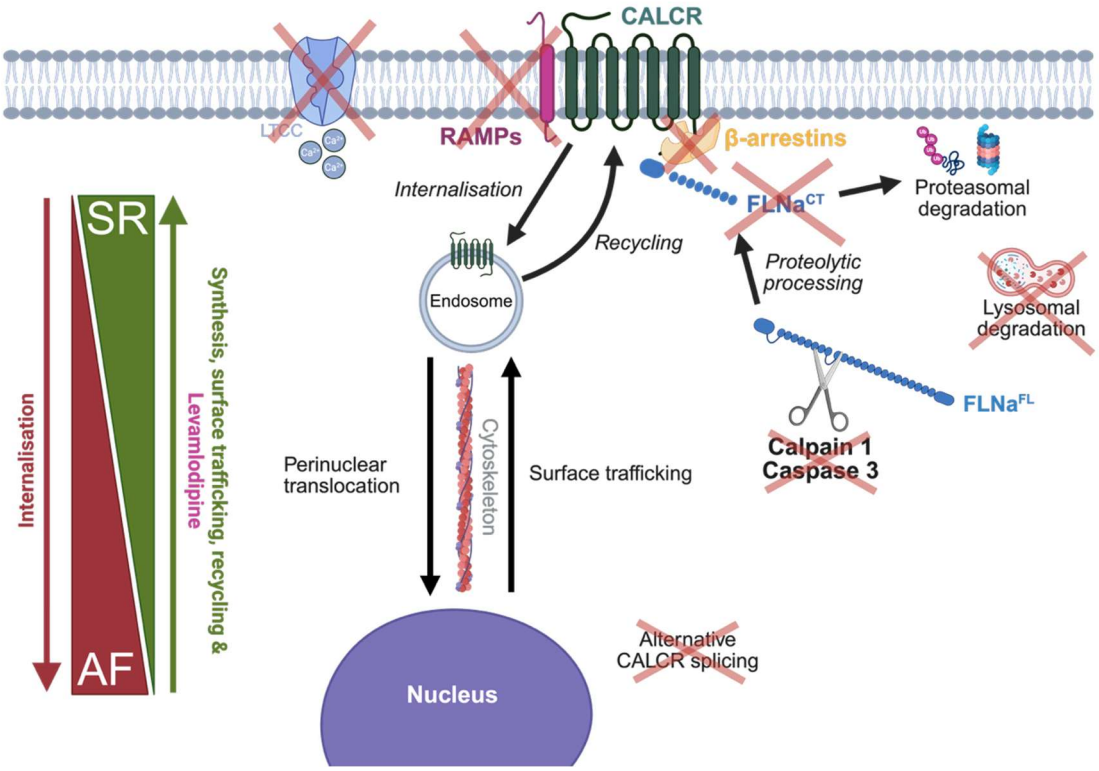


Figure 7.1: Schematic summarising the principal findings of this thesis. In SR-ACFs, CALCR is predominantly localised at the cell periphery and at the cell membrane, enabling activation by CT and downstream antifibrotic signalling. In AF-ACFs, CALCR exhibits increased internalisation and perinuclear accumulation. Multiple candidate mechanisms including FLNa dysregulation, RAMPs, β-arrestin- and CME-mediated internalisation, N-glycosylation, and alternative splicing of CALCR were investigated and no evidence was found to support their position as primary drivers of this phenotype. Treatment with levamlodipine restores CALCR localisation and re-establishes CT-dependent antifibrotic signalling. This effect appears to occur independently of canonical LTCC inhibition, suggesting a non-classical, pleiotropic mechanism involving modulation of membrane dynamics, trafficking pathways, or receptor recycling.

7.3 Limitations and future directions

7.3.1 The primary human ACF model

All mechanistic experiments were conducted on primary human ACFs maintained in two-dimensional, monocultures. While this system offers essential advantages – including direct disease-relevance and compatibility with genetic/pharmacological manipulations requiring large numbers of cells – it lacks key features of the *in vivo* atrial microenvironment that may be relevant to CALCR trafficking. These include the lack of cyclic mechanical stretch, three-dimensional extracellular matrix architecture, and paracrine signals from neighbouring cell types. The absence of cardiomyocytes, an endogenous source of myocardial CT production, means that functional experiments supplied CT at a concentration (100 nM) that may not reflect the physiological paracrine levels experienced by ACFs. Similarly, culturing ACFs on surfaces of supraphysiological stiffness (e.g. plastic plates which have a Young's modulus several orders of magnitude greater than even extensively fibrotic heart tissue) can stimulate unique transcriptional programmes that promote ACF activation, proliferation, and myofibroblast transdifferentiation.[271-273] Three-dimensional co-culture models or organoid systems incorporating cardiomyocytes with soft hydrogels or engineered heart tissue of biological stiffness could provide a more physiologically accurate representation of the CT-CALCR axis.

Moreover, prolonged cell culture has been shown to induce changes in ACF gene expression and electrophysiological properties.[113,274] However, we aimed to minimise these effects by performing all experiments on cells within their first 5 passages which was a compromise to ensure sufficient cellular material while minimising confounding culture-related changes.[1] Cognisant of these limitations, an *in vivo* study is underway to assess the effects of levamlodipine and exogenous calcitonin on atrial structural remodelling.

All experiments used ACFs isolated from the left atrial appendage of donors undergoing cardiac surgery. Therefore, the control (SR) donors are not free of heart disease. This is a limitation imposed by tissue availability and ethical access which largely precludes sampling from disease-free hearts. The study was not designed to precisely age- and comorbidity-match groups and SR donors invariably differed from AF donors beyond rhythm status alone which could introduce potential confounding in SR versus AF comparisons. Furthermore, I focussed on patients with persistent AF and, therefore, whether the results described are consistent in less advanced disease warrants future investigation and has implications for the timing of CALCR-restoring interventions. The inter-donor variability that dominated the transcriptomic data, hit identification, and complicated pharmacological dose-response analyses reflects the biological heterogeneity of human AF, in which multiple upstream pathological pathways converge on a common phenotype. Similarly, although the left atrial appendage, the tissue from which all ACFs were isolated and a common source of cardiac thromboembolism, is widely used in preclinical research, it differs in embryological origin and haemodynamic environment when compared with the true left atrium which may limit generalisability.

7.3.2 Measurement of CALCR localisation

The CALCR-DAPI overlap coefficient, used in Chapters 3 and 4, is a measure of global receptor distribution relative to the nuclear compartment. As discussed in Chapter 3, the redistribution of CALCR to cytoskeletal fractions on subcellular fractionation is consistent with perinuclear accumulation rather than true nuclear import, but the precise organellar location – ER, Golgi, early endosomes, recycling endosomes, lysosomes, or perinuclear space – was not resolved. This is a mechanistic gap because different intracellular destinations imply different upstream mechanisms. The P/C ratio used in the HTS platform provided a quantitative ratiometric measure with sufficient dynamic range for screening purposes but is likewise blind to compartment-specific information.

Therefore, co-localisation assays using markers for specific endosomal compartments (e.g. EEA1 or Rab5 for early endosomes, Rab11 for recycling endosomes, Rab7 for late endosomes, LAMP1 for lysosomes, GM130 for the cis-Golgi) are a priority for future work.[275,276] Super resolution microscopy and techniques to assess protein proximity (e.g. Förster/bioluminescence resonance energy transfer or proximity ligation assays) could more precisely define the spatial relationship between CALCR and specific trafficking machinery.[172,270] Similarly, surface labelling strategies (e.g. SNAP-tag, biotinylation, or fluorescent protein conjugation) would enable direct measurement of CALCR internalisation kinetics and recycling rates, which would substantially clarify whether the primary defect in AF-ACFs is receptor internalisation and/or recycling.[277] However, caution should be applied when interpreting the results of any experiments that require modified CALCR constructs which may have altered trafficking dynamics and/or be expressed at non-physiological levels thereby promoting interactions that do not ordinarily occur. Once the compartment is identified, targeted siRNA knockdown of candidate recycling regulators identified in the SR CALCR interactome data would test whether disruption of these pathways in SR-ACFs phenocopies the AF CALCR internalisation.

7.3.3 Limitations of mechanistic experiments

Ongoing work is addressing some of the limitations of mechanistic experiments. Specifically, in Chapter 3, the exploratory cycloheximide chase assay was performed in a single donor and will be repeated in additional donors. Likewise, the *in vivo* data presented in Chapter 6 are derived from a single biological replicate (for both the 3-month vs 9-month comparison and the levamlodipine treatment in the ACFs from a 9-month-old animal) which severely limits the conclusions that can be drawn from this early, hypothesis generating study. The planned *in vivo* study – using early combination therapy with levamlodipine and salmon calcitonin in CREM-Tg mice, with subsequent assessment of atrial fibrosis and AF burden – will be necessary to determine whether

the pharmacological rescue of CALCR surface expression translates to meaningful attenuation of *in vivo* AF pathology. This is the most immediate translational priority.

Relatedly, the RNA sequencing analysis was performed on AF-ACFs from only four donors which, although typical for studies of this kind, limited the statistical power for differential expression analysis and necessitated the use of unadjusted p-values to identify downregulated KEGG pathways.[1,43,177] The small sample size also makes it difficult to distinguish reproducible treatment-driven transcriptional changes from donor-specific effects, although the PCA analysis does support the presence of a consistent intra-donor levamlodipine signature. Increasing the donor number would substantially improve statistical power and confidence in pathway enrichment analyses.

Knockdown of *ARRB2* and *CACNA1C* was assessed by RT-qPCR but not verified at the protein level. Post-transcriptional regulation and protein half-life considerations mean that mRNA knockdown does not guarantee equivalent protein depletion within the experimental timeframe. Protein-level confirmation by WB is ongoing and will be necessary before the negative results from these experiments can be considered definitive.

Additionally, the hit characterisation studies presented in Chapter 6 mostly used levamlodipine at 10 μM which exceeds typical clinical plasma concentrations (~10nM), although local myocardial concentrations may be substantially higher due to lipophilic drug partitioning.[254,278] This does not invalidate *in vitro* conclusions but this pharmacokinetic gap is an important consideration for the translational interpretation of findings and for the design of *in vivo* studies.

7.4 Final conclusions

This thesis made three substantive contributions to the field of AF biology and GPCR trafficking.

1. It has systematically studied FLNa and six other candidate mechanisms and found no evidence they are major regulators of CALCR surface expression in primary human ACFs, establishing that the AF-associated CALCR localisation defect is mechanistically complex and not entirely captured by existing cell line-based, overexpression models.
2. It generated the most comprehensive characterisation of the disease-specific CALCR interactome to date, revealing AF-associated remodelling of endocytic and recycling machinery. Combined with the direct mechanistic interrogation, these suggested that receptor recycling and surface delivery, rather than enhanced internalisation, are the likely principal trafficking defects.
3. Of greatest translational significance, it demonstrated through a rigorous, high-throughput phenotypic screening approach that levamlodipine – an approved cardiovascular drug – pharmacologically reverses CALCR internalisation and restores CALCR-dependent antifibrotic CT signalling in primary human AF-ACFs.

The endogenous CT-CALCR antifibrotic axis represents a physiological brake on atrial fibrosis that is dysfunctional in persistent AF. The work presented here provides proof-of-principle that this brake can be pharmacologically re-engaged using an approved, well-tolerated drug in a primary human cell model. While substantial work remains to define the mechanism and validate its efficacy *in vivo*, these findings advance the field towards a fundamentally new approach to atrial fibrosis management – one that aims to restore endogenous paracrine cardioprotective signalling. Given the inadequacy of current strategies for targeting atrial fibrosis in clinical practice, this approach merits further investigation.

CHAPTER 8: APPENDICES

Appendix 1: List of the 169 unique CALCR interactors in SR-ACFs

NBAS	LRPAP1	CEMIP
RNF212B	MCM7	SCFD1
CCS	RPL22	AP3S1
TP53I11	NNMT	DDX17
HNRNPDL	GPD2	UPF1
RER1	MAP2K3	RAB8B
DHX15	STT3A	LPP
ZW10	ME1	RPL36AL
HNRNPR	NASP	ERGIC1
EPB41L2	PDLIM4	FUBP1
SCO2	RAB13	UPRT
EDIL3	HNRNPA3	FUBP3
CTNND1	KPNA2	PAWR
DPM1	SLC16A1	ZNF382
PRPF40A	SNU13	PSMB7
ECI2	SPCS3	PLIN2
BANF1	UFM1	DNAJC2
PRKRA	HBB	CHP1
EIF3J	MAP1A	HNRNPAB
SCO1	MRPS22	CORO1B
DCTN3	ERH	PI4K2A
TRIO	U2AF1	HNRNPUL1
GLRX3	TAP2	CCDC32
RSL1D1	PTPN12	NUP58
MYO1D	LRP1	OSBPL11
CAVIN2	GALNT1	MRPL13
BAG2	AKAP13	UACA
CP	GRSF1	UPF2
C3	PTPN13	PDLIM7
JCHAIN	G3BP1	DDX21
LMNA	MRPL49	FARSB
HRG	SNTB2	SPATS2L
RPLP0	MRPL58	MRPL22
COL5A2	FLOT2	GDAP2
COL1A2	RBM39	BCLAF1
PFKM	SEPTIN2	FKBP11
RPSA	EIF4H	UGGT2
HNRNPA1	NONO	EIF3K
RO60	SKIC2	DNAJB11
UMPS	ATP6AP1	STK39
PDHB	ADRM1	ABCF2
ADH5	SRSF7	PUF60
HNRNPL	IMMT	SLC39A10
ENG	FKBP15	NOB1
DDX5	UBR4	VPS4A
EIF2AK2	BRWD3	STUB1

PTMS	HSDL2	FARSA
BGN	VPS13C	NCKAP1
OSBP	TRMT10C	SUGT1
FBL	ZC3HAV1	MRPS23
SFPQ	GCC2	MAP4K5
JAK1	PNPLA6	SRPRB
PSMA2	NDUFAF2	GMPPB
DDX6	NUP93	CDC42BPB
S100A4	LRRC47	NFS1
YWHAQ	ASCC1	
LOX	ABCF1	

Appendix 2: List of the 427 unique CALCR interactors in AF-ACFs

IGHV3-49	UBTF	MRPS25	EDC4	SRRT
IGKV3D-20	CTPS1	MRPS35	RPL22L1	AP1M1
SH3PXD2B	NDUFV2	MRPS9	LARP1	FUT8
PSMD12	TRIM21	HSPG2	MTHFD1L	RAB34
PGRMC1	EIF2S2	ATP2C1	FIP1L1	SKIC8
DFFA	PZP	SLC25A3	GIGYF2	NAT10
IPO5	COL5A1	AMPD2	RAPH1	XRN2
IGF2BP3	GSTM3	FABP5	H3C13	TRIOBP
DNM1L	ATP6V1B2	EXOSC10	LARP4	RAB3GAP2
PIK3C2A	ACO1	NUCB1	BZW1	ACBD3
EXOC5	SDHB	TAP1	PHF5A	CHMP4B
PES1	MMUT	CEBPZ	HDGFL2	OSBPL3
PPP6C	UQCRC2	RELA	HUWE1	BICC1
TXNDC9	MCC	PTPN11	TMED4	EPS8L2
PDCD5	ATP2B4	KLC1	HOOK3	RPF2
CASK	RRM1	SRSF1	CARM1	AAMDC
ARPC2	MCM3	ARHGAP1	SULF1	LRRC40
ZNF185	PSMA1	LGALS3BP	CHERP	MRPL47
TM9SF1	PSMA3	PPID	CCAR1	EMC7
PPM1G	ANXA13	VAC14	PARP9	ENY2
EIF3H	MAPK3	NEXN	FTSJ3	IL1RAP
ASAP2	PSMB4	TWF1	XRN1	ARHGAP35
PJA2	NDUFS1	TRIM26	PALS1	OLA1
PAPSS1	EPHA2	ILF2	CPSF7	ECHDC1
TXNL1	CLIP1	TRAP1	OTUD6B	MDN1
EIF4G3	GSTT1	MYO1E	VPS37A	DCAF13
TGOLN2	SERPINB1	PRKAA1	WDR36	ARL8B
CHMP2A	ALDH1B1	PPFIA1	DTX3L	ANO10
PLRG1	PYCR1	HNRNPA0	BRIX1	MRPL16
ZNRD2	CSTF2	SRSF9	NEK7	BET1L
SPAG9	PFN2	SRSF5	PHLDA1	ERAP1
OPA1	CTNNB1	PPIG	PCNP	FAM120A
EVI5	THBS2	SF3B2	ATXN2L	EHD3
ACSL4	ARL2	MYO9B	PRPF31	MRPL15
DIAPH1	FEN1	TCIRG1	GEMIN6	HACD3
PRMT3	TXLNA	SQSTM1	PSPC1	EMC3
SNX2	CSK	ASAH1	PSMF1	ABRACL
TOM1	ACTR1B	CAMK2G	NCSTN	STIM2
DKC1	PAFAH1B1	SNW1	CNOT9	CTTNBP2NL
CNOT3	MAP2K4	KRR1	MYO18A	EPS15L1
PEX14	RECQL	CUL3	TFG	NXF1
CS	ATRX	CUL4B	STAM	CLIP2
MRPL33	GYG1	MOGS	TAF15	TJP2
TACC1	PXN	NID2	OSTF1	ZC3H7B
SRSF10	CARS1	BOP1	TNPO1	SUN2
SF3B1	YLPM1	ARHGEF7	UTP4	NRBP1

MYCBP2	RBM25	UBAP2L	MRPL24	LNPEP
PSMD10	NUP153	SCRIB	GCC1	DBNL
STK10	RANBP2	TTLL12	KCTD12	STOML2
ENDOD1	GMPS	PDIA5	SNRNP40	MRTO4
ELP1	EMD	PDCD11	PTCD3	RALY
SNX4	CPT1A	BMS1	S100A16	ACIN1
TRIM16	VASP	USP10	CERS2	BLOC1S6
SVIL	ANXA11	NOLC1	SUCLG2	PSME2
MAP4K4	STAT2	SPCS2	GMPPA	CCPG1
AIFM1	CRIP2	KARS1	SCYL1	CORO1C
TXNDC12	METAP1	EEA1	RBM14-RBM4	AKAP8L
NDUFB10	AP2S1	PCBP2	FMNL2	PRPF19
PLAT	EIF5	SF3B4	VPS35	MAGED2
KRT14	PSMD4	SEC23A	GFM1	SNX6
AHSG	DRG2	MAPRE2	CCNL2	MACF1
GNAI2	CSE1L	SF1	SRPK1	SRRM2
ICAM1	NPEPPS	TRIP6	RUFY1	EIF3L
RPLP1	RRP1	ZYX	YME1L1	FNDC3A
KRT8	ATP5ME	CCDC6	SDF2	DIS3
IGKV4-1	ARPC4	IFI16	POP1	MRPS17
EIF4E	CD81	NDUFA5	TTC1	AP3M1
SERPINE2	IL2	TXNRD1	PHB2	YARS2
APRT	ACTR2	SMU1	COPS8	SBDS
YES1	ABCE1	MAP7D1	COL12A1	CHTOP
RHOC	RHOA	CCDC88A	ACO2	SAMHD1
SRPRA	SNRPE	FILIP1L	DDX50	HBS1L
COL4A2	SNRPD1	ARHGAP29	TXNDC17	DAAM1
KRT16	PSMC6	AGK	MRPL45	MYO5A
MRPL3	TBPL1	RRP12	SDF4	PRRC2C
ACAA1	RPS26	MRPL2	NOL10	PPME1
SNRPC	RPS27A	ATAD3B	AARSD1	YTHDF2
SNRPA1	TRA2B	ECPAS	TMEM43	ATP6V1D
COX5B	PPP3R1	MICOS13	PDCD10	MAGED1
COL6A2	SKP1	RNF213	WDR18	LRRFIP2
SLC25A4	UBE2I	KANK2	UTP14A	NCOR2
COX4I1	YBX1	ATG16L1	GNL3	BZW2
DSP	CSNK2B	SPECC1L	RIOK2	OAS3
PDGFRA	TUBA4A	CIAPIN1	ELOVL1	
POR	RPP38	DHX57	LSM14B	
ATP2A2	GTF2I	ERAP2	HINT2	

Appendix 3: Full list of the compounds that reduced cell count by ≥2 SD for each donor

Donor 1	Donor 2	Donor 3
Pralsetinib	Revaprazan (hydrochloride)	Nitrofurantoin
Mobocertinib	Dioscin	Sulfameter
Toltrazuril	Bepridil (hydrochloride hydrate)	Benzbromarone
Menadione	Amlodipine (besylate)	Brimonidine
Cetraxate (hydrochloride)	Tafluprost	Bendazac L-Lysine
Pimavanserin (hemitartrate)	Zinc Pyrithione	Antazoline (hydrochloride)
Fangchinoline	Tegaserod (maleate)	Sennoside B
Tolmetin (sodium dihydrate)	Candesartan Cilexetil	Candesartan Cilexetil
Lopinavir	Amorolfine (hydrochloride)	Temoporfin
Bronopol	Tafenoquine (Succinate)	Dyclonine (hydrochloride)
Ursolic acid	Butoconazole (nitrate)	Tocofersolan
(S)-Crizotinib	Simeprevir	Tafenoquine (Succinate)
Vinpocetine	Estrone sulfate (potassium)	Digoxigenin
Oxiconazole nitrate	Dyclonine (hydrochloride)	Tafluprost
Lapatinib ditosylate	Bilastine	Revaprazan (hydrochloride)
Aclacinomycin A hydrochloride	Hexaminolevulinate (hydrochloride)	Zinc Pyrithione
Arterolane	Butylparaben	Simeprevir
Cabozantinib (S-malate)	Dicyclomine (hydrochloride)	Tegaserod (maleate)
Halofuginone (hydrobromide)	Dirithromycin	Butoconazole (nitrate)
Robenidine hydrochloride	Nelfinavir (Mesylate)	Mevastatin
Cobimetinib (hemifumarate)	Enrofloxacin (monohydrochloride)	Norethisterone enanthate
Saxagliptin	Riluzole hydrochloride	Ebselen
Oxyclozanide	Closantel (sodium)	Nebivolol (hydrochloride)
Ruboxistaurin	Clindamycin palmitate (hydrochloride)	Cilengitide
L-Tryptophan	Nebivolol (hydrochloride)	Nelfinavir (Mesylate)
Maytansine	Digitonin	Amsacrine (hydrochloride)
20(S)-Ginsenoside Rg3	AKBA	Closantel (sodium)
Ixabepilone	Oxethazaine	Digitonin
Andrographolide	Mevastatin	Chlorhexidine
Finafloxacin	Sanguinarine (chloride)	AKBA
Telotristat etiprate	Astemizole	Toremifene (citrate)
Sofalcone	Amsacrine (hydrochloride)	Ebastine
Nelfinavir	Sertaconazole (nitrate)	Sertaconazole (nitrate)
Fluvastatin (sodium)	Ebselen	Sanguinarine (chloride)
Edoxaban (tosylate)	Chlorhexidine	Fluspirilene
Sonidegib	Azelnidipine	Astemizole
Quinacrine (dihydrochloride)	Menadione bisulfite (sodium)	Clotrimazole
Anidulafungin	Toremifene (citrate)	Azelnidipine
Masitinib	Moxidectin	Moxidectin
Costunolide	Fluspirilene	Fenretinide
Hexestrol	Fenretinide	Sunitinib

Gossypol (acetic acid)	Ebastine	Y-33075 (dihydrochloride)
Rucaparib (monocamsylate)	Cilengitide	Ouabain (Octahydrate)
Lapatinib	Norethisterone enanthate	Nintedanib esylate
Vemurafenib	Triclabendazole	Telotristat ethyl
Mitoxantrone (dihydrochloride)	Otilonium (bromide)	Doramectin
Domiphen (bromide)	Costunolide	Costunolide
CB-5083	Masitinib (mesylate)	Fedratinib (hydrochloride hydrate)
Dyclonine (hydrochloride)	Maleimide	Otilonium (bromide)
Vorapaxar (sulfate)	Fedratinib (hydrochloride hydrate)	Cetylpyridinium (chloride)
Ceritinib	Bromhexine (hydrochloride)	Benzethonium chloride
Chlorhexidine (dihydrochloride)	Oxiconazole nitrate	Visomitin
Afoxolaner	Ouabain (Octahydrate)	Saikosaponin D
Sanguinarine (chloride)	Y-33075 (dihydrochloride)	Bosutinib
Dioscin	Saikosaponin A	Saikosaponin A
Lacidipine	CB-5083	CB-5083
Dienestrol	Visomitin	Robenidine hydrochloride
Raloxifene (hydrochloride)	Bedaquiline	Pimavanserin (hemitartrate)
Nelfinavir (Mesylate)	Cetylpyridinium (chloride)	Maleimide
Almonertinib	Robenidine hydrochloride	Octyl gallate
Sclareol	Doramectin	Bedaquiline
Thioridazine (hydrochloride)	Pimavanserin (hemitartrate)	Triclabendazole
Ceritinib dihydrochloride	Etofenamate	Oxiconazole nitrate
Clindamycin palmitate (hydrochloride)	Dronedarone	Efavirenz
Econazole	Olverembatinib	Olverembatinib
Cilengitide (TFA)	Benzethonium chloride	Dronedarone
Mobocertinib (succinate)	Octyl gallate	Aurothioglucose
Mitoxantrone	Efavirenz	Hydroxyprogesterone caproate
Odevixibat	Lomerizine dihydrochloride	(S)-Crizotinib
Ensartinib (dihydrochloride)	Colchicine	Digitoxin
18?-Glycyrrhetinic acid	Saikosaponin D	Estradiol valerianate
Fluralaner	Vandetanib	Regorafenib
Bosutinib	Rilpivirine	Mibefradil (dihydrochloride)
Erythromycin estolate	(S)-Crizotinib	Ceritinib
Menadione bisulfite (sodium)	Mibefradil (dihydrochloride)	Fingolimod (hydrochloride)
Verteporfin	Bronopol	Isoconazole (nitrate)
Amsacrine (hydrochloride)	Estradiol valerianate	Cinacalcet
Felodipine	Ceritinib	Rifamycin S
Otilonium (bromide)	Fingolimod (hydrochloride)	Vortioxetine (hydrobromide)
Ivermectin	Vortioxetine (hydrobromide)	Ivacaftor
Tafenoquine (Succinate)	Cinacalcet	Entrectinib
Sulconazole (mononitrate)	Ivacaftor	Fenticonazole (Nitrate)
Puromycin (dihydrochloride)	Fenticonazole (Nitrate)	Clioquinol
Dabigatran etexilate	Entrectinib	Octenidine (dihydrochloride)
Ripretinib	Isoconazole (nitrate)	Pimozide
Chlorhexidine	Desogestrel	Amiodarone (hydrochloride)
Closantel (sodium)	Ethacridine (lactate)	Avermectin B1
Oxethazaine	Hexylresorcinol	Thonzonium (bromide)

Maleimide	Domiphen (bromide)	Cetylpyridinium (chloride monohydrate)
Digitonin	Ensartinib (dihydrochloride)	Cetrimonium (bromide)
Epirubicin (hydrochloride)	alpha-Hederin	Mobocertinib (succinate)
Palbociclib (isethionate)	Amiodarone (hydrochloride)	Desogestrel
Amsacrine	Malachite green (oxalate)	Domiphen (bromide)
Sunitinib (Malate)	Clomiphene (citrate)	Malachite green (oxalate)
Voxilaprevir	Crystal Violet	Dehydrocostus Lactone
Mefloquine (hydrochloride)	Montelukast (sodium)	Crystal Violet
Benzethonium chloride	Pimozide	8-Hydroxyquinoline
Mevastatin	Dehydrocostus Lactone	Auranofin
Tetradecyl sulfate (sodium)	Auranofin	Milbemycin oxime
Sodium lauryl sulfoacetate	Milbemycin oxime	Siramesine (hydrochloride)
Osimertinib	Siramesine (hydrochloride)	alpha-Hederin
Ebastine	Cetylpyridinium (chloride monohydrate)	Cyclo(RGDyK) (trifluoroacetate)
Sertindole	Mobocertinib (succinate)	Prazosin (hydrochloride)
Zinc Pyrithione	Octenidine (dihydrochloride)	Fenbendazole
Gossypol	8-Hydroxyquinoline	Travoprost
Ponesimod	Thonzonium (bromide)	Anidulafungin
Malachite green (oxalate)	Cetrimonium (bromide)	Trilaciclib (hydrochloride)
Cilengitide	Econazole (nitrate)	Lapatinib (ditosylate)
alpha-Hederin	Lapatinib (ditosylate)	Lapatinib
Troglitazone	Anidulafungin	Osimertinib mesylate
Almonertinib (hydrochloride)	Lapatinib	Dichlorophen
Daunorubicin (hydrochloride)	Olverembatinib (dimesylate)	Olverembatinib (dimesylate)
Afatinib	Oxibendazole	Lacidipine
Crizotinib	Lasofoxifene (Tartrate)	Lasofoxifene (Tartrate)
Ebselen	Almonertinib	Cloxiquine
Cetylpyridinium (chloride)	Flupentixol dihydrochloride	Almonertinib
Dacomitinib	Osimertinib mesylate	Flupentixol dihydrochloride
Tegaserod (maleate)	Dichlorophen	Staurosporine
Clomiphene (citrate)	Afoxolaner	Oxyclozanide
Octyl gallate	Staurosporine	Fluralaner
Siramesine (hydrochloride)	Fluralaner	Troglitazone
Saikosaponin D	Dronedarone (Hydrochloride)	Afoxolaner
Osimertinib mesylate	Lacidipine	Mefloquine (hydrochloride)
Toremifene (citrate)	Cloxiquine	Dronedarone (Hydrochloride)
Olverembatinib (dimesylate)	Troglitazone	Flunarizine (dihydrochloride)
Idarubicin (hydrochloride)	Oxyclozanide	Belumosudil
Amiodarone (hydrochloride)	Ivermectin	Odevixibat
Amylmetacresol	Mefloquine (hydrochloride)	Fidaxomicin
Nebivolol (hydrochloride)	Elbasvir	Plicamycin
Saikosaponin A	Gossypol (acetic acid)	Triptolide
Netupitant	Halofantrine (hydrochloride)	Pitavastatin (Calcium)
Fluspirilene	Zotepine	Ripretinib
Sertaconazole (nitrate)	Nilotinib (monohydrochloride monohydrate)	Eltrombopag (Olamine)
Everolimus	Gossypol	Amphotericin B
Astemizole	Palbociclib (isethionate)	Deslanoside

Olmutinib	Belumosudil	Crizotinib (hydrochloride)
Bedaquiline	Crizotinib (hydrochloride)	Halofantrine (hydrochloride)
Candesartan Cilexetil	Voxilaprevir	Sonidegib
Dehydrocostus Lactone	Disulfiram	Pexidartinib
Doxorubicin (hydrochloride)	Osimertinib	Nilotinib (monohydrochloride monohydrate)
Penfluridol	Bazedoxifene (acetate)	Epirubicin (hydrochloride)
Auranofin	Verteporfin	Quizartinib
Bexarotene	Sertraline (hydrochloride)	Nintedanib
Econazole (nitrate)	Idarubicin (hydrochloride)	Ziprasidone (hydrochloride monohydrate)
Desogestrel	Ceritinib dihydrochloride	Ceritinib dihydrochloride
Aprepitant	Bithionol	Doxorubicin (hydrochloride)
Afatinib (dimaleate)	Vortioxetine	Palbociclib (isethionate)
Crizotinib (hydrochloride)	Odevixibat	Verteporfin
Vortioxetine	Epirubicin (hydrochloride)	Osimertinib
Visomitin	Abemaciclib (methanesulfonate)	Gossypol (acetic acid)
8-Hydroxyquinoline	Olmutinib	Disulfiram
Fingolimod (hydrochloride)	Doxorubicin (hydrochloride)	Vortioxetine
Ponatinib	Sonidegib	Idarubicin (hydrochloride)
Azelnidipine	Ruboxistaurin	Voxilaprevir
Dronedarone	Everolimus	Olmutinib
Magnolol	Afatinib	Sertraline (hydrochloride)
Ticagrelor	Sodium lauryl sulfoacetate	Abemaciclib (methanesulfonate)
AKBA	Nordihydroguaiaretic acid	Bazedoxifene (acetate)
Isoconazole (nitrate)	Ticagrelor	Fingolimod
Clotrimazole	Sorafenib (Tosylate)	Gossypol
Amorolfine (hydrochloride)	Fedratinib	Bithionol
Sertraline (hydrochloride)	Fluticasone (propionate)	Vinblastine (sulfate)
Rolapitant	Sunitinib (Malate)	Everolimus
N-Ethylmaleimide	Tamoxifen (Citrate)	Vemurafenib
Fenticonazole (Nitrate)	Aprepitant	Cerivastatin (sodium)
Butoconazole (nitrate)	Afatinib (dimaleate)	Pralsetinib
Celecoxib	Almonertinib (hydrochloride)	Fluvastatin (sodium)
Vortioxetine (hydrobromide)	Dacomitinib	Afatinib
Disulfiram	Ponatinib	Afatinib (dimaleate)
Simeprevir	Amsacrine	Fostamatinib Disodium
Rifamycin S	Telotristat etiprate	Rolapitant
Staurosporine	Celecoxib	Regorafenib (Hydrochloride)
Fingolimod	Sertindole	Sunitinib (Malate)
Lomitapide	Daunorubicin (hydrochloride)	Fostamatinib (disodium hexahydrate)
Melflufen (hydrochloride)	Lomitapide	Amsacrine
Milbemycin oxime	Melflufen (hydrochloride)	Quinacrine (dihydrochloride)
Cloxiquine	Fluvastatin (sodium)	Fedratinib
Clofoctol	Quinacrine (dihydrochloride)	Celecoxib
Montelukast (sodium)	Dienestrol	Ticagrelor
Hexylresorcinol	Sulconazole (mononitrate)	Mitoxantrone
Flupentixol dihydrochloride	Chlorquinaldol	Daunorubicin (hydrochloride)
Estradiol valerianate	Chlorhexidine (dihydrochloride)	Sodium lauryl sulfoacetate

Fenretinide	Miconazole (nitrate)	Dacomitinib
Bithionol	Penfluridol	Mitoxantrone (dihydrochloride)
Miconazole (nitrate)	Triclosan	Sertindole
Olverembatinib	Econazole	Sorafenib (Tosylate)
Parthenolide	Felodipine	Almonertinib (hydrochloride)
Crystal Violet	Tioconazole	Sorafenib
Dichlorophen	Clofoctol	Lomitapide
Honokiol	Menadione	Ponatinib
Triclosan	Thioridazine (hydrochloride)	Homoharringtonine
Dronedarone (Hydrochloride)	Puromycin (dihydrochloride)	Melflufen (hydrochloride)
Cinacalcet (hydrochloride)	Atorvastatin	Ospemifene
Casticin	(R)-Fangchinoline	Ponesimod
Lapatinib (ditosylate)	Lovastatin	Tamoxifen (Citrate)
Fedratinib	Gramicidin	Niclosamide
Tirbanibulin (Mesylate)	Aclacinomycin A hydrochloride	Chlorhexidine (dihydrochloride)
Mebendazole	Crizotinib	Lanatoside C
Chlorquinaldol	Fostamatinib	Nifedipine
Rotenone	18?-Glycyrrhetinic acid	Chlorquinaldol
(R)-Fangchinoline	Tetradecyl sulfate (sodium)	Puromycin (dihydrochloride)
Y-33075 (dihydrochloride)	Escin	Felodipine
Regorafenib	Cinacalcet (hydrochloride)	Econazole
Gramicidin	Parthenolide	Penfluridol
Prazosin (hydrochloride)	Magnolol	Triclosan
Octenidine (dihydrochloride)	Honokiol	Tioconazole
Fostamatinib (disodium hexahydrate)	Tetrandrine	Dienestrol
Thonzonium (bromide)	Salbutamol (hemisulfate)	Sulconazole (mononitrate)
Sorafenib (Tosylate)	Cangrelor (tetrasodium)	Clofoctol
Fedratinib (hydrochloride hydrate)	Osimertinib (dimesylate)	Thioridazine (hydrochloride)
Tocofersolan	Docusate (Sodium)	Miconazole (nitrate)
Bazedoxifene (acetate)	Cilengitide (TFA)	Ciclopirox
Cetrimonium (bromide)	Cinobufotalin	9-Aminoacridine
Cetylpyridinium (chloride monohydrate)	Perifosine	Fangchinoline
Efavirenz	Cefprozil (monohydrate)	Lovastatin
		(R)-Fangchinoline
		Ethidium (bromide)
		Curcumin
		Aclacinomycin A hydrochloride
		Fostamatinib
		Crizotinib
		Gramicidin
		Tetradecyl sulfate (sodium)
		Harringtonine
		Magnolol
		Halofuginone
		Honokiol
		Halofuginone (hydrobromide)
		Cinacalcet (hydrochloride)

	Parthenolide
	Escin
	Vinorelbine (ditartrate)
	Alectinib (Hydrochloride)
	Netupitant
	Brigatinib
	Gilteritinib hemifumarate
	Cinobufotalin
	Cilengitide (TFA)
	Lumefantrine
	Osimertinib (dimesylate)
	Toceranib (phosphate)
	Abemaciclib
	Miconazole
	Tetrandrine
	(-)-Securinine
	Perifosine

Appendix 4: RNA quality, sequencing depth, and alignment quality-control metrics for RNAseq libraries.

RNAseq was performed using AF-ACFs from four independent donors following vehicle (Veh) or levamlodipine besylate (LB) treatment. RNA integrity was assessed using a Fragment Analyzer and is reported as RNA Quality Number (RQN). RQN values ranged from 9.5–10.0, indicating highly intact RNA. All libraries generated >65 million reads, with >96% of bases achieving a Phred quality score of Q30 or greater. More than 99% of reads mapped to the reference genome, of which >97% mapped uniquely.

Sample	RQN	Total Reads	Mean Quality Score	Yield (Mbases)	Bases >Q30 (%)	Total Mapped Reads	% Total Mapped Reads	Unique Mapped Reads	% Unique Mapped Reads
Donor 1-Veh	9.7	81,616,912	39.30	25,003	96.59	80,872,094	99.09	79,377,938	97.26
Donor 1-LB	9.5	87,220,721	39.26	26,766	96.42	86,556,783	99.24	84,869,498	97.30
Donor 2-Veh	9.7	80,836,655	39.30	24,776	96.57	80,252,614	99.28	78,724,790	97.39
Donor 2-LB	9.8	63,719,867	39.32	19,511	96.65	63,196,114	99.18	62,036,748	97.36
Donor 3-Veh	10.0	69,219,004	39.28	21,210	96.45	68,680,854	99.22	67,294,638	97.22
Donor 3-LB	10.0	71,598,259	39.29	21,945	96.53	71,041,753	99.22	69,587,999	97.19
Donor 4-Veh	10.0	72,468,873	39.31	22,181	96.62	71,968,194	99.31	70,526,980	97.32
Donor 4-LB	9.7	75,061,315	39.29	23,021	96.53	74,485,281	99.23	72,885,231	97.10

Appendix 5: Genes upregulated by levamlodipine in AF-ACFs.

List of the 241 genes upregulated by levamlodipine treatment in AF-ACFs (adjusted p-value < 0.05 and log2FoldChange > 1). Ordered by adjusted p-value.

FABP3	GDF15	SERINC2	AC008897.3
DHRS3	ERVV-2	BIRC3	AC135048.1
NKD2	FCRLA	MT2A	HEY1
SREBF1	AC116351.1	DMKN	BATF2
TYMP	AC144652.1	HSD17B7	CLMN
IGFBP1	ACSL3	ACLY	IL1B
LSS	MVK	MAFF	AL032819.2
TRIB3	OASL	AC007405.3	OAS1
PCYT2	IDI2-AS1	ZMIZ1-AS1	RFX8
CDHR1	ACACA	DDX58	SLC30A3
AP001469.1	TSC22D3	FADS2	SQLE
ITIH1	MVD	IL1A	STAR
FDPS	MLPH	CXCL3	DBH
RAB27B	TMEM97	HMGCR	FER1L6
PCSK9	MMAB	LRP8	P2RX1
DUSP4	THEMIS2	SMIM10L2B	AL157871.2
GALNT12	PTGS2	PCDHAC2	IFIT3
ODF3B	FDFT1	SLC2A6	AK7
RUSC1-AS1	CXCL2	LINC02257	NCF2
STARD4	SHMT1	RPLP0P2	ERICH2
DDIT4	RSAD2	AC009549.1	BHLHE40
LINC00520	GCH1	CEACAMP10	ISG15
HSD17B12	CXCL5	AL138828.1	MX2
AC004988.1	DHCR7	SPP1	CCL7
MME	XAF1	PDE4D	SCD
NCR3LG1	ATF3	FGFBP3	HRK
LYNX1	HMGCS1	AC112198.2	HES6
JAKMIP2	AP003068.4	KRT34	FBXO39
QPRT	STC1	LBHD1	ABCG1
RRAGD	KCNG1	NRROS	OAS2
IDI1	ACSS2	PNPLA3	MIR4635
STARD8	UNC13A	DUSP6	CXCL1
IRF7	HSPA6	IGFN1	PPP1R14C
MSMO1	INSIG1	AC036214.1	PRAL
SCARB1	IL21R	FAM213A	FAAH
FADS1	CYP51A1	PTGES	B3GNT5
RARRES1	TM7SF2	AC004264.1	CKMT2
PRUNE2	ATP6V0D2	AC011511.5	TCTEX1D4
SLCO4C1	FLVCR1	U62317.1	RTN4R
KLHDC7B	DNER	RELB	ELFN2
TNFRSF9	LAMP3	ADTRP	CCDC17
DHCR24	HSD11B1	NPY1R	SOD2
INHBE	AC089983.1	SV2A	SIGLEC9

ADAMTS14	BEX2	PFKFB4	HERC5
SYT7	AC254633.1	MX1	CHST6
LPIN1	KCP	CSF3	ICAM1
MLXIPL	RAB33A	UQCC3	KLHL30-AS1
LDLR	TMEM154	SLC16A13	LIF
SLC8A2	TMEM233	TDRKH	IFI6
MID1IP1	NSDHL	IL4I1	SLC17A7
PLA2G3	ITGAX	AC100861.1	MIR3189
EBP	NPC1	AP000808.1	NPPA
AC124798.1	UNC13D	CMPK2	MCF2L2
ELOVL6	PHLDA2	DLGAP1-AS2	FOLR3
NAMPT	AC114947.2	TAC1	ASPRV1
ACAT2	HSD17B7P2	SNAI3-AS1	MMP1
FASN	CCL5	MISP	IFIH1
NPPA-AS1	GBP5	CXCL8	GPR3
WARS	LINC01705	HELZ2	
ALDOC	SGIP1	LINC02154	
ADGRG1	AL445490.1	SNAI3	

Appendix 6: Genes downregulated by levamlodipine in AF-ACFs.

List of the 258 genes downregulated by levamlodipine treatment in AF-ACFs (unadjusted p-value < 0.05 and log2FoldChange < -1). Purple text indicates those genes with adjusted p-values < 0.05. Ordered by adjusted p-value.

LMOD1	ANXA8	CTAGE1	DEPDC1
PRSS23	RIMS1	DDIAS	STARD4-AS1
SCUBE3	RXFP1	LINC01711	SPAG5
SLC6A4	SPAAR	PLK4	ANLN
KRT14	GPR17	RASL11B	CILP2
FGF1	CDKN3	CCDC81	AC104137.1
ACTA2	HLF	CBLN2	CDCA8
CLEC3B	ALPK2	ADRA2A	PIK3CG
GAP43	AC023421.2	SBSPON	ESPNL
RASSF2	OSR2	CGN	CDC45
CNN1	AC114760.2	KIF20A	RPS6KA2-IT1
LINC01614	ITLN2	FRRS1L	CDH1
GREM2	SAPCD2	CCNB1	SOST
AC037198.1	ANXA8L1	TMSB15A	CENPE
KRT7	HGD	SULT1B1	CEP55
ADH1B	GJA4	PCLAF	AURKA
LINC01018	MGAT3	HMMR	EXO1
ACTA2-AS1	GINS4	AC018647.1	TPX2
H19	AF165147.1	FGF9	TLL1
CD244	TMPO-AS1	OXTR	PLK1
OGN	CSF2RB	NREP	HPGD
AC027237.3	ERBB3	LINC02511	PENK
CLIC3	CENPM	TSPAN2	ARHGAP11A
TENM2	KCNS1	PPP1R1B	CCNA2
SLC1A7	SLC38A4	HSD17B6	CFHR1
THBS1	SYNPO2L	KCNK2	KIF23
ELN	LINC02544	GDF7	KCNB1
KRT7-AS	C11orf87	NEURL1B	BUB1
JPH2	DHRS9	KIF2C	NCAPG2
PRSS35	RAB7B	BIRC5	MKI67
DLGAP1	PADI2	AP002364.1	CDCA2
INMT	RSPO1	CPA4	NUSAP1
LINC01013	ZNF488	PRR11	GTSE1
AC013652.1	SLAMF7	AC105105.1	TNFSF15
CEMIP	DRD1	SEMA5B	AC068491.4
CRABP2	ADGRG6	TMC3	NCAPH
GATA5	KCNS2	TNNT2	AC022211.1
WISP2	NPR3	KRT16	HOXA3
HUNK	TUBA1B	FRZB	CST6
ACKR3	AC027808.2	TK1	LINC01151

GSG1	KLHDC8A	AL592430.1	KIF14
PITX2	AP003355.2	PRC1	DEPDC1B
CMAHP	SMILR	RIPOR2	ASPM
HRCT1	AC112229.3	BUB1B	TTK
MYO7B	CNTN1	C1QTNF2	PBK
IL1RAPL2	LSP1	FRMPD3	FANCD2
PLCXD3	TOX	LINC01697	EME1
SULT1E1	E2F8	CCNB2	KRT87P
RASD1	AL096865.1	DLGAP5	TROAP
AC037198.2	AQP3	CIT	FMO2
COL21A1	KCNA4	MYBL2	APOBEC3B
CRISPLD2	TRPC6	OIP5	NEK2
PDK4	KRT80	CYP24A1	SKA3
SLC7A4	ERCC6L	SOX18	KNL1
LINC00968	DIAPH3	NA	MIR23B
FAM46B	FLNC-AS1	NOSTRIN	RAD54L
LGR5	AL512413.1	IQGAP3	KIFC1
HR	PLPPR4	NUF2	CPA1
PIMREG	ANGPTL4	RACGAP1	SPC24
ANK3	AL133553.1	AL121578.3	ZNF367
LSAMP	AL445183.2	CDC20	BLM
CCDC190	AC099850.3	TRIP13	KIF4A
AL355916.1	CDC25C	SHCBP1	TOP2A
PI15	LINC00578	CENPF	
ACTG2	AL590004.4	AC011767.1	

CHAPTER 9: REFERENCES

1. Moreira, L.M.*, et al.* Paracrine signalling by cardiac calcitonin controls atrial fibrogenesis and arrhythmia. *Nature* **587**, 460-465 (2020).

2. Tracy, T.S.J. Heart and Soul in Aristotle. *The Society for Ancient Greek Philosophy Newletter* **90**(1974).

3. Harvey, W. *Exercitatio Anatomica de Motu Cordis et Sanguinis in Animalibus*, (Frankurt: Fitzeri, 1628).

4. Aird, W.C. Discovery of the cardiovascular system: from Galen to William Harvey. *J Thromb Haemost* **9 Suppl 1**, 118-129 (2011).

5. Lippi, G., Sanchis-Gomar, F. & Cervellin, G. Global epidemiology of atrial fibrillation: An increasing epidemic and public health challenge. *Int J Stroke* **16**, 217-221 (2021).

6. Staerk, L.*, et al.* Lifetime risk of atrial fibrillation according to optimal, borderline, or elevated levels of risk factors: cohort study based on longitudinal data from the Framingham Heart Study. *BMJ* **361**, k1453 (2018).

7. Nattel, S., Lip, G.Y.H., Filgueiras-Rama, D. & Dobrev, D. Challenges and opportunities in improving the management of atrial fibrillation: recent research advances and their clinical translation. *Cardiovasc Res* **117**, 1609-1611 (2021).

8. Staerk, L., Sherer, J.A., Ko, D., Benjamin, E.J. & Helm, R.H. Atrial Fibrillation: Epidemiology, Pathophysiology, and Clinical Outcomes. *Circ Res* **120**, 1501-1517 (2017).

9. Odutayo, A.*, et al.* Atrial fibrillation and risks of cardiovascular disease, renal disease, and death: systematic review and meta-analysis. *BMJ* **354**, i4482 (2016).

10. Ruddox, V.*, et al.* Atrial fibrillation and the risk for myocardial infarction, all-cause mortality and heart failure: A systematic review and meta-analysis. *Eur J Prev Cardiol* **24**, 1555-1566 (2017).

11. Van Gelder, I.C.*, et al.* 2024 ESC Guidelines for the management of atrial fibrillation developed in collaboration with the European Association for Cardio-Thoracic Surgery (EACTS). *Eur Heart J* **45**, 3314-3414 (2024).

12. Burdett, P. & Lip, G.Y.H. Atrial fibrillation in the UK: predicting costs of an emerging epidemic recognizing and forecasting the cost drivers of atrial fibrillation-related costs. *Eur Heart J Qual Care Clin Outcomes* **8**, 187-194 (2022).

13. Sgreccia, D.*, et al.* Comparing Outcomes in Asymptomatic and Symptomatic Atrial Fibrillation: A Systematic Review and Meta-Analysis of 81,462 Patients. *J Clin Med* **10**(2021).

14. Kloosterman, M.*, et al.* Sex-related differences in risk factors, outcome, and quality of life in patients with permanent atrial fibrillation: results from the RACE II study. *Europace* **22**, 1619-1627 (2020).

15. Potpara, T.S. & Lip, G.Y. Lone atrial fibrillation: what is known and what is to come. *Int J Clin Pract* **65**, 446-457 (2011).

16. Nattel, S. & Harada, M. Atrial remodeling and atrial fibrillation: recent advances and translational perspectives. *J Am Coll Cardiol* **63**, 2335-2345 (2014).

17. Weng, L.C.*, et al.* Heritability of Atrial Fibrillation. *Circ Cardiovasc Genet* **10**(2017).

18. Andersen, J.H., Andreasen, L. & Olesen, M.S. Atrial fibrillation-a complex polygenetic disease. *Eur J Hum Genet* **29**, 1051-1060 (2021).

19. Haissaguerre, M.*, et al.* Spontaneous Initiation of Atrial Fibrillation By Ectopic Beats Originating in the Pulmonary Veins. *NEJM* **339**(1998).

20. Wijesurendra, R.S. & Casadei, B. Mechanisms of atrial fibrillation. *Heart* **105**, 1860-1867 (2019).

21. Wijffels, M.C.E.F., Kirchhof, C.J.H.J., Dorland, R. & Allessie, M.A. Atrial Fibrillation Begets Atrial Fibrillation: A Study in Awake Chronically Instrumented Goats. *Circulation* **92**, 1954-1968 (1995).

22. Zhao, S.*, et al.* Aging-associated mechanisms of atrial fibrillation progression and their therapeutic potential. *The Journal of Cardiovascular Aging* **4**(2024).

23. Brundel, B.*, et al.* Atrial fibrillation. *Nat Rev Dis Primers* **8**, 21 (2022).

24. Voigt, N.*, et al.* Enhanced sarcoplasmic reticulum Ca2+ leak and increased Na+-Ca2+ exchanger function underlie delayed afterdepolarizations in patients with chronic atrial fibrillation. *Circulation* **125**, 2059-2070 (2012).

25. Kato, T., Iwasaki, Y.K. & Nattel, S. Connexins and atrial fibrillation: filling in the gaps. *Circulation* **125**, 203-206 (2012).

26. Camm, A.J.*, et al.* The Increasing Role of Rhythm Control in Patients With Atrial Fibrillation: JACC State-of-the-Art Review. *J Am Coll Cardiol* **79**, 1932-1948 (2022).

27. Hindricks, G.*, et al.* 2020 ESC Guidelines for the diagnosis and management of atrial fibrillation developed in collaboration with the European Association for Cardio-Thoracic Surgery (EACTS): The Task Force for the diagnosis and management of atrial fibrillation of the European Society of Cardiology (ESC) Developed with the special contribution of the European Heart Rhythm Association (EHRA) of the ESC. *Eur Heart J* **42**, 373-498 (2021).

28. Voigt, N. & Dobrev, D. Ion Channel Remodelling in Atrial Fibrillation. *European Cardiology* **7**, 97-103 (2011).

29. Heijman, J., Guichard, J.B., Dobrev, D. & Nattel, S. Translational Challenges in Atrial Fibrillation. *Circ Res* **122**, 752-773 (2018).

30. Valembois, L.*, et al.* Antiarrhythmics for maintaining sinus rhythm after cardioversion of atrial fibrillation. *Cochrane Database Syst Rev* **9**, CD005049 (2019).

31. Kirchhof, P.*, et al.* Early Rhythm-Control Therapy in Patients with Atrial Fibrillation. *N Engl J Med* **383**, 1305-1316 (2020).

32. Saglietto, A.*, et al.* Impact of atrial fibrillation catheter ablation on mortality, stroke, and heart failure hospitalizations: A meta-analysis. *J Cardiovasc Electrophysiol* **31**, 1040-1047 (2020).

33. Marrouche, N.F.*, et al.* Catheter Ablation for Atrial Fibrillation with Heart Failure. *N Engl J Med* **378**, 417-427 (2018).

34. Packer, D.L.*, et al.* Effect of Catheter Ablation vs Antiarrhythmic Drug Therapy on Mortality, Stroke, Bleeding, and Cardiac Arrest Among Patients With Atrial Fibrillation: The CABANA Randomized Clinical Trial. *JAMA* **321**, 1261-1274 (2019).

35. Darby, A.E. Recurrent Atrial Fibrillation After Catheter Ablation: Considerations For Repeat Ablation And Strategies To Optimize Success. *J Atr Fibrillation* **9**(2016).

36. Li, D., Fareh, S., Leung, T.K. & Nattel, S. Promotion of Atrial Fibrillation by Heart Failure in Dogs. *Circulation* **100**, 87-95 (1999).

37. Henderson, N.C., Rieder, F. & Wynn, T.A. Fibrosis: from mechanisms to medicines. *Nature* **587**, 555-566 (2020).

38. Virchow, R. *Die Cellularpathologie in ihrer Begründung auf physiologische und pathologische Gewebelehre*, (Berlin : Verlag von August Hirschwald, 1859).

39. Ziegler, E. *General pathology or the science of the causes, nature and course of the pathological disturbances which occur in the living subject*, (William Wood and Company, New York, 1896).

40. Plikus, M.V.*, et al.* Fibroblasts: Origins, definitions, and functions in health and disease. *Cell* **184**, 3852-3872 (2021).

41. Carrel, A. On the Permanent Life of Tissues Outside of the Organism. *J Exp. Med.* **15**, 516-528 (1912).

42. Buechler, M.B.*, et al.* Cross-tissue organization of the fibroblast lineage. *Nature* **593**, 575-579 (2021).

43. Leblanc, F.J.A.*, et al.* Single-nucleus multi-omics implicates androgen receptor signaling in cardiomyocytes and NR4A1 regulation in fibroblasts during atrial fibrillation. *Nat Cardiovasc Res* **4**, 433-444 (2025).

44. Turner, N.A. Inflammatory and fibrotic responses of cardiac fibroblasts to myocardial damage associated molecular patterns (DAMPs). *J Mol Cell Cardiol* **94**, 189-200 (2016).

45. Litvinukova, M.*, et al.* Cells of the adult human heart. *Nature* **588**, 466-472 (2020).

46. Moore-Morris, T., Cattaneo, P., Puceat, M. & Evans, S.M. Origins of cardiac fibroblasts. *J Mol Cell Cardiol* **91**, 1-5 (2016).

47. Yamaguchi, T. Atrial structural remodeling and atrial fibrillation substrate: A histopathological perspective. *J Cardiol* **85**, 47-55 (2025).

48. Takahashi, Y.*, et al.* Histological validation of atrial structural remodelling in patients with atrial fibrillation. *Eur Heart J* **44**, 3339-3353 (2023).

49. Corradi, D.*, et al.* Persistent lone atrial fibrillation: clinicopathologic study of 19 cases. *Heart Rhythm* **11**, 1250-1258 (2014).

50. Morfino, P.*, et al.* Treatment of cardiac fibrosis: from neuro-hormonal inhibitors to CAR-T cell therapy. *Heart Fail Rev* **28**, 555-569 (2023).

51. Sohns, C. & Marrouche, N.F. Atrial fibrillation and cardiac fibrosis. *Eur Heart J* **41**, 1123-1131 (2020).

52. Marrouche, N.F.*, et al.* Association of atrial tissue fibrosis identified by delayed enhancement MRI and atrial fibrillation catheter ablation: the DECAAF study. *JAMA* **311**, 498-506 (2014).

53. Marrouche, N.F.*, et al.* Effect of MRI-Guided Fibrosis Ablation vs Conventional Catheter Ablation on Atrial Arrhythmia Recurrence in Patients With Persistent Atrial Fibrillation: The DECAAF II Randomized Clinical Trial. *JAMA* **327**, 2296-2305 (2022).

54. Naot, D., Musson, D.S. & Cornish, J. The Activity of Peptides of the Calcitonin Family in Bone. *Physiol Rev* **99**, 781-805 (2019).

55. Frohlich, E. & Wahl, R. Calcitonin and procalcitonin: Revisiting the overlooked role of C cells. *Metabolism* **175**, 156434 (2026).

56. Hurley, D.L., Tiegs, R.D., Wahner, H.W. & Heath, H. Axial and Appendicular Bone Mineral Density in Patients with Long-term Deficiency or Excess of Calcitonin. *NEJM* **317**, 537-541 (1987).

57. Machens, A., Lorenz, K. & Dralle, H. Time to calcitonin normalization after surgery for node-negative and node-positive medullary thyroid cancer. *Br J Surg* **106**, 412-418 (2019).

58. Hung, C.L.*, et al.* Is Partial or Total Thyroidectomy Associated with Risk of Long-Term Osteoporosis: A Nationwide Population-Based Study. *World J Surg* **42**, 2864-2871 (2018).

59. Woo, T. & Adachi, J.D. Role of bisphosphonates and calcitonin in the prevention and treatment of osteoporosis. *Best Pract Res Clin Rheumatol* **15**, 469-481 (2001).

60. Lin, H.Y.*, et al.* Expression Cloning of an Adenylate Cyclase-Coupled Calcitonin Receptor. *Science* **254**, 1022-1024 (1991).

61. Yang, D.*, et al.* G protein-coupled receptors: structure- and function-based drug discovery. *Signal Transduct Target Ther* **6**, 7 (2021).

62. Liang, Y.L.*, et al.* Phase-plate cryo-EM structure of a class B GPCR-G-protein complex. *Nature* **546**, 118-123 (2017).

63. Dal Maso, E.*, et al.* The Molecular Control of Calcitonin Receptor Signaling. *ACS Pharmacol Transl Sci* **2**, 31-51 (2019).

64. Cary, B.P.*, et al.* New Insights into the Structure and Function of Class B1 GPCRs. *Endocr Rev* **44**, 492-517 (2023).

65. Uhlen, M.*, et al.* Proteomics. Tissue-based map of the human proteome. *Science* **347**, 1260419 (2015).

66. Chen, Y.*, et al.* The calcitonin receptor stimulates Shc tyrosine phosphorylation and Erk1/2 activation. Involvement of Gi, protein kinase C, and calcium. *J Biol Chem* **273**, 19809-19816 (1998).

67. Bower, R.L.*, et al.* Molecular Signature for Receptor Engagement in the Metabolic Peptide Hormone Amylin. *ACS Pharmacol Transl Sci* **1**, 32-49 (2018).

68. Magalhaes, A.C., Dunn, H. & Ferguson, S.S. Regulation of GPCR activity, trafficking and localization by GPCR-interacting proteins. *Br J Pharmacol* **165**, 1717-1736 (2012).

69. Dal Maso, E.*, et al.* Characterization of signalling and regulation of common calcitonin receptor splice variants and polymorphisms. *Biochem Pharmacol* **148**, 111-129 (2018).

70. Gorn, A.H.*, et al.* Cloning, characterization, and expression of a human calcitonin receptor from an ovarian carcinoma cell line. *J Clin Invest* **90**, 1726-1735 (1992).

71. Frendo, J.L.*, et al.* An isoform of the human calcitonin receptor is expressed in TT cells and in medullary carcinoma of the thyroid. *FEBS Letters* **342**, 214-216 (1994).

72. Nakamura, M.*, et al.* Allelic variants of human calcitonin receptor in the Japanese population. *Hum Genet* **99**, 38-41 (1996).

73. Laporte, S.A. & Scott, M.G.H. β-Arrestins: Multitask Scaffolds Orchestrating the Where and When in Cell Signalling. in *Beta-Arrestins. Methods in Molecular Biology*, Vol. 1957 (eds. Scott, M. & Laporte, S.) (Humana Press, New York, NY, 2019).

74. Andreassen, K.V.*, et al.* Prolonged calcitonin receptor signaling by salmon, but not human calcitonin, reveals ligand bias. *PLoS One* **9**, e92042 (2014).

75. Liu, J.*, et al.* Multi-faceted roles of beta-arrestins in G protein-coupled receptor endocytosis. *Nat Commun* (2025).

76. Wootten, D.*, et al.* Receptor activity modifying proteins (RAMPs) interact with the VPAC2 receptor and CRF1 receptors and modulate their function. *Br J Pharmacol* **168**, 822-834 (2013).

77. Pioszak, A.A. & Hay, D.L. RAMPs as allosteric modulators of the calcitonin and calcitonin-like class B G protein-coupled receptors. *Adv Pharmacol* **88**, 115-141 (2020).

78. Barbash, S., Lorenzen, E., Persson, T., Huber, T. & Sakmar, T.P. GPCRs globally coevolved with receptor activity-modifying proteins, RAMPs. *Proc Natl Acad Sci U S A* **114**, 12015-12020 (2017).

79. McLatchie, L.*, et al.* RAMPs regulate the transport and ligand specificity of the calcitonin-receptor-like receptor. *Nature* **393**, 333-339 (1998).

80. Hay, D.L. & Pioszak, A.A. Receptor Activity-Modifying Proteins (RAMPs): New Insights and Roles. *Annu Rev Pharmacol Toxicol* **56**, 469-487 (2016).

81. Hay, D.L., Garelja, M.L., Poyner, D.R. & Walker, C.S. Update on the pharmacology of calcitonin/CGRP family of peptides: IUPHAR Review 25. *Br J Pharmacol* **175**, 3-17 (2017).

82. Hay, D.L., Chen, S., Lutz, T.A., Parkes, D.G. & Roth, J.D. Amylin: Pharmacology, Physiology, and Clinical Potential. *Pharmacological Reviews* **67**, 564-600 (2015).

83. Christopoulos, G.*, et al.* Multiple Amylin Receptors Arise from Receptor Activity-Modifying Protein Interaction with the Calcitonin Receptor Gene Product. *Molecular Pharmacology* **56**, 235-242 (1999).

84. Routledge, S.J., Ladds, G. & Poyner, D.R. The effects of RAMPs upon cell signalling. *Mol Cell Endocrinol* **449**, 12-20 (2017).

85. Cao, J.*, et al.* Cryo-EM Structure of the Human Amylin 1 Receptor in Complex with CGRP and Gs Protein. *Biochemistry* **63**, 1089-1096 (2024).

86. Shead, K.D., Salyahetdinova, V. & Baillie, G.S. Charting the importance of filamin A posttranslational modifications. *Biochem J* **481**, 865-881 (2024).

87. Bandaru, S., Ala, C., Zhou, A.X. & Akyurek, L.M. Filamin A Regulates Cardiovascular Remodeling. *Int J Mol Sci* **22**(2021).

88. Zheng, X.*, et al.* Hypoxia-induced and calpain-dependent cleavage of filamin A regulates the hypoxic response. *Proc Natl Acad Sci U S A* **111**, 2560-2565 (2014).

89. Oh, C.H.*, et al.* A family of Melnick-Needles syndrome: a case report. *BMC Pediatr* **20**, 391 (2020).

90. Tirupula, K.C.*, et al.* G protein-coupled receptors directly bind filamin A with high affinity and promote filamin phosphorylation. *Biochemistry* **54**, 6673-6683 (2015).

91. Seck, T., Baron, R. & Horne, W.C. Binding of filamin to the C-terminal tail of the calcitonin receptor controls recycling. *J Biol Chem* **278**, 10408-10416 (2003).

92. Rafizadeh, S.*, et al.* Functional interaction with filamin A and intracellular Ca2+ enhance the surface membrane expression of a small-conductance Ca2+-activated K+ (SK2) channel. *Proc Natl Acad Sci U S A* **111**, 9989-9994 (2014).

93. Heijman, J.*, et al.* Enhanced Ca(2+)-Dependent SK-Channel Gating and Membrane Trafficking in Human Atrial Fibrillation. *Circ Res* **132**, e116-e133 (2023).

94. Nygaard, S.C., Kuestner, R.E., Moore, E.E. & Stroop, S.D. Phosphorylation of the Human Calcitonin Receptor by Multiple Kinases is Localized to the C-Terminus. *Journal of Bone and Mineral Research* **12**(1997).

95. He, M., Zhou, X. & Wang, X. Glycosylation: mechanisms, biological functions and clinical implications. *Signal Transduct Target Ther* **9**, 194 (2024).

96. Lee, S.M.*, et al.* Calcitonin Receptor N-Glycosylation Enhances Peptide Hormone Affinity by Controlling Receptor Dynamics. *J Mol Biol* **432**, 1996-2014 (2020).

97. Lee, S.M.*, et al.* N-Glycosylation of Asparagine 130 in the Extracellular Domain of the Human Calcitonin Receptor Significantly Increases Peptide Hormone Affinity. *Biochemistry* **56**, 3380-3393 (2017).

98. Whitaker, G.M., Lynn, F.C., McIntosh, C.H. & Accili, E.A. Regulation of GIP and GLP1 receptor cell surface expression by N-glycosylation and receptor heteromerization. *PLoS One* **7**, e32675 (2012).

99. Chalhoub, G. & McCormick, P.J. Chapter Nine - Palmitoylation and G-protein coupled receptors. in *Prog Mol Biol Transl Sci*, Vol. 193 (ed. Shukla, A.K.) 195-211 (Academic Press, 2022).

100. Renner, U.*, et al.* Localization of the mouse 5-hydroxytryptamine(1A) receptor in lipid microdomains depends on its palmitoylation and is involved in receptor-mediated signaling. *Mol Pharmacol* **72**, 502-513 (2007).

101. Buenaventura, T.*, et al.* Agonist-induced membrane nanodomain clustering drives GLP-1 receptor responses in pancreatic beta cells. *PLoS Biol* **17**, e3000097 (2019).

102. Wilkinson, R. Treatment of hypercalcaemia associated with malignancy. *BMJ* **288**(1984).

103. Takahashi, S.*, et al.* Downregulation of calcitonin receptor mRNA expression by calcitonin during human osteoclast-like cell differentiation. *J Clin Invest* **95**, 167-171 (1995).

104. Rakopoulos, M., Ikegame, M., Findlay, D.M., Martin, T.J. & Moseley, J.M. Short Treatment of Osteoclasts in Bone Marrow Culture With Calcitonin Causes Prolonged Suppression of Calcitonin Receptor mRNA. *Bone* **17**(1995).

105. Waring, M.J.*, et al.* An analysis of the attrition of drug candidates from four major pharmaceutical companies. *Nat Rev Drug Discov* **14**, 475-486 (2015).

106. Yildirim, Z., Swanson, K., Wu, X., Zou, J. & Wu, J. Next-Gen Therapeutics: Pioneering Drug Discovery with iPSCs, Genomics, AI, and Clinical Trials in a Dish. *Annu Rev Pharmacol Toxicol* **65**, 71-90 (2025).

107. Hay, M., Thomas, D.W., Craighead, J.L., Economides, C. & Rosenthal, J. Clinical development success rates for investigational drugs. *Nat Biotechnol* **32**(2014).

108. Onakpoya, I.J., Heneghan, C.J. & Aronson, J.K. Post-marketing withdrawal of 462 medicinal products because of adverse drug reactions: a systematic review of the world literature. *BMC Med* **14**, 10 (2016).

109. Pushpakom, S.*, et al.* Drug repurposing: progress, challenges and recommendations. *Nat Rev Drug Discov* **18**, 41-58 (2019).

110. Sourimant, J., Aggarwal, M. & Plemper, R.K. Progress and pitfalls of a year of drug repurposing screens against COVID-19. *Curr Opin Virol* **49**, 183-193 (2021).

111. Swinney, D.C. & Anthony, J. How were new medicines discovered? *Nat Rev Drug Discov* **10**, 507-519 (2011).

112. Krishnamurthy, N., Grimshaw, A.A., Axson, S.A., Choe, S.H. & Miller, J.E. Drug repurposing: a systematic review on root causes, barriers and facilitators. *BMC Health Serv Res* **22**, 970 (2022).

113. Poulet, C.*, et al.* Altered physiological functions and ion currents in atrial fibroblasts from patients with chronic atrial fibrillation. *Physiol Rep* **4**(2016).

114. Livak, K.J. & Schmittgen, T.D. Analysis of relative gene expression data using real-time quantitative PCR and the 2(-Delta Delta C(T)) Method. *Methods* **25**, 402-408 (2001).

115. Bolte, S. & Cordelieres, F.P. A guided tour into subcellular colocalization analysis in light microscopy. *J Microsc* **224**, 213-232 (2006).

116. Gorlin, J.B.*, et al.* Human endothelial actin-binding protein (ABP-280, nonmuscle filamin): a molecular leaf spring. *J Cell Biol* **111**, 1089-1105 (1990).

117. Loy, C.J., Sim, K.S. & Yong, E.L. Filamin-A fragment localizes to the nucleus to regulate androgen receptor and coactivator functions. *Proc Natl Acad Sci U S A* **100**, 4562-4567 (2003).

118. Jobin, M.L.*, et al.* Filamin A organizes gamma-aminobutyric acid type B receptors at the plasma membrane. *Nat Commun* **14**, 34 (2023).

119. Salimi, R.*, et al.* Blocking the Cleavage of Filamin A by Calpain Inhibitor Decreases Tumor Cell Growth. *Anticancer Res* **38**, 2079-2085 (2018).

120. Di Donato, M.*, et al.* Filamin A cooperates with the androgen receptor in preventing skeletal muscle senescence. *Cell Death Discov* **9**, 437 (2023).

121. Macias-Diaz, A.*, et al.* Filamin A C-terminal fragment modulates Orai1 expression by inhibition of protein degradation. *AJP Cell* **328**(2025).

122. Baudry, M., Su, W. & Bi, X. The Calpain Proteolytic System. in *Encyclopedia of Cell Biology* 852-864 (2023).

123. Brundel, B.J.*, et al.* Activation of proteolysis by calpains and structural changes in human paroxysmal and persistent atrial fibrillation. *Cardiovascular Research* **54**, 380-389 (2002).

124. Goette, A.*, et al.* Calpains and cytokines in fibrillating human atria. *AJP Heart Circ Physiol* **283**(2002).

125. Brundel, B.J., Kampinga, H.H. & Henning, R.H. Calpain inhibition prevents pacing-induced cellular remodeling in a HL-1 myocyte model for atrial fibrillation. *Cardiovasc Res* **62**, 521-528 (2004).

126. Umeda, T.*, et al.* Limited proteolysis of filamin is catalyzed by caspase-3 in U937 and Jurkat cells. *J Biochem* **130**, 535-542 (2001).

127. Browne, K.A., Johnstone, R.W., Jans, D.A. & Trapani, J.A. Filamin (280-kDa actin-binding protein) is a caspase substrate and is also cleaved directly by the cytotoxic T lymphocyte protease granzyme B during apoptosis. *J Biol Chem* **275**, 39262-39266 (2000).

128. Heuze, M.L.*, et al.* ASB2 targets filamins A and B to proteasomal degradation. *Blood* **112**, 5130-5140 (2008).

129. Razinia, Z.*, et al.* The E3 ubiquitin ligase specificity subunit ASB2alpha targets filamins for proteasomal degradation by interacting with the filamin actin-binding domain. *J Cell Sci* **124**, 2631-2641 (2011).

130. Maire, K.*, et al.* Fine-tuning levels of filamins a and b as a specific mechanism sustaining Th2 lymphocyte functions. *Nat Commun* **15**, 10574 (2024).

131. Nagano, T.*, et al.* Filamin A-interacting protein (FILIP) regulates cortical cell migration out of the ventricular zone. *Nat Cell Biol* **4**, 495-501 (2002).

132. Goldberg, A.L. Development of proteasome inhibitors as research tools and cancer drugs. *J Cell Biol* **199**, 583-588 (2012).

133. Klionsky, D.J.*, et al.* Guidelines for the use and interpretation of assays for monitoring autophagy (3rd edition). *Autophagy* **12**, 1-222 (2016).

134. Miao, Y.*, et al.* Cycloheximide (CHX) Chase Assay to Examine Protein Half-life. *Bio Protoc* **13**, e4690 (2023).

135. Kosugi, S., Hasebe, M., Tomita, M. & Yanagawa, H. Systematic identification of cell cycle-dependent yeast nucleocytoplasmic shuttling proteins by prediction of composite motifs. *PNAS* **106**, 10171-10176 (2009).

136. Ono, Y., Saido, T.C. & Sorimachi, H. Calpain research for drug discovery: challenges and potential. *Nat Rev Drug Discov* **15**, 854-876 (2016).

137. Rawlings, N.D.*, et al.* The MEROPS database of proteolytic enzymes, their substrates and inhibitors in 2017 and a comparison with peptidases in the PANTHER database. *Nucleic Acids Res* **46**, D624-D632 (2018).

138. Dube, D.K.*, et al.* Effect of MG-132 on myofibrillogenesis and the ubiquitination of GAPDH in quail myotubes. *Cytoskeleton (Hoboken)* **78**, 375-390 (2021).

139. Kucharski, M., Mrowiec, P. & Oclon, E. Current standards and pitfalls associated with the transfection of primary fibroblast cells. *Biotechnol Prog* **37**, e3152 (2021).

140. Shaiken, T.E. & Opekun, A.R. Dissecting the cell to nucleus, perinucleus and cytosol. *Sci Rep* **4**, 4923 (2014).

141. Peverelli, E.*, et al.* Filamin A (FLNA) plays an essential role in somatostatin receptor 2 (SST2) signaling and stabilization after agonist stimulation in human and rat somatotroph tumor cells. *Endocrinology* **155**, 2932-2941 (2014).

142. Matsuyama, M. & Iwamiya, T. Novel and effective plasmid transfection protocols for functional analysis of genetic elements in human cardiac fibroblasts. *PLoS One* **19**, e0309566 (2024).

143. Sakoda, T., Kasahara, N., Hamamori, Y. & Kedes, L. A High-Titer Lentiviral Production System Mediates Efficient Transduction of Differentiated Cells Including Beating Cardiac Myocytes. *J Mol Cell Cardiol* **31**, 2037-2047 (1999).

144. Moore, E.E.*, et al.* Functionally Different Isoforms of the Human Calcitonin Receptor Result from Alternative Splicing of the Gene Transcript. *Mol Endocrinol* **9**, 959-968 (1995).

145. Ritchie, M.E.*, et al.* limma powers differential expression analyses for RNA-sequencing and microarray studies. *Nucleic Acids Res* **43**, e47 (2015).

146. Verschueren, E.*, et al.* Scoring Large-Scale Affinity Purification Mass Spectrometry Datasets with MiST. *Curr Protoc Bioinformatics* **49**, 8 19 11-18 19 16 (2015).

147. Ge, S.X., Jung, D. & Yao, R. ShinyGO: a graphical gene-set enrichment tool for animals and plants. *Bioinformatics* **36**, 2628-2629 (2020).

148. Benjamini, Y. & Hochberg, Y. Controlling the False Discovery Rate: A Practical and Powerful Approach to Multiple Testing. *J. R. Statist. Soc. B* **57**, 289-300 (1995).

149. Kanehisa, M., Furumichi, M., Sato, Y., Ishiguro-Watanabe, M. & Tanabe, M. KEGG: integrating viruses and cellular organisms. *Nucleic Acids Res* **49**, D545-D551 (2021).

150. Mellacheruvu, D.*, et al.* The CRAPome: a contaminant repository for affinity purification-mass spectrometry data. *Nat Methods* **10**, 730-736 (2013).

151. Kovtun, O., Dickson, V.K., Kelly, B.T., Owen, D.J. & Briggs, J.A.G. Architecture of the AP2/clathrin coat on the membranes of clathrin coated vesicles. *Sci Adv* **6**, 9 (2020).

152. Milesi, C.*, et al.* Redundant and nonredundant organismal functions of EPS15 and EPS15L1. *Life Sci Alliance* **2**(2019).

153. Andreev, J.*, et al.* Identification of a New Pyk2 Target Protein with Arf-GAP Activity. *Mol. Cell. Biol.* **19**, 2338-2350 (1999).

154. Lamaze, C., Chuang, T.-H., Terlecky, L.J., Bokoch, G.M. & Schmid, S.L. Regulation of receptor-mediated endocytosis by Rho and Rac. *Nature* **382**(1996).

155. Ellis, S. & Mellor, H. Regulation of endocytic traffic by rho family GTPases. *Trends Cell Biol.* **10**, 85-88 (2000).

156. Szewczyk-Roszczenko, O.K.*, et al.* The Chemical Inhibitors of Endocytosis: From Mechanisms to Potential Clinical Applications. *Cells* **12**(2023).

157. McCluskey, A.*, et al.* Building a better dynasore: the dyngo compounds potently inhibit dynamin and endocytosis. *Traffic* **14**, 1272-1289 (2013).

158. Vercauteren, D.*, et al.* The Use of Inhibitors to Study Endocytic Pathways of Gene Carriers: Optimization and Pitfalls. *Molecular Therapy* **18**, 561-569 (2010).

159. Park, M.H., Jo, M., Kim, Y.R., Lee, C.K. & Hong, J.T. Roles of peroxiredoxins in cancer, neurodegenerative diseases and inflammatory diseases. *Pharmacol Ther* **163**, 1-23 (2016).

160. Pfenniger, A., Yoo, S. & Arora, R. Oxidative stress and atrial fibrillation. *J Mol Cell Cardiol* **196**, 141-151 (2024).

161. Reilly, S.N.*, et al.* Atrial sources of reactive oxygen species vary with the duration and substrate of atrial fibrillation: implications for the antiarrhythmic effect of statins. *Circulation* **124**, 1107-1117 (2011).

162. Ibarrola, J.*, et al.* Galectin-3 down-regulates antioxidant peroxiredoxin-4 in human cardiac fibroblasts: a new pathway to induce cardiac damage. *Clin Sci (Lond)* **132**, 1471-1485 (2018).

163. Kim, M.S., Zhong, J. & Pandey, A. Common errors in mass spectrometry-based analysis of post-translational modifications. *Proteomics* **16**, 700-714 (2016).

164. Seaman, M.N. The retromer complex - endosomal protein recycling and beyond. *J Cell Sci* **125**, 4693-4702 (2012).

165. Zhang, X.*, et al.* Mutation in nuclear pore component NUP155 leads to atrial fibrillation and early sudden cardiac death. *Cell* **135**, 1017-1027 (2008).

166. Han, M.*, et al.* Lamin A mutation impairs interaction with nucleoporin NUP155 and disrupts nucleocytoplasmic transport in atrial fibrillation. *Hum Mutat* **40**, 310-325 (2019).

167. Laniel, A.*, et al.* Class A and B GPCRs trigger rapid Galpha(s) translocation to late and slow recycling endosomes. *Commun Biol* **8**, 1715 (2025).

168. van Dam, E.M. & Stoorvogel, W. Dynamin-dependent Transferrin Receptor Recycling by Endosome-derived Clathrin-coated Vesicles. *Mol Biol Cell* **13**(2002).

169. Goley, E.D. & Welch, M.D. The ARP2/3 complex: an actin nucleator comes of age. *Nat Rev Mol Cell Biol* **7**, 713-726 (2006).

170. Hetrick, B., Han, M.S., Helgeson, L.A. & Nolen, B.J. Small molecules CK-666 and CK-869 inhibit actin-related protein 2/3 complex by blocking an activating conformational change. *Chem Biol* **20**, 701-712 (2013).

171. Pavlos, N.J. & Friedman, P.A. GPCR Signaling and Trafficking: The Long and Short of It. *Trends Endocrinol Metab* **28**, 213-226 (2017).

172. Brouwers, B.*, et al.* Human MC4R variants affect endocytosis, trafficking and dimerization revealing multiple cellular mechanisms involved in weight regulation. *Cell Rep* **34**, 108862 (2021).

173. Pegoraro, G. & Misteli, T. High-throughput Imaging as a versatile and unbiased discovery tool. *Methods* **96**, 1-2 (2016).

174. Kubben, N., Brimacombe, K.R., Donegan, M., Li, Z. & Misteli, T. A high-content imaging-based screening pipeline for the systematic identification of anti-progeroid compounds. *Methods* **96**, 46-58 (2016).

175. Zhang, J.H., Chung, T.D. & Oldenburg, K.R. A Simple Statistical Parameter for Use in Evaluation and Validation of High Throughput Screening Assays. *J Biomol Screen* **4**, 67-73 (1999).

176. Bar, H. & Zweifach, A. Z' Does Not Need to Be >0.5. *SLAS Discov.* **25**, 1000-1008 (2020).

177. Zhang, H.*, et al.* Multiscale drug screening for cardiac fibrosis identifies MD2 as a therapeutic target. *Cell* (2024).

178. Gomes, R.N., Cardona-Timoner, M., Silva, E.D., Pombinho, A. & Nascimento, D.S. A high-throughput analysis of novel anti-fibrotics in human adult cardiac fibroblasts. *Biomed Pharmacother* **188**, 118216 (2025).

179. Deb, B., Ganesan, P., Feng, R. & Narayan, S.M. Identifying Atrial Fibrillation Mechanisms for Personalized Medicine. *J Clin Med* **10**(2021).

180. Suh, S.S., Mohan, M.S. & Davis, M.W. P-250: Amlodipine: pharmacokinetics of the maleate vs besylate salts. *American Journal of Hypertension* **17**, 123A-124A (2004).

181. Park, J.-Y.*, et al.* Pharmacokinetic and pharmacodynamic characteristics of a new S-amlodipine formulation in healthy Korean male subjects: A randomized, open-label, two-period, comparative, crossover study. *Clinical Therapeutics* **28**, 1837-1847 (2006).

182. Sheraz, M.A., Ahsan, S.F., Khan, M.F., Ahmed, S. & Ahmad, I. Formulations of Amlodipine: A Review. *J Pharm (Cairo)* **2016**, 8961621 (2016).

183. Zhang, X.-P., Loke, K.E., Seema, M., Suresh, C. & Hintze, T.H. Paradoxical Release of Nitric Oxide by an L-Type Calcium Channel Antagonist, the R+ Enantiomer of Amlodipine. *Journal of Cardiovascular Pharmacology* **39**, 208-214 (2002).

184. Thacker, H.P. S-amlodipine — the 2007 clinical review. *J Indian Med Assoc* **105**(2007).

185. Dalal, J.*, et al.* S-Amlodipine: An Isomer with Difference-Time to Shift from Racemic Amlodipine. *Int J Hypertens* **2018**, 8681792 (2018).

186. Hunt, N.J.*, et al.* Manipulating fenestrations in young and old liver sinusoidal endothelial cells. *Am J Physiol Gastrointest Liver Physiol* **316**, G144-G154 (2019).

187. He, G.F.*, et al.* The role of L-type calcium channels in mouse oocyte maturation, activation and early embryonic development. *Theriogenology* **102**, 67-74 (2017).

188. Slack, R.J., Macdonald, S.J.F., Roper, J.A., Jenkins, R.G. & Hatley, R.J.D. Emerging therapeutic opportunities for integrin inhibitors. *Nat Rev Drug Discov* **21**, 60-78 (2022).

189. Dong, X., *et al.* Force interacts with macromolecular structure in activation of TGF-beta. *Nature* **542**, 55-59 (2017).

190. Munger, J.S., *et al.* The Integrin αvβ6 Binds and Activates Latent TGFb1: A Mechanism for Regulating Pulmonary Inflammation and Fibrosis. *Cell* (1999).

191. Henderson, N.C., *et al.* Targeting of alphav integrin identifies a core molecular pathway that regulates fibrosis in several organs. *Nat Med* **19**, 1617-1624 (2013).

192. Murray, I.R., *et al.* alphav integrins on mesenchymal cells regulate skeletal and cardiac muscle fibrosis. *Nat Commun* **8**, 1118 (2017).

193. Hohmann, T. & Dehghani, F. The Cytoskeleton-A Complex Interacting Meshwork. *Cells* **8**(2019).

194. Delon, I. & Brown, N.H. Integrins and the actin cytoskeleton. *Curr Opin Cell Biol* **19**, 43-50 (2007).

195. Ley, K., Rivera-Nieves, J., Sandborn, W.J. & Shattil, S. Integrin-based therapeutics: biological basis, clinical use and new drugs. *Nat Rev Drug Discov* **15**, 173-183 (2016).

196. Floyd, C.N. & Ferro, A. Indications for anticoagulant and antiplatelet combined therapy. *BMJ* **359**, j3782 (2017).

197. Yang, Y., Li, Y., Gu, H., Dong, M. & Cai, Z. Emerging agents and regimens for multiple myeloma. *J Hematol Oncol* **13**, 150 (2020).

198. Zinzani, P.L., *et al.* CHRONOS-4: phase 3 study of copanlisib plus rituximab-based immunochemotherapy in relapsed indolent B-cell lymphoma. *Blood Adv* **8**, 4866-4876 (2024).

199. Soldatov, N.M. Molecular diversity of L-type Ca2+ channel transcripts in human fibroblasts. *PNAS* **89**(1992).

200. Chen, J.B., *et al.* Multiple Ca2+ signaling pathways regulate intracellular Ca2+ activity in human cardiac fibroblasts. *J Cell Physiol* **223**, 68-75 (2010).

201. Mukherjee, S., *et al.* Disruption of Calcium Signaling in Fibroblasts and Attenuation of Bleomycin-Induced Fibrosis by Nifedipine. *Am J Respir Cell Mol Biol* **53**, 450-458 (2015).

202. Rinne, A. & Pluteanu, F. Ca(2+) Signaling in Cardiovascular Fibroblasts. *Biomolecules* **14**(2024).

203. Feng, J., *et al.* Ca(2+) Signaling in Cardiac Fibroblasts and Fibrosis-Associated Heart Diseases. *J Cardiovasc Dev Dis* **6**(2019).

204. Davis, J., Burr, A.R., Davis, G.F., Birnbaumer, L. & Molkentin, J.D. A TRPC6-dependent pathway for myofibroblast transdifferentiation and wound healing in vivo. *Dev Cell* **23**, 705-715 (2012).

205. Khorasani, N.*, et al.* Computational modelling of cardiac fibroblast signalling reveals a key role for Ca(2+) in driving atrial fibrillation-associated fibrosis. *J Physiol* (2025).

206. Zeigler, A.C., Richardson, W.J., Holmes, J.W. & Saucerman, J.J. A computational model of cardiac fibroblast signaling predicts context-dependent drivers of myofibroblast differentiation. *J Mol Cell Cardiol* **94**, 72-81 (2016).

207. Ong, H.L., de Sousza, L.B. & Ambudkar, I.S. Role of TRPC Channels in Store-Operated Calcium Entry. in *Calcium Entry Pathways in Non-excitable Cells. Advances in Experimental Medicine and Biology.*, Vol. 898 (ed. Rosado, J.A.) (Springer, 2016).

208. Wang, J.*, et al.* Junctophilin-2 Regulates Store-Operated Calcium Entry to Drive Cardiac Fibroblast Activation, Fibrotic Repair, and Angiogenesis After Myocardial Infarction. *Circulation* **152**, 699-716 (2025).

209. Zhang, B.*, et al.* Store-Operated Ca(2+) Entry (SOCE) contributes to angiotensin II-induced cardiac fibrosis in cardiac fibroblasts. *J Pharmacol Sci* **132**, 171-180 (2016).

210. Schuttler, D.*, et al.* Animal Models of Atrial Fibrillation. *Circ Res* **127**, 91-110 (2020).

211. Muller, F.U.*, et al.* Heart-directed expression of a human cardiac isoform of cAMP-response element modulator in transgenic mice. *J Biol Chem* **280**, 6906-6914 (2005).

212. Kirchhof, P.*, et al.* Overexpression of cAMP-response element modulator causes abnormal growth and development of the atrial myocardium resulting in a substrate for sustained atrial fibrillation in mice. *Int J Cardiol* **166**, 366-374 (2013).

213. Muller, F.U.*, et al.* Identification and expression of a novel isoform of cAMP response element modulator in the human heart. *FASEB J* **12**, 1191-1199 (1998).

214. Zhao, S.*, et al.* Atrial proteomic profiling reveals a switch towards profibrotic gene expression program in CREM-IbDeltaC-X mice with persistent atrial fibrillation. *J Mol Cell Cardiol* **190**, 1-12 (2024).

215. Liu, T.*, et al.* BindingDB in 2024: a FAIR knowledgebase of protein-small molecule binding data. *Nucleic Acids Res* **53**, D1633-D1644 (2025).

216. Liu, T., Lin, Y., Wen, X., Jorissen, R.N. & Gilson, M.K. BindingDB: a web-accessible database of experimentally determined protein-ligand binding affinities. *Nucleic Acids Res* **35**, D198-201 (2007).

217. Daina, A., Michielin, O. & Zoete, V. SwissTargetPrediction: updated data and new features for efficient prediction of protein targets of small molecules. *Nucleic Acids Res* **47**, W357-W364 (2019).

218. Love, M.I., Huber, W. & Anders, S. Moderated estimation of fold change and dispersion for RNA-seq data with DESeq2. *Genome Biol* **15**, 550 (2014).

219. Ho, K.S.*, et al.* Multiomic and electrophysiologic analyses reveal that an inherited MRC2 variant causes fibroblast dysfunction and increased atrial fibrillation susceptibility. *Am J Physiol Heart Circ Physiol* **329**, H1055-H1071 (2025).

220. Szklarczyk, D.*, et al.* STITCH 5: augmenting protein-chemical interaction networks with tissue and affinity data. *Nucleic Acids Res* **44**, D380-384 (2016).

221. Zhang, S.*, et al.* Discovery of a Highly Selective and Potent TRPC3 Inhibitor with High Metabolic Stability and Low Toxicity. *ACS Med Chem Lett* **12**, 572-578 (2021).

222. Wang, J.*, et al.* Discovery of a potent and selective TRPC3 antagonist with neuroprotective effects. *Bioorg Med Chem* **117**, 118021 (2025).

223. Maier, T.*, et al.* Discovery and pharmacological characterization of a novel potent inhibitor of diacylglycerol-sensitive TRPC cation channels. *Br J Pharmacol* **172**, 3650-3660 (2015).

224. Lin, B.L.*, et al.* In vivo selective inhibition of TRPC6 by antagonist BI 749327 ameliorates fibrosis and dysfunction in cardiac and renal disease. *Proc Natl Acad Sci U S A* **116**, 10156-10161 (2019).

225. Washburn, D.G.*, et al.* The discovery of potent blockers of the canonical transient receptor channels, TRPC3 and TRPC6, based on an anilino-thiazole pharmacophore. *Bioorg Med Chem Lett* **23**, 4979-4984 (2013).

226. Wei, Y.*, et al.* Benzothiazole Amides as TRPC3/6 Inhibitors for Gastric Cancer Treatment. *ACS Omega* **6**, 9196-9203 (2021).

227. Aprile, S.*, et al.* 1,2,4-Oxadiazole-Bearing Pyrazoles as Metabolically Stable Modulators of Store-Operated Calcium Entry. *ACS Med Chem Lett* **12**, 640-646 (2021).

228. Iannarone, V.J., Cruz, G.E., Hilliard, B.A. & Barbe, M.F. The answer depends on the question: Optimal conditions for western blot characterization of muscle collagen type 1 depends on desired isoform. *J Biol Methods* **6**, e117 (2019).

229. Guo, L., Xiang, W., Pan, Z., Gu, H. & Jiang, X. Post-translational modifications of collagen and its related diseases in metabolic pathways. *Acta Pharm Sin B* **15**, 1773-1795 (2025).

230. Lin, M., Aladejebi, O. & Hockerman, G.H. Distinct properties of amlodipine and nicardipine block of the voltage-dependent Ca2+ channels Cav1.2 and Cav2.1 and the mutant channels Cav1.2/dihydropyridine insensitive and Cav2.1/dihydropyridine sensitive. *Eur J Pharmacol* **670**, 105-113 (2011).

231. Mohammad, S.*, et al.* Constitutive traffic of melanocortin-4 receptor in Neuro2A cells and immortalized hypothalamic neurons. *J Biol Chem* **282**, 4963-4974 (2007).

232. Kisling, A.*, et al.* Loss of Function in Dopamine D3 Receptor Attenuates Left Ventricular Cardiac Fibroblast Migration and Proliferation in vitro. *Front Cardiovasc Med* **8**, 732282 (2021).

233. Johnson, T.L.*, et al.* The dopamine D3 receptor knockout mouse mimics aging-related changes in autonomic function and cardiac fibrosis. *PLoS One* **8**, e74116 (2013).

234. Neumann, J., Hofmann, B., Dhein, S. & Gergs, U. Cardiac Roles of Serotonin (5-HT) and 5-HT-Receptors in Health and Disease. *Int J Mol Sci* **24**(2023).

235. Jahnel, U., Rupp, J., Ertl, R. & Nawrath, H. Positive inotropic response to 5-HT in human atrial but not in ventricular heart muscle. *Naunyn-Schmiedeberg's Arch Pharmacol* **346**, 482-485 (1992).

236. Tarbit, E., Singh, I., Peart, J.N., Bivol, S. & Rose'Meyer, R.B. Increased release of serotonin from rat primary isolated adult cardiac myofibroblasts. *Sci Rep* **11**, 20376 (2021).

237. Hutcheson, J.D., Setola, V., Roth, B.L. & Merryman, W.D. Serotonin receptors and heart valve disease--it was meant 2B. *Pharmacol Ther* **132**, 146-157 (2011).

238. Janssen, W.*, et al.* 5-HT2B receptor antagonists inhibit fibrosis and protect from RV heart failure. *Biomed Res Int* **2015**, 438403 (2015).

239. Jaffre, F.*, et al.* Serotonin and angiotensin receptors in cardiac fibroblasts coregulate adrenergic-dependent cardiac hypertrophy. *Circ Res* **104**, 113-123 (2009).

240. Tabana, Y., Babu, D., Fahlman, R., Siraki, A.G. & Barakat, K. Target identification of small molecules: an overview of the current applications in drug discovery. *BMC Biotechnol* **23**, 44 (2023).

241. Kawecki, F.*, et al.* Inter-donor variability of extracellular matrix production in long-term cultures of human fibroblasts. *Biomater Sci* **10**, 3935-3950 (2022).

242. Catt, K. & Dufau, M. Spare Gonadotrophin Receptors in Rat Testis. *Nature New Biology* **244**, 219-222 (1973).

243. Chidiac, P. RGS proteins destroy spare receptors: Effects of GPCR-interacting proteins and signal deamplification on measurements of GPCR agonist potency. *Methods* **92**, 87-93 (2016).

244. Shirzad, H., Mousavinezhad, S.A., Panji, M. & Ala, M. Amlodipine alleviates renal ischemia/reperfusion injury in rats through Nrf2/Sestrin2/PGC-1alpha/TFAM Pathway. *BMC Pharmacol Toxicol* **24**, 82 (2023).

245. Lee, Y.J., Park, H.H., Koh, S.H., Choi, N.Y. & Lee, K.Y. Amlodipine besylate and amlodipine camsylate prevent cortical neuronal cell death induced by oxidative stress. *J Neurochem* **119**, 1262-1270 (2011).

246. Mason, R.P., Marche, P. & Hintze, T.H. Novel vascular biology of third-generation L-type calcium channel antagonists: ancillary actions of amlodipine. *Arterioscler Thromb Vasc Biol* **23**, 2155-2163 (2003).

247. Yang, G. & Qiu, Y. Effects of amlodipine combined with atorvastatin on Th17/Treg imbalance and vascular microcirculation in hypertensive patients

with atherosclerosis: A double-blind, single-center randomized controlled trial. *Medicine (Baltimore)* **102**, e32384 (2023).

248. Toba, H.*, et al.* Calcium Channel Blockades Exhibit Anti-Inflammatory and Antioxidative Effects by Augmentation of Endothelial Nitric Oxide Synthase and the Inhibition of Angiotensin Converting Enzyme in the NG-Nitro-L-Arginine Methyl Ester-Induced Hypertensive Rat Aorta: Vasoprotective Effects beyond the Blood Pressure-Lowering Effects of Amlodipine and Manidipine. *Hypertens Res* **28**, 689-700 (2005).

249. Panneerpandian, P., Rao, D.B. & Ganesan, K. Calcium channel blockers lercanidipine and amlodipine inhibit YY1/ERK/TGF-beta mediated transcription and sensitize the gastric cancer cells to doxorubicin. *Toxicol In Vitro* **74**, 105152 (2021).

250. Nissen, E.*, et al.* Effect of antihypertensive agents on cardiovascular events in patients with coronary disease and normal blood pressure: the CAMELOT study: a randomized controlled trial. *JAMA* **292**, 2217-2225 (2004).

251. Dahlof, B.*, et al.* Prevention of cardiovascular events with an antihypertensive regimen of amlodipine adding perindopril as required versus atenolol adding bendroflumethiazide as required, in the Anglo-Scandinavian Cardiac Outcomes Trial-Blood Pressure Lowering Arm (ASCOT-BPLA): a multicentre randomised controlled trial. *Lancet* **366**, 895-906 (2005).

252. Ostrom, R.S. & Insel, P.A. The evolving role of lipid rafts and caveolae in G protein-coupled receptor signaling: implications for molecular pharmacology. *Br J Pharmacol* **143**, 235-245 (2004).

253. Zhou, Z., Zong, J. & Xu, N. Review of methods for the determination of cellular cholesterol content: principles, advantages, limitations, applications, and perspectives. *Anal Sci* **41**, 1697-1714 (2025).

254. Mason, R.P., Campbell, S.F., Wang, S.D. & Herbette, L.G. Comparison of location and binding for the positively charged 1,4-dihydropyridine calcium channel antagonist amlodipine with uncharged drugs of this class in cardiac membranes. *Mol Pharmacol* **36**(1989).

255. Heath, B., Xia, J. & Kass, R.S. Molecular pharmacology of UK-118, 434-05, a permanently charged amlodipine analog. *International Journal of Cardiology* **62**(1997).

256. Tulenko, T.N., Chen, M., Mason, P.E. & Mason, R.P. Physical effects of cholesterol on arterial smooth muscle membranes: evidence of immiscible cholesterol domains and alterations in bilayer width during atherogenesis. *Journal of Lipid Research* **39**, 947-956 (1998).

257. Trion, A.*, et al.* Anti-Atherosclerotic Effect of Amlodipine, Alone and in Combination With Atorvastatin, in APOE*3-Leiden/hCRP Transgenic Mice. *J Cardiovasc Pharmacol* **47**(2006).

258. Chou, C.L., Li, C.H. & Fang, T.C. Benefits of Valsartan and Amlodipine in Lipolysis through PU.1 Inhibition in Fructose-Induced Adiposity. *Nutrients* **14**(2022).

259. Wohlfahrt, T.*, et al.* PU.1 controls fibroblast polarization and tissue fibrosis. *Nature* **566**, 344-349 (2019).

260. Alqudah, M.A.Y., Al-Samman, R., Azaizeh, M. & Alzoubi, K.H. Amlodipine inhibits proliferation, invasion, and colony formation of breast cancer cells. *Biomed Rep* **16**, 50 (2022).

261. Zhang, Y.Z.*, et al.* The inhibitory mechanisms of amlodipine in human vascular smooth muscle cell proliferation. *Hypertens Res* **23**, 403-406 (2000).

262. Verhey, K.J. & Ohi, R. Causes, costs and consequences of kinesin motors communicating through the microtubule lattice. *J Cell Sci* **136**(2023).

263. Chen, H.*, et al.* Kif23 Promotes Myocardial Fibrosis by Suppressing Ces1d-Dependent Lipid Metabolism. *Hypertension* **83**, 116-129 (2026).

264. Reyat, J.S.*, et al.* PITX2 deficiency leads to atrial mitochondrial dysfunction. *Cardiovasc Res* **120**, 1907-1923 (2024).

265. Brandenburg, S.*, et al.* Junctophilin-2 expression rescues atrial dysfunction through polyadic junctional membrane complex biogenesis. *JCI Insight* **4**(2019).

266. Beavers, D.L.*, et al.* Mutation E169K in junctophilin-2 causes atrial fibrillation due to impaired RyR2 stabilization. *J Am Coll Cardiol* **62**, 2010-2019 (2013).

267. Lam, C.K.*, et al.* Identifying the Transcriptome Signatures of Calcium Channel Blockers in Human Induced Pluripotent Stem Cell-Derived Cardiomyocytes. *Circ Res* **125**, 212-222 (2019).

268. Takeuchi, F.*, et al.* Transcriptomic Response in the Heart and Kidney to Different Types of Antihypertensive Drug Administration. *Hypertension* **79**, 413-423 (2022).

269. Dzeshka, M.S., Lip, G.Y., Snezhitskiy, V. & Shantsila, E. Cardiac Fibrosis in Patients With Atrial Fibrillation: Mechanisms and Clinical Implications. *J Am Coll Cardiol* **66**, 943-959 (2015).

270. Chen, G. & Obal, D. Detecting and measuring of GPCR signaling - comparison of human induced pluripotent stem cells and immortal cell lines. *Front Endocrinol (Lausanne)* **14**, 1179600 (2023).

271. Landry, N.M., Rattan, S.G. & Dixon, I.M.C. An Improved Method of Maintaining Primary Murine Cardiac Fibroblasts in Two-Dimensional Cell Culture. *Sci Rep* **9**, 12889 (2019).

272. Ebrahimighaei, R.*, et al.* Extracellular matrix stiffness controls cardiac fibroblast proliferation via the nuclear factor-Y (NF-Y) transcription factor. *Biochim Biophys Acta Mol Cell Res* **1871**, 119640 (2024).

273. Herum, K.M., Lunde, I.G., McCulloch, A.D. & Christensen, G. The Soft- and Hard-Heartedness of Cardiac Fibroblasts: Mechanotransduction Signaling Pathways in Fibrosis of the Heart. *J Clin Med* **6**(2017).

274. Sahadevan, P. & Allen, B.G. Isolation and culture of adult murine cardiac atrial and ventricular fibroblasts and myofibroblasts. *Methods* **203**, 187-195 (2022).

275. Bay, A.E., Schreiner, R. & Rodriguez-Boulan, E. Structural and functional analysis of endosomal compartments in epithelial cells. *Methods Cell Biol* **130**, 271-288 (2015).

276. Bui, S., Stark, D., Li, J., Zhang, J. & Wang, Y. Common Markers and Small Molecule Inhibitors in Golgi Studies. *Methods Mol Biol* **2557**, 453-493 (2023).

277. Wolf, P., Gavins, G., Beck-Sickinger, A.G. & Seitz, O. Strategies for Site-Specific Labeling of Receptor Proteins on the Surfaces of Living Cells by Using Genetically Encoded Peptide Tags. *Chembiochem* **22**, 1717-1732 (2021).

278. Li, X.*, et al.* Bioequivalence of levamlodipine besylate tablets in healthy Chinese subjects: a single-dose and two-period crossover randomized study. *BMC Pharmacol Toxicol* **21**, 80 (2020).